ISOTOPIC CONSTRAINTS ON SOURCES AND CYCLING OF RIVERINE DISSOLVED INORGANIC CARBON IN THE AMAZON BASIN

Emilio Mayorga

A dissertation submitted in partial fulfillment
of the requirements for the degree of

Doctor of Philosophy

University of Washington

2004

Program Authorized to Offer Degree: School of Oceanography

University of Washington
Graduate School

This is to certify that I have examined this copy of a doctoral dissertation by

Emilio Mayorga

and have found that it is complete and satisfactory in all respects,
and that any and all revisions required by the final
examining committee have been made.

Chair of Supervisory Committee:

_____
Jeffrey E. Richey

Reading Committee:

_____
Charles Nittrouer

_____
Paul D. Quay

_____
Jeffrey E. Richey

Date: _____

In presenting this dissertation in partial fulfillment of the requirements for the Doctoral degree at the University of Washington, I agree that the Library shall make its copies freely available for inspection. I further agree that extensive copying of the dissertation is allowable only for scholarly purposes, consistent with "fair use" as prescribed in the U.S. Copyright Law. Requests for copying or reproduction of this dissertation may be referred to ProQuest Information and Learning, 300 North Zeeb Road, Ann Arbor, MI 48106-1346, to whom the author has granted "the right to reproduce and sell (a) copies of the manuscript in microform and/or (b) printed copies of the manuscript made from microform."

Signature: _____

Date: _____

University of Washington

Abstract

ISOTOPIC CONSTRAINTS ON SOURCES AND CYCLING OF RIVERINE DISSOLVED INORGANIC CARBON IN THE AMAZON BASIN

Emilio Mayorga

Chair of the Supervisory Committee:
Professor Jeffrey E. Richey
School of Oceanography

Dissolved inorganic carbon (DIC) and CO_2 gas are fundamental components of riverine biogeochemical functioning. Amazonian and humid tropical rivers represent a large, neglected source of CO_2 to the atmosphere. Carbon isotopes are invaluable tools for examining sources and cycling of inorganic carbon. However, ^{14}C-DIC has never been analyzed in Amazonia, while ^{13}C-DIC studies have concentrated on the mainstem and surroundings, despite large basin landscape heterogeneity.

I used geochemical and ^{13}C-^{14}C isotopic measurements on basin-wide samples to address the following DIC and CO_2 topics: isotopic variability and its primary causes; sources and age of respired organic carbon (OC) dominating CO_2 production; terrestrial sources; and downstream evolution. To facilitate interpretation within a consistent river system view, I developed an Amazon river network dataset and algorithm. I also compiled into a common database new and previously published geochemical data. I characterized lithological sources through major ions geochemistry.

Dominant sources of riverine DIC isotopic variability are: presence of carbonate lithologies (common throughout the Andes, especially Peru), relative contribution of C_3 and C_4 plant material to respiration, and atmospheric CO_2 invasion in turbulent rivers. Lowland rivers are predominantly supersaturated in pCO_2 and carry young DIC. Aged lowland DIC occurs only in carbonate lithologies, some small streams, and low-oxygen environments. A small, contemporary OC fraction dominates respiration; C_4 vegetation exerts a disproportionate influence on lowland fluvial respiration. CO_2 is typically more supersaturated and depleted in $\delta^{13}C$ at high water. In the shields, sandy soils and deforested regions export contemporary inorganic carbon; certain forested clayey soils export aged inorganic carbon.

Extensive Andean erosion carries unweathered carbonate sediments into depositional areas. Dissolution then results in slowed replacement of ^{14}C-depleted DIC in the mainstem; $\delta^{13}C$-DIC reflects equilibrium between evasion and respiration in addition to very gradual downstream increase in contributions from C_3 respiration.

Respiration maintains CO_2 supersaturation, flushing out terrestrial DIC via exchange and gas evasion. DIC gradually approaches atmospheric ^{14}C-CO_2 downstream. Turbulence in steep Andean rivers and rocky Shield rivers accelerates gas exchange. In the Andes, tectonic activity and lithological heterogeneity leads to localized influence by marginal processes such as black shale oxidation and lithospheric CO_2 degassing.

TABLE OF CONTENTS

LIST OF FIGURES

LIST OF TABLES

Page

ACKNOWLEDGEMENTS

I would like to express my gratitude to my advisor, Jeffrey Richey, for continued support and encouragement as I meandered across a range of topics, and especially during some difficult circumstances. I thank Committee members Paul Quay and Charles Nittrouer, and former members John Hedges and Chris Field (Carnegie Institute of Washington), for scientific guidance and assistance. I have also benefited from discussions with Allan Devol and Dennis Lettenmaier. Financial support was provided by a NASA Earth Systems Science graduate fellowship, a mini-grant from the Lawrence Livermore National Laboratory (LLNL) Center for Accelerator Mass Spectrometry (CAMS), and funding to our research group from NSF's Division of Environmental Biology, NASA's Office of Earth Science, and Brazils's Fundação de Amparo à Pesquisa do Estado de São Paulo (FAPESP).

Many people provided invaluable assistance in the field. In particular I would like to thank A. K. Aufdenkampe, A. V. Krusche, C. A. Llerena Pinto, and B. Forsberg. Additional assistance in my own field work and in other expeditions was provided by B. J. Dickson, L. Maurice-Bourgoin, M. McClain, T. Pimentel, J. Quintanilla, J. L. Semizo, and many others. Chemical analyses were carried out at several laboratories at the UW, and at LLNL-CAMS, the Centro de Estudos Nucleares na Agricultura (CENA, Piracicaba, Brazil), and the Instituto Nacional de Pesquisas da Amazonia (INPA, Manaus, Brazil). I especially would like to thank Paul Quay's stable isotopes lab for ^{13}C analyses (UW), T. Brown and the staff at LLNL-CAMS for ^{14}C analyses, CENA for numerous analyses, and S. Remington and S. Alin for processing an important set of samples. I benefited greatly from the hospitality and resources at CENA, INPA, LLNL-CAMS, and the Universidad

Agraria La Molina (Lima, Peru). The administrative staff at the UW School of Oceanography was always extremely helpful and effective in assisting me to overcome many stumbling blocks.

I am in debt to present and past graduate students, staff, and postdocs associated with the UW rivers group. They include M. McClain, S. Wilhelm, W. Lin, K. Balster, S. Remington, P. Rattanaviwatpong, H. Greenberg, B. Gustafson, S. Rodda, M. Costa-Cabral, S. Alin, and R. Aalto. Early discussions with T. Dunne, R. Weeks, and M. Smith influenced the direction of this work. C. Masiello's assistance with ^{14}C sample analysis and discussions about carbon isotope dynamics were invaluable to the development of this research. M. Logsdon has deeply influenced my thinking on computing and information systems, and was instrumental to the work presented in Chapter 3. Above all, my collaboration with A. Aufdenkampe permeates this entire work; this dissertation is his as much as it is mine.

I would like to thank my co-workers at Snohomish County, the SWM GIS team, for their constant encouragement to complete this dissertation. But most importantly, I am deeply grateful for the support and encouragement from my entire family, my parents, siblings, in-laws, María Alejandra, Meilin, and especially my wife, Inés.

DEDICATION

To John Hedges,
for his example of a scientif mentor.

To my grandmother, abuelita Alicia,
for instilling a love of science and of a scientific tradition in our family.

And especially to Inés,
for her patience, love, and support.

CHAPTER 1: INTRODUCTION

The Amazon River Basin – the world's largest basin, from the Andean Cordillera to the Atlantic Ocean – contains within its border a large variety of river and subbasin types. Biogeochemical cycling of carbon in this river system therefore involves heterogeneous processes and controls; they span biological, chemical, climatological, and geological components, in fluvial systems ranging from first-order streams to wetlands, seasonally inundated floodplains, and the world's largest river, the Amazon mainstem proper. This study focuses on the use of carbon isotopes (^{14}C and ^{13}C) and other geochemical measurements on many rivers across the basin to elucidate dominant sources and controls on dissolved inorganic carbon (DIC) and carbon dioxide (CO_2) gas. To enable the interpretation of geochemical data from diverse river sites throughout the basin, I integrated this dataset with spatial information using Geographical Information Systems (GIS) and systematically combined it with geochemical data from previous studies. To provide background information, I present extensive reviews of riverine biogeochemistry in Amazonia, and of processes impacting inorganic carbon and carbon isotope cycling in rivers.

Chapter 2 provides a review and synthesis of biogeochemical research in Amazonian rivers, focusing in particular on results from the CAMREX program. In spite of large variability in river types, Amazonian rivers exhibit remarkable consistencies in the processes that control the fate and transport of bioactive elements. River-borne material resides in three compositionally distinct size fractions that have contrasting transport properties and reaction histories. Coarse particulates are the freshest, degrading to form fine particulate and dissolved fractions, which continually interact with each other via sorption processes. Variability in the composition and

dynamics of river-borne material from one river (or season) to another is often less than differences between size fractions within a single river (or season). However, it is often this variability that offers the most insight regarding important processes.

Chapter 3 presents a new high-resolution Amazon river network dataset developed to enable basin-wide modeling and river data integration at multiple scales. In contrast with methods based on elevation, this dataset relies on a new algorithm that uses river vector data to create gridded flow-direction maps covering entire drainage areas. I used the resulting dataset to extract drainage areas, distances along rivers, and basin-averaged properties for each riverine biogeochemical observation.

Chapters 4 through 6 discuss sources and cycling of DIC and CO_2 in Amazonian rivers. First, Chapter 4 reviews relevant literature in the basin and other rivers. This review includes a basic discussion of isotopic and DIC geochemistry, the quantitative mass balance of a river reach, and the main processes impacting a reach, including soil and groundwater terrestrial sources. Chapter 5 then compares the isotopic composition of organic and inorganic carbon to examine sources of respired CO_2, concluding that a small, contemporary fraction of organic matter dominates respiration, sustaining CO_2 supersaturation and evasion. Finally, Chapter 6 provides an extensive discussion of patterns of DIC and CO_2 cycling throughout the basin. While pointing out the principal sources of geochemical and isotopic variability, I also emphasize important topics and more intensively sampled regions. I divide the river sites into lowland, mountain, and "mixed" sites, and into regionally distinct groups; use inorganic geochemistry to qualitatively identify dominant lithological sources; isolate the signature of the smallest streams which reflect terrestrial inputs; and examine trends in downstream and seasonal evolution of inorganic carbon from the Andes to the lowlands and across deforested lowland regions.

CHAPTER 2: PROCESSING OF BIOACTIVE ELEMENTS IN THE AMAZON RIVER SYSTEM

INTRODUCTION

The Amazon Basin drains a vast and heterogeneous region of Northern South America, encompassing large areas of seven nations and important population centers such as Manaus, Porto Velho, Iquitos, Cusco, and La Paz (Fig. 2.1). Despite the acceleration of human impact in the form of deforestation and land use change, mining and oil extraction, dam construction, and urbanization, larger tracts remain relatively pristine, and the main river channels remain largely unaffected by engineering (Lewis *et al.* 1995; Richey *et al.* 1997). The Amazon is of undeniable importance for local communities in particular, and Amazonian nations in general; but as the largest river system in the world it also plays a significant continental and global role in modulating climate, biogeochemical cycles, and terrestrial inputs to the ocean (Devol *et al.* 1994; Meade 1994; Devol & Hedges 2001; Marengo & Nobre 2001).

An understanding of biogeochemical dynamics and controls in river systems is a central requirement of any effort to rationally manage fluvial resources and minimize the impact of human activity on riverine ecosystems. The cycling of bioactive materials (oxygen, carbon, nitrogen, phosphorus, etc.) in rivers, however, is mediated by physical and biological components, such as hydrology, sediment dynamics, and bacterial metabolism. In addition, the linkages between a river and the land it drains are often complex. An integrated approach that crosses disciplinary and landscape boundaries is required to fully elucidate the biogeochemistry of a river system.

In this chapter I review and synthesize current understanding of the biogeochemistry of the Amazon River system. My goal is to provide a conceptual framework from which observations can be evaluated, rather than summarize all available data as has been done in the extensive reviews by Guyot (1993) and Lewis *et al.* (1995). In this overview, no new data or analyses are presented nor are observations discussed in extensive detail. Rather, I provide numerous references to the many papers that do so.

I begin by briefly introducing the geography of the Amazon Basin and the history of geochemical and related research on the region's rivers. I then describe the principal fractions of bioactive materials carried by rivers – their characteristics, sources and interactions – paying special attention to the role of size in fate and transport. Finally, I illustrate with examples largely from the Amazon mainstem the principal patterns of spatial and temporal variability typical of river systems and discuss how their controls can change regionally and with river scale. Through such a presentation I hope to facilitate the interpretation and use of natural riverine biogeochemical observations in tropical river systems like the Amazon, a task that is of critical importance for evaluating likely impacts of human perturbations. While I refer to relevant research by other groups, I write this chapter from my perspective as a member of the CAMREX (**C**arbon in the **AM**azon **R**iver **EX**periment) project, with origins in oceanography that are evident in my view of river processes.

GEOGRAPHICAL AND HISTORICAL PERSPECTIVES OF THE AMAZON

The Amazon river and its basin

The Amazon basin covers a continental-scale region of approximately six million km^2 (not including the Tocantins basin; Fig. 2.1 and 2.2). Such a large area

will inevitably encompass very dissimilar environments, climates, and ecosystems. The main physiographic features of the basin and the river system have been extensively reviewed elsewhere (Sternberg 1975; Sioli 1984b; Lewis *et al.* 1995), and I provide only a brief outline. The main structural elements include the Precambrian, highly weathered Guayana and Brazilian Shields, the Andean mountains to the west, the Andean alluvial foreland, and a central continental alluvium or trough (Fig. 2.1). Soils in the lowlands are generally deep and highly weathered, with prominent occurrences of sandy podzols in the Shields. The soils in floodplains and alluvial regions around mainstems draining the Andes originate in the cordillera and are much less weathered. The climate is generally humid, with mean annual rainfall of approximately 2000 mm. However, precipitation in some regions in the northwest and the Andean piedmont can be much larger, whereas large regions in the east, south, and the high Andes can be drier or arid. More specifically, 10 -15% of the basin receives less than 1,500 mm of rainfall per year, while 6 -10% receives at least 3,000 mm of rainfall per year (unpub. data). The length of the dry season in particular has a large role in determining the type of vegetation that may be sustained. The lowlands are primarily covered by evergreen to semi-deciduous rain forest, but large regions have distinct savanna-like vegetation systems, often seasonally inundated in low-lying areas. River discharge generally displays strong seasonality, with changes in stage height of as much as 10 meters in the Amazon mainstem driving changes in the extent of inundation within the central lowlands from 100,000 km^2 in November to 350,000 km^2 in May (Richey *et al.* 2002). Discharge to the ocean is approximately 220,000 $m^3 s^{-1}$.

History of geochemical research in the Amazon

The variety of environments, massive scale of drainage areas and rivers, and relatively low levels of human impacts, has long attracted geochemical and ecological researchers to the region. Initial investigations centered on large rivers in the Brazilian Amazon, especially the Solimões-Amazonas mainstem, surrounding floodplains and major tributaries, and the region around Manaus (Sioli 1984b). Early observations of three types of river water based on color (Wallace 1853) were later developed extensively and systematized by H. Sioli (Furch 1984; Sioli 1984a). Whitewater rivers have a characteristic muddy color, relatively high concentrations of dissolved solids, and alkaline to neutral pH; their high sediment load originates in Andean or alluvial regions. Examples include the Rios Solimões and Madeira, and other lowland rivers draining mountainous Andean regions. Blackwater rivers are tea-colored from high concentrations of dissolved organic matter (DOM), have negligible suspended sediment loads and medium transparencies, are very dilute in dissolved ions, and are usually acidic; they typically drain areas of low relief and sandy podzol soils. The Rio Negro is the classic example. Finally, clearwater rivers can have high transparencies and are clear or olive-green in color. Their dissolved load is typically low but varies across systems, and they have a wide range in pH, from acidic to alkaline, and low suspended sediment loads. Examples are the Rios Tapajos and Xingu. The group led by H. Sioli, K. Furch, W. Junk and associates from the Max-Planck Institut für Limnologie (Plön, Germany) and the Instituto Nacional de Pesquisas da Amazônia (Manaus, Brazil) is responsible for most of the early studies on the geochemistry and ecology of rivers and floodplains in the Central Amazon (reviewed in Sioli 1984b). Others made important contributions to the characterization of inorganic and organic constituents of these rivers of the central

basin (Klinge & Ohle 1964; Williams 1968), and Gibbs (1967) extended his surveys of river mineralogy and inorganic geochemistry from the lowlands to the Andes.

The cruises of the Research Vessel *Alpha Helix* in 1976-1977 from the Atlantic to Iquitos comprised one of the most influential initiatives in early Amazon research. These expeditions united researchers from diverse fields and nationalities, spawning a substantial number of important publications on sedimentology (Curtis *et al.* 1979; Meade *et al.* 1979; Nordin Jr. *et al.* 1980; Sholkovitz & Price 1980), biogeochemistry (Fisher & Parsley 1979; Richey *et al.* 1980; Longinelli & Edmond 1983; Stallard & Edmond 1983; Cai *et al.* 1988), and biology (Fisher 1979; Wissmar *et al.* 1981). The Alpha Helix project gave birth to the CAMREX research group, which has continued to unite researchers in Amazon biogeochemical research for the last 20 years. The more than 120 CAMREX publications have focused on understanding physical and biogeochemical dynamics throughout the basin using a large variety of approaches. These include studies of cross-sectionally integrated fluxes of water, sediments and bioactive elements (Meade *et al.* 1985; Richey *et al.* 1986; Ferreira *et al.* 1988; Richey *et al.* 1990); floodplain sediment dynamics (Mertes *et al.* 1996; Dunne *et al.* 1998); sediment diagenesis in river bars, floodplains and deltas (Victoria *et al.* 1989; Johnsson & Meade 1990; Martinelli *et al.* 1993; Keil *et al.* 1997); nutrient dynamics in rivers, floodplains and *terra firme* streams (Forsberg *et al.* 1988; Martinelli *et al.* 1992; McClain *et al.* 1994; Devol *et al.* 1995; McClain *et al.* 1997); biogenic gas production rates and air-water exchange fluxes (Devol *et al.* 1987; Richey *et al.* 1988; Devol *et al.* 1994; Richey *et al.* 2002); biochemical tracers of organic matter (OM) sources and processes (Ertel *et al.* 1986; Hedges *et al.* 1986a; Hedges *et al.* 1994; Hedges *et al.* 2000; Aufdenkampe *et al.* 2001); isotopic tracers of organic matter sources and cycling (Araujo-Lima *et al.* 1986; Hedges *et al.* 1986b;

Martinelli *et al.* 1991; Quay *et al.* 1992; Victoria *et al.* 1992; Forsberg *et al.* 1993; Quay *et al.* 1995; Brandes *et al.* 1996); isotopic tracers of water cycling (Martinelli *et al.* 1996a); microbiological metabolism of organic matter (Benner *et al.* 1995; Amon & Benner 1996a; Amon & Benner 1996b); and remote sensing driven models of sediment dynamics (Mertes *et al.* 1993).

Other groups have made very substantial contributions to biogeochemical research in the Amazon Basin. Several studies have focused on hydrological, nutrient and geochemical dynamics on hillslopes and in small catchments north of Manaus (Franken & Leopoldo 1984; Brinkmann 1985; Nortcliff & Thornes 1988; Nortcliff *et al.* 1990; Forti & Neal 1992; Konhauser *et al.* 1994). Others have examined the sources and mechanisms yielding high DOM concentrations in the sandy soils of the Rio Negro basin (Leenheer 1980; St. John & Anderson 1982). In the floodplains of the Central Amazon, J. Melack and associates have carried out extensive biogeochemical, hydrological, and ecological studies in lakes, small catchments, and the inundated area (Lenz *et al.* 1986; Lesack & Melack 1996; Williams & Melack 1997; Sippel *et al.* 1998). Studies in other regions of the basin have been primarily focused on terrestrial, hillslope and stream processes. These include the work in the upper Rio Negro at San Carlos, Venezuela (Stark & Jordan 1978; Tiessen *et al.* 1994); in the Caquetá basin at Araracuara, Colombia (Duivenvoorden & Lips 1995); and in the Pachitea basin in the Andean piedmont of central Perú (Elsenbeer *et al.* 1996). In the Peruvian Amazon a group from the University of Turku, Finland, maintained long-term studies of the relationships between geomorphology, river evolution, succession, and floodplain mineral nutrients (Salo *et al.* 1986; Puhakka *et al.* 1992; Kalliola *et al.* 1993). In the Bolivian headwaters of Rio Madeira the PHICAB (Programa Hidrológico y Climatológico de la Cuenca Amazónica de

Bolivia) project conducted extensive research on the hydrology, sediment dynamics, and geochemistry of rivers beginning in the 1980s (Guyot 1993; Guyot & Wasson 1994; Guyot *et al.* 1999). This French-led project has been extended into the Brazilian Amazon, where it is currently active as HiBAm (**Hi**drologia e **G**eoquímica da **B**acia **Am**azônica; Guyot *et al.* 1998; Mounier *et al.* 1999; Patel *et al.* 1999; Mounier *et al.* 2002). Additional research in the Andean Amazon has been reviewed by McClain et al. (1995).

ROLE OF SIZE ON FATE AND TRANSPORT

Three distinct physical size classes of materials transported in rivers

Riverine transport of bioactive elements from land to sea forms a major link in the global biogeochemical system. The diversity of matter carried within river water is extraordinary – weathered products of rocks and plants sustain all forms of living organisms. The entire continuum of material size is represented, ranging from individual molecules to boulders and trees. Early on in the study of rivers, materials in water were separated into fractions by size (Williams 1968; Meybeck 1982). Coarse particulate, fine particulate, and dissolved fractions were thus operationally defined using sieve pore sizes ranging from 20 to 65 μm to separate particulate fractions, and filter pore sizes ranging from 0.1 to 1.0 μm to isolate dissolved constituents. These exact size cutoffs often differ slightly between research groups, chosen arbitrarily and largely out of convenience. In nature the size distribution of materials across these ranges is actually quite smooth. Despite this, the three size classes – coarse, fine and dissolved – consistently exhibit very distinct transport dynamics, degradation patterns and compositional characteristics. In addition, these

three fractions remain compositionally distinct despite interacting with each other on a continual basis (Fig. 2.3, 2.4, 2.5).

Coarse particles

Essentially all the material transported by rivers starts out in the coarse particulate size class. Rock and decaying vegetation are physically and chemically weathered and eroded until they finally reach the river. While the coarse size class includes boulders and dead trees, most riverine studies have focused on sand sizes (defined as 63 μm – 2 mm within CAMREX). Because these coarse suspended sediments (CSS) settle quickly to the streambed, suspended concentrations are strongly dependent on stream flow velocities (Meade *et al.* 1985; Devol *et al.* 1995) and increase substantially with depth in the river (Curtis *et al.* 1979; Richey *et al.* 1986). Thus CSS transport is highly episodic or seasonal, with most occurring during flood events. For instance, the mainstem of the Amazon near Manaus has depth averaged CSS concentrations of 10-20 mg L^{-1} during low water and 45-70 mg L^{-1} at high water (Devol *et al.* 1995). The bedload, or the CSS travelling very close to, or even as part of, the fluid riverbed, is estimated to be a small fraction of total coarse sediment flux in the Amazon mainstem (Dunne *et al.* 1998) but it may be important in smaller rivers. As for all the size classes, coarse particulates consist of both inorganic mineral material and organic material derived from the remains of living organisms.

Within the Amazon Basin, quartz is the dominant mineral in CSS with 25-75% of the total (Gibbs 1967); other primary silicates such as feldspars, micas, and chlorite comprise the remainder at 2-25% each. These primary minerals in rivers, surrounding soils, and aquifers each exhibit distinctive weathering rates and products. Thus through weathering processes, the lithology, relief and climate of a watershed together determine the composition of the finer, secondary minerals such as alumino-

silicate clays and iron and aluminum oxides and the composition of major dissolved inorganic ions, such as Ca^{2+}, Na^{+}, Mg^{2+}, HCO_3^{-}, Cl^{-} and Si species (Fig. 2.3) (Stallard & Edmond 1983; Stallard & Edmond 1987). The composition of CSS as a function of hydrograph remains unstudied, but hydrodynamic sorting of CSS components would be expected to produce spatial and temporal variations in CSS composition within a reach.

In the Amazon mainstem and other large turbid rivers, organic matter (OM) is a small but important portion of the CSS fraction, comprising only 0.6-3.3% by mass (Richey *et al.* 1990; Devol *et al.* 1995). However as CSS concentrations decrease in rivers, OM contributions increase to as high as 10-30% in the clearest waters (Hedges *et al.* 1994, and unpublished data). In all cases, microscopic studies reveal that most coarse particulate organic matter (CPOM) in rivers resembles partially degraded plant fragments, often retaining visible cell structure (Keil *et al.* 1997). CPOM is less dense than mineral grains of the same size, hence explaining its higher contribution to CSS in river channels under low flow. 10-20% of CPOM can be identified biochemically as amino acids, carbohydrates and lignins – the primary molecular building blocks of living organisms – relative to 25-60% within biomass sources (Fig. 2.5) (Hedges *et al.* 1986a; Hedges *et al.* 1994; Hedges *et al.* 2000). Biochemical source indicators, such as carbon to nitrogen ratio and the ratio of cinamyl to vanilyl lignin phenols, all show that Amazon Basin CPOM is primarily derived from tree leaves (Fig. 2.6a) (Devol & Hedges 2001). Several other lines of evidence, including stable carbon isotope compositions, confirm these conclusions but also show minor contributions from grasses for certain rivers (data not shown, Quay *et al.* 1992; Victoria *et al.* 1992). Biochemical indicators of degradation, such as the contribution of fucose and rhamnose sugars to total carbohydrates and acid to aldehyde ratios in

lignin phenols, all support evidence from microscopic studies and major biochemical composition that CPOM is sparingly degraded and rather fresh (Fig 2.6b). Radiocarbon analysis of CPOM and low density soil POM confirms their recent origin in most cases (Hedges *et al.* 1986b; Trumbore *et al.* 1995; this thesis, Chapter 5). It is clear that CPOM is actively degrading and leaching, supplying microbes with substrate and releasing dissolved organic and inorganic compounds into the river. These rates have not been directly measured, but are likely to be quite high. Stream and river budgets suggest that CPOM continuously enters the river mostly from bank vegetation and detritus falling directly into the water (McClain *et al.* 1997).

Coarse suspended river sediments are thus a heterogeneous mixture of sand sized mineral grains and discrete plant fragments (Fig. 2.3). Both inorganic and organic constituents of CSS are generally fresh and supply the dissolved pool as they degrade. CSS deposits on the river bed and in sand bars form a relatively porous sediment buffer or “hyporheic” zone (Boulton *et al.* 1998) that acts as a biological reactor, supplying the river with its products and forming new riverine environments that can be colonized by vegetation.

Fine particles

Fine suspended sediments (FSS) consist of clays and silts, material between 0.45 and 63 μm in size as defined by CAMREX. Maintained in suspension by the slightest turbulence, FSS is often referred to as the "wash load" by geomorphologists, because once introduced to a stream or river, FSS will generally not settle. Notable environments that often prevent FSS from washing directly out to sea are lakes, reservoirs, and floodplains. For instance, evidence suggests that within the Amazon – with its extensive annually flooded plains – a typical FSS particle passes through floodplain deposits several times between the Peruvian border and the Atlantic

(Martinelli *et al.* 1993; Dunne *et al.* 1998). Given the patterns of channel migration, each cycle of floodplain deposition and re-suspension requires a few thousand years (Mertes *et al.* 1996). Because FSS is mobilized by erosion events, concentrations are also a function of river discharge, although the tendency for FSS to not be redeposited results in weaker correlations than those observed for CSS (Devol *et al.* 1995). The mainstem of the Amazon near Manaus exhibits FSS concentrations of 70-120 mg L^{-1} during low water and annual maximums of 210-340 mg L^{-1} during the rising hydrograph (Devol *et al.* 1995).

Mineralogy within the FSS fraction can be quite diverse. Silt size grains (5-63 μm) often retain many of the characteristics of the CSS fraction while at the same time showing signs of being more weathered (Fig. 2.4a). Fine quartz is important in more weathered lowland basins whereas other primary silicate minerals dominate in rivers draining the Andes (Gibbs 1967). Clays and oxides are aggregated with the larger minerals in important quantities. The clay size fraction (0.45-5 μm) is composed mostly of phylo alumino-silicate clay minerals, which are the weathering products of primary silicates (Fig. 2.3, 2.4b). As can be seen in figures 2.4a and 2.4b, mineral diversity within FSS is very large and depends on the geology (source minerals) and climate (weathering rates) of the watershed. As a result, mineralogical compositions within the Amazon are constantly evolving downstream with inputs from tributary watersheds and from weathering during temporary storage in the floodplain (Johnsson & Meade 1990; Martinelli *et al.* 1993). All FSS samples do have common characteristics however. This size fraction is generally high in surface area and high in cation and anion exchange capacity. As such, significant quantities of certain inorganic ions (e.g. NH_4^+, PO_4^{3-} and most metals) and organic compounds (e.g. natural organic matter, contaminants, etc.) can potentially be adsorbed to the

mineral surfaces of FSS. Thus FSS actively interacts with the dissolved fraction, often acting as a buffer or reservoir for dissolved compounds (Fig. 2.3).

As with the CSS, organic matter contributes only a small fraction of FSS, generally 0.5-2.0% by weight in turbid rivers (Richey *et al.* 1990; Devol *et al.* 1995). Unlike CPOM however, fine particulate organic matter (FPOM) is tightly associated with the mineral phase (Fig. 2.3). In the Amazon and other rivers of the world, generally over 90% of the FPOM can not be physically separated from the mineral material (Keil *et al.* 1997; Mayer *et al.* 1998). With low-density material removed, the organic surface loadings of these sediments is consistently 0.5-1.1 mg C m^{-2} of mineral surface area, leading in part to the conclusion that sorption of natural DOM to minerals is the primary pathway in which FPOM is formed (Mayer 1994; Hedges & Keil 1995). Evidence suggests however that mineral-associated organic matter does not form uniform coatings over the surfaces, but rather as organic gel-like assemblages that cover <20% of the surfaces (Mayer 1999; Filius *et al.* 2000). However, sorbed organic matter affects mineral surface properties significantly by increasing cation exchange capacity and by offering hydrophobic phases into which organic contaminants (e.g. pesticides, petroleum products, etc.) and heavy metals readily sorb (Benedetti *et al.* 1996). Biochemically, a smaller fraction of FPOM is identifiable as carbohydrates or lignins when compared to CPOM (Fig. 2.5), but often a larger fraction is identifiable as amino acids. FPOM appears to come largely from leaf material as does CPOM (Fig. 2.6a), but often falls slightly outside of the biochemical range that is possible by mixing biomass alone, as might be expected of diagenetically altered material (Devol & Hedges 2001). Specific degradation parameters show this clearly (Fig. 2.6b), however riverine FPOM is still relatively fresh compared to riverine DOM or deep-sea sediments (Hedges *et al.* 1994). This

appears to be the result of physical protection from microbial attack that is offered by the intimate association of FPOM with mineral surfaces (Keil *et al.* 1994; Baldock & Skjemstad 2000; Kaiser & Guggenberger 2000).

FSS is thus a diverse but tightly associated mixture of minerals and organic matter that interacts strongly with other size fractions (Fig. 2.3). Fine minerals are formed from the weathering of coarse minerals, and FPOM largely results from sorptive interactions with dissolved organics. However, the major characteristics of FPOM most likely form within soils prior to erosion into rivers. Mineralogical and biochemical evidence all points to this conclusion (Devol & Hedges 2001), including carbon-14 dates hundreds to thousands of years old (Hedges *et al.* 1986b; this thesis, Chapter 5). However, whereas high relief source basins are the ultimate source for >90% of river-borne FSS (Meade 1994), stable carbon isotopes show that at Obidos >60% of the associated FPOM originates in the lowlands (Quay *et al.* 1992; Hedges *et al.* 2000). With such high levels of surface exchange and activity, deposited FSS forms highly fertile soils and sediments, often far from the river channel.

Dissolved matter

Just as for the particulate size classes, the dissolved fraction (<0.45 μm as defined by CAMREX) is composed of matter spanning a continuum of sizes, from truly dissolved individual molecules to colloidal minerals and organic gels. The distinguishing physical feature of material in the <0.45 μm size class is that it will stay in suspension indefinitely due to Brownian motion alone. Thus, the transport of material in the dissolved pool is determined by the advection and mixing of the waters that carry it. However, fluxes are not only determined by hydrology but also by processes that transfer material in and out of the dissolved phase, such as degradation, adsorption and coagulation. Perhaps the most important characteristic of

dissolved material is that it has the potential to be directly bioavailable. Microbial organisms, plant roots, and many animal tissues will transport dissolved molecules across cellular membranes, both passively and actively. Likewise, contaminants exhibit their highest toxicity when in the dissolved phase. The only way to measure the mass of the entire dissolved pool is by evaporation, however it is much more typical to measure the concentration of individual compounds or compound classes.

The inorganic material within the dissolved fraction includes all major ions, nutrients, dissolved gases, and colloidal minerals. The major inorganic ion composition of the Amazon mainstem is very similar to the world river average, dominated by HCO_3^-, Ca^{2+}, Na^+, $Si(OH)_4$ + $SiO(OH)_3^-$, Cl^-, Mg^{2+} and SO_4^{2-} in order of importance (Stallard & Edmond 1983). Diversity within the Amazon basin parallels the pattern of other rivers of the world, with a wide range of ionic compositions and concentrations controlled largely by geology and weathering regime with minor inputs from precipitation (Stallard & Edmond 1983; 1987). Once within the river, these ions mix conservatively, such that conductivity and alkalinity serve as excellent tracers for water sources (Stallard & Edmond 1983; Devol *et al.* 1995). Of the bioactive compounds, phosphate shows the least systematic variability, generally 0.4-2.0 μM in turbid rivers as a result of buffering with larger mineral-bound reservoirs in the FSS (Forsberg *et al.* 1988; Devol *et al.* 1995). On the other hand, inorganic nitrogen compounds – NO_3^- and NH_4^+ – cycle rapidly via remineralization of organic matter and other microbial process such as nitrification and denitrification (McClain *et al.* 1994; Brandes *et al.* 1996; Boulton *et al.* 1998). Dynamics of dissolved gasses, such as O_2 and CO_2, are also largely controlled by the respiration of organic matter because river, floodplain and lake waters are dominantly heterotrophic (Cole *et al.* 1994; Cole & Caraco 2001). These within-river fluxes

(more below) are in quasi- steady state balance with atmospheric gas exchange (Quay *et al.* 1992; Devol *et al.* 1995). Waters of the Amazon are characteristically supersaturated in CO_2 with respect to atmospheric equilibrium (by commonly a factor of 20-50) and act as a significant source of CO_2 to the atmosphere (Richey *et al.* 2002). Thus the dissolved inorganic constituents of river waters are constantly evolving as a result of interactions with non-dissolved phases within the river corridor.

Dissolved organic matter (DOM) exists as a mixture of simple molecules, complex biomacromolecules, their partial degradation products and molecular assemblages or gels. Total concentrations, measured as dissolved organic carbon (DOC), depend strongly upon the mineralogy of the basin, highlighting the importance of sorption to DOM dynamics. Watersheds with soils dominated by quartz sands having low surface area produce black water rivers with 7-40 mg L^{-1} of DOC, whereas watersheds rich in clays produce surface waters with low DOC (2-7 mg L^{-1}) (Sioli 1984a; Nelson *et al.* 1993; McClain *et al.* 1997). To better understand the composition and dynamics of DOM, ultrafiltration techniques have employed membranes with pores as small as 1 nm to separate and concentrate DOM into various size fractions (Hedges *et al.* 1994; Küchler *et al.* 1994; Amon & Benner 1996a; Amon & Benner 1996b; Mounier *et al.* 1999; Patel *et al.* 1999; Mounier *et al.* 2002). Generally, ultrafiltered DOM (UDOM) refers to organic material with molecular weights >1000 g mol^{-1} or daltons (HMW, or high molecular weight DOM in the CAMREX convention), including very high molecular weight subsets variously named VHMW DOM or colloidal organic carbon (COC) by different research groups (1000 dalton is approximately equivalent to a molecule of 1 nm diameter). Inorganic

colloids also appear in UDOM fractions, comprising from 5-10% of the total mass in the Amazon lowlands to as much as 80-90% in the high Andes (Hedges *et al.* 2000).

In Amazon lowland rivers, 70-90% of total DOM can be isolated as UDOM (Hedges *et al.* 1994), with yields decreasing upstream to 40-50% in the Andes (Hedges *et al.* 2000). Relative to the two particulate classes, UDOM contains the smallest fraction, 2.5-4.5%, identifiable as major biochemicals (Fig. 2.5), although UDOM also appears to be largely derived from tree leaves (Fig. 2.6a). DOM shows the most extensive signs of degradation of all three fractions (Fig. 2.6b) (Ertel *et al.* 1986; Hedges *et al.* 1986a; Hedges *et al.* 1994), yet radiocarbon analysis places the average age to be no more than a couple of decades (Hedges *et al.* 1986b; this thesis, Chapter 5). Care must be taken however when interpreting many biochemical trends between DOM and FPOM. It is known that biochemical fractionation of DOM occurs during sorption. Newly sorbed OM tends to be higher in molecular weight, more hydrophobic, more enriched in nitrogen and hydrolyzable amino acids, and have different amino acid compositions that the DOM from which it came (Gu *et al.* 1995; Kaiser & Zech 1997; Aufdenkampe *et al.* 2001). Other untested biochemical parameters may also result in part from sorptive fractionation.

Cumulative evidence suggests that DOM is produced largely from the degradation and/or leaching of leaf detritus similar to that in CPOM (Devol & Hedges 2001). Once in solution, biomacromolecules such as proteins and carbohydrates are easily hydrolyzed (a least partially) by exoenzymes for subsequent microbial uptake. As a result degradation tends to decrease both the size and bioavailability of HMW DOM to form the low molecular weight (LMW, ~200-1000 daltons) fraction (Amon & Benner 1996a). However, as all particulate and dissolved organic carbon fractions degrade, microbial activity and photochemistry can generate a pool of the smallest

molecules (<200 daltons) – free amino acids, free sugars, and organic acids such as acetate and citrate (Amon & Benner 1996b; Moran & Zepp 1997). Despite the likelihood that this very low molecular weight (VLMW) DOM represents an exceedingly small proportion of total DOM in rivers, these compounds are generally extremely bioavailable and could drive significant biological fluxes. The relative proportions of VHMW, HMW, LMW and VLMW DOM fractions would be expected to evolve down river as a result of their different degradation rates. Coagulation and disassociation of DOM in and out of colloidal gel phases or mineral surfaces complicates these size dynamics significantly however, as many of these processes respond to changes in pH and to ratios of polyvalent to monovalent ions in solution (such as Ca^{2+}/Na^{+}) (Chin *et al.* 1998; Kaiser 1998).

The dissolved fraction is particularly characterized by diversity and contrasts (Fig. 2.3). Organics and inorganics exist in both truly dissolved and colloidal phases. This mixture contains the most labile material carried by the river (e.g. NH_4^+, free amino acids, etc.) and also relatively non-labile weathering end-products (e.g. inorganic ions that determine alkalinity, LMW DOM, etc.). Some material is swept away with the water directly to sea, whereas transit times for other components are delayed considerably by interactions with mineral particles.

River metabolism

The CSS, FSS and dissolved fractions are compositionally distinct, yet interact with each other on a continual basis through the processes of degradation and sorption. The dynamics of one fraction can not be completely understood without considering the dynamics of the other two. Likewise, when considering whole-river processes, such as river metabolism, all three fractions must be considered together because nutrients and substrates (or pollutants) can reside in more than one fraction.

A notable omission in the above discussion of river-borne material is microorganisms. Bacterial biomass accounts for only 15-50 μg OC L^{-1} (0.75-2.5 $x10^9$ cells L^{-1}) or <5% of total organic carbon (Wissmar *et al.* 1981; Benner *et al.* 1995), thus contributing insignificantly to the mass of any fraction. However, the microbial community mediates nearly all biochemical transformations in the natural environment, including the weathering of rocks, and as such the activity of microorganisms is implicit in every discussion of biogeochemistry.

Just as rivers provide microorganisms with a wide array of substrates, nutrients and energy sources, rivers contain within their corridors a diverse set of physicochemical environments within which nearly all biochemical transformations can occur. Most rivers in the Amazon are dominated by heterotrophic respiration over photosynthesis (R/P ratio > 3) due to low light penetration in turbid rivers and in canopy-covered streams (Quay *et al.* 1995). Community respiration rates in the Amazon and major tributaries show a wide range, from 0.2-2 μmol C L^{-1} hr^{-1} (Richey *et al.* 1990; Benner *et al.* 1995; Devol *et al.* 1995), with no consistent seasonal or river-type patterns. These rates appear to be substrate limited rather than nutrient limited (Benner *et al.* 1995), further evidence that the bulk of dissolved and particulate OM in rivers is of limited bioavailability but that a small pool of labile compounds fuels the majority of respiration (Amon & Benner 1996a). Water flow in and out of suboxic and anoxic hyporheic zones in river beds is a likely source of labile fermentation products to the river. Methane gradients from banks to the main river channel can be quite large (Richey *et al.* 1988; Devol *et al.* 1994), but quantification of fluxes for other associated fermentation products has not yet been attempted. Lastly, in less turbid waters photochemical reactions can be important in both oxidizing DOM and in releasing VLMW organic compounds from more

recalcitrant material for bacterial consumption (Amon & Benner 1996b; Moran & Zepp 1997). As light penetration increases, so does photosynthesis. In floodplain lakes, grassland streams, clearwater rivers and to some extent blackwater rivers, respiration to photosynthesis ratios approach one (Quay *et al.* 1995). Depth integrated gross photosynthesis in these waters is comparable to the more productive regions of the oceans, with rates as high as 160 mmol C m^{-2} d^{-1} (Wissmar *et al.* 1981; Quay *et al.* 1995). All of these various biological process are cumulatively important. Concentrations of CO_2 over the Amazon surface exhibit a diurnal cycle with amplitudes of 70 to 150 ppm (Quay *et al.* 1989). Thus, to say that large rivers "breath" is not simply metaphorical.

VARIABILITY AND SCALE IN THE RIVER SYSTEM

Importance of natural variability and river scale for biogeochemical processing

The conceptualization of bioactive materials as interacting size classes with distinct properties has led to invaluable insight regarding dominant biogeochemical transformations in riverine environments (Devol & Hedges 2001). A fuller understanding of biogeochemical dynamics in a river system, however, requires an additional dimension: an examination of the range and patterns of natural variability in concentrations, compositions, and process rates, and of their principal environmental sources and controls (Meyer *et al.* 1988). In a fluvial system draining a continental-scale basin, natural variability is manifested across all spatial and temporal scales. Most obviously, concentrations and compositions usually vary within a channel cross-section, both laterally and with depth (Richey *et al.* 1986). This observation is especially relevant for suspended sediments (Curtis *et al.* 1979), and for highly labile molecules with well-defined sources in the form of discrete

inputs or diffusing from the sediment-water interface, such as CH_4 (Richey *et al.* 1988; Devol *et al.* 1994). Such variability highlights the need for careful, channel-integrated quantitative sampling in order to obtain representative cross-section averages, especially in larger rivers (Richey *et al.* 1986).

Regional differences in climate, soils, geomorphology, and vegetation also lead to dramatic contrasts, such as the river water typology already discussed. The progressive downstream growth of rivers that in Amazonia leads to massive channels and vast drainage areas results in not only the mixing of river waters draining dissimilar terrains, but also the creation of geomorphologically distinct riverine landforms and floodplains (Gregory *et al.* 1991), and longitudinal biogeochemical trends. Likewise, episodic events, the seasonal evolution of climate, and subsequent ecosystem and sediment responses, can result in substantial temporal changes in the biogeochemical functioning of rivers.

Some dominant forms of biogeochemical variability in Amazonian rivers will be described, focusing on the Amazon mainstem and mouths of major tributaries where more data are available and where CAMREX concentrated its efforts in the past. This large-river bias is a common feature of tropical South American research, in contrast with a focus on small catchments in temperate regions (Lewis *et al.* 1995). River size and system scale are important considerations that will be interwoven in this discussion. I will also emphasize factors such as the interactions of bioactive materials with geomorphology, sediment, and hydrological dynamics, and the sensitivity of different species to reach- vs. basin-scale controls.

Regional heterogeneity, downstream evolution, and large-scale structure

The biogeochemistry of running waters in the Amazon basin is exceedingly diverse. Several examples of this diversity have already been discussed. Spatial

heterogeneity can be manifested at multiple scales, from large regional differences between Andean and lowland streams, through downriver longitudinal geochemical trends and interactions with a changing floodplain environment, down to sub-regional variability and micro-scale changes. The value of broad classification schemes such as the visual water typology described earlier is diminished when considering subtle sub-regional changes in biogeochemical composition and controls. For example, turbid whitewater rivers closer to their Andean headwaters in Perú and Bolivia display substantial contrasts in the sorptive partitioning history and proportion of HMW DOM (Hedges *et al.* 2000); these differences may be attributable to differences in climate, terrain, and especially lithology and mineralogy (see Fig. 2.4, Ucayali, Marañón, and Madeira rivers). Moreover, smaller rivers at high elevations are often not turbid at all during the dry, low-water season (personal observation; Kvist & Nebel 2001). Similarly, streams within each of the lowland physiographic domains (Fig. 2.1) can display geochemical composition and dynamics unlike those of the assumed norm, as a result of localized features (Sioli 1984a; Kvist & Nebel 2001). Larger rivers tend to average out these small-scale fluctuations and result in the expected water color type.

The downstream growth of a river yields important biogeochemical consequences, including: a progressively diminishing role of local impacts and inputs compared to upstream influences; mixing of waters from dissimilar regions through the confluence of large tributaries; and creation of particular floodplain environments through the geomorphological action of the river and its water and sediment regimes (Vannote *et al.* 1980; Gregory *et al.* 1991; Leopold 1994). Longitudinal trends and "resetting" of the biogeochemistry of the channel often result from these factors. In the Rio Beni, Bolivia (Fig. 2.2), such a pattern is seen in the increasingly finer

suspended sediment sizes downstream as the river reaches the piedmont area (Guyot *et al.* 1999); it is also observed in the ^{13}C content of organic matter, which evolves from relatively enriched values in the highlands resulting from an elevation isotopic effect on C3 vegetation (Körner *et al.* 1988), to a progressive decrease towards the lowlands, followed by a sharp increase in ^{13}C of UDOM that may be a result of input from C4 grasses, and finally a sharp decrease after confluence with the larger Rio Madre de Dios (see Fig. 6a in Hedges *et al.* 2000).

On a larger scale, CAMREX has investigated changes in concentration, composition, fluxes, and process rates along a 1800-km reach of the Solimões-Amazonas mainstem (Fig. 2.2). While there are often clear differences between longitudinal trends during rising and falling stage (see below), some patterns are persistent (Fig. 2.7). Most biochemical tracers of OM composition, sources, and degradation show relatively insignificant changes downstream, despite the input of very large tributary fluxes and floodplain exchanges (Hedges *et al.* 1986a; Hedges *et al.* 1994); these tracers suggest that organic matter dynamics are operating in an apparent steady-state. ^{13}C of FPOC, on the other hand, generally becomes more depleted from Vargem Grande to Manacapurú, reflecting the gradual replacement of Andean FPOC with lowland-derived organic carbon from C3 plants (Quay *et al.* 1992). Suspended sediment concentrations generally decrease to Manacapurú, though sediment fluxes may follow different patterns and the channel exchanges vast amounts of sediments with the floodplain (Meade *et al.* 1985; Dunne *et al.* 1998). Associated particulate species usually track the trends in suspended sediment concentrations (Hedges *et al.* 1986a; Richey *et al.* 1990). Conservative dissolved species such as alkalinity, originating primarily in the Andes and alluvial foreland rivers, present largely a downstream dilution effect from the input of lowland

tributaries with low base cation content. For many bioactive dissolved species such as CO_2, on the other hand, the contribution of lowland tributaries and the floodplain is often the opposite, resulting in persistent increases downstream (Richey *et al.* 1990). DOC concentrations are relatively unchanging in the mainstem, except for substantial increases due to the confluence of the blackwater Rio Negro. In fact, the input of such a large and distinctive tributary often results in substantial changes in the biogeochemical signature of the mainstem.

Several studies have indicated that the Amazon floodplain is a source of respiration products as well as highly labile organic matter that fuels respiration in the channel, but this input does not appear to affect the composition of bulk river organic matter (Devol & Hedges 2001). The biogeochemical impact of the floodplain, however, is likely to be variable across the mainstem, given the diversity of geomorphological and ecological functioning of the floodplain in different reaches, driven by large-scale morphotectonic features (Mertes *et al.* 1996; Dunne *et al.* 1998). This diverse and changing role is also likely to be important in other floodplain regions throughout the basin (Puhakka *et al.* 1992; Guyot 1993; Kvist & Nebel 2001).

At a small scale, the extrapolation and regionalization of intensive stream and hillslope studies remains a difficult problem. Few studies of this type have been carried out in the basin (Nortcliff & Thornes 1988; Elsenbeer *et al.* 1996; Lesack & Melack 1996; McClain *et al.* 1997), and their research emphases have varied. A dual challenge exists: defining the appropriate boundaries for regionalization of results from stream studies, and scaling small-stream results to their resulting larger rivers – and conversely, down-scaling from large to small rivers. These issues remain largely unexplored in the Amazon basin, though studies in North American rivers are beginning to point the way forward (Smith *et al.* 1997; Peterson *et al.* 2001).

Temporal variability and episodic disturbance

Variability in biogeochemical processing with time can have important ecosystem impacts and must be considered in designing sampling or monitoring systems. It can occur at all temporal scales, from short rainfall events, to regular diurnal cycles and seasonal changes in rainfall; and from interannual climate variability driven by El Niño, to rare episodic disturbance such as earthquakes and mass wasting of hillslopes in the Andes. The consequences in a river are regulated by hydrological regimes and ecosystem and geomorphological responses. In large rivers, the relative timing and magnitude of events in different tributary basins also play a role.

Longitudinal trends along the Amazon mainstem often show marked contrasts between rising and falling stages, resulting from the combined effect of changing relative contributions of tributaries vs. Andean source waters, local hydraulic conditions, and the contribution of the floodplain in comparison with in-channel transformations (Richey *et al.* 1990; Devol & Hedges 2001). Trends in suspended sediment concentration and associated bioactive constituents vary with the hydrograph, showing relatively uniform distributions or lack of clear longitudinal patterns during falling water, but higher concentrations and downstream decreases during rising portions of the hydrograph (Fig. 2.7). These seasonal changes reflect variations in both sources and transport of particulate materials during different stages of the hydrograph, the role of local hydraulic and turbulent conditions as measured by river surface slope, and large-scale changes in sediment dynamics and geomorphological functioning of the floodplain (Meade *et al.* 1985; Devol *et al.* 1995; Dunne *et al.* 1998). However, such well-defined patterns often break down after the confluence of the Rios Negro and Madeira, the two largest tributaries.

Dissolved conservative species with sources in the Andes, such as alkalinity and Ca^{2+} (Fig. 2.7), show only a dilution effect downstream, where their seasonal variations are controlled largely by the relative contribution and timing of the hydrographs from the headwaters and the major tributaries (Richey *et al.* 1990). Dissolved bioactive species, on the other hand, are controlled largely by river stage, where stage is a proxy for channel-floodplain interactions (Richey *et al.* 1990; Devol *et al.* 1995). As discussed earlier, oxygen and CO_2 show a local steady-state between transport, respiration, and gas exchange across the river surface. Changing river stage results in variations in the longitudinal patterns of these dissolved gases, with increasing CO_2 super-saturation and decreasing O_2 concentrations downstream observed primarily during falling waters (Fig. 2.7). Lastly, DOC and PO_4^{3-} show little seasonal variability in their upstream-downstream distributions.

A more detailed picture of temporal variability in the mainstem is obtained from a ten-year time series of monthly measurements at the Marchantaria sampling station, in the Rio Solimões before its confluence with the Rio Negro (Fig. 2.2). Many species present regular, damped variability (Figs. 2.8a, 2.8b). This decadal time series facilitated a more rigorous empirical examination of factors controlling the seasonal changes in river constituents (Devol *et al.* 1995). Sediment and geochemical constituents were regressed against likely controls based on water provenance and hydraulic characteristics: % of water derived from Andean inputs, % derived from "local" water (floodplain and small tributaries feeding the mainstem), river slope, and discharge. Three groups of species with similar controls were found (Table 2.1). Particulate species are controlled by source strength and the hydrodynamics of sediment deposition and remobilization. Conservative dissolved species reflected their sources and dilution effects, and bioactive species vary with the

discharge hydrograph. These results are congruent with those gleaned from mainstem cruises.

Variability in streams and mid-sized rivers has been scarcely studied in the Amazon basin. In contrast to large rivers, changes in these systems can occur rapidly in response to storms, often resulting in large and rapid changes in concentrations (Elsenbeer *et al.* 1996; Lesack & Melack 1996). In the Bolivian Andes, Guyot (1993) has shown that most annually averaged organic carbon transport occurs in particulate form and is dominated by very high concentrations during a short period of time when FSS concentrations are extremely high. Concentrations of both particulate and dissolved species can vary quickly within a few days. Rosenqvist *et al.* (2002) have demonstrated that methane fluxes occur predominantly during flood recession.

Little is yet known about riverine biogeochemical responses to interannual forcings in the Amazon basin. Richey *et al.* (1989a) showed that the mainstem discharge data near Manaus presents substantial variability at frequencies of about 3 years, corresponding to El Niño and La Niña events. Marengo & Nobre (2001) have shown that the impact of ENSO (El Niño-Southern Oscillation) events on climate and river hydrographs vary across the basin. Tian *et al.* (1998) and Asner *et al.* (2000) have recently demonstrated via models and remote sensing that carbon cycling in terrestrial ecosystems in the basin also varies with ENSO events. This combined evidence of hydrological and terrestrial biogeochemical responses to interannual climate variability strongly suggests that processing of bioactive materials in the river system will also respond to such forcing. In large rivers, however, this response will be modulated by the relative regional impacts, the influx of tributaries, and the relative timing of their hydrographs. Likewise, large episodic disturbance, such as earthquakes and mass wastings in steep Andean slopes (Aalto *et al.*, 2003), are likely

to have substantial and long-lasting biogeochemical impacts on small and mesoscale rivers, as has been shown in small watersheds in Puerto Rico disturbed by hurricanes (Schaefer *et al.* 2000).

CONCLUSIONS

The Amazon River Basin – from the Andean Cordillera to the Atlantic Ocean – contains within its border a large variety of river and basin types. Nevertheless, these rivers exhibit remarkable consistencies in the processes that control the fate and transport of bioactive elements. River-borne material resides in three compositionally distinct size fractions that have contrasting transport properties and reaction histories. Coarse particulates are the freshest, degrading to form the fine particulate and dissolved fractions, which continually interact with each other via sorption processes. Organic matter in these fractions contains most of the bioactive material in the river, yet inorganic material is of critical importance due to its ability to complex and protect organic matter from degradation.

Variability in the composition and dynamics of river-borne material from one river (or season) to another is often much less than differences between size fractions within a single river (or season). However, it is often this variability that offers the most insight regarding important processes. Understanding how these processes scale with basin size is of critical importance. The watersheds of streams and small rivers most often represent a single geologic and climatic zone. Each small river thus exhibits the narrow range of characteristics typical of its limited basin, yet these rivers respond to episodic forcing (storms, landslides, fires, development) quite quickly and strongly. Large rivers can contain high sub-basin heterogeneity with respect to ecosystems, geology, climate, and timing of weather events. Material carried by

these large rivers integrates this heterogeneity, yet the relative influence of each sub-basin is continually changing with time and with distance downstream. Thus the response of large rivers to environmental change is damped relative to its constituent drainages.

The cumulative understanding of natural undisturbed river systems sets the foundation for subsequent work to elucidate human impacts on rivers and to eventually develop sustainable management plans. For example, knowing which size fraction the material of interest (nutrients, pollutants, eroded sediments, etc.) can potentially reside in is a critical first step in evaluating its transport dynamics and bioavailability. The next step might be to evaluate issues of scale. How does the human flux of this material compare to the natural riverine fluxes (transport, degradation, production, etc.) at that location? The answers to this question are likely to change across regions and with the time scale of interest. The evaluation of human impacts on river systems is rarely a simple and straightforward task – the natural world is too variable and complex for textbook solutions to every problem. However, systematic and well planned study of a natural system can yield the information necessary for sound management. Fortunately, a number of such studies are currently in place in the Amazon basin, including CAMREX, AARAM (Andean Amazon Rivers Analysis and Management), and HiBAm.

Table 2.1. Hydrologic variables controlling seasonal biogeochemical variability at the Machantaria sampling site, in the Solimões mainstem near Manaus. Biogeochemical parameters are grouped according to the dominant control variable resulting from multiple linear regression.

Andean Group

Controlled by the relative contribution of river water from Vargem Grande, serving as a proxy of the Andean drainage of the Amazon mainstem.

Fine suspended sediments (FSS), alkalinity (Alk), calcium (Ca^{2+}), and sulphate (SO_4^{2-})

Stage Height Group

Controlled by the local stage height at Marchantaria.

Dissolved oxygen (O_2), dissolved carbon dioxide gas (CO_2), nitrate (NO_3^-), pH, sodium (Na^+), chloride (Cl^-), and % carbon by weight in coarse suspended sediments.

Local Group

Controlled by the relative contribution of river water from small, local tributaries in the central lowlands and the floodplain.

Silicate ($Si(OH)_4$), potassium (K^+), and % carbon and nitrogen by weight in fine suspended sediments.

Surface Slope Group

Controlled by the river surface slope around Marchantaria, as a proxy of local turbulence.

Coarse suspended sediments (CSS), fine particulate organic carbon (FPOC), coarse particulate organic carbon and nitrogen (CPOC and CPON), and total particulate phosphorus (TPP).

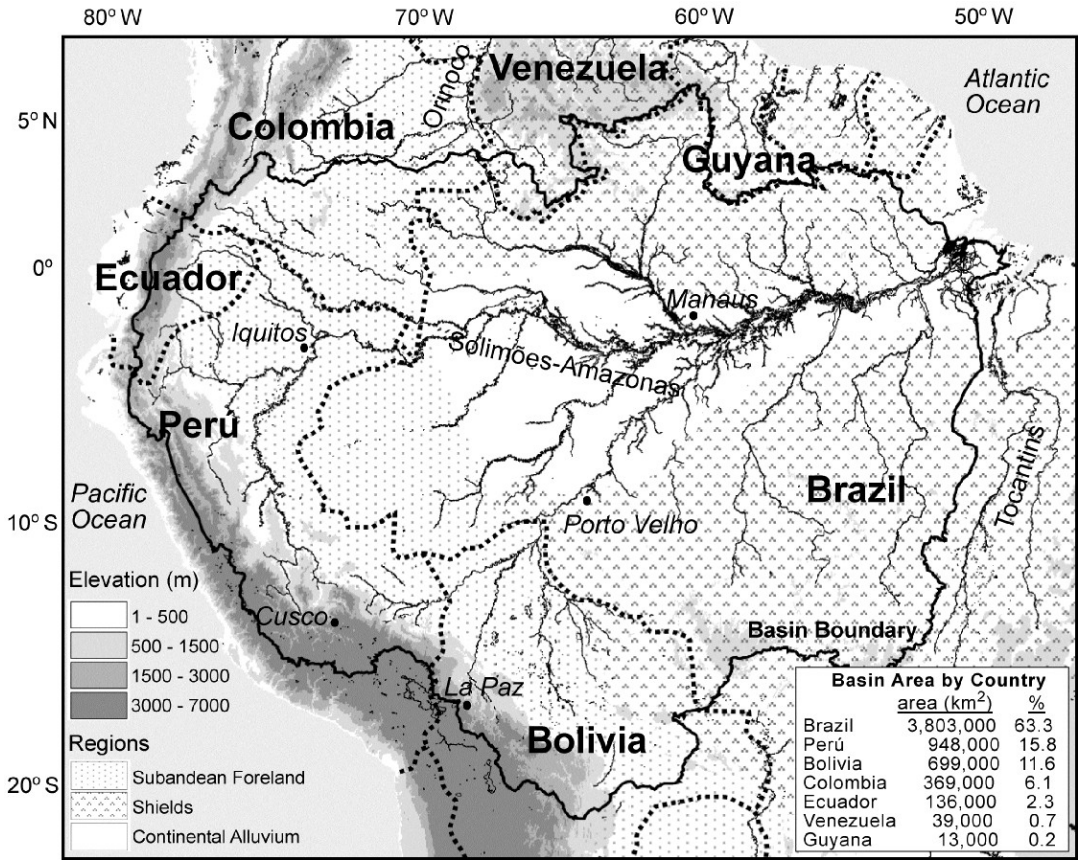

Figure 2.1. General physiographic features of the Amazon basin. The basin boundary is shown as a thick black line. National boundaries are shown as thick dotted lines. Major cities in the basin are included. The portion of the total basin area encompassed in each country is listed in the inset table; total basin area is 6,007,000 km^2 (see Chapter 3). Also shown are elevation and the main morphostructural regions.

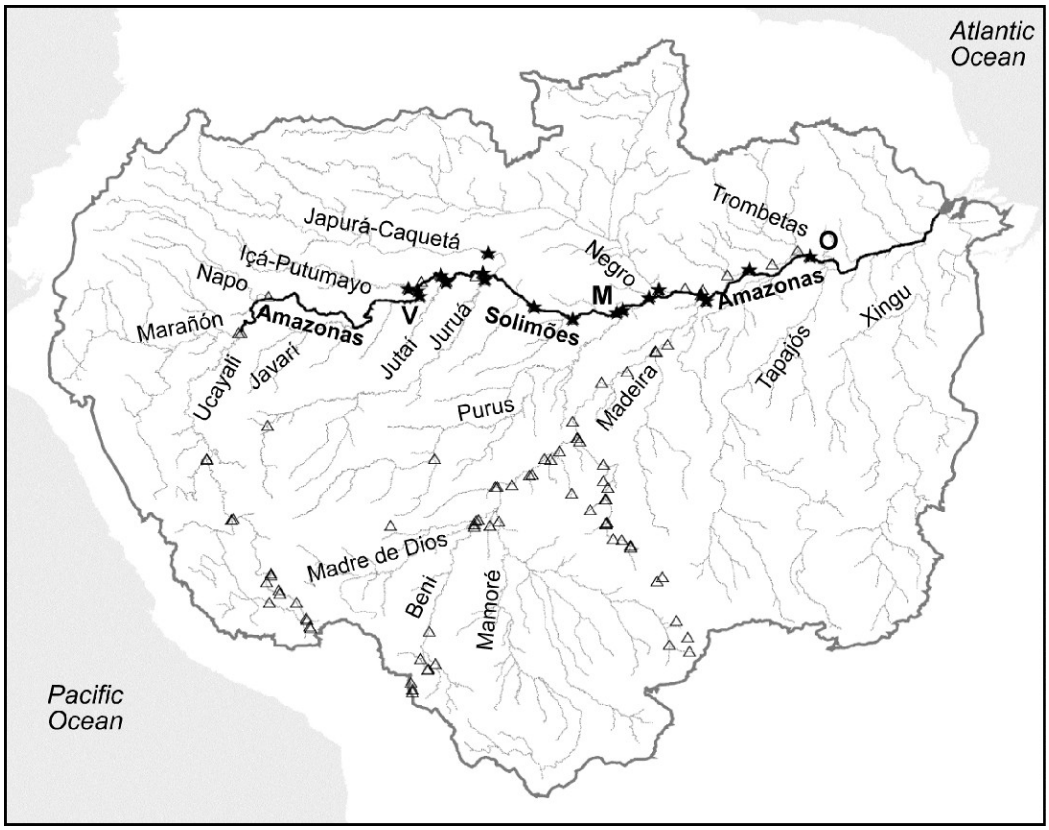

Figure 2.2. Amazon river network and CAMREX river sampling sites. The names of the mainstem and major tributaries are shown. The Amazon mainstem (thick black line) first begins under the name of "Amazonas" in the confluence of the Ucayali and Marañón in Perú. As it enters Brazil, its name changes to "Solimões", and becomes the "Amazonas" again after the confluence of the Rio Negro. The total length of the river is about 6,500 km, from its mouth to its source in the Ucayali headwaters south of Cusco (see Chapter 3). CAMREX mainstem sampling stations are shown as solid stars, from Vargem Grande (V) to Óbidos (O). 11 mainstem sites and the mouths of the 7 major tributaries were sampled through cross-sectional composites during 12 cruises between 1982 and 1991. All other CAMREX sampling sites are shown as open triangles. The site of the Marchantaria-Manacapurú time series is labelled "M".

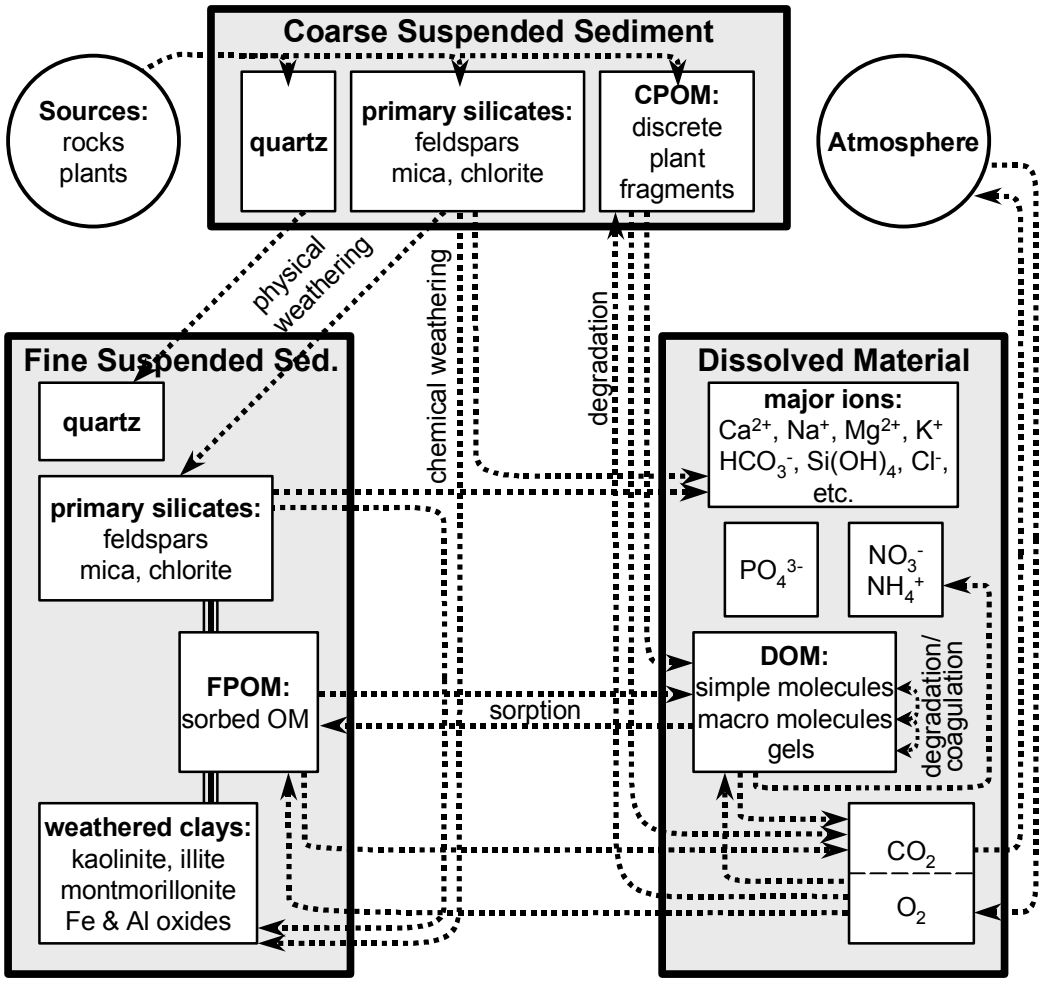

Figure 2.3. Conceptual model for the composition of the three principal size fractions carried by rivers, and the processes that are responsible for continuous interactions between them. Microbial mediation of these processes is implicit for many of these arrows. Bars connecting boxes within the fine particulate fraction represent the physical associations between mineral and organic components.

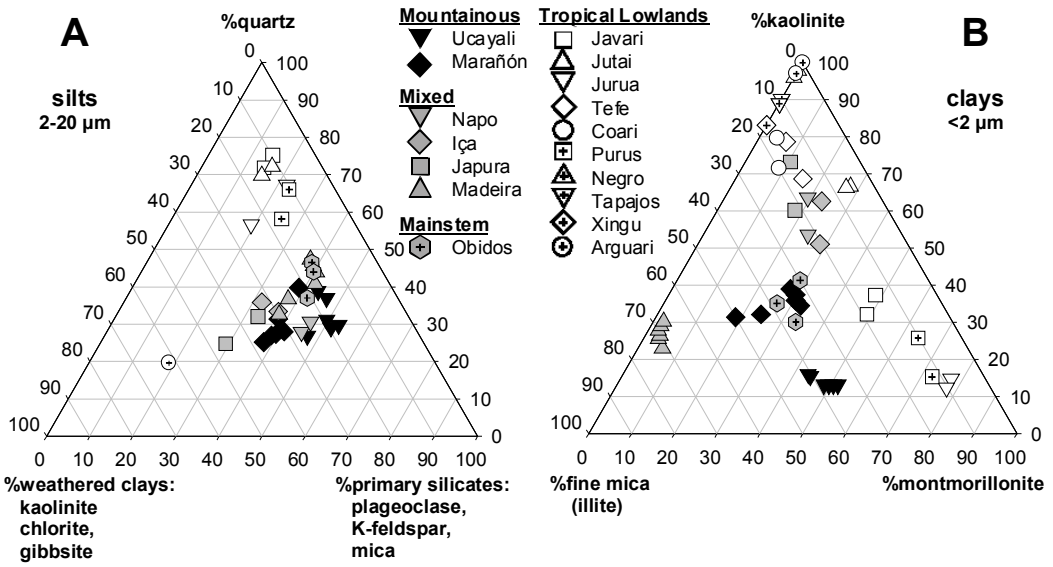

Figure 2.4. Major mineralogical composition of **A)** silt sized sediments (2-20 µm) and **B)** clay sized sediments (<2 µm) within the Amazon Basin. "Mixed" refers to river basins that drain both mountainous and lowland environments. Data from Gibbs (1967).

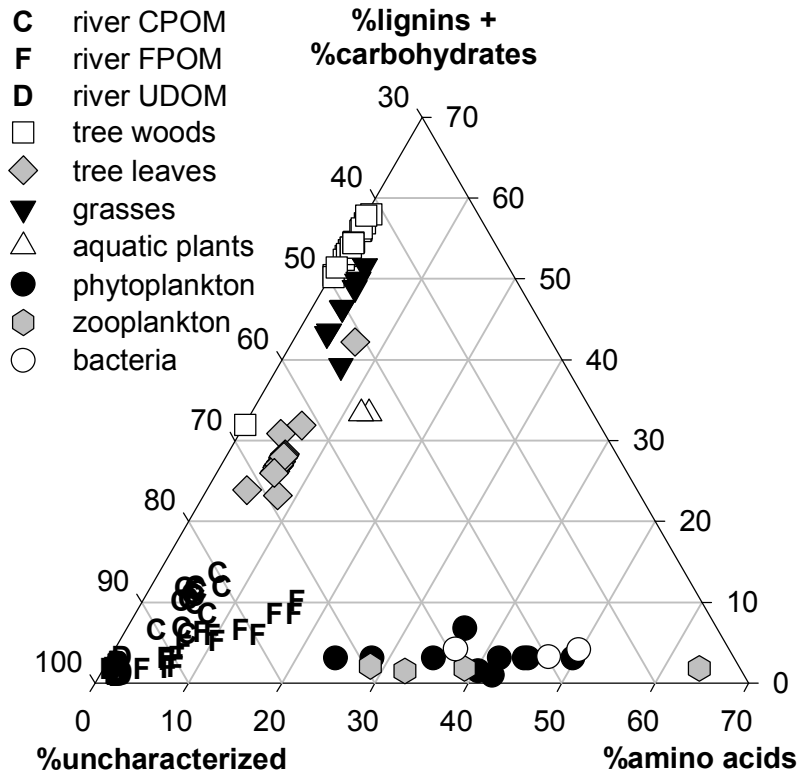

Figure 2.5. Major biochemical composition of coarse and fine particulate organic matter (OM) and ultrafiltered dissolved OM carried by rivers of the Amazon Basin, relative to the composition of source materials. River data from Ertel *et al.* (1986), Hedges *et al.* (1986a), Hedges *et al.* (1994), Hedges *et al.* (2000) and source data from these papers and from Cowie & Hedges (1984, 1992), Goni & Hedges (1992) and unpublished data. Notice that upper and right axes terminate at 70% of the respective biochemicals, due to all samples containing at least 30% of OM not identifiable in these biochemical classes. All DOM compositions fall in the grouping at >95% uncharacterized.

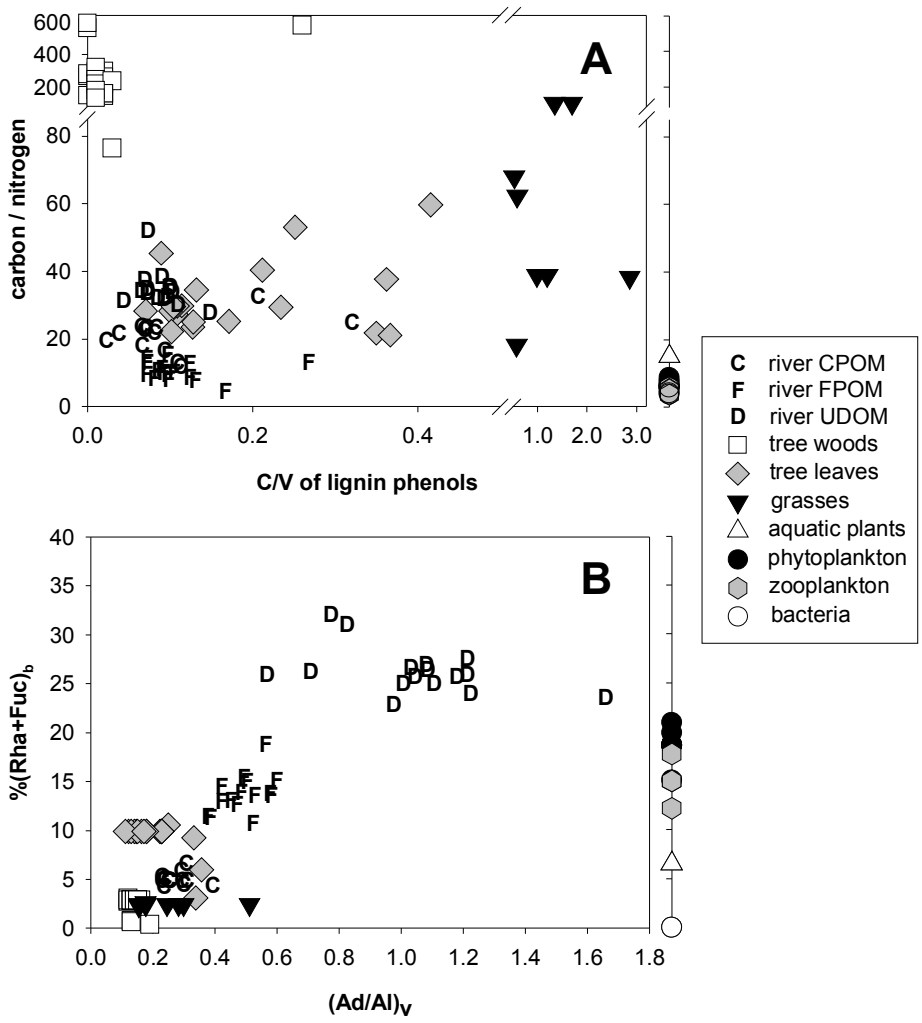

Figure 2.6. Biochemical parameters commonly used to interpret **A)** organic matter sources and **B)** organic matter degradation. Riverine coarse and fine particulate OM and ultrafiltered dissolved OM are again presented relative to common source materials. In A, the ratio of cinamyl to vanilyl lignin phenols (C/V) clearly distinguishes between woods, leaves, grasses and all aquatic organisms (which contain no lignin and are thus plotted to the right). In B, FPOM and UDOM are outside the range of plant sources with respect to both the acid to aldehyde ratio of lignin phenols, (Ad/Al)v, and the percent contribution of sugars rhamnose and fucose to total carbohydrates, $\%(Rha+Fuc)_b$ -- two parameters that increase with increasing degradation within sediments. Data obtained from the references listed for Fig. 2.5. Average $\%(Rha+Fuc)_b$ values were used for some woods and leaves for which no measurements were made.

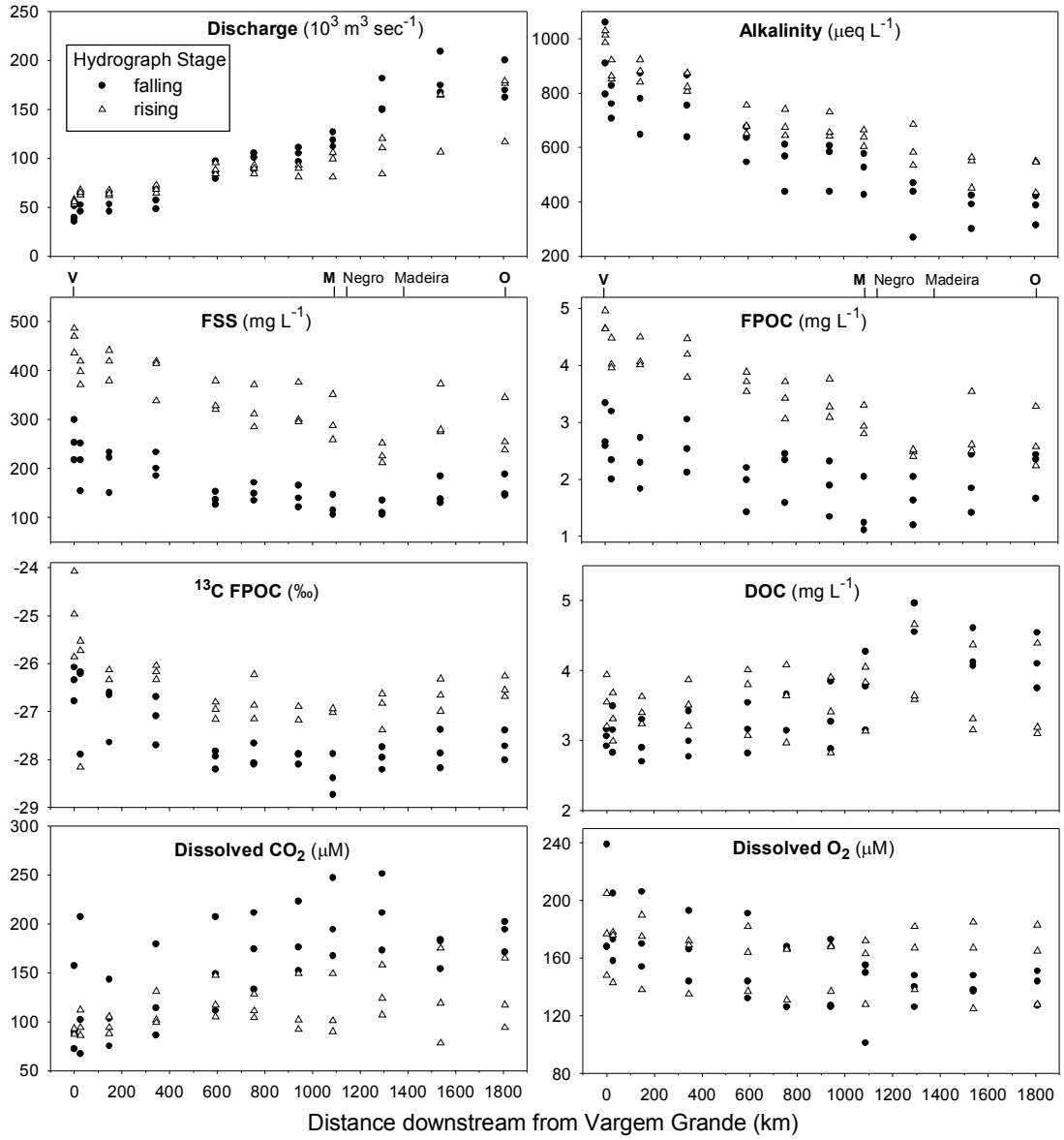

Figure 2.7. Longitudinal trends along an 1800 km reach in the Solimões-Amazonas mainstem from Vargem Grande to Óbidos in Brazil. The data have been divided into falling (closed circles) and rising (open triangles) stages according to major hydrograph periods, to highlight seasonal differences. Variables shown are river discharge, alkalinity, fine suspended sediment (FSS), fine particulate organic carbon (FPOC), carbon-13 content of FPOC, dissolved organic carbon (DOC), dissolved CO_2 gas, and dissolved oxygen. The sampling station labels at the top of the graph are the same as in Fig. 2.2. Data from Richey *et al.* (1990) and Quay *et al.* (1992).

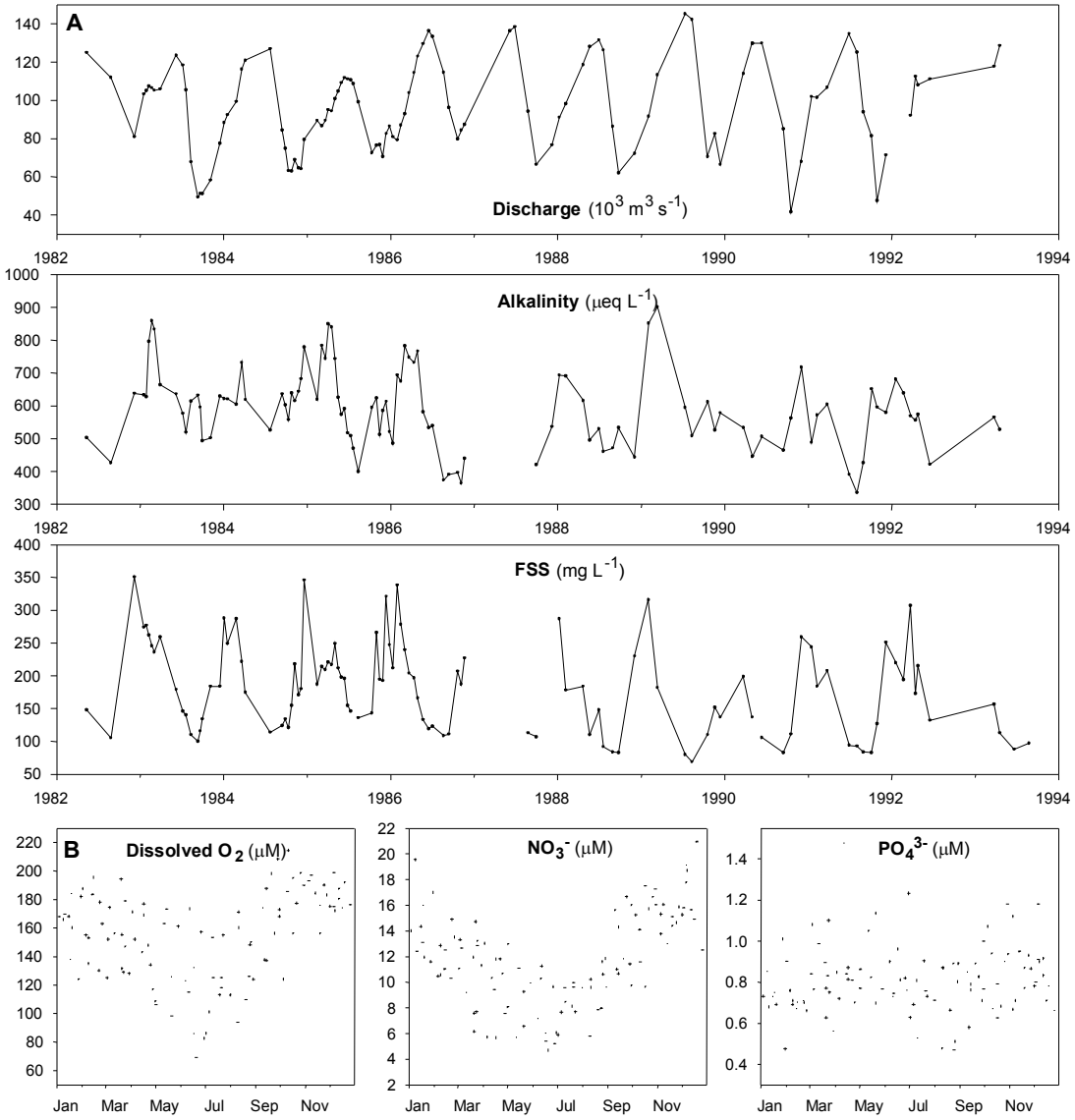

Figure 2.8. Hydrological and biogeochemical time series from Marchantaria, in the Solimões mainstem near Manaus (see Fig. 2.2). Data were collected at approximately monthly intervals from 1982 through 1993. **A)** Complete time series, shown for river discharge, alkalinity, and FSS. **B)** Annual composites for dissolved oxygen, nitrate (NO_3^-), and phosphate (PO_4^{3-}) are presented to illustrate the dominant seasonal variability patterns; these time series are created by plotting each value against the day in the year (1-366) when the sample was collected. Data from Devol *et al.* (1995).

CHAPTER 3: ESTIMATING CELL-TO-CELL LAND SURFACE DRAINAGE PATHS FROM DIGITAL CHANNEL NETWORKS, WITH AN APPLICATION TO THE AMAZON BASIN

INTRODUCTION

River channel networks are fundamental land surface features that integrate diverse and distant regions through the transport of water, sediments, and chemical constituents. The dynamics at a given channel reach can be understood only in the context of the characteristics of its drainage area and the upstream river network. A systematic linkage of the land to its drainage channels involves the delineation of flow paths from each element on the land surface to a channel reach and down the river network to the mouth. Such integration is required in many significant earth science and resource management applications, including the validation of land surface hydrology models using observed river discharge (Lohmann *et al.* 1998) and studies of the effects of basin characteristics and land use on river nutrient and carbon fluxes (Ludwig *et al.* 1996; Smith *et al.* 1997; Krysanova *et al.* 1998).

Surface flow paths are commonly derived from a gridded digital elevation model (DEM), where the elevation values are stored in regular grid cells. Several algorithms exist to determine the direction of water flow from cell to cell based on terrain analysis and DEMs (Moore *et al.* 1991; Martz & Garbrecht 1992). The most convenient and widely used method is the D8 algorithm (Maidment 1993; Hogg *et al.* 1997), in which the direction of flow out of each cell corresponds to the direction of steepest descent to one of the eight surrounding cells. A consequence of this method is that water and materials in a cell can flow to only one of its neighbors, a simplification that may result in drainage artifacts (Costa-Cabral & Burges 1994). Nevertheless, other important parameters can be derived easily and unambiguously

once unique flow direction paths are delineated; examples include flow accumulation grids (the number of cells draining to any given cell), distance along the network, river networks at a desired scale, and drainage basins (e.g., Vörösmarty *et al.* 2000a; Vörösmarty *et al.* 2000b). Utilities to calculate these parameters from flow direction grids have been incorporated in most Geographical Information Systems (GIS) software, such as ArcInfo (ESRI 1997) and GRASS (USA-CERL 1991).

The use of DEMs and unique cell-to-cell flow paths greatly facilitates the extraction of surface flow characteristics, river networks, and drainage basins, and the development of hydrological and biogeochemical applications. Nevertheless, DEMs of sufficient resolution and accuracy do not exist in large areas of the world, especially in developing countries and in low-relief forested regions such as the Amazon lowlands; low-relief areas are specially challenging even when high-resolution DEMs are available. In such cases, alternative methods are needed to derive cell-to-cell surface flow paths covering the entire land surface, at a resolution high enough to support a variety of applications. Döll & Lehner (2002) discuss additional limitations of deriving drainage directions from DEMs.

Vector maps of channel networks are widely available, detailed, and verifiable sources of relevant information. Compared to elevation, channels are more easily and accurately extracted from aerial and satellite remote sensing, and errors more easily identified and corrected. However, available digital networks are often used only for visual display or proximity analysis (river buffers); datasets supporting primarily such applications may include a number of topological network complexities, including disconnected reaches, two-bank channel representation, and flow bifurcation. For small watersheds, topologically corrected networks are often used in network analysis, and in hydraulic channel routing models based on lumped sub-

watersheds or hydrological representative units where watershed boundaries may be extracted manually (Fread 1992; Maidment 1993).

The use of digitized channel networks to assist in delineating basin-wide land and river surface flow paths has been limited. In the "stream burning" method, a river network from an external source is incised into a DEM by artificially lowering the elevation of cells that are part of this network, forcing flow paths to drain into and follow the imposed network (Graham *et al.* 1999; Liang & Mackay 2000; Renssen & Knoop 2000). This scheme reduces the impact of inaccuracies in DEMs, but it still requires an adequate DEM while ensuring realistic flow paths only at the larger scales for which a river network is available. Sekulin *et al.* (1992) used a channel network and a nearest-neighbor method only to extract gridded drainage areas without the use of a DEM. In this chapter I present a related but more exhaustive approach that uses topologically simplified channel networks to derive gridded cell-to-cell surface flow paths in rivers and across the entire land surface; it is intended for use in regions where existing DEMs are inadequate but detailed channel network maps are available. With a complete land and river flow direction grid created, surface flow path analysis functions can be applied in the same manner as with flow direction grids derived from DEMs. After describing the method, I illustrate and evaluate it with a large-scale application to the entire Amazon basin using a corrected version of the Digital Chart of the World (Danko 1992) river network; the derived datasets are freely available and may be used in hydrological and biogeochemical modeling and in studies linking river observations to their corresponding drained areas, particularly in connection with the Large-scale Biosphere-atmosphere experiment in Amazonia (LBA).

METHODS

Figure 3.1 shows a general description of the steps involved in the approach presented here to create a complete flow direction grid from river network maps. These steps are grouped into three stages, described below. All data processing and algorithm implementation was carried out using a combination of custom C programs and ArcInfo software.

Preparation and gridding of input vector datasets

The need to create a basin-wide land and river flow direction grid depicting unique cell-to-cell paths imposes certain requirements and limitations on the vector network: *a*, the entire network must be interconnected; *b*, channels that form loops or are split into parallel braided channels must be simplified to single channels following single, well defined directions; and *c*, channels represented as polygons or with individual river bank vectors must be simplified to single-curve center lines to avoid multiple parallel gridded flow paths. The Amazon delta region in Northeastern Brazil illustrates these network complexities (Figure 3.2). Correction or simplification of such features may be facilitated through automated methods in a GIS, but ultimately must rely on visual inspection and manual corrections. Errors in drainage network configuration must be checked and corrected against ancillary data such as atlases and air photography. Commonly available network datasets will typically require extensive pre-processing.

Two other datasets are required. First, unique cell-to-cell flow paths require a single outlet. Rivers in estuaries and deltas are often split into multiple channels and mouths (see Fig. 3.2), and this complexity is depicted faithfully in vector channel networks. A single mouth point must be chosen manually; all other draining channels may either be forced to reverse their direction of flow or may be cut off at arbitrary

points. Reliance on DEMs and D8 to extract flow directions and river networks sidesteps the issue because the use of elevation gradients and unique cell-to-cell paths enforces an arbitrary unique mouth point, even when additional processing is involved. Second, the basin boundary corresponding to the chosen mouth point is needed. This polygon may be created manually by visual inspection or may originate in other datasets or methods; however, it must be consistent with the channel network map. The accuracy of this basin boundary may be difficult to quantify and is dependent on the background information used to extract the boundary – DEMs, atlases, or the river network dataset itself.

At this point, the river network can be gridded using an extent that encompasses the basin boundary. The choice of cell resolution involves a balance between smaller cells to accurately represent channel sinuosity, avoid connecting adjacent channels, and avoid breaking off meander loops at their necks; and larger cells to minimize processing time and file sizes. The optimal cell size is selected through trial and error. Finally, the gridded river network and basin boundary must be evaluated carefully to ensure that artifacts such as improperly connected channels are not introduced during gridding.

Flow direction algorithm

The goal of the algorithms is to create a basin-wide, land and river flow direction grid. The input datasets are the gridded versions of the pre-processed river network, basin, and mouth coordinates. For convenience, the network and basin are first combined into a single grid using different integer cell values or flags. In the first step, in-channel cell-to-cell flow paths are assigned, leading to the mouth. These paths are determined as the shortest path from each channel cell to the mouth, traversing the river network; flow can move from a cell to any one of its eight

possible neighbors within the network. An undesired consequence of this approach is that meanders and general curvature are often smoothed or shortened, thus reducing total channel length (Fig. 3.3). At this stage the mouth cell itself is assigned an arbitrary direction of flow pointing away from the basin.

Next, each "land" cell in the basin — one not in the channel network — is allocated to the channel cell closest to it along a straight line (the shortest Euclidean distance). To accomplish this, cells surrounding the land cell are scanned along progressively larger one-cell-wide square "rings" in a clockwise direction starting at the upper left corner of the ring. The distance and angle between the center of the land cell and that of its allocated river cell is recorded. A land-river line crossing cells outside the basin implies flow paths leaving and reentering the basin. Such physically impossible flow paths are invalid. Scanning proceeds until the first valid river cell assignment is made and such path is confirmed to be the shortest possible cell-to-cell distance. The invalidation of flow paths crossing the pre-defined basin boundaries can have an undesirable effect once all land cells have been processed. A land cell near a basin boundary can become “trapped” by the boundary when no valid straight-line path to the center of a channel cell can be allocated. Such unallocated cells are identified and reprocessed as a special case. In this step, all land cells successfully allocated are treated as channel cells together with real channel cells, and the allocation mechanism is repeated with this much larger set of targets. Identification and reprocessing of unallocated cells continues until every land cell has been assigned a valid path. Finally, the angle of the land-stream connecting line is truncated to the nearest direction pointing from the center of the cell to the center of one of its eight neighboring cells. For example, a shortest-distance path with an angle of 60° NE will be rounded off to a cell-to-cell path at 45° NE. Truncation is a key

step that in effect changes the interpretation of the path direction from a long-distance nearest neighbor angle into a cell-to-cell flow direction.

At this point, a valid drainage direction map exists that can trace the path followed by a parcel of water from any point on the basin to the outlet. However, some artifacts result from gridding a vector network (Congalton 1997) and applying a shortest-distance network path algorithm. These include short parallel drainage paths adjacent to the channel, and small clusters of pixels that are no longer part of the channel proper. Drainage paths from land cells may be diverted through these artifacts before they reach valid channel cells. To minimize this problem, I make use of the flow direction map generated above to identify potential artifact cells. The premise is that these cells cluster around the main derived channel cells and drain a relatively small number of cells, according to the flow accumulation map derived from the preliminary flow direction map. The steps are illustrated in Figure 3.4. First, a support area threshold is chosen to extract a new river network from the drainage direction map (Hogg *et al.* 1997). This new network is made up of both cells in the original gridded network and others previously considered land cells (Fig. 3.4a); the latter are artificially generated channels which are assigned a flag value of 4 and disregarded (Fig. 3.4b). Conversely, the flow accumulation threshold splits the original network into "channel" (above the threshold) and "non-channel" (below-threshold) cells. From this set of all original-network cells, channel cells are flagged as 1, and non-channel cells are flagged as 2 (Fig. 3.4b). Next, flag-2 cells are further divided into valid original network cells and potential artifacts using a set of kernel calculations centered on each below-threshold cell from the original network. In the first step, flag-2 cells adjacent and perpendicular to a flag-1 cell are identified as potential artifacts and flagged as 3 (Fig. 3.4c). Second, a 3×3 kernel is used to flag

additional potential artifacts. If a flag-2 cell has no flag-2 neighbors in the kernel (it is isolated) and has at least one flag-3 neighbor (it has adjacent potential artifacts), it is flagged as 3 (Fig. 3.4d). The final step identifies below-threshold cells that connect flag-1 and flag-2 cells but were incorrectly flagged as potential artifacts. If the cell is flagged as 3 and is adjacent and perpendicular to a flag-2 cell, it is recoded back to 2 (Fig. 3.4e).

Network cell flagging is carried out for a large range of flow accumulation thresholds. I select the threshold value that maximizes the number of artifact channel cells identified (flag 3). Cells flagged as 1 or 2 using this optimal support area are then selected to form a new base river network. A number of small, valid stream channels will still be dropped, while some artifacts will remain. Finally, the flow direction algorithm described earlier is applied on this new network (Fig. 3.1). The resulting drainage direction map is the final, cleaned product.

Final dataset products

Additional products can be derived from the final flow direction map, base network, basin mask, and location of the basin outlet. I apply standard network traversal methods on the flow direction map to create flow accumulation and flow length gridded maps. In the flow length product, each cell holds the length of the complete drainage path from the cell to the basin outlet; the length of a horizontal or vertical path is equal to cell width, while the length of a diagonal path is equal to $\sqrt{2}$ times cell width. Together, these maps and the final gridded network make up the complete, final dataset.

RESULTS AND DISCUSSION

The CAMREX research group (Carbon in the AMazon River Experiment) has studied the biogeochemistry, hydrology, and geomorphology of Amazonian rivers over the last two decades (Richey *et al.* 1989b; Dunne *et al.* 1998; Devol & Hedges 2001; Richey *et al.* 2002). Sampled rivers range from 1st order streams to the mainstem Amazon a few hundred kilometers above the mouth; systematic analysis of this extensive dataset requires the co-registration of sampling sites with a detailed basin-wide river network and extraction of watershed boundaries at a range of scales. The CAMREX group is also engaged in spatially distributed hydrological and biogeochemical modeling for the entire basin. These activities dictate the need for a single drainage dataset consisting of a high-resolution basin-wide river network and an associated drainage direction map to facilitate water routing modeling and watershed boundary extraction. The highest-resolution dataset currently available that spans the entire Amazon basin is HYDRO1k, a 1-km product derived from the GTOPO30 DEM (USGS 1998; Verdin & Verdin 1999). However, GTOPO30 and HYDRO1k are impacted by very low relief and poor data quality in the lowlands, and some artifacts in the highlands. A preliminary evaluation suggested that it was effectively unusable in the central Amazon (see comparison below). The next best datasets (Graham *et al.* 1999; Vörösmarty *et al.* 2000a; Costa *et al.* 2002; Döll & Lehner 2002) are derivatives of ETOPO5 and TerrainBase, 5-minute resolution global DEMs (NGDC 1988; NGDC 1997). However, these datasets suffer from similar problems and the resolution was too coarse for my research requirements. Instead, I have used the Digital Chart of the World (DCW, Danko 1992) vector river network and the method presented in this paper to create a new, high-resolution flow direction map and derived datasets at 0.005° resolution (decimal degrees; approx. 500

meters) for the Amazon basin proper, excluding the Rio Tocantins basin. In this section I describe the procedures used to prepare these datasets and the creation of a flow direction map. Finally, I evaluate the resulting datasets against HYDRO1k and a database of drainage areas for hydrographic gages co-registered with the DCW-derived river network.

Data sources and pre-processing

This dataset was processed in geographic coordinates (degrees latitude & longitude). A resolution of 0.005° was chosen through trial and error as an acceptable balance between excessive file size and presence of river network gridding errors.

Basin boundary. I delineated the boundary of the Amazon basin (excluding the Tocantins basin) by manually tracing mountain ridges and watershed divides in ETOPO5, using the DCW networks and published paper maps as reference. This basin boundary was created before GTOPO30 became available. ETOPO5's coarse resolution and associated topographic distortion may have resulted in considerable uncertainty in the accuracy of the boundary.

River network. The original DCW global river network vector dataset is distributed as two subsets: lakes and large rivers represented as polygons by their two banks, and smaller rivers represented as centerline arcs only. Using the previously created Amazon basin boundary, I first selected the DCW polygons and arcs within the basin. The two subsets were then combined while eliminating topological errors. The polygonal dataset was processed first. Isolated polygons were assumed to represent small lakes and in-channel islands and were eliminated. Remaining polygons were then gridded at a resolution finer than 0.005°, reduced to single-cell

thickness channels using ArcInfo's "thin" function, and converted back to vectors. Next, the main task was to combine this new centerline representation of large channels with the DCW center line vector subset. The polygonal channels were originally connected to channels in the center line subset at their banks, but the connection was broken when polygonal channels were simplified to centerlines. I developed a semi-automatic procedure to extend the terminal end of connecting arcs in the original centerline-only subset to the new channel centerlines, to reestablish connectivity. The combined vector dataset was then extensively evaluated against the original DCW network and paper reference maps. The type of manual corrections carried out include: addition of missing network branches and reaches, correction of wrong confluence locations, and break up of network bifurcations. Finally, when gridding created an incorrect connection between two channels, the smaller channel was moved away to increase the separation.

Mouth location. The Amazon delta is a complex region without a single clear mouth. I chose as the mouth a terminal point of the northern mainstem sub-channel that starts out below the confluence of the Amazon mainstem and Rio Xingu and drains north of Ilha de Marajó (Marajó island) and Ilha Grande de Gurupá, at 51.4175° West, 0.4275° South (see Fig. 3.2). The stream network in the delta area was greatly simplified to force all flow into this single mouth point.

Flow direction algorithm and final products

Applying the procedures described in the Methods section to these Amazon basin datasets, I first obtained a set of network flag counts for a sequence of flow accumulation thresholds ranging from 5 to 10,000 0.005° cells (Fig. 3.5). Artifact cells identified reached a maximum at a threshold of 200 cells. This threshold was

used to create a new base network for the flow direction algorithm (Fig. 3.1). Finally, I created flow accumulation and flow length maps based on the resulting flow direction map, using standard algorithms. I used flow accumulation to derive a new river network that combines original network cells with synthetic flow paths not present in the original network. Cells that receive no drainage from other network cells were assumed to be Strahler first-order streams. This assumption is probably appropriate in most humid, lowland forested parts of the basin but is problematic in more arid regions. Nevertheless, it allowed me to assign a Strahler stream order to all river reaches in the basin and to group reaches of similar scale when necessary. Using this scheme, the mainstem below the confluence of Rios Solimões and Negro near Manaus to its mouth is a 10^{th} order reach. For comparison, this reach is 6^{th} order in the STN-30p global 0.5° drainage direction dataset (Vörösmarty *et al.* 2000a).

To assist in future basin analysis, I divided the Amazon basin into major tributary subbasins and the local drainages and floodplain area around the Amazonas-Solimões mainstem. This division involved two assumptions. First, I defined the beginning of the mainstem at the confluence of the Rios Marañón and Ucayali in northeastern Perú. Traditionally, the river is named Amazonas from this point to the Brazilian border, where it becomes known as Solimões; below its confluence with Rio Negro it is known again as Amazonas. My definition reflects the mainstem's globally significant size beginning in Perú. Second, I designated as a major tributary every subbasin whose outlet cell draining directly into the mainstem has a flow accumulation value of at least 40,000 cells (approx. 12,230 km^2). 32 major subbasins were extracted, in addition to the Amazonas- Solimões mainstem drainage area. Figure 3.6 shows the resulting subbasin boundaries, together with river reaches with a Strahler order of 6 and higher. Table 3.1 lists some hydrographic properties of the

major tributaries and the mainstem floodplain drainage area. The complete grid dataset, including flow direction, flow accumulation, flow length, drainage network, and subbasins, can be downloaded from the LBA data distribution site, http://lba.cptec.inpe.br/beija-flor/. The 0.005° grids have a dimension of 5,300 rows by 6,400 columns and extend from 80.5° W to 48.5° W and 20.5° S to 6.0° N.

Like other flow direction datasets and associated river networks, the CAMREX dataset has certain limitations, some of which have already been discussed. The method presented here results in lower sinuosity and overall reduction of channel length as a consequence of shortest-path channel flow allocation (Fig. 3.3). Further pre-processing of the vector network before gridding may eliminate the reliance on shortest Euclidean paths. The following sequence of steps may represent a promising approach: a, automated scanning and editing of all arcs in the network to ensure that they point downstream; b, assignment to each arc of cumulative distance from mouth; c, gridding the network while transferring cumulative distances values to the cells; and d, flow direction allocation based on cumulative distance cell values along the gridded channel network.

Additional limitations remain in the CAMREX dataset. Some channel distortions originally present in the DCW were not corrected. Channel bifurcations can not be represented correctly. The Amazon and some tributary mainstems are often wider than one 500-meter cell, but drainage paths are only one-cell wide. In addition, a number of small DCW streams were deleted during the initial pre-processing stage. Known, geographically specific problem areas are described in Figure 3.6.

Validation

The only drainage direction map available at a scale similar to mine is HYDRO1k (Verdin & Verdin 1999). This dataset has the advantage of being consistent with topography. However, the river networks represented in HYDRO1k in the Amazon lowlands contain severe drainage errors as a consequence of low relief and poor quality of the source elevation data in that region. Figure 3.7 shows a sample network error in the Juruá headwaters near Perú. In HYDRO1k, the entire Juruá headwater system drains incorrectly as parallel channels into the Javari basin to the North. Other portions are captured by the Purus on the East (not shown). Large errors in channel location and topology are also observed in the Rio Negro mainstem, the Amazonas mainstem near the Perú-Brazil border, and the Japurá-Caquetá headwaters. These problems would be difficult to correct without additional high-quality topographic data, unless a detailed channel network were incised into the DEM to enforce correct drainage paths. Therefore, HYDRO1k can not be used reliably for validating the DCW-derived Amazon dataset.

I co-registered with the CAMREX network dataset 224 hydrographic gages that include associated drainage areas in their original metadata; their published drainage areas range from 227 km^2 to approximately 4,620,000 km^2 at Óbidos, on the Amazonas mainstem. 210 sites are in Brazil (ANEEL 1987) and 14 in Bolivia (Guyot *et al.* 1988; Guyot *et al.* 1989; Carrasco N. & Bourges 1992; Guyot 1993). Discharge or stage data are also available. Geo-reference information associated with the gages was of variable quality. For Brazil, data was received electronically. Latitude and longitude coordinates were present in most cases, but their accuracy and origin are not known. Metadata also included river, roads, or town names in most cases. Uncertainty in data sources and reliability is especially problematic near river

confluences and for relatively small watersheds where local stream names were not accessible to me. For Bolivia, gage location, drainage area, and all additional information was gleaned from publications and digitized manually. Registration of all gage sites against the river network was carried out and verified manually, using descriptive information when the coordinates yielded ambiguous locations. Even when coordinates were available, site location had to be shifted towards the digital network in most cases. Finally, drainage areas were extracted for all co-registered sites using the flow direction and flow accumulation maps.

I used this hydrographic database and extracted basin areas to evaluate the CAMREX drainage direction map. Figure 3.8a presents a comparison of extracted vs. published area values. While overall there is good agreement, the relative error is larger in smaller basins. I examined the distribution of the percent error of CAMREX vs. published drainage area (A_{CAMREX} and A_{pub}, respectively), where percent error is calculated as 100 ($A_{CAMREX} - A_{pub}$) / A_{pub} (Fig. 3.8b). The histogram is divided into four basin area (A_{pub}) classes: ≤ 2000 km^2, 2000 km^2 to 10,000 km^2, 10,000 km^2 to 20,000 km^2, and $> 20{,}000$ km^2. Summary results for all basins and for each area class are presented in Table 3.2. Overall, the median and mean errors are ~ 4.5 and 16%, respectively. 55% (73%) of estimated areas are within 10% (20%) of published areas. This level of agreement is similar to that shown by STN-30p when compared to a global database of published drainage areas (Vörösmarty *et al.* 2000a). However, 23 basins have an error of > 50%, with a maximum as high as ~ 372%. Results by area class show that the error gradually increases as the size of the basin decreases, and for basins ≤ 2000 km^2 the majority of the areas are severely overestimated. When these 19 basins are removed, the median and mean errors are reduced to ~ 3.6

and 7.4%, respectively (Table 3.2), and 60% (79%) of estimated areas are within 10% (20%) of published areas.

2000 km^2 may represent an effective limit of reliability for the extraction of basin areas in this dataset. However, other considerations must be taken into account. First, the accuracy of published basin areas is unknown. Second, determining the exact location of hydrographic gages on the CAMREX network was more difficult for smaller basins due in part to the inaccessibility of local river names. Third, the stream density of any given area in the original DCW network in the Amazon basin appears to reflect the ease of interpretation from air photos and degree of effort spent digitizing that area, rather than an inherent stream density. Consequently, the limit of reliability for basin extraction is unlikely to be a uniform threshold but will vary across the basin to values smaller or larger than 2000 km^2. More tests are needed to estimate the reliability throughout the basin. Additional analysis is also required to determine the reason for the observed positive bias in small basins, to assess the contribution of the flow-direction method and inaccuracies in published basin areas, location of gages, and the DCW network.

I did not attempt to reduce the disagreement by adjusting the locations of sites with larger errors. Future work may involve adjustments of site location as well as improvements in channel representation. A potential source of more accurate river networks is radar imagery from the JERS-1 sensor spanning almost the entire basin (Siqueira *et al.* 2000); Muller *et al.* (1999) have demonstrated the potential of such data for channel extraction in the Rio Negro subbasin of the Amazon.

CONCLUSIONS

I developed a method for creating a gridded, land and stream drainage direction map based on a vector river network and independent of topography. This scheme is intended for use in situations where an adequate digital elevation model is not available. It may be applied at a wide range of scales, as its reliability is dependent primarily on the accuracy and resolution of the river network dataset. The most time-consuming step involves the pre-processing of the vector river dataset to create a connected and topologically simple gridded network. While an obvious weakness of this method is its potential inconsistency with topographic data, the ability to create flow direction maps from vector networks can expand the use of river transport modeling and automatic watershed extraction, and foster the co-registration of field measurements against a consistent dataset. An additional strength is the ability to easily improve the accuracy of all or parts of a basin through seamless insertion of improved river networks when these become available.

I applied the method to the Digital Chart of the World river network in the Amazon basin at a nominal 0.005° resolution. This dataset required extensive pre-processing to create a consistent, usable network. The derived CAMREX basin-wide flow direction map was used to identify 32 major subbasins draining into the mainstem. I geo-registered 224 hydrographic gages against the processed network, and used the published drainage area for each site to evaluate the CAMREX drainage direction map. Drainage areas for these sites ranged from 227 km^2 to approximately 4,620,000 km^2. The overall level of agreement is comparable to that shown by global-scale datasets when compared to global databases for hydrographic sites (Vörösmarty *et al.* 2000a). However, the relative error increases in smaller basins and becomes very large in basins smaller than 2000 km^2. While this basin area may

be seen as an effective limit of reliability for the CAMREX dataset, I suggest that such a threshold in fact will vary across the basin depending on the accuracy of the original DCW network and of my co-registration of hydrographic sites against the network.

The CAMREX drainage direction map represents an improvement over currently available alternatives (Graham *et al.* 1999; Verdin & Verdin 1999; Vörösmarty *et al.* 2000a; Costa *et al.* 2002; Döll & Lehner 2002) for regional research in the Amazon basin. The complete gridded dataset can be downloaded from the LBA data distribution web site. I have also co-registered 280 CAMREX and other biogeochemical sampling sites from mountain and lowland rivers in Brazil, Bolivia, and Perú; these sites are linked to a relational database holding corresponding biogeochemical measurements. Future updates may involve improvements to the network with more accurate and finer-scale networks; corrections to the Amazon basin boundary; and adjustments to the site location to reduce the relative error. Nevertheless, I anticipate that the availability of high-quality 90-meter and 30-meter DEMs from the Shuttle Radar Topography Mission (SRTM) in the coming years (Farr & Kobrick 2000) and subsequent extraction of a drainage direction map will bring dramatic improvements over this and other existing datasets.

Table 3.1. Major Amazon subbasins and drainage area of the mainstem. Subbasin number of the mainstem drainage is 1; values increase upstream from the mouth. Basin names are taken from the local name of the main tributary trunk. When the trunk has different names across national boundaries, both names are included. Names in bold are subbasins that are not originally made up of a single tributary system but were simplified to remove network bifurcations. Outlet distance is the distance from the subbasin outlet to the mouth of the Amazon. Length is the longest drainage distance from a subbasin source point to the outlet.

Number	Name	Area	Length	Subbasin Outlet		
				Longitude	Latitude	Distance
		km^2	km	°W	°S	km
1	Amazonas-Solimões	6,020,438	3,557	51.42	0.43	0
2	**Macapá**	16,147	318	51.45	0.5	9
3	**Marajó-Pará**	84,027	784	51.44	0.5	10
4	Jari	51,893	769	51.87	1.17	108
5	Xingu	515,651	2,275	51.96	1.43	141
6	Paru de Este	43,640	731	52.63	1.56	221
7	Maicuru	21,917	547	53.98	2.03	398
8	Curuá-Una	24,505	315	54.08	2.34	435
9	Tapajós	498,063	2,291	54.65	2.37	516
10	Curuá	28,099	484	54.8	2.08	560
11	Trombetas-Nhamundá	157,568	744	55.83	1.93	691
12	**Mamuru**	17,533	237	56.66	2.6	819
13	**Ilha Tupinambarana**	68,222	948	56.71	2.6	825
14	Uatumã	59,282	701	57.55	2.41	935
15	Urubu	13,892	405	58.06	2.84	1,019
16	Madeira	1,381,696	3,518	58.75	3.36	1,135
17	**Madeirinha**	13,634	288	58.84	3.36	1,146
18	Negro	719,216	2,362	59.87	3.14	1,274
19	**Manacapuru**	13,100	291	60.64	3.32	1,376
20	Purus	362,981	2,561	61.47	3.67	1,493
21	**Badajós**	21,575	413	62.33	3.76	1,614
22	Coari	52,715	599	63.09	4.07	1,714
23	Tefé	25,877	571	64.6	3.32	1,923
24	Japurá-Caquetá	267,735	1,953	65.49	2.57	2,066
25	Juruá	218,183	2,096	65.7	2.6	2,093
26	Jutaí	55,826	912	66.95	2.73	2,278
27	Içá-Putumayo	125,740	1,770	67.93	3.13	2,440
28	Jandiatuba	26,927	493	68.69	3.47	2,575
29	Javari-Yavarí	98,366	893	69.94	4.33	2,839
30	Napo	110,378	1,081	72.69	3.37	3,268
31	Nanay	17,564	348	73.16	3.7	3,340
32	Marañón	358,496	1,561	73.52	4.48	3,492
33	Ucayali	341,235	2,269	73.52	4.48	3,492

Table 3.2. Summary statistics of the relative error (%) between extracted and published drainage areas, by published area class. The last column includes only sites with drainage area greater than 2000 km^2.

	Drainage Area Classes (km^2)					
	<= 2000	2000 to 10,000	10,000 to 20,000	> 20,000	All Sites	> 2000
Count	19	51	40	114	224	205
Minimum	-6.9	-61	-59	-30	-61	-61
Maximum	372	272	82	49	372	272
Median	94	7.8	5.5	2.2	4.5	3.6
Mean	108	16	6.8	3.8	16	7.4

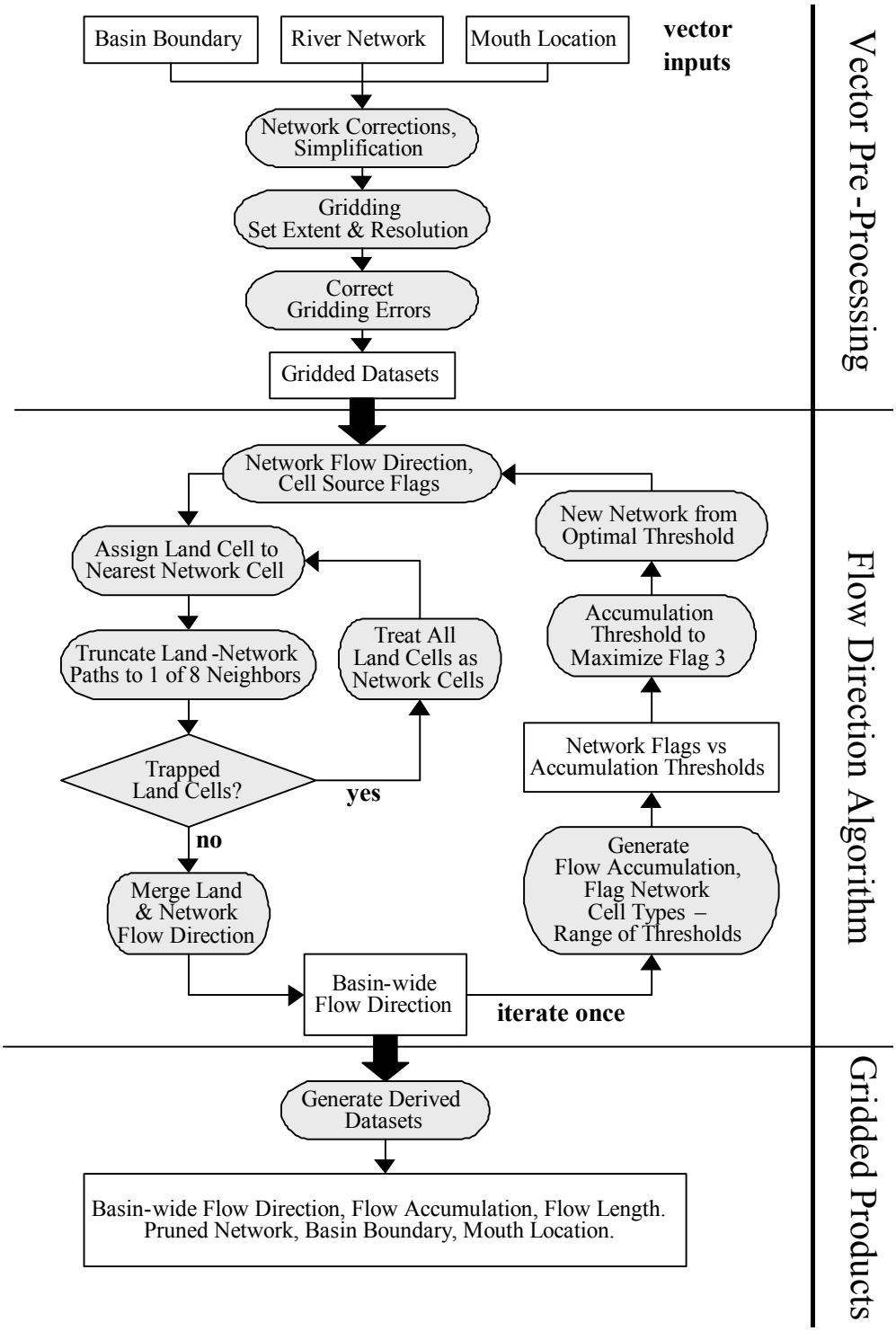

Figure 3.1. Overview of steps to generate basin-wide drainage paths from vector river network and associated datasets.

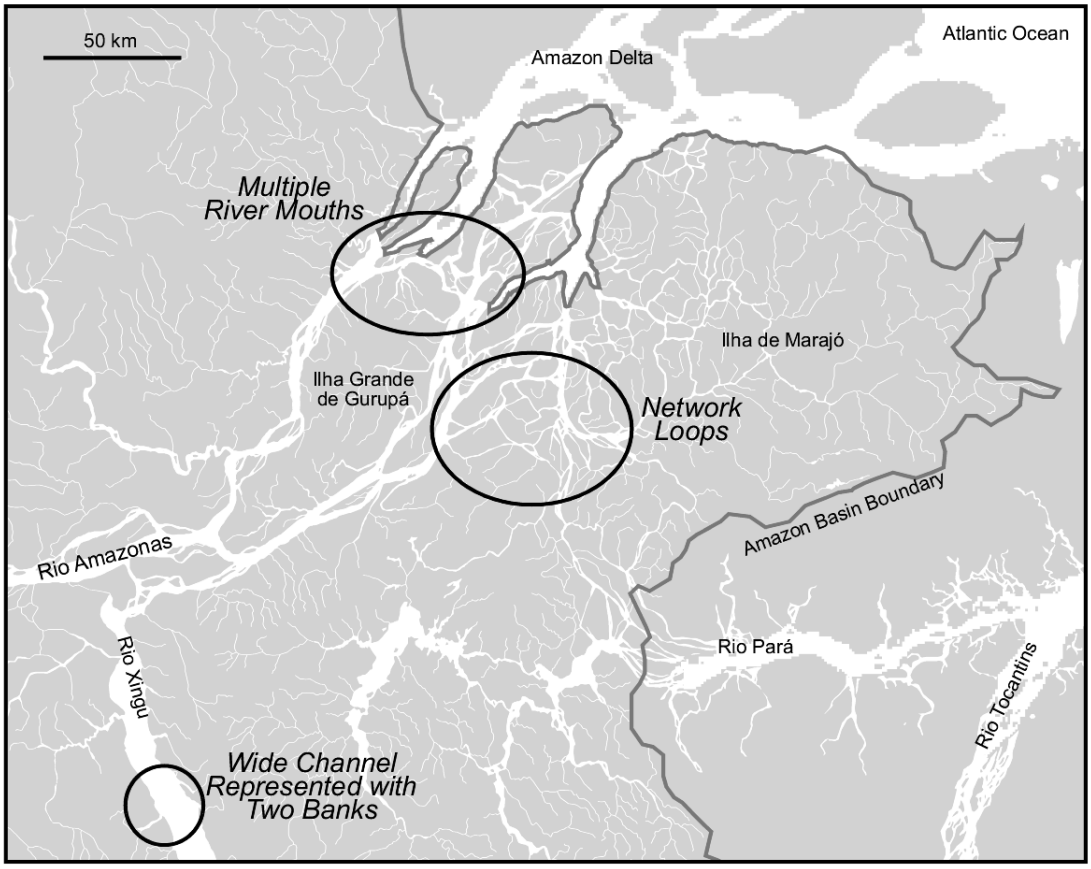

Figure 3.2. Amazon River mouth region illustrating challenges encountered when using a vector river network dataset to derive drainage direction maps constrained to unambiguous, unique cell-to-cell paths. The ovals highlight three common types of problems.

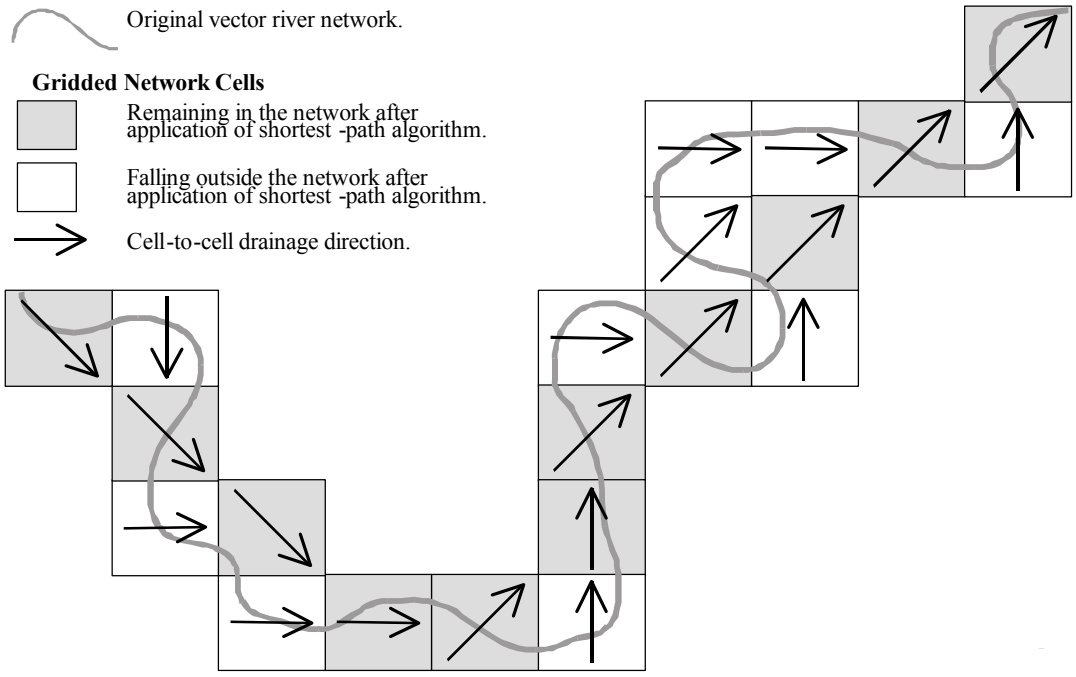

Figure 3.3. Gridding of a vector river network reach and application of a shortest cell-to-cell path distance scheme to extract in-channel drainage paths on the gridded network. This example illustrates meander smoothing and overall shortening of network path lengths when applying the shortest-distance scheme.

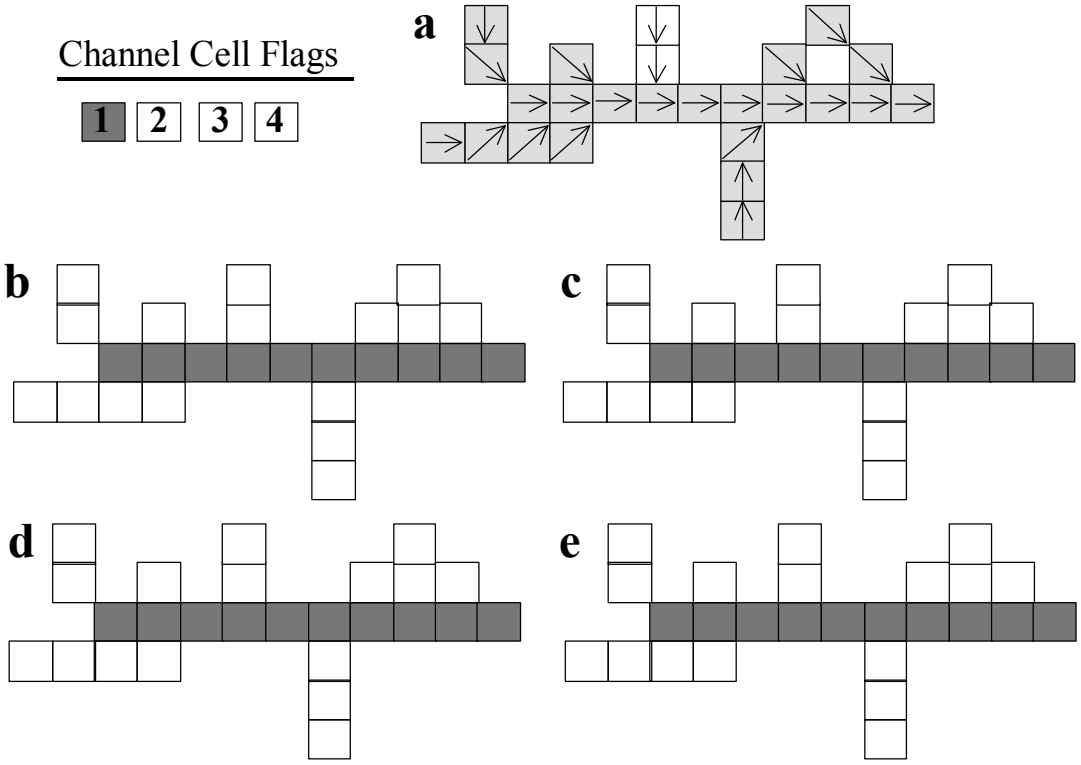

Figure 3.4. Use of flow-accumulation thresholds to identify and minimize artifact channel cells resulting from gridding and channel flow-direction steps. **A)** Schematic river network reach showing cell flow-direction paths; dark cells are original gridded channels and white cells are former "land" cells with a flow accumulation exceeding the current threshold. **B)** Segmentation of the set of cells from (B) into three subsets or flags: original network cells meeting the support area threshold (1), original network cells not meeting the threshold (2), and former land cells that meet the threshold (4). **C)** First pass to identify potential artifacts (flag 3) from flag-2 cells. **D)** Second pass to identify further potential artifacts. **E)** Locate flag-3 cells likely to be valid and recode to 2, to retain in the network.

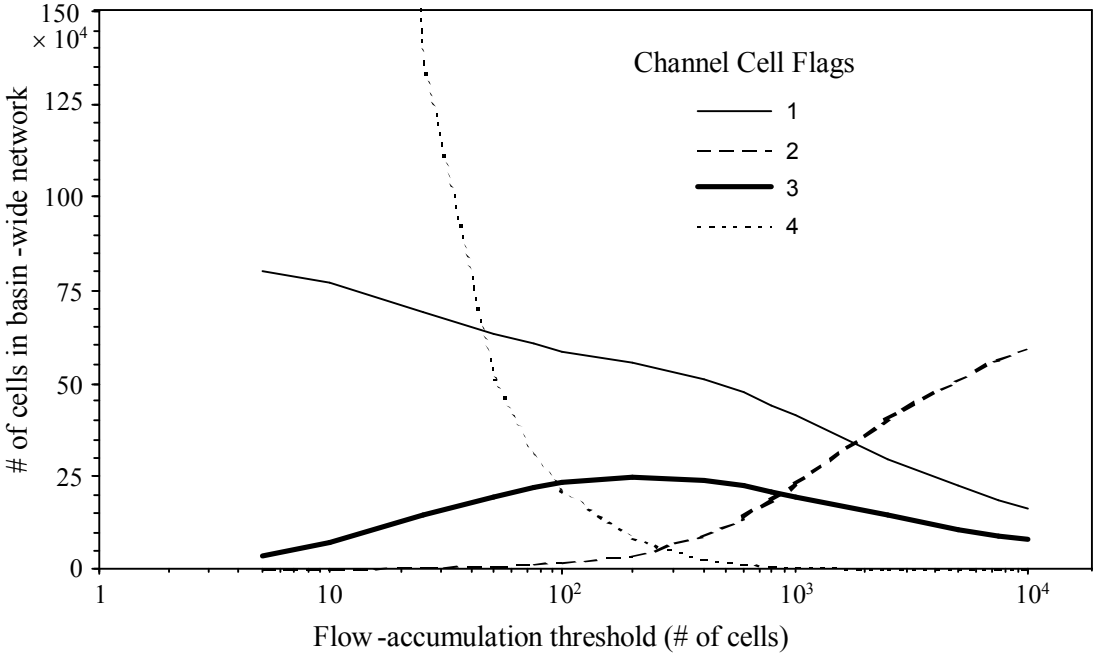

Figure 3.5. Network cell flags vs. flow-accumulation threshold (log-scale) for the Amazon basin. There were 838,008 0.005° cells in the original gridded network. See Fig. 3.4 for an explanation of each cell flag value.

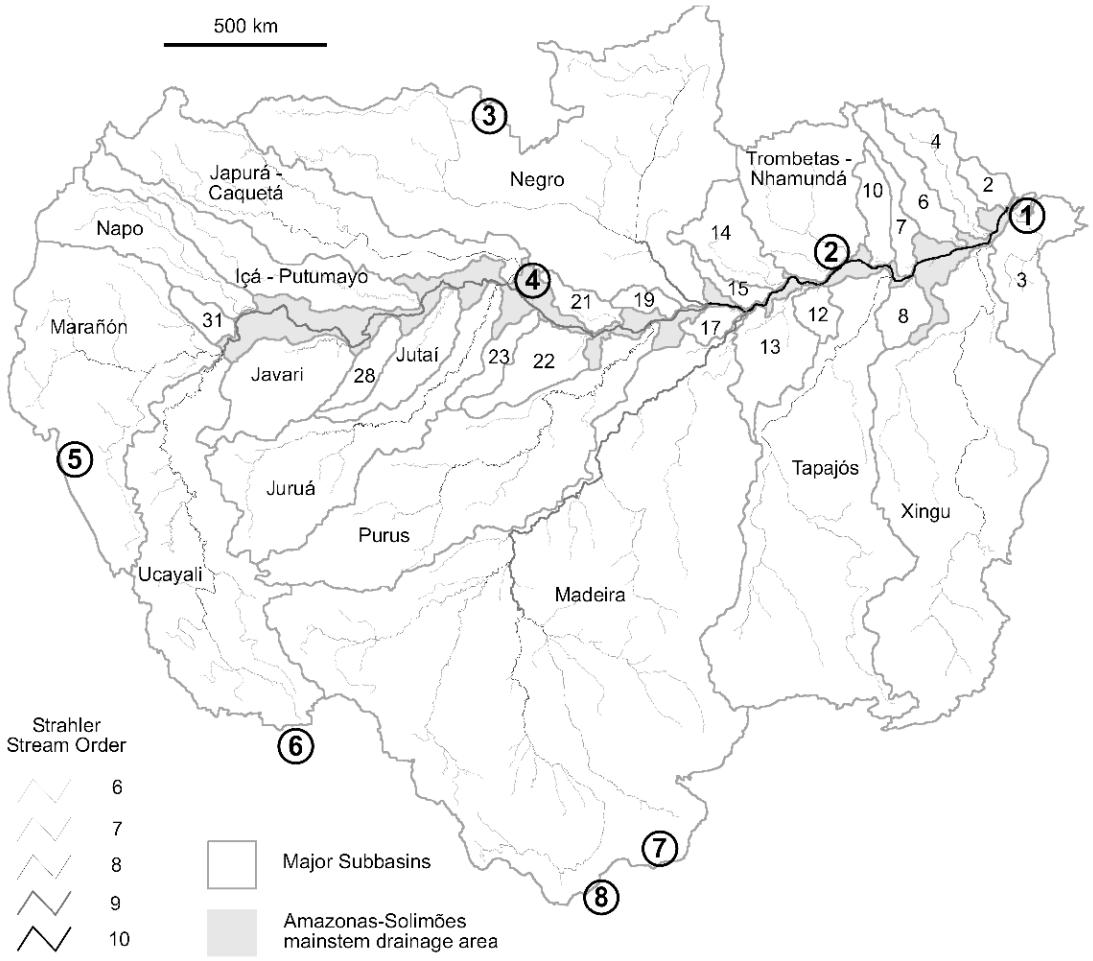

Figure 3.6. Amazon major subbasins and river network extracted from the drainage direction map. River reaches with a Strahler order of 6 and higher are shown. Each of the larger subbasins is labeled with the name of its mainstem(s); smaller basins are labeled with their subbasin numbers (see Table 3.1). Circled numbers indicate prominent hydrographic ambiguities and data problems: (1) Mouth of the Amazon, with multiple channels draining into the Ocean, bifurcations, small coastal catchments, and connection to the Tocantins river. (2) Combined Trombetas and Nhamundá confluence into the mainstem. (3) Linkage to the Orinoco Basin via the Negro-Casiquiare connecting channel. (4) Bifurcation of the Japurá-Caquetá confluence into the mainstem. (5) Marañón headwaters mainstem dropped from the DCW network and reconstructed manually. (6) Apurimac source headwaters dropped from the basin. (7) Ambiguous hydrological connectivity in the Bañados del Izozog wetlands. (8) Itenez headwaters in the Itonamas-Parapeti river dropped from the basin.

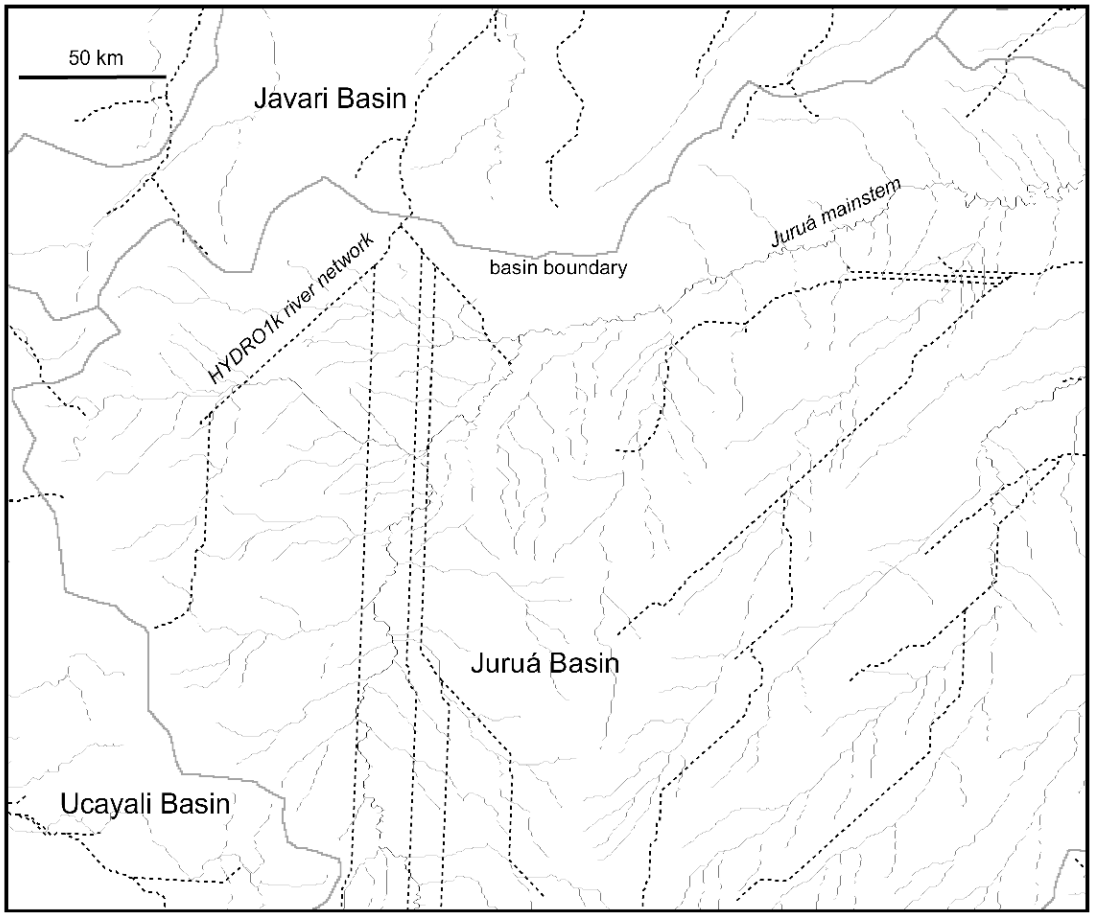

Figure 3.7. Comparison of CAMREX river network (solid lines) and HYDRO1k network (dotted lines) in the Juruá headwaters, in the lowlands of the central Amazon basin. The basin boundaries shown are the subbasin boundaries shown in Fig. 3.6 and created from the CAMREX drainage direction map. In this region, HYDRO1k drains the entire Juruá headwater system as parallel straight channels into the Javari basin to the North.

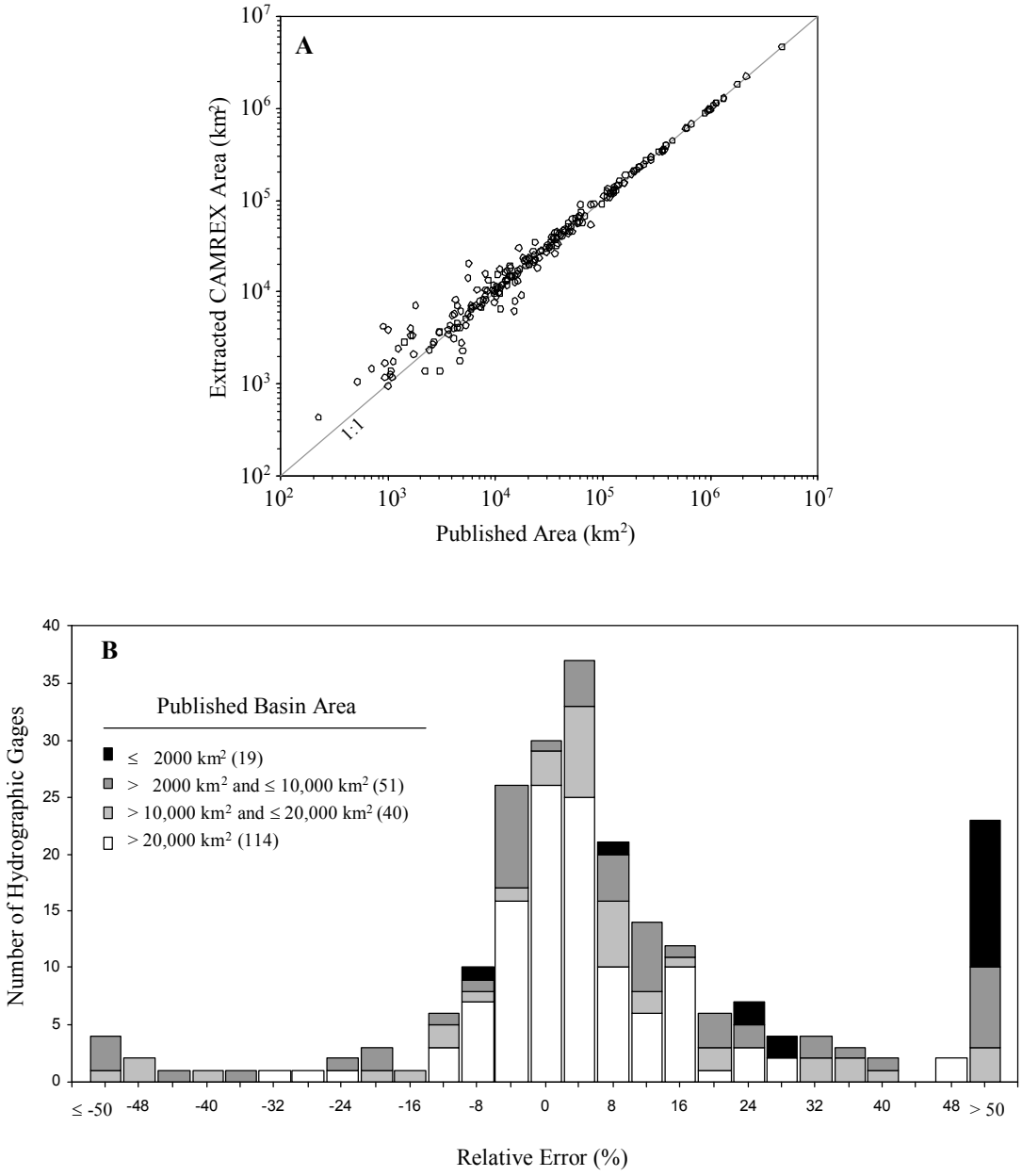

Figure 3.8. Drainage basin areas derived from the CAMREX drainage direction map compared with published drainage areas from the hydrographic gage database (n = 224). **A)** Scatter plot of CAMREX vs. published areas; the 1:1 line is also plotted. **B)** Frequency distribution of relative error partitioned into four drainage area classes. The number of gage stations in each area class is shown in parenthesis.

CHAPTER 4: OVERVIEW OF RIVERINE DIC, CO_2, AND CARBON ISOTOPE SYSTEMATICS, FOCUSING ON AMAZONIAN RIVERS

INTRODUCTION

Carbon in all its forms plays a key role in riverine ecosystems. Organic carbon (OC) sustains heterotrophic activity that produces CO_2, and interacts with trace metals and minerals through complexation and sorption reactions (Spitzy & Ittekkot 1991; Hope *et al.* 1994; Cole & Caraco 2001). Dissolved inorganic carbon (DIC) serves as a source for carbon fixation by autotrophs and as a key control on geochemical reactions. Organic and inorganic carbon interact closely through biologically mediated processes. In turn, they are part of an open fluvial system that receives exports from terrestrial environments in the form of organic carbon, respired soil CO_2, and weathering products (Stallard & Edmond 1987; Hope *et al.* 1994; Jones & Mulholland 1998a; Finlay 2003; Mortatti & Probst 2003); processes allocthonous carbon within its channels (Richey *et al.* 1988; Benner *et al.* 1995; Cole & Caraco 2001; Mulholland *et al.* 2001); impacts the surrounding terrestrial areas through flooding and geomorphological action (Salo *et al.* 1986; Forsberg *et al.* 1988; Puhakka *et al.* 1992; Räsänen *et al.* 1992; Mertes 1997; Dunne *et al.* 1998; Melack & Forsberg 2001); sequesters organic carbon for tens to thousands of years through floodplain sediment deposition (Victoria *et al.* 1992; Dunne *et al.* 1998; Stallard 1998; Aalto *et al.* 2003; Martinelli *et al.* 2003); interacts with the atmosphere via gas exchange (Jones & Mulholland 1998b; Hope *et al.* 2001; Richey *et al.* 2002; Finlay 2003); and ultimately transports carbon to the oceans or inland lakes (Richey *et al.* 1990; Ludwig *et al.* 1996; Aumont *et al.* 2001; Blair *et al.* 2003).

The prospect of global climate change resulting from anthropogenic increase of atmospheric CO_2 has accelerated the need to understand all components of the

global carbon cycle (Sundquist 1993; Bousquet *et al.* 2000; Canadell *et al.* 2000; Falkowski *et al.* 2000; Schimel *et al.* 2001; Gurney *et al.* 2002) and recognize the central role of CO_2 in modulating global climate throughout Earth's history (Berner & Kothavala 2001; Crowley & Berner 2001; Berner 2003; Royer *et al.* 2004). In particular, a global imbalance between known anthropogenic sources and ocean sinks of CO_2 indicates the existence of a global "missing sink" possibly as high as 2.0 Pg C yr^{-1} and likely to be concentrated on land (Sarmiento & Gruber 2002). While there has been much emphasis on the Northern Hemisphere as the primary location of this sink (Bousquet *et al.* 2000; Pacala *et al.* 2001; Gurney *et al.* 2002), the role of the tropics remains ambiguous and poorly constrained (Phillips *et al.* 1998; Malhi & Grace 2000; Clark 2002; Gurney *et al.* 2002; Richey *et al.* 2002; Townsend *et al.* 2002). The net carbon balance in Amazonia is currently the focus of intensive studies under the Large-Scale Biosphere-Atmosphere Experiment in Amazonia (LBA) initiative (Andreae *et al.* 2002; Avissar *et al.* 2002; Davidson & Artaxo 2004; Keller *et al.* 2004).

Recently, there has been increased recognition that rivers are closely linked to their terrestrial watersheds and corridors (Jones & Mulholland 1998a; Richey *et al.* 2002; Davidson & Artaxo 2004), and that closure of terrestrial carbon budgets in the humid tropics requires the inclusion of high CO_2 fluxes evading from rivers (Richey *et al.* 2002). This is especially relevant in the Amazon basin, where Richey *et al.* (2002) have estimated CO_2 evasion fluxes from rivers as high as 0.5 Pg C yr^{-1}, nearly an order of magnitude greater than fluvial exports of organic carbon to the ocean (Richey *et al.* 1990). In Amazonian rivers, assessing DIC sources and cycling is therefore critical both to improve our understanding of local riverine ecosystem

dynamics and their response to human impacts, and to better constrain CO_2 evasion fluxes to the atmosphere and their linkage to terrestrial ecosystems.

Major ion and alkalinity observations from rivers have been used to examine dominant weathering regimes throughout the Amazon basin. Together with climate, lithology is a primary control on chemical erosion and therefore on DIC and alkalinity loads in rivers (Stallard 1985; Amiotte-Suchet & Probst 1995; Edmond *et al.* 1996; Gaillardet *et al.* 1999; Galy & France-Lanord 1999; Kump *et al.* 2000; Berner & Kothavala 2001; Chen *et al.* 2002; Mortatti & Probst 2003). In a seminal study surveying the mainstem, adjacent environments, and large areas of the Peruvian and Bolivian Andes, Stallard & Edmond (1981; 1983; 1987) examined the dominant sources of the dissolved inorganic load across the Amazon basin. The highest rates of chemical erosion occur in the Andes as a result of exposure of unstable, highly weatherable sedimentary lithologies such as marine limestones and evaporites like gypsum and halite. High rates of tectonic uplift and the resulting physical erosion continually expose weatherable bedrock material, leading to large rates of weathering of silicates, carbonates and evaporites, and associated large fluxes of alkalinity and bicarbonate (HCO_3^-). This denudation regime is described as "weathering-limited", because erosion is limited by the supply of loose material created by chemical weathering (Stallard & Edmond 1983; Stallard 1985; Stallard 1988; Edmond *et al.* 1996). In the lowlands, particularly on the stable continental cratons of the Guyana and Brazilian shields (Fig. 2.1), intense weathering over perhaps hundreds of millions of years has stripped most cations from the soils and built very deep soil profiles, leaving the bedrock and saprolite largely beyond the reach of actively circulating subsurface waters that provide runoff to streams. Rivers in these regions are generally acidic and depleted in major ions and alkalinity, while most of its DIC is in

the form of dissolved CO_2. This denudation regime is described as "transport-limited", because erosion is limited by the ability of transport processes to remove material (Stallard & Edmond 1983; Stallard 1985; Stallard 1988; Edmond *et al.* 1995). Nonetheless, weatherable lithologies are found in the lowlands as outcrops of silicates in the shields (Stallard & Edmond 1983; Ballester *et al.* 2003; Holmes *et al.* 2004; Krusche *et al.* in prep.) and marine sediments in the Subandean Foreland (Fig. 2.1), including the Juruá, Purus, and Javari rivers in the Western end of the Brazilian Amazon (Stallard & Edmond 1983; Palmer & Edmond 1992).

The work of Stallard and Edmond has been recently extended through the use of observed river geochemistry and inverse models at large scales throughout the basin to calculate the consumption of atmospheric and soil CO_2 during carbonate and silicate weathering (Probst *et al.* 1994; Gaillardet *et al.* 1997; Gaillardet *et al.* 1999; Mortatti & Probst 2003); some of these studies (Probst *et al.* 1994; Mortatti & Probst 2003) relied primarily on data collected under the CAMREX program. In addition to inverse approaches relying on river observations, a forward model ("GEM-CO2") based on lithological maps and empirical weathering rate relationships has been used to estimate CO_2 consumption during weathering, and export of DIC and alkalinity to rivers (Amiotte-Suchet & Probst 1993; 1995; Amiotte-Suchet *et al.* 2003).

Most previous examinations of DIC cycling have concentrated on the Amazon mainstem, its surrounding floodplain, and the mouths of major tributaries. High suspended sediment loads in the mainstem impede light penetration and lead to negligible photosynthetic rates (Wissmar *et al.* 1981). As part of the CAMREX project, Devol *et al.* (1987) and Richey *et al.* (1988) found high rates of respiration roughly equivalent to the rates of outgassing, and pCO_2 levels 10-30 times as high as atmospheric pCO_2. Floodplain environments generally have higher pCO_2

concentrations than the mainstem, the result of more intense respiration rates and reduced gas diffusivity compared to turbulent river channels (Devol *et al.* 1987; Melack & Forsberg 2001). Along an 1,800-km mainstem lowland transect from Vargem Grande to Obidos (see Fig. 2.2), dilution by low-alkalinity lowland tributaries decreases DIC concentrations by half from elevated levels of ~ 1,110 μM at the upstream end (Richey *et al.* 1990) caused by substantial carbonate dissolution in the Andean and piedmont headwaters of the mainstem upstream of Vargem Grande (Stallard & Edmond 1983; 1987). During falling waters, mainstem pCO_2 increases and pH decreases downstream as a result of tributary and floodplain inputs (Richey *et al.* 1990).

Riverine DIC and CO_2 have not been examined in detail outside of the mainstem and floodplain corridor. Stallard & Edmond (1987) used their alkalinity and pH observations to estimate pCO_2 and supersaturation throughout the basin. Their findings agree with subsequent work carried out by CAMREX in mainstem and floodplain waters, already discussed. In Andean rivers, they estimated lower CO_2 supersaturation (< 10 times atmospheric pCO_2), attributing this result to higher rates of CO_2 outgassing due to higher turbulence caused by topographic relief. DIC in the Peruvian Andes calculated from their data is often substantially higher than at Vargem Grande as a result of extensive dissolution of carbonate sediments. In Bolivia, the PHICAB/IRD program (Guyot *et al.* 1992; Guyot 1993) conducted extensive geochemical surveys of Andean and lowland rivers draining into the Rio Madeira. While no attempt has been made to estimate pCO_2 from this dataset, Andean DIC values calculated from their data are generally lower than those in Peru, consistent with a reduced presence of carbonate outcrops compared to the Peruvian Andes (Stallard & Edmond 1983).

Contact between land and rivers and lateral transfers from the watershed to the stream in the humid lowlands of the Amazon basin occurs predominantly in smaller rivers and streams, which represent the largest fraction of total river length (McClain & Elsenbeer 2001). Studies examining biogeochemical transfers from soils, hillslopes, and groundwater to streams have focused on nutrients, dissolved organic carbon (DOC), and major ions (Nortcliff & Thornes 1978; Elsenbeer *et al.* 1995; McClain *et al.* 1997; Williams & Melack 1997; McClain & Elsenbeer 2001; Thomas *et al.* 2004). As in most forested ecosystems (Raich & Potter 1995; Schlesinger & Andrews 2000; Raich *et al.* 2002), soil respiration in lowland Amazonia is high (Chambers *et al.* 2004; Keller *et al.* 2004; Salimon *et al.* 2004; Sotta *et al.* 2004) and leads to CO_2 concentrations in soils much higher than atmospheric levels (Davidson & Trumbore 1995; Trumbore 2000; Sotta *et al.* 2004). Nonetheless, the lateral transfer of DIC and CO_2 from soils to streams and subsequent fate of this terrestrial carbon in streams remain largely uninvestigated in the Amazon. Studies in temperate systems suggest that water highly supersaturated in CO_2 is exported from the land and quickly degassed downstream, leading to decreases in pCO_2 and associated increases in pH along streams (Dawson *et al.* 1995; Choi *et al.* 1998; Jones & Mulholland 1998a; 1998b; Neal *et al.* 1998b; Schindler & Krabbenhoft 1998; Andrews & Schlesinger 2001; Hope *et al.* 2001; Dawson *et al.* 2002; Finlay 2003). Similar mechanisms are certain to be important in Amazonia as well (Richey *et al.* 2002).

Natural ^{13}C and ^{14}C isotopes of DIC provide a unique capability to identify the biological and geological sources of inorganic carbon to rivers, processes leading to its transformation in transit, and residence times on land and within rivers (Mook & Tan 1991; Kendall *et al.* 1995; Bullen & Kendall 1998; Raymond & Hopkinson 2003). ^{13}C-DIC in particular has been widely used across a range of river systems

(Aravena & Suzuki 1990; Mook & Tan 1991; Aravena *et al.* 1992; Tan & Edmond 1993; Cameron *et al.* 1995; Kendall *et al.* 1995; Flintrop *et al.* 1996; Rose & Davisson 1996; Yang *et al.* 1996; Atekwana & Krishnamurthy 1998; Amiotte-Suchet *et al.* 1999; Aucour *et al.* 1999; Barth & Veizer 1999; Galy & France-Lanord 1999; James *et al.* 1999; Telmer & Veizer 1999; Karim & Veizer 2000; Cole & Caraco 2001; Palmer *et al.* 2001; Raymond & Bauer 2001b; Hélie *et al.* 2002; Barth *et al.* 2003; Finlay 2003; Raymond & Hopkinson 2003; Yoshimura *et al.* 2004). The use of ^{14}C-DIC has been much more limited (Aravena & Suzuki 1990; Aravena *et al.* 1992; Rose & Davisson 1996; James *et al.* 1999; Cole & Caraco 2001; Palmer *et al.* 2001; Raymond & Hopkinson 2003) and absent altogether in the Amazon and tropical rivers in general, due in large part to the cost associated with the Accelerator Mass Spectrometry (AMS) technique used for sensitive analysis requiring only small samples (Vogel *et al.* 1987; Vogel *et al.* 1995; Gove 2000; Levin & Hesshaimer 2000).

Analyses of ^{13}C-DIC along the Amazon mainstem (Longinelli & Edmond 1983; Quay *et al.* 1989; Quay *et al.* 1992) has yielded additional insight on DIC and CO_2 cycling. A persistent downstream trend of ^{13}C depletion indicates a progressive influence on the mainstem from DIC derived from ^{13}C-depleted C_3 plant material (typically forests, see Hedges *et al.* 1986a; Martinelli *et al.* 1998), contributed by lowland tributaries. Furthermore, isotopic and respiration data strongly suggest that ^{13}C-enriched C_4 grasses from the floodplain ("*varzea*") (Devol *et al.* 1987; Quay *et al.* 1992; Waichman 1996; Melack & Forsberg 2001) are a disproportionately important source of organic matter used in respiration.

In Chapters 5 and 6, I will present the results of an extensive survey of DIC and its carbon isotopes in rivers throughout the Amazon basin which extends DIC and

^{13}C-DIC observations to many rivers beyond the mainstem and mouths of major tributaries, and adds ^{14}C-DIC measurements for the first time. In Chapter 5 I focus on the relationship between organic carbon and DIC in Amazonian rivers, as determined from their isotopic composition. In this chapter, I first discuss the geochemistry and systematics of DIC, CO_2, ^{13}C, and ^{14}C; then make use of a mass balance approach to discuss the dominant processes controlling DIC and carbon isotopes in a river reach, with emphasis on observations and dominant processes in Amazonian rivers. The quantitative framework and literature review presented in this chapter will serve to facilitate the qualitative interpretation of DIC trends in Chapter 6 and lay a foundation for future carbon modeling work in Amazonian rivers and riverine corridors.

δ^{13}C AND Δ^{14}C NOTATION

^{13}C is commonly reported in per mil (‰) notation with respect to the Pee Dee Belemnite (PDB) standard:

$$\delta^{13}C = [{}^{13}R_{sample} / {}^{13}R_{PDB} - 1] \times 1000, \quad (4.1)$$

where $^{13}R_{sample}$ and $^{13}R_{PDB}$ are the sample and standard $^{13}C/^{12}C$ isotopic ratios, respectively (Clark & Fritz 1997). ^{14}C is commonly reported in the conventional Δ^{14}C (‰) notation (Stuiver & Polach 1977):

$$\Delta^{14}C = [{}^{14}R_{sample} / {}^{14}R_{ABS} - 1] \times 1000, \quad (4.2)$$

where $^{14}R_{sample}$ is the sample $^{14}C/^{12}C$ isotopic ratio normalized to a common δ^{13}C value of -25‰ to remove mass-dependent isotopic fractionation effects, as follows (Stuiver & Robinson 1974; Stuiver & Polach 1977):

$$\begin{aligned} {}^{14}R_{sample} &= ({}^{14}C/{}^{12}C)_{sample} \times [(1 - 25/1000)^2 / (1 + \delta^{13}C_{sample}/1000)^2] \\ &= ({}^{14}C/{}^{12}C)_{sample} \times 0.975^2 / (1 + \delta^{13}C_{sample}/1000)^2. \end{aligned} \quad (4.3)$$

$^{14}R_{ABS}$ corresponds to the absolute Modern Carbon standard, defined as 95% of the $^{14}C/^{12}C$ ratio (or equivalently, the ^{14}C activity) of the international NBS Oxalic Acid 1 standard (Ox1) in 1950 normalized to a $\delta^{13}C$ value of -19‰ (Stuiver & Polach 1977). Analogous to the expression for $^{14}R_{sample}$, but incorporating the 95% factor and a correction for decay between 1950 and the year of measurement (y) with a 5730 yr half-life:

$$^{14}R_{ABS} = 0.95 \times (^{14}C/^{12}C)_{Ox1} \times 0.981^2 / (1 + \delta^{13}C_{Ox1}/1000)^2 \times e^{(y-1950)/8267}. \qquad (4.4)$$

In practice, many Accelerator Mass Spectrometry (AMS) laboratories (Vogel *et al.* 1987; Vogel 1992) measure $^{14}C/^{13}C$ rather than $^{14}C/^{12}C$ ratios. J. Southon (internal pub., Center for Accelerator Mass Spectrometry, Lawrence Livermore National Laboratory) presents modified but equivalent formulas for $\Delta^{14}C$ based on $^{14}C/^{13}C$ measurements. When sample collection year (z) differs from analysis year (y), a correction for radioactive decay since the collection year is needed (Stuiver & Polach 1977). $^{14}R_{sample}$ in eqtn. 4.2 is multiplied by the decay correction factor, $e^{(y-z)/8267}$.

The Modern Carbon standard represents the atmospheric ^{14}C composition in the late 19th century before large-scale addition of ^{14}C-free fossil-fuel CO_2 and before the initiation of thermonuclear weapon testing (Stuiver & Polach 1977). Thus, positive $\Delta^{14}C$ values indicate the presence of ^{14}C from atmospheric weapon testing, while negative values indicate the occurrence of significant radioactive decay (Clark & Fritz 1997; Levin & Hesshaimer 2000; Randerson *et al.* 2002).

DIC, alkalinity, and pCO_2

Dissolved inorganic carbon is equal to the total concentration ([]) of aqueous carbonate species:

$$DIC = [H_2CO_3^*] + [HCO_3^-] + [CO_3^{2-}] \quad (4.5)$$

where $[H_2CO_3^*]$ is a short-hand for the analytic sum of dissolved CO_2 and carbonic acid concentrations ($[CO_2(aq)] + [H_2CO_3]$) that is mainly composed of $CO_2(aq)$ (Stumm & Morgan 1981). The activity ({})of each carbonate species is controlled by pH ($-\log(\{H^+\})$) according to the equilibrium constant expressions:

$$K_1 = \{H^+\}\{HCO_3^-\} / \{H_2CO_3^*\} \quad (4.6)$$

$$K_2 = \{H^+\}\{CO_3^{2-}\} / \{HCO_3^-\} \quad (4.7)$$

For convenience, these expressions can be redefined in terms of concentrations by assuming a constant ionic medium (Stumm & Morgan 1981) and rearranging activity coefficients γ_z , where z is the species charge absolute value and $\gamma_0 = 1$:

$$^cK_1 = \gamma_1^{-2} K_1 = [H^+][HCO_3^-] / [H_2CO_3^*] \quad (4.8)$$

$$^cK_2 = \gamma_2^{-1} K_2 = [H^+][CO_3^{2-}] / [HCO_3^-] \quad (4.9)$$

The concentration of each DIC species can be calculated using the ionization fractions f_0, f_1, and f_2: $[H_2CO_3^*] = f_0$ DIC, $[HCO_3^-] = f_1$ DIC, and $[CO_3^{2-}] = f_2$ DIC (Stumm & Morgan 1981). Ionization fractions are calculated as a function of $[H^+]$ and the equilibrium constants:

$$f_0 = [H^+]^2 / D \quad (4.10)$$

$$f_1 = {}^cK_1 [H^+] / D \quad (4.11)$$

$$f_2 = {}^{c}K_1 \, {}^{c}K_2 \, / \, D \tag{4.12}$$

where $D = [H^+]^2 + {}^{c}K_1 [H^+] + {}^{c}K_1 \, {}^{c}K_2$ and $f_0 + f_1 + f_2 = 1$. Note that the symbol α is often used instead of f. Finally, $CO_2(g)$ dissolution is represented through Henry's Law, expressing the equilibrium between $H_2CO_3^*$ and CO_2 partial pressure (pCO_2):

$$K_H = \{H_2CO_3^*\} / pCO_2 \tag{4.13}$$

The temperature dependence of the above equilibrium constants can be calculated using relationships from Clark & Fritz (1997) in terms of pK (-log(K)), where temperature is in ^{o}C:

$$pK_1 = 1.1 \times 10^{-4} \, T^2 - 0.012 \, T + 6.58 \tag{4.14}$$

$$pK_2 = 9 \times 10^{-5} \, T^2 - 0.0137 \, T + 10.62 \tag{4.15}$$

$$pK_H = -7 \times 10^{-5} \, T^2 + 0.016 \, T + 1.11 \tag{4.16}$$

The above expressions yield pK_1, pK_2, and pK_H values of 6.47, 10.49, and 1.26 at $10^{o}C$, respectively; and 6.34, 10.32, and 1.49 at $27^{o}C$. K_H is in units of $\mu M \, ppm^{-1}$, or $M \, atm^{-1}$.

As ionic strength could often not be estimated accurately in this study (see Chapter 6), equilibrium calculations will be based on the simplifying assumption that $\gamma = 1$ and ${}^{c}K = K$ (see eqtns. 4.7 and 4.8). For clarity, I will refer to ${}^{c}K$ as K and use concentrations in place of activities in further discussions, except when noted.

In freshwaters, titration alkalinity (Alk, in eq L^{-1}) may be generally represented by the electroneutrality condition (Stumm & Morgan 1981; Neal 2001):

$$Alk = [HCO_3^-] + 2 \, [CO_3^{2-}] + [OH^-] - [H^+] \tag{4.17}$$

This equation can be expressed in terms of DIC, ionization fractions, and $[H^+]$:

$$Alk = DIC \, (f_1 + 2f_2) + (K_w / [H^+] - [H^+]). \tag{4.18}$$

K_w is the equilibrium constant for dissociation of water into $[OH^-]$ and $[H^+]$. Its temperature dependence is calculated as:

$$pK_w = 606.52 + 0.09761\ T_k - 31286\ T_k^{-1} + 21.71 \times 10^5\ T_k^{-2} - 94.973 \log(T_k), \quad (4.19)$$

where T_k is temperature in Kelvin (Szaran 1998).

pCO_2 can be calculated from DIC and pH by combining eqtn. 4.13 and the definition of the ionization fraction f_0:

$$pCO_2 = f_0 \cdot DIC / K_H \quad (4.20)$$

To calculate the degree of CO_2 saturation with respect to the atmosphere, pCO_2 / pCO_2^{atm}, mean sea-level tropospheric pCO_2 ($pCO_2^{atm}(0)$) can be adjusted for the effect of pressure via an exponential function of site elevation (h, in meters) as follows (Karim & Veizer 2000):

$$pCO_2^{atm}(h) = pCO_2^{atm}(0)\ e^{-h/8400} \quad (4.21)$$

Neal *et al.* (1998a) present an extensive set of equations for calculating the degree of CO_2 saturation.

^{13}C and ^{14}C of CO_2(g)

While isotopic analysis yields measurements for bulk DIC, individual carbonate species are typically involved in dominant biogeochemical processes and exchanges. CO_2 gas in particular participates in air-water gas exchange and the key biological processes of respiration and photosynthesis. The isotopic composition of CO_2(g) in equilibrium with DIC is therefore important for assessing the relative role of a variety of DIC sources and processes. The definition of $\Delta^{14}C$ already includes a normalization for mass-dependent fractionation effects (see above), such as equilibrium between carbonate species; $\Delta^{14}C\text{-}CO_2(g) = \Delta^{14}C\text{-DIC}$. $\delta^{13}C\text{-}CO_2(g)$, on the other hand, must be calculated by accounting for equilibrium fractionation among

carbonate species and the pH-dependent relative distribution of each species (Zhang *et al.* 1995; Clark & Fritz 1997; Zeebe & Wolf-Gladrow 2001).

δ^{13}DIC can be described in terms of the isotopic composition and relative distribution of each carbonate species using a mass balance formulation and the ionization fractions defined earlier, where the error introduced by the use of δ values rather than mass fractional abundance (e.g., $^{13}r = {}^{13}C/({}^{12}C + {}^{13}C)$) is negligible (Zeebe & Wolf-Gladrow 2001):

$$\delta^{13}\text{C-DIC} = f_0 \cdot \delta^{13}\text{C-}H_2CO_3^* + f_1 \cdot \delta^{13}\text{C-}HCO_3^- + f_2 \cdot \delta^{13}\text{C-}CO_3^{2-} \quad (4.22)$$

Equilibrium isotopic fractionation between reactant X and product Y may be represented by the enrichment factor $\varepsilon_{X\text{-}Y}(‰) = (\delta X - \delta Y)/(1 + \delta Y \cdot 10^{-3}) \approx \delta X - \delta Y$ (isotopic fractionation can also be described in terms of the fractionation factor, $\alpha_{X\text{-}Y} = \varepsilon_{X\text{-}Y} \cdot 10^{-3} + 1 = R_X/R_Y$) (Clark & Fritz 1997; Zeebe & Wolf-Gladrow 2001). Carbonate species enrichment factors as a function of temperature in ^oC are estimated from Zhang *et al.* (1995), where $CO_2(g)$ is the reaction product:

$$\varepsilon_{H2CO3^*\text{-}g} = 0.0049\ T - 1.31 \quad (4.23)$$

$$\varepsilon_{HCO3\text{-}g} = -0.1141\ T + 10.78 \quad (4.24)$$

$$\varepsilon_{CO3\text{-}g} = -0.052\ T + 7.22 \quad (4.25)$$

For example, $\varepsilon_{H2CO3^*\text{-}g}$ is a short-hand for $\varepsilon_{H2CO3^*\text{-}CO2g}$ and is approximately equal to $\delta^{13}\text{C-}H_2CO_3^* - \delta^{13}\text{C-}CO_2(g)$. The above expressions yield $\varepsilon_{H2CO3^*\text{-}g}$, $\varepsilon_{HCO3\text{-}g}$, and $\varepsilon_{CO3\text{-}g}$ values of -1.26, 9.64, and 6.70‰ at 10^{o}C, respectively; and -1.18, 7.70, and 5.82‰ at 27^{o}C. $\delta^{13}\text{C-}CO_2(g)$ is then calculated by replacing $\delta^{13}\text{C-}H_2CO_3^*$, $\delta^{13}\text{C-}HCO_3^-$, and $\delta^{13}\text{C-}CO_3^{2-}$ in eqtn. 4.22 with the corresponding enrichment factor expressions with respect to $CO_2(g)$, and rearranging to yield:

$$\delta^{13}C\text{-}CO_2(g) = \delta^{13}C\text{-DIC} - f_0\,\varepsilon_{H2CO3^*\text{-}g} - f_1\,\varepsilon_{HCO3\text{-}g} - f_2\,\varepsilon_{CO3\text{-}g} \quad (4.26)$$

ATMOSPHERIC CO_2

Atmospheric CO_2 concentration has experienced large changes since the 19th century as a result of anthropogenic perturbations. The rise in global mean pCO_2 from a pre-industrial value of approximately 280 ppm to 375 ppm in 2003 is well documented and is largely the result of the combustion of fossil fuels (Conway *et al.* 1994; Keeling *et al.* 1995; Barnola 1999; Rayner *et al.* 1999a; Keeling & Whorf 2004). Annual growth rates of pCO_2 in the second half of the 20th century ranged from about 0.5 to nearly 3.0 ppm yr^{-1}, with considerable interannual variability related to large-scale forcings such as El Niño, large volcanic eruptions, and changes in fossil-fuel emissions (Conway *et al.* 1994; Keeling *et al.* 1995; Dettinger & Ghil 1998; Gérard *et al.* 1999; Rayner *et al.* 1999a; Rayner & Law 1999; Rayner *et al.* 1999b; Keeling & Whorf 2004).

The isotopic composition of atmospheric CO_2 has also experienced large changes of anthropogenic origin. Fossil-fuel combustion and biomass burning release CO_2 with a $\delta^{13}C$ composition representative of C_3 vegetation, about -27‰ (Trolier *et al.* 1996; Francey *et al.* 1999; Rayner *et al.* 1999a). Input of light $^{13}CO_2$ has resulted in a depletion of atmospheric $^{13}CO_2$ (the ^{13}C "Suess" effect) from pre-industrial values of approximately -6.4‰ to about -8‰ in the late 1990s (Keeling *et al.* 1995; Trolier *et al.* 1996; Francey *et al.* 1999). Due to radioactive decay, fossil fuels are completely depleted in ^{14}C, leading to a decrease in atmospheric $\Delta^{14}C\text{-}CO_2$ relative to a pre-industrial value of ~0‰ (Levin & Hesshaimer 2000; Randerson *et al.* 2002). However, testing of thermonuclear bombs in the 1950s and 1960s resulted in a large increase in atmospheric $^{14}CO_2$, masking out the Suess depletion (Levin & Hesshaimer

2000; Randerson *et al.* 2002; Levin & Kromer in press). A $\Delta^{14}C$ peak of close to 1000‰ was reached in the late 1960s in the Northern Hemisphere, and atmospheric $^{14}CO_2$ has steadily decreased since then to below 100‰ today (Fig. 4.1). In the Amazon basin, the seasonal North-South movement of the Intertropical Convergence Zone (ITCZ) brings varying mixtures of air masses from the Southern and Northern hemispheres (Marengo & Nobre 2001), likely leading to variable atmospheric $\Delta^{14}C$ compositions; however, most of the basin remains north of the ITCZ (Waliser & Gautier 1993; Waliser & Somerville 1994; Marengo & Nobre 2001), suggesting that Northern Hemisphere air masses exert the strongest influence. See Chapter 5 for additional discussion.

In the Amazon basin, Longinelli & Edmond (1983) and Quay *et al.* (1989) measured the $\delta^{13}C$ composition of CO_2 in air above the mainstem Amazon. River degassing of CO_2 depleted in $\delta^{13}C$ resulted in up to 30% higher pCO_2 compared to mean tropospheric partial pressure for that latitude, and relatively depleted $\delta^{13}C$-CO_2 values of -12.7 to -7.7‰ (Quay *et al.* 1989). Lower nocturnal mixed layer heights and vigorous mixing by solar heating during the day produced a distinct CO_2 diurnal cycle characterized by accumulation of evaded CO_2 at night and mixing with the tropospheric air during the day (Quay *et al.* 1989). Longinelli & Edmond (1983) observed generally more depleted $\delta^{13}C$-CO_2 values and an East-West decrease from the Amazon mouth to Iquitos, Peru, (~3,400 km upriver), a trend not detected by Quay *et al.* (1989). $\Delta^{14}C$ measurements of tropospheric CO_2 are not available for the region. As described later in Chapter 5, I estimated it by applying a +8‰ offset relative to annual averages at a European continental reference station (see also Fig. 4.1).

DIC mass balance

The mass balance of DIC in a river reach (Fig. 4.2) can be expressed by the following equation, disregarding the effect of dispersion (Quay *et al.* 1986; Richey *et al.* 1990; Richey *et al.* 1991):

$$d(V \cdot DIC_r)/dt = I - Q_o \cdot DIC_r + V \cdot R - V \cdot P + G \quad (4.27)$$

where V = river reach volume, DIC_r = river [DIC], I = total DIC input flux via transport, Q_o = reach outflow water discharge, R = heterotrophic respiration rate per unit volume, P = net autochthonous photosynthesis rate per unit volume (net primary production from phytoplankton, periphyton, and submerged vegetation), and G = net CO_2 gas exchange with the overlying atmosphere (positive value corresponds to net CO_2 invasion). This mass balance expression does not explicitly include exchange with a distinct floodplain environment (e.g., Richey *et al.* 1990).

The input flux term can be expanded to consider multiple sources (Fig. 4.2):

$$I = Q_{in} \cdot DIC_{in} + Q_{tr} \cdot DIC_{tr} + Q_{gw} \cdot DIC_{gw} + I_{rip} \quad (4.28)$$

where subscripts are in = river reach upstream inflow, tr = tributary inflow, and gw = groundwater inflow; and I_{rip} = riparian area CO_2 contributions from submerged root respiration (Richey *et al.* 1991; Devol *et al.* 1995). DIC in groundwater includes respired CO_2 from roots and soil organic matter decomposition, and bicarbonate from mineral weathering (Fig. 4.2; see additional discussion below).

Total heterotrophic respiration is the sum of respiration of organic carbon from multiple sources (Fig. 4.2):

$$R = R_{in} + R_{tr} + R_{terr} + R_{rip} + R_{alg} \quad (4.29)$$

where terr = *terra firme* organic carbon transported to the reach via subsurface DOC flux and POC erosion, rip = riparian area vegetation leaching and direct litterfall, and alg = algal organic carbon. *Terra firme* and riparian ecosystems may be composed of C_3 or C_4 vegetation types (O'Leary 1981; Ehleringer & Monson 1993; Lloyd & Farquhar 1994; Martinelli *et al.* 1994; Ehleringer *et al.* 1997; Martinelli *et al.* 1998; Still *et al.* 2003). In the Amazon basin, deforested areas are dominated by C_4 pastures (Desjardins *et al.* 1994; Neill *et al.* 1997; Alves *et al.* 1999; Bernardes *et al.* 2004), which can grow directly over small streams (Neill & Davidson 2000; Thomas *et al.* 2004). C_4 macrophytes are also dominant in the floodplain of the Amazon mainstem, and are likely important in the floodplains and river corridors around other nutrient-rich rivers but are generally absent from nutrient-poor black-water rivers (Hedges *et al.* 1986a; Junk 1989; Martinelli *et al.* 1991; Victoria *et al.* 1992; Melack & Forsberg 2001). Aquatic photosynthetic production is very limited midchannel in turbid rivers draining the Andes and other high-relief areas, but may be significant in mainstem littoral areas, floodplain lakes, and low-sediment lowland rivers (Wissmar *et al.* 1981; Quay *et al.* 1995). See Chapter 2 for additional discussion of river metabolism in Amazonian rivers.

The flux of CO_2 between atmosphere and water is commonly represented as a function of gas transfer velocity and concentration gradient via a stagnant-film gas transfer model (Quay *et al.* 1986; Devol *et al.* 1987; Richey *et al.* 1988; Choi *et al.* 1998; Raymond *et al.* 2000; Cook *et al.* 2003):

$$G = A \cdot f \cdot (D_{CO2} / z) \cdot K_H \cdot (pCO_2^{atm} - pCO_2^{s}) \qquad (4.30)$$

where A = river surface area, f = chemical enhancement factor, D_{CO2} = CO_2 molecular diffusion coefficient, z = empirical thickness of the stagnant boundary layer, K_H = Henry's Law constant (see eqtn. 4.13), and pCO_2^{atm} and pCO_2^{s} are the

partial pressures of CO_2 in the atmosphere and in solution, respectively. Chemical enhancement is important ($f > 1$) only at high pH and low gas transfer velocity (D_{CO2} / z) (Wanninkhof & Knox 1996), a rare condition in the Amazon basin. The thickness of the boundary layer (z) decreases with water turbulence and wind speed, leading to increased transfer velocity (Devol *et al.* 1987; Richey *et al.* 1988; Genereux & Hemond 1992; Cirpka *et al.* 1993; Aucour *et al.* 1999; Raymond & Cole 2001; Cook *et al.* 2003); high turbulence can also result in enhanced mixing with air via bubble injection (Cirpka *et al.* 1993; Cook *et al.* 2003). A large majority of rivers in the Amazon basin are supersaturated with respect to atmospheric CO_2, resulting in net evasion ($G < 0$) from the water surface (Devol *et al.* 1987; Stallard & Edmond 1987; Richey *et al.* 1988; Richey *et al.* 2002).

DIC isotopic mass balance

An isotopic mass balance can be constructed using an approach analogous to the one used in eqtn. 4.27 for DIC (Quay *et al.* 1986). For ^{13}C:

$$d(V \cdot DIC_r \cdot {}^{13}R_r)/dt = I \cdot {}^{13}R_I - Q_o \cdot DIC_r \cdot {}^{13}R_r + V \cdot R \cdot {}^{13}R_{rOC} - V \cdot P \cdot {}^{13}R_P + G \cdot {}^{13}R_G \quad (4.31)$$

where ^{13}R denotes the $^{13}C/^{12}C$ ratio of each flux, source, or storage term as follows: $^{13}R_r$ = DIC in the reach, $^{13}R_I$ = DIC in combined transport input, $^{13}R_{rOC}$ = heterotrophically respired organic carbon, $^{13}R_P$ = organic carbon produced by autochthonous photosynthesis, and $^{13}R_G$ = CO_2 of net gas exchange.

As discussed above, the transport input flux term is composed of multiple sources. Each source may be characterized by a distinct isotopic signature. For example, lowland tributaries draining into the Amazon mainstem are significantly depleted in $\delta^{13}C$-DIC compared to the mainstem (Quay *et al.* 1992). Respiratory fractionation between organic carbon substrate and the resulting CO_2 has been

generally found to be negligible (Smith & Kroopnick 1981; Ekblad *et al.* 2002; Cleveland *et al.* 2004), although controversial evidence exists for a small (< 3‰) depletion in CO_2 during microbial respiration (Blair *et al.* 1985) and a small enrichment (< 6‰) during carbon uptake and CO_2 release by fungi (Henn & Chapela 2000). Similar to the heterogeneity of transport input sources, heterotrophs may respire organic carbon from multiple substrates with distinct isotopic signatures (Martinelli *et al.* 1994; Waichman 1996). However, many transport and respiration sources may be isotopically undistinguishable (Martinelli *et al.* 1994), particularly if they originate largely from C_3-derived respiration without significant mineral weathering contributions. In the absence of significant C_3-to-C_4 gradation between terra firme and riparian or floodplain vegetation communities, it may be impossible to isolate the contribution from each landscape element by using carbon isotopes alone. See above and Chapter 5 for more extensive discussion on Amazon biogeography and isotopic signatures of C_3 and C_4 plants. In the central Amazon, bottle incubations have been carried out to determine the $\delta^{13}C$ signature of respired CO_2. Quay *et al.* (1992) used mainstem water to determine a respiratory CO_2 signature of -22±3‰, attributing it to a source mixture of 40% C_4 and 60% C_3 organic carbon. Using water from multiple environments in a floodplain lake (open water, floating meadow, and flooded forest), Waichman (1996) obtained respiratory CO_2 with -18.5±3.3‰ (-27.7 to -13.5‰), yielding a C_4 source contribution of 46 to 79% with the assumption that respiration does not fractionate. C_4 plants appear to be a disproportionately important source of organic matter used in respiration, but contribute only a minor component of the organic carbon load (Quay *et al.* 1992; Melack & Forsberg 2001).

Phytoplankton take up $CO_2(aq)$ preferentially relative to other carbonate species and ^{12}C relative to the heavier ^{13}C isotope (Laws *et al.* 1995); fractionation

during photosynthesis can be expressed as $^{13}R_P = {}^{13}R_{CO2aq}/\alpha_P$, where α_P is the photosynthetic fractionation factor with respect to CO_2(aq). Under ideal conditions of CO_2(aq), nutrient, and light availability, α_P reaches maximum values of 1.025 to 1.028 (Laws *et al.* 1995; Bidigare *et al.* 1997), a depletion of up to 28‰ during photosynthetic carbon fixation that will enrich the remaining DIC. $^{13}R_{CO2aq}$ (= $^{13}R_{H2CO3*}$) can be calculated from $\delta^{13}C\text{-}H_2CO_3^*$, which is obtained by substituting $\delta^{13}C\text{-}CO_2(g) = \delta^{13}C\text{-}H_2CO_3^* - \varepsilon_{H2CO3*\text{-}g}$ into eqtn. 4.26. Phytoplankton ^{13}C composition ranging from -32 to -47‰ have been observed or estimated in rivers in the Amazon and Orinoco basins (Hedges *et al.* 1986a; Mook & Tan 1991; Tan & Edmond 1993).

Gas exchange ^{13}C flux is expressed by adapting eqtn. 4.30, taking into account kinetic and equilibrium fractionation effects (Quay *et al.* 1986; Zhang *et al.* 1995):

$$G\cdot{}^{13}R_G = A\cdot f\cdot(D_{CO2} / z)\cdot K_H\cdot\alpha_k\cdot\alpha_{H2CO3*\text{-}g}\cdot(pCO_2^{atm}\cdot{}^{13}R_{atm} - pCO_2^{s}\cdot{}^{13}R_{CO2g}) \qquad (4.32)$$

where $\alpha_k \approx 0.9991$ is the temperature-insensitive kinetic fractionation factor for CO_2 gas transfer across the water surface (Siegenthaler & Munnich 1981; Zhang *et al.* 1995), $^{13}R_{atm}$ = the $^{13}C/^{12}C$ ratio of atmospheric CO_2 (discussed above), and $^{13}R_{CO2g} = {}^{13}R_{DIC}/\alpha_{DIC\text{-}g}$; $\alpha_{DIC\text{-}g}$ can be gleaned from eqtn. 4.26. Gas exchange generally leads to ^{13}C enrichment of DIC in rivers (Finlay 2003), particularly in the Amazon lowlands where respiratory CO_2 produces DIC depleted in $\delta^{13}C$ relative to atmospheric CO_2 (Longinelli & Edmond 1983; Quay *et al.* 1992). At low pCO_2 supersaturation levels, CO_2 invasion with $\delta^{13}C \approx$ -8‰ may be a significant flux and will enrich ^{13}C-DIC. Under supersaturated conditions and neutral pH where DIC is dominated by bicarbonate, CO_2 evasion involves the export of a species depleted in ^{13}C relative to bulk DIC due to equilibrium fractionation between bicarbonate and CO_2(g).

A river reach DIC mass balance for ^{14}C can be constructed in a similar fashion as eqtn. 4.31 for ^{13}C. Such a mass balance is formulated in terms of the $^{14}C/^{12}C$ ratio ^{14}R, which can be calculated from $\Delta^{14}C$ and $\delta^{13}C$ values through eqtns. 4.1 to 4.3 (Braziunas *et al.* 1995). ^{14}R in this case is the true isotopic ratio, not the ^{13}C-normalized ratio used in eqtns. 4.2 and 4.3. ^{14}C enrichment factors (ε) are approximately twice as large as those for ^{13}C (Clark & Fritz 1997; Zeebe & Wolf-Gladrow 2001). As transport through the reach is fast, radioactive decay can be neglected. However, the variability in residence times of carbon in sources such as organic matter supporting respiration provides a tracer of sources and cycling time that complements ^{13}C. Residence time on the order of decades can be discerned by the impact of bomb-induced changes in atmospheric $^{14}CO_2$, while radioactive decay can serve to distinguish residence times of hundreds to tens of thousands of years. Dissolution of ^{14}C-dead carbonate sediments is another important source of DIC with a distinctive isotopic signature (Deines *et al.* 1974; Cheng 1992; Clark & Fritz 1997; Taylor 1997). The large dynamic range in $\Delta^{14}C$ from -1000‰ for ^{14}C-free materials to over 500‰ for carbon originating in the atmosphere from the late 1960s to early 1970s (Fig. 4.1) presents distinct advantages for separating carbon sources.

CO_2 dynamic equilibrium in rivers

Based on gas exchange and respiration observations, CO_2 (and dissolved oxygen) has been proposed to be in quasi steady state along the Amazon mainstem, such that CO_2 production by *in situ* respiration plus transport of recently respired CO_2 from floodplains are approximately balanced by evasion to the atmosphere ($-G \approx V \cdot R$, from eqtn. 4.27) (Devol *et al.* 1987; Richey *et al.* 1990). A dynamic equilibrium between respiration and gas exchange was supported by Quay *et al.* (1992), who

determined that the $\delta^{13}C$ of respired CO_2 (-22‰) is equal to that of CO_2 outgassing from the water surface. At the same time, downstream output fluxes of both DIC (Richey *et al.* 1990) and $\delta^{13}C$-DIC (Quay *et al.* 1992) at Obidos (Fig. 2.2) were found to be largely balanced by upstream and tributary fluxes at different mainstem reaches, throughout the year. At the Marchantaria site (Fig. 2.2), monthly observations over 10 years indicate that dO_2/dt is small relative to respiration or gas exchange rates, supporting a quasi steady state between these processes (Devol *et al.* 1995); however, CO_2 balance required an additional CO_2 input inferred to be advected in from flooded floodplains and originate in submerged C_3 root respiration.

DIC AND CO_2 IN SOILS AND GROUNDWATER

CO_2 and DIC in soils and groundwater originate primarily from biological respiration and weathering of carbonate and silicate minerals (Fig. 4.2). While carbonate and weatherable silicate lithologies are rare in the Amazon lowlands (Stallard & Edmond 1983; Stallard 1985), respiration by roots and heterotrophic decomposition of organic matter lead to high rates of CO_2 production and efflux from the soil surface (Davidson & Trumbore 1995; Davidson *et al.* 2000; Chambers *et al.* 2004; Goulden *et al.* 2004; Keller *et al.* 2004; Sotta *et al.* 2004). Weathering of carbonate and silicate lithologies by carbonic acid (CO_2) yields HCO_3^- that is transported to streams in groundwater (Stallard 1988; 1995; Clark & Fritz 1997; Jones & Mulholland 1998a; Telmer & Veizer 1999; Kump *et al.* 2000; Andrews & Schlesinger 2001; Bade *et al.* 2004).

Soil respiration and CO_2

Large soil respiration fluxes are the result of favorable conditions for commonly accepted environmental controlling factors, including generally high temperature, soil moisture, and biomass productivity (Raich & Potter 1995; Davidson *et al.* 1998; Davidson *et al.* 2000; Schlesinger & Andrews 2000; Wang *et al.* 2000; Amundson 2001; Savage & Davidson 2001; Raich *et al.* 2002; Reichstein *et al.* 2003). However, soil respiration represents the aggregation of multiple processes controlled by different factors; for example, autotrophic root respiration may experience seasonal variability different from that of heterotrophic respiration (Davidson & Trumbore 1995; Trumbore *et al.* 1995; Davidson *et al.* 2000; Hanson *et al.* 2000; Wang *et al.* 2000; Chambers *et al.* 2004; Sotta *et al.* 2004).

Observed annual soil respiration efflux in lowland Amazonian forests ranges from approximately 1 to 2 kg C m^{-2} yr^{-1} (Table 3 in Sotta *et al.* 2004). Maximum respiration occurs at medium levels of soil moisture, near field capacity, where microbial access to oxygen and soluble organic matter is optimal (Davidson *et al.* 1998; Davidson *et al.* 2000; Savage & Davidson 2001). At sites with well-drained soils and a prolonged dry season, particularly in eastern and southern regions of the basin, low dry-season soil moisture leads to reduction in soil respiration (Davidson & Trumbore 1995; Meir *et al.* 1996; Davidson *et al.* 2000; Keller *et al.* 2004; Salimon *et al.* 2004; Vasconcelos *et al.* 2004). In contrast, in the central Amazon near Manaus, where the dry season is more limited, soil respiration shows limited seasonal variability (Chambers *et al.* 2004). Higher soil moisture has been observed to inhibit respiration as a result of reduced diffusion of oxygen (Davidson *et al.* 2000; Chambers *et al.* 2004); this factor appears to produce lower soil CO_2 efflux in valley soils near Manaus, relative to slope and plateau soils (Chambers *et al.* 2004).

Seasonal variability of soil respiration in drier regions may be driven largely by microbial response to soil desiccation. Deep roots allow trees to extract water from deeper soil horizons and sustain primary production and respiration throughout the dry season, while the zone of maximal root CO_2 production may shift downward following receding soil water (Davidson & Trumbore 1995; Trumbore *et al.* 1995; Davidson *et al.* 2000; Goulden *et al.* 2004; Sotta *et al.* 2004). At the forested Paragominas site in the eastern Amazon, Davidson & Trumbore (1995) estimated that 20-30% of measured CO_2 surface flux is produced below 1 meter, while Trumbore *et al.* (1995) estimated that root respiration contributes 50-65% of the surface CO_2 flux; Chambers *et al.* (2004) obtained a similar estimate of root contribution to surface CO_2 flux near Manaus, excluding respiration from fine surface litter.

CO_2 dynamics within Amazonian forest soils has been studied extensively only at the Paragominas site, where concentration and ^{13}C and ^{14}C isotopes were analyzed down to a depth of 8 meters on multiple dates in the wet and dry seasons (Davidson & Trumbore 1995; Trumbore *et al.* 1995; de Camargo *et al.* 1999). pCO_2 increased with depth from about 15,000 ppm in the upper meter to nearly 80,000 ppm at 8 meter depth – more than 200 times atmospheric concentration. At the Cuieiras Reserve north of Manaus, Sotta *et al.* (2004) measured similar soil pCO_2 concentrations near the surface in a one-week period early in the wet season; pCO_2 increased from about 2,000 ppm at 1 cm depth to nearly 9,000 ppm at 40 cm. In a white sand (Spodosol) forested site at Campinas, north of Manaus, A. Aufdenkampe (pers. comm.) observed pCO_2 levels 100 times that of the atmosphere in soil water below the water table. Richey *et al.* (2002) used the soil CO_2 observations from Paragominas (Davidson & Trumbore 1995) together with estimates of lateral subsurface runoff and of the total length of low-order streams in the central Amazon

(derived from Chapter 3) to come up with a first-order estimate of the total flux of CO_2 from soils to streams. Nonetheless, the lateral transfer of DIC and CO_2 from soils to streams and subsequent fate of this terrestrial carbon in streams remain largely uninvestigated in the Amazon.

Sources and turnover times of organic matter fueling soil respiration have been studied using ^{13}C and ^{14}C isotopes of CO_2 and soil organic carbon (SOC). In Amazonian (14C-CO2 observations in Paragominas, Trumbore *et al.* 1995; de Camargo *et al.* 1999) as well as temperate (Gaudinski *et al.* 2000; Bowling *et al.* 2003; Fessenden & Ehleringer 2003) and boreal (Ekblad & Högberg 2001; Högberg *et al.* 2001) soils, CO_2 appears to originate primarily from root respiration of recently fixed metabolites and heterotrophic respiration of labile, fast-cycling SOC fractions (Trumbore 2000). Soil CO_2 is commonly no more than a few years old, even at depth (Trumbore *et al.* 1995; de Camargo *et al.* 1999; Gaudinski *et al.* 2000; Trumbore 2000; Wang *et al.* 2000), in contrast with bulk SOC which is generally greatly depleted in ^{14}C (Trumbore 1993; Trumbore *et al.* 1995; Pessenda *et al.* 1998a; Pessenda *et al.* 1998b; de Camargo *et al.* 1999; Gaudinski *et al.* 2000; Trumbore 2000; Freitas *et al.* 2001; Telles *et al.* 2003). In addition, Telles *et al.* (2003) showed that while SOC age increases rapidly with depth in clay-rich Ultisol and Oxisol soils in the Amazon, organic carbon in sandy stream valley Spodosols near Manaus remains young down to at least 50 cm depth.

Theoretical and field analyses have shown that diffusion of CO_2 in soils can lead to a ^{13}C fractionation of up to 4.4‰, such that CO_2 leaving the soil surface is depleted with respect to soil CO_2 (Dörr & Münnich 1980; Cerling *et al.* 1991; Aravena *et al.* 1992; Amundson *et al.* 1998; Amiotte-Suchet *et al.* 1999). However, at steady state $\delta^{13}C$ of CO_2 produced within soils will be the same as that of soil CO_2

efflux, assuming that downward export is insignificant (Cerling *et al.* 1991; Amundson *et al.* 1998). As soil $\delta^{13}C$-CO_2 observations in the Amazon are currently limited to Paragominas (Trumbore *et al.* 1995; de Camargo *et al.* 1999), where corresponding observations of $\delta^{13}C$-CO_2 efflux were not made, it is not possible to assess whether diffusion fractionation is a significant factor. Measurements of soil $\delta^{13}C$-CO_2 efflux in forests are also limited, but have been carried out at multiple sites; values range from –24.8‰ to –29.4‰ (Quay *et al.* 1989; Feigl *et al.* 1995; Buchmann *et al.* 1997; Ometto *et al.* 2002; Salimon *et al.* 2004). The soil CO_2 source is separated from atmospheric contributions using a simple mixing model, as the y-intercept of a $\delta^{13}C$-CO_2 vs. $1/[CO_2]$ plot ("Keeling plots", Pataki *et al.* 2003). Observations of total ecosystem respiration (aboveground + belowground) yielded a seasonal variability of about 4‰ at Santarem, where the dry season is prominent (Ometto *et al.* 2002); Manaus and a site in French Guiana did not show such isotopic variability (Buchmann *et al.* 1997; Ometto *et al.* 2002).

Heterotrophic soil respiration utilizes SOC to produce CO_2. However, SOC in forests that have not experienced substantial Quaternary land cover change typically is progressively enriched in ^{13}C down the soil profile by a few per mil in the tropics (Trumbore *et al.* 1995; Martinelli *et al.* 1996b; de Camargo *et al.* 1999; Powers & Schlesinger 2002; Telles *et al.* 2003; Salimon *et al.* 2004) and elsewhere (Amundson *et al.* 1998; Wang *et al.* 1998; Ehleringer *et al.* 2000; Poage & Feng 2004). The only exception to this ^{13}C depth trend in the Amazon occurs in Manaus Spodosols, where $\delta^{13}C$-SOC remains at ~ –29.5‰ all throughout the upper 50 cm (Telles *et al.* 2003). While the causes of the depth trend are not clear, they appear to be related to selective sorption of DOC and decomposition of organic matter (Amundson *et al.* 1998; Ehleringer *et al.* 2000; Aufdenkampe *et al.* 2001; Kaiser *et al.* 2001; Cleveland *et al.*

2004; Poage & Feng 2004). At Paragominas, $\delta^{13}C$-CO_2 also becomes enriched from –25.3‰ at the surface to –23.1‰ at 8 m depth, roughly paralleling the change in $\delta^{13}C$-SOC from –27.3‰ to –23.4‰ (Trumbore *et al.* 1995; de Camargo *et al.* 1999).

At sites where vegetation shifts between C_3 and C_4 dominance may have occurred, changes in the isotopic composition of SOC with depth have been exploited as a tool to examine organic carbon turnover times and determine past climate conditions using land cover types as proxies. In Amazonian lowlands, such studies have addressed Quaternary changes near contemporary forest-savanna boundaries, anthropogenic replacement of forest with C_4 pasture, and development of secondary forests after pasture abandonment (Desjardins *et al.* 1994; Trumbore *et al.* 1995; Martinelli *et al.* 1996b; Koutika *et al.* 1997; Neill *et al.* 1997; Bernoux *et al.* 1998; Pessenda *et al.* 1998a; Pessenda *et al.* 1998b; de Camargo *et al.* 1999; Freitas *et al.* 2001; Sanaiotti *et al.* 2002; Salimon *et al.* 2004).

Despite substantial advancements in our understanding of soil respiration and CO_2 dynamics, large uncertainties still exist, including the biochemical nature and isotopic composition of soil organic matter used by heterotrophs at different depths; the isotopic signature of CO_2 respired by roots at different depths; the role of DOC flux and sorption in supporting heterotrophic respiration down the soil profile (Kalbitz *et al.* 2000; Aufdenkampe *et al.* 2001; Neff & Asner 2001; Guggenberger & Kaiser 2003; Michalzik *et al.* 2003); and the flux, isotopic composition, age, seasonal variability, and controls on downward CO_2 export into groundwater, and subsequently into streams and rivers.

Weathering and DIC

Earlier (see Chapter 2 and the Introduction to this chapter) I reviewed the distribution of lithologies across the Amazon basin. Broadly, readily weatherable lithologies are rare in the lowlands but abundant in the Andean mountains, their depositional fans, and rivers and floodplains draining those regions (Stallard & Edmond 1983).

While evaporites dissolve readily, weathering of carbonate and silicate minerals proceeds through reaction with acids (Drever 1988). Dissolved CO_2 generated by biological activity in soils is the dominant acid involved in such weathering on land masses (Berner *et al.* 1983; Stallard & Edmond 1983; 1987; Drever 1988; Stallard 1988; Drever 1994; Gaillardet *et al.* 1999; Galy & France-Lanord 1999). Less common acid sources include CO_2 dissolved from air, from oxidation of kerogen (metamorphosed organic matter), and from volcanic or metamorphic lithospheric degassing; and sulfuric acid from oxidation of reduced sulfides such as pyrite, commonly found in black shale (e.g., Galy & France-Lanord 1999; Yoshimura *et al.* 2001).

Congruent dissolution of the carbonate mineral calcite with carbonic acid proceeds via the reaction:

$$CaCO_3(s) + CO_2 + H_2O = Ca^{2+} + 2HCO_3^- \qquad (4.33)$$

One mole of HCO_3^- originates from the mineral, while the other mole originates from dissolved CO_2. In contrast, all the HCO_3^- produced through incongruent weathering of aluminosilicate minerals originates from dissolved CO_2. For example, weathering of anorthite (a Ca-plagioclase feldspar) to kaolinite proceeds as follows:

$$CaAl_2Si_2O_8(s) + 2CO_2 + 3H_2O = Al_2Si_2O_5(OH)_4(s) + Ca^{2+} + 2HCO_3^- \qquad (4.34)$$

Weathering of the more stable albite aluminosilicate (a Na-plagioclase feldspar) to kaolinite proceeds as follows:

$$2NaAlSi_3O_8(s) + 2CO_2 + 3H_2O = Al_2Si_2O_5(OH)_4(s) + 2Na^+ + 4SiO_2 + 2HCO_3^- \quad (4.35)$$

Production of HCO_3^- during weathering increases DIC, alkalinity, and pH in soil and groundwater, with carbonate weathering proceeding faster and producing twice as much HCO_3^- as silicate weathering. Carbonate dissolution may advance to precipitation saturation with respect to carbonate minerals. Final DIC concentration and alkalinity reached are dependent on the openness of weathering sites to continual exchange with a large supply of soil CO_2 (Deines *et al.* 1974; Clark & Fritz 1997; Aucour *et al.* 1999). Open system conditions are dominant in the unsaturated soil zone and in saturated groundwater near the water table, while closed conditions are more common deeper in the aquifer. For silicates, a continued supply of CO_2 implies that weathering and production of HCO_3^- are limited only by weathering kinetics and availability of minerals. For carbonates, dissolution under open conditions will result in equilibrium saturation at higher DIC and alkalinity, and lower pH, compared to dissolution in a closed system, and high pCO_2 will persist (Deines *et al.* 1974; Clark & Fritz 1997). Weathering typically involves both open and closed systems, or partially open conditions (Deines *et al.* 1974; Cheng 1992; Clark & Fritz 1997; Taylor 1997; Aucour *et al.* 1999).

The isotopic composition of DIC resulting from weathering is strongly dependent on weathering regime and the origin of CO_2 used as the acid. Factors controlling the variability of soil CO_2 carbon isotopes in the Amazon basin and elsewhere were discussed earlier. As DIC from silicate weathering originates from the source CO_2 only, its isotopic composition reflects that of soil CO_2 and, for $\delta^{13}C$, the equilibrium fractionation between $CO_2(g)$ and HCO_3^- that results in an enrichment

of 7-10‰ (see discussion above). Carbonates of marine sedimentary origin are ^{14}C-free ($\Delta^{14}C$ = -1000‰) and have a ^{13}C content similar to the PDB standard ($\delta^{13}C \approx 0\pm2$‰) (Clark & Fritz 1997; Bullen & Kendall 1998; Aucour *et al.* 1999; Zeebe & Wolf-Gladrow 2001; Gonfiantini & Zuppi 2003). In a fully closed system the isotopic composition of HCO_3^- produced will reflect a 1:1 mixture of carbon from CO_2(g) and carbonates; for $\delta^{13}C$, additional factors include equilibrium fractionation between CO_2(g) and HCO_3^-, (at T = 25°C, $\varepsilon_{HCO3\text{-}g}$ = 7.9‰; see above) and a small enrichment during mineral dissolution to HCO_3^- ($\varepsilon_{CaCO3\text{-}HCO3}$ = -1.1‰ for calcite at T = 25°C) (Zhang *et al.* 1995; Clark & Fritz 1997); for example, calcite with $\delta^{13}C$ = 0‰ weathering in a closed system at T = 25°C with carbonic acid dissolved from C_3 soil CO_2(g) with $\delta^{13}C$ = -27‰ and $\Delta^{14}C$ = 110‰ (estimated 1996 atmospheric $\Delta^{14}C$-CO_2 in tropical South America; see discussion above) will produce HCO_3^- with $\delta^{13}C$ = 0.5*[(0+1.1) + (-27+7.9)] = -9.0‰ and $\Delta^{14}C$ = 0.5*[-1000 + 110] = -445‰. In contrast, weathering in a fully open system will involve continual isotopic exchange with CO_2(g), and the isotopic composition of DIC will reflect equilibrium with CO_2(g) (Deines *et al.* 1974; Cheng 1992; Clark & Fritz 1997; Taylor 1997; Aucour *et al.* 1999). As carbonate weathering typically occurs in partially open systems, the isotopic signature of DIC will fall between those two end members. Extensive research has been published on field conditions during carbonate weathering in soils and aquifers, and the resulting DIC and isotopic behavior (e.g., Bullen & Kendall 1998; Aucour *et al.* 1999; Taylor *et al.* 2001; Yoshimura *et al.* 2001; Emblanch *et al.* 2003; Gonfiantini & Zuppi 2003; Yoshimura *et al.* 2004). However, I am not aware of any similar studies in the Amazon basin or the Andean region focusing on the isotopic composition of carbonate minerals, environmental conditions during

weathering, or DIC isotopic composition in deep aquifers or the near-stream subsurface.

Interest in more comprehensive understanding of weathering is increasing (Anderson *et al.* 2004). Factors that control rates of chemical erosion have been examined in several reviews using data from lab experiments, soil sites, streams draining small, monolithological watersheds, and large rivers (Berner *et al.* 1983; Bluth & Kump 1994; White & Blum 1995; Berner & Berner 1997; Edmond & Hu 1997; Gaillardet *et al.* 1999; Kump *et al.* 2000), though conflicting results are often observed between small-scale experiments and large-scale observations (Kump *et al.* 2000). Common large-scale controls include temperature, rainfall, runoff, lithology, and tectonics, including topographic relief. Such information has been synthesized as empirical models that predict the flux of alkalinity and bicarbonate into rivers and oceans, and weathering CO_2 consumption, based on spatially distributed climate and lithological data (Amiotte-Suchet & Probst 1993; 1995; Gibbs *et al.* 1999; Aumont *et al.* 2001; Munhoven 2002; Amiotte-Suchet *et al.* 2003); applications have ranged from regional to global scale, and contemporary, future, and past climate conditions.

Globally averaged models like BLAG (Berner *et al.* 1983) and GEOCARB (Berner & Lasaga 1989; Berner 1991; 1994; Berner & Kothavala 2001) have been applied to characterize the global carbon cycle throughout the Phanerozoic. At long time scales, over millions of years, consumption of CO_2 during carbonate dissolution is balanced by re-release during carbonate precipitation in the oceans, with no net effect on atmospheric CO_2; in contrast, continental weathering of Ca and Mg silicates consumes atmospheric CO_2 and exports Ca and Mg cations and bicarbonate from rivers to oceans, leading to long-term sequestration via precipitation of carbonate sediments, and large impacts on atmospheric CO_2 and climate (Berner *et al.* 1983;

Berner & Lasaga 1989; France-Lanord & Derry 1997; Broecker & Sanyal 1998; Berner 1999; Kump *et al.* 2000; Berner 2003; Cohen *et al.* 2004; Royer *et al.* 2004). Studies of long-term weathering have generated controversy over the relative role of temperature, lithology, and tectonics in controlling the variability of chemical erosion and therefore its impact on atmospheric CO_2 and climate (Berner & Berner 1997; Edmond & Hu 1997; France-Lanord & Derry 1997; Ruddiman 1997; Ruddiman *et al.* 1997; Broecker & Sanyal 1998; Kump *et al.* 2000). Further studies addressing the scaling of weathering processes from sites to continents, and fluxes to rivers, will be invaluable for improving our understanding of both short and long-term controls on atmospheric CO_2 (Anderson *et al.* 2004).

CONCLUSIONS

Carbon plays a critical role in river ecosystems. Improved understanding of DIC and CO_2 sources and cycling in Amazonia will result in enhanced capability to manage local impacts of deforestation and quantify regional CO_2 budgets. ^{13}C and ^{14}C isotopes of DIC are invaluable tools for addressing such issues. However, the use of ^{13}C-DIC in Amazonia has been limited to the mainstem and surrounding riverine environments, while ^{14}C-DIC has never been used before. In this chapter I present an overview of DIC and carbon isotope geochemistry. Focusing on the mass balance of a river reach, I examine the biological, physical, and geological processes and sources that impact DIC and its carbon isotopes in rivers. This quantitative framework and the review of previous relevant research in rivers, soils, and groundwater in the Amazon basin and elsewhere provide the necessary background for discussion of the basin wide survey presented in the next two chapters, and for future synthesis and modeling work.

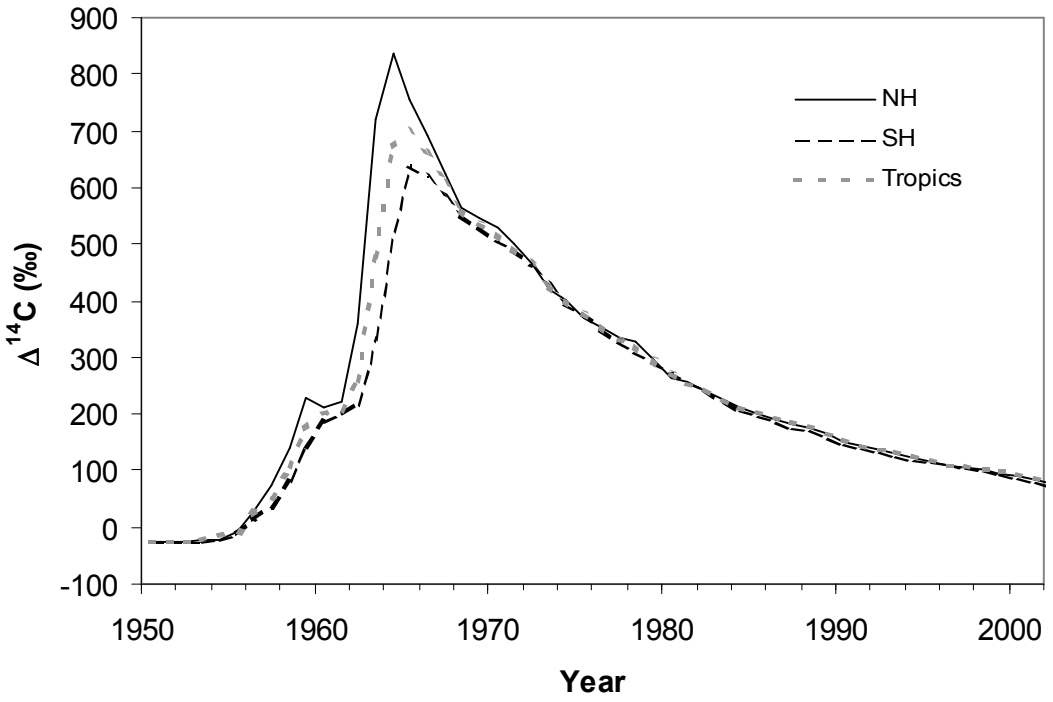

Figure 4.1. Hemispheric trends in tropospheric $\Delta^{14}C$-CO_2 since 1950. Data represent annual means for the Tropics (30 ^{o}N to 30 ^{o}S) and extratropical Northern Hemisphere (NH) and Southern Hemisphere (SH), from I. Levin (pers. comm.). See Chapter 5 for additional discussion of seasonal and latitudinal variability.

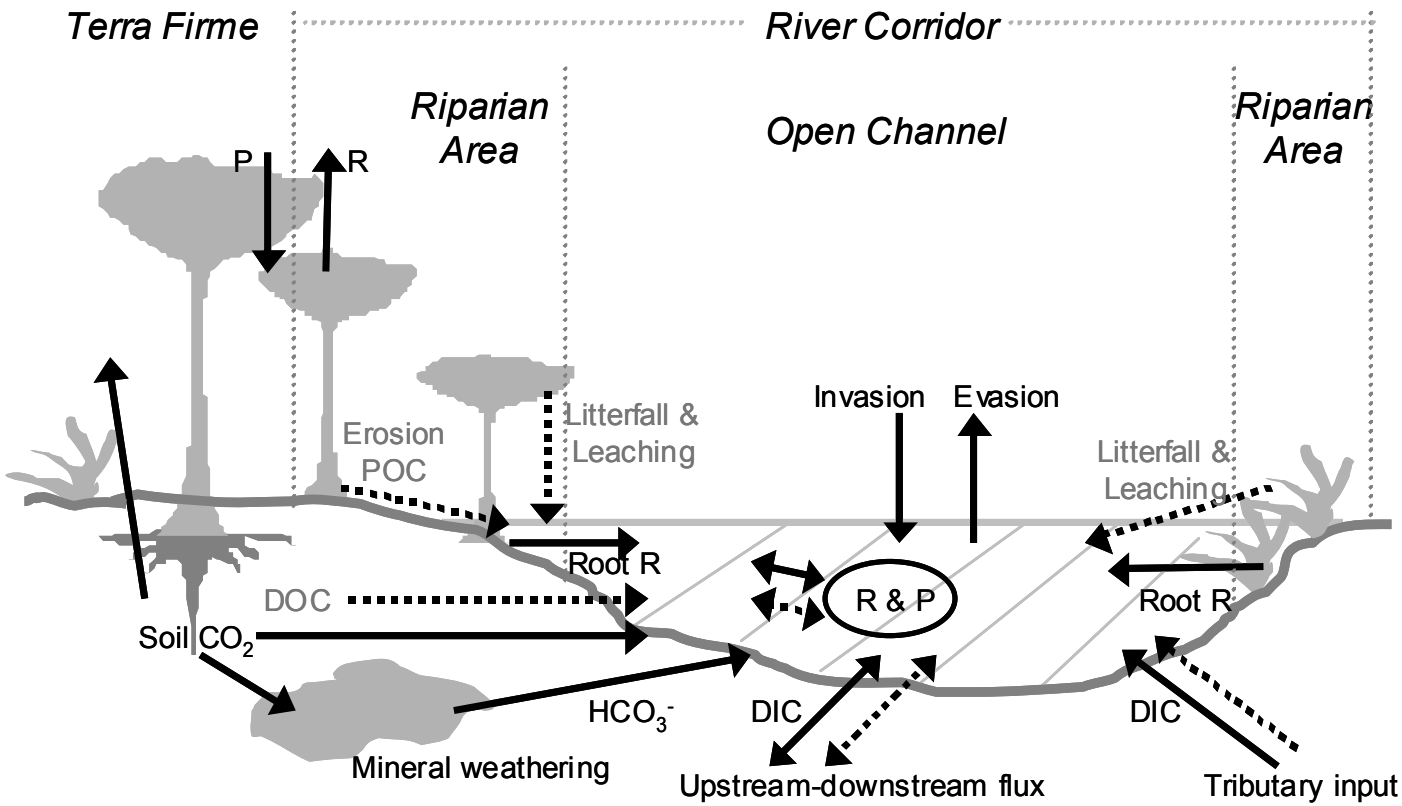

Figure 4.2. Sources and cycling of carbon in a river, its corridor, and the adjacent *terra firme* area. Solid arrows represent inorganic carbon fluxes in the form of CO_2, except as noted. Dotted arrows represent organic carbon fluxes in the form of total OC (POC + DOC), except as noted. R and P are heterotrophic respiration and photosynthesis (net primary production), respectively. Organic carbon fluxes are described using gray text. Vegetation types shown include trees (C_3 photosynthetic pathway) and macrophytes + pastures (predominantly C_4 but also C_3).

CHAPTER 5. RESPIRATION OF CONTEMPORARY ORGANIC MATTER DRIVES OUTGASSING OF CO_2 FROM AMAZONIAN RIVERS

INTRODUCTION

Rivers in humid tropics were recently shown to outgas CO_2 at much higher rates than previously appreciated, with evasion fluxes in Amazonian rivers (0.5 Pg C yr^{-1}) more than 10 times the exports to the ocean as total organic carbon (OC) or dissolved inorganic carbon (DIC) (Richey *et al.* 2002). However, little agreement exists about sources of CO_2, and the few direct estimates of respiratory source age range from contemporary to thousands of years (Cole & Caraco 2001; Raymond & Bauer 2001a; Raymond & Hopkinson 2003). Rivers are predominantly supersaturated with respect to CO_2, resulting in large gas evasion fluxes that can be a significant component of regional net carbon budgets (Cole & Caraco 2001; Hope *et al.* 2001; Richey *et al.* 2002). In the Amazon basin lowlands, riverine CO_2 concentrations are generally 5-30 times supersaturated with respect to atmospheric equilibrium (Richey *et al.* 2002), and such conditions are likely to be prevalent throughout the humid tropics. Dissolved CO_2 in excess of equilibrium concentrations set by weathering reactions originates predominantly from *in situ* respiration and inputs of groundwater supersaturated from soil respiration, and in some cases direct CO_2 input from submerged root respiration by riparian vegetation (Quay *et al.* 1992; Jones & Mulholland 1998a; Cole & Caraco 2001; Mulholland *et al.* 2001). Except at low supersaturation levels, atmospheric CO_2 invasion has a negligible role compared to the large CO_2 evasion fluxes (Quay *et al.* 1992; Jones & Mulholland 1998a; Cole & Caraco 2001; Mulholland *et al.* 2001). In turn, the importance of groundwater CO_2 inputs decreases downstream of small streams as a result of evasion and replacement by *in situ* respiration fluxes (Jones & Mulholland 1998a; Mulholland *et al.* 2001).

Despite the fundamental role of *in situ* respiration for riverine CO_2 cycling, sources and turnover times of organic carbon fueling respiration remain poorly constrained. Stable and radio- carbon isotope (^{13}C and ^{14}C) data can provide such constraints, yet no previous study has used a dual-isotope approach to address these questions in tropical regions. Isotope studies in eastern USA temperate rivers appear to offer, at first glance, conflicting findings. In the Hudson River, up to 70% of the centuries-old terrestrial OC entering the river is respired in transit, and the average age of riverine OC decreases downstream (Cole & Caraco 2001). On the other hand, in the York River, the youngest components of dissolved OC (DOC) are preferentially respired (Raymond & Bauer 2001a). One study that comprehensively interpreted dissolved inorganic carbon radioisotope data in the Parker River estuary found modern DIC that could be explained by respiration of DOC produced within the estuary (Raymond & Hopkinson 2003). In the Amazon mainstem, indirect evidence suggests a large source of respired CO_2 from rapidly cycling, uncharacterized OC fractions (Quay *et al.* 1992; Waichman 1996; Devol & Hedges 2001; Melack & Forsberg 2001; Richey *et al.* 2002). Reconciling these results is critical to advance our understanding of CO_2 outgassing from rivers and its role in regional to continental net carbon balance under natural and perturbed conditions.

METHODS

Sample collection and analysis

Samples analyzed for ^{14}C-DIC were collected between 1991 and 2003, whereas ^{14}C-OC samples are from 1995-1996 (Table 5.1). Samples were collected at mid depth from the deepest section of the channel (the thalweg). DIC samples were obtained from a Niskin bottle by overfilling (2x) 250 mL glass bottles from the

bottom, preserving with $HgCl_2$ and immediately capping with a greased ground glass stopper (Quay *et al.* 1992). CPOC (63-2000 μm) was isolated either by sieving pump outflow or with a plankton net. FPOC (0.1-63 μm) was isolated by tangential flow microfiltration and DOC (1000 atomic mass units to 0.1 μm) by tangential flow ultrafiltration followed by freeze drying (Hedges *et al.* 2000). Ultrafiltration yields ranged from 40% in the Andes up to 80% in the lowlands (Hedges *et al.* 2000; Aufdenkampe *et al.* submitted). In the lab, the top half of DIC samples was drawn into a vacuum line (eliminating particles) and stripped of CO_2 after acidification (Quay *et al.* 1992). Organic samples were combusted with CuO in evacuated, sealed quartz tubes (Quay *et al.* 1992).

Purified CO_2 was analyzed for stable isotopes and radiocarbon by dual-inlet isotope ratio mass spectrometry (IRMS) and Accelerator Mass Spectrometry (AMS) (Vogel *et al.* 1987), respectively. ^{13}C is reported in the conventional $\delta^{13}C$ delta notation vs. the Pee Dee Belemnite (PDB) standard (Clark & Fritz 1997). Radiocarbon values are reported as age-corrected $\Delta^{14}C$ adjusted for sample $\delta^{13}C$ (Stuiver & Polach 1977). Absolute $\Delta^{14}C$ and $\delta^{13}C$ analysis errors (1σ) are typically <6‰ and <0.2‰, respectively. Isotopes for all carbon fractions were not always analyzed at each site. A few sites were analyzed more than once for ^{14}C, in different years.

Additional analyses include, in most cases, pH, major ions, alkalinity, and total carbon fraction concentrations (Table 5.2). Major ions were quantified by ion chromatography. Alkalinity was measured by Gran titration, or estimated from temperature, pH, and DIC when not measured. CO_2 concentrations were either measured directly by headspace equilibration (Aufdenkampe, manuscript in preparation) or estimated from temperature, pressure, pH, DIC, and alkalinity.

Radiocarbon trends in atmospheric CO_2

Measurements from Schauinsland Station, Germany, were used to characterize atmospheric $\Delta^{14}C\text{-}CO_2$ from 1991 to 2003 (Levin & Hesshaimer 2000; Levin & Kromer in press). The uncharacterized effect of seasonal and short-term atmospheric variability is minimized by comparing river ^{14}C only against time-weighted annual means (Levin & Kromer in press). A constant +8‰ offset was added to Schauinsland annual means to account for a 5‰ depletion from regional fossil-fuel emissions at Schauinsland relative to the well-mixed, mid-latitude European troposphere (Jungfraujoch site, Levin & Kromer in press), and approximately 3‰ further depletion at the mid-latitude troposphere relative to tropical South America (Levin & Hesshaimer 2000; Randerson *et al.* 2002). The resulting estimated annual atmospheric $\Delta^{14}C\text{-}CO_2$ values from 1991 to 2003 are 144.2, 139.0, 131.3, 125.4, 119.1, 110.4, 107.7, 104.5, 97.2, 94.2, 87.2, 80.0, and 74.4‰. Atmospheric $\Delta^{14}C\text{-}CO_2$ composition within the Amazon basin is unknown, but seasonal and regional variability may be as large as 10‰ (Randerson *et al.* 2002). Riverine $\Delta^{14}C$ values within 5‰ of my estimated atmospheric annual average for the sampling year likely represent carbon turnover times of one year or less.

Results and Discussion

To identify dominant sources and turnover times of riverine carbon throughout the Amazon basin, I analyzed ^{14}C and ^{13}C signatures of DIC, DOC, and suspended fine and coarse particulate OC fractions (FPOC and CPOC). Samples were collected on multiple expeditions from a diverse set of lowland and mountain rivers (Fig. 5.1, Table 5.1). While DIC is composed of several species in solution ($CO_2(aq)$, $HCO_3^-(aq)$, and $CO_3^{2-}(aq)$), respiration, autochthonous photosynthesis, gas

exchange, and other important processes interact with DIC primarily through exchange of CO_2 gas. Isotopic fractionation occurs during conversion from one carbonate species to another (Clark & Fritz 1997). Thus, to facilitate the direct interpretation of CO_2 sources, I base my analysis on the isotopic composition of CO_2 gas in thermodynamic equilibrium with bulk DIC (Fig. 5.2, Table 5.3). $\delta^{13}C\text{-}CO_2(g)$ is calculated from measured $\delta^{13}C$-DIC and isotopic equilibrium fractionations between DIC species, which are in turn dependent on pH and temperature (Zhang *et al.* 1995; Clark & Fritz 1997). $\Delta^{14}C$ is unaffected because this term is defined to be insensitive to mass-dependent fractionation (Stuiver & Polach 1977); $\Delta^{14}C\text{-}CO_2(g)$ is the same as $\Delta^{14}C$-DIC. This survey represents the most extensive dual-isotope carbon inventory published to date over a wide variety of rivers from a single large-scale basin, allowing a unique, integrated assessment of carbon cycling throughout a river network. This dataset is also the first reported ^{14}C analysis on DIC in Amazonian rivers, and complements but greatly exceeds previous surveys of ^{14}C of OC fractions (Hedges *et al.* 1986b; Raymond & Bauer 2001a). It provides multiple lines of isotopic evidence that a rapidly cycling, contemporary OC subfraction fuels respiration and sustains CO_2 supersaturation and evasion across most mid-size to large Amazonian rivers.

The first evidence for this assertion is that dissolved CO_2 gas in nearly all lowland rivers has a $\Delta^{14}C$ signature bound within the atmospheric $\Delta^{14}C\text{-}CO_2$ composition range for the lowland DIC sampling period (1996-2003, Fig. 5.2, Table 5.3). Testing of thermonuclear bombs in the 1950s and 1960s resulted in a large increase in atmospheric $^{14}CO_2$, reaching a peak in the late 1960s and steadily decreasing afterwards (Levin & Hesshaimer 2000; Randerson *et al.* 2002). Continual change in atmospheric radiocarbon content necessitates that I assess mean age for

modern carbon (post 1890, Stuiver & Polach 1977) through the offset between each riverine $\Delta^{14}C$ value and the annually averaged atmospheric $\Delta^{14}C$-CO_2 for the corresponding sampling year (Levin & Kromer in press). For sites with repeated measurements over time, the need for considering the atmospheric offset rather than the absolute $\Delta^{14}C$-CO_2 is clear (Fig. 5.3). From 1996 to 2003, riverine $\Delta^{14}C$-CO_2 at each of four supersaturated sites in mid to large rivers within two lowland basins decreased by 32-41‰, equivalent to the annually averaged atmospheric $\Delta^{14}C$-CO_2 decrease of 36‰ (110.4 to 74.4‰, or -5.6±2.3‰ yr^{-1}) (Fig. 5.3). Thus, atmospheric offsets remained roughly constant, suggesting persistent and constant respiratory OC turnover times for each basin. Furthermore, the range of these offsets suggests that CO_2 outgassing from these rivers was photosynthetically sequestered from the atmosphere <4 years previously within the mid-sized Rio Ji-Parana basin (sites 24, 25 & 28; $\Delta^{14}C$ offsets of 13±6‰, n=8) and 4-7 years previously at the mouth of the Rio Negro (site 32; $\Delta^{14}C$ offsets of 29±9‰, n=3).

The rapid carbon turnover observed within these lowland river sites is also likely to be typical in the broad survey of rivers throughout the Amazon. However, demonstrating this requires first assessing the influence of carbonate weathering on river geochemistry. Such weathering is a source of high DIC concentrations enriched in $\delta^{13}C$ and with $\Delta^{14}C$ as low as -500‰ when, as is most common, it involves the dissolution of ^{14}C-dead carbonate minerals (Fig. 5.2) by carbonic acid (CO_2) from respired modern plant matter in soils through the dissolution reaction $CaCO_3(s) + CO_2(aq) + H_2O = Ca^{2+}(aq) + 2HCO_3^-(aq)$ (Fig. 5.2). I used the relative proportion of silica, alkalinity, and major anion concentrations to identify sites draining substantial carbonate lithologies (Stallard & Edmond 1983) (Fig. 5.4). This approach identifies all mountain and mixed sites, and five lowland sites from the Guaporé, Purus, and

Juruá headwaters and the Juruá mouth (Fig. 5.1, sites 10, 41, 42, 43 & 45), as rivers strongly or potentially influenced by carbonate dissolution. The remaining 25 lowland sites (38 samples, including those presented in Fig. 5.3) have little potential for direct carbonate mineral contributions to DIC and contain dissolved CO_2 that is predominantly contemporary (Tables 5.3 & 5.4, Fig. 5.2).

Carbonate-free lowland sites can be roughly divided into two groups based on their radiocarbon offset relative to atmospheric CO_2. Rivers in the largest group (32 samples from 21 sites) range from first-order streams to one of the largest rivers in the world (Rio Negro), yet all carry contemporary CO_2(g) with atmospheric $\Delta^{14}C$-CO_2 offsets ranging from -3 to +37‰ (mean 13±11‰), indicating a mean CO_2 age of approximately 2 years, and <5 years in 74% of the observations. In rivers from the Ji-Parana region, relatively low supersaturation (pCO_2 = 1530±930 ppm, n=13) and enriched $\delta^{13}C$-CO_2 (-17.5±2.2‰, n=21) suggest that atmospheric invasion could be a significant source of CO_2. Invasion of atmospheric CO_2 (pCO_2 approx. 370 ppm and $\delta^{13}C$ approx. -8‰) (Clark & Fritz 1997; Levin & Hesshaimer 2000; Randerson *et al.* 2002) should lead to an inverse correlation between $\delta^{13}C$-CO_2 and pCO_2. The absence of such correlation in the Ji-Parana indicates that while atmospheric invasion can not be ruled out, it is likely a relatively small CO_2 source. Finally, the second group of carbonate-free sites consists of 6 samples in 3 streams (sites 22, 29 & 31) and 2 mid-sized rivers (sites 6 & 7) in the Brazilian Shield in the Ji-Parana region that have considerable negative $\Delta^{14}C$ offsets (-67 to -11‰, mean -32±21‰), indicating mean source age of several decades. Relatively depleted $\delta^{13}C$-CO_2 values (-20.0±1.7‰) compared to those in generally larger rivers from the first group in the Ji-Parana region suggest that these streams may be dominated by groundwater influx of aged soil CO_2 with a significant terrestrial C_3 plant source.

Previous studies in the highly supersaturated Amazon mainstem have indicated the existence of a quasi steady state between evasion and *in situ* respiration with respect to CO_2 and $^{13}CO_2$ fluxes (Devol *et al.* 1987; Quay *et al.* 1992; Devol *et al.* 1995); $\delta^{13}C$ of CO_2 evading from the river is the same as that produced during respiration (Quay *et al.* 1992), while tributary DIC and ^{13}C-DIC inputs account for mainstem downstream changes (Devol *et al.* 1987; Richey *et al.* 1990; Quay *et al.* 1992). Data to enable a similar determination are insufficient for carbonate-free lowland rivers in this study. Nonetheless, with the exception of Ji-Parana headwaters (sites 28-31), the downstream rate of change of DIC isotopes is relatively small (see Chapter 6). In addition to that trend, high respiration rates (A. Krusche and A. Aufdenkampe, unpublished data) and CO_2 supersaturation (Table 5.2) coupled with evidence for a likely small role for atmospheric CO_2 invasion, together suggest that dynamic equilibrium between evasion and respiration with respect to CO_2, $^{13}CO_2$, and $^{14}CO_2$ is a reasonable, though tentative, first-order assumption in these systems. The implication is that $\delta^{13}C$ and $\Delta^{14}C$ of evaded CO_2 gas should be equivalent to the isotopic signature of respired OC.

CO_2 in carbonate-free rivers is generally isotopically distinct from the associated OC fractions (DOC, FPOC, and CPOC; Table 5.3, Fig. 5.2). A $\Delta^{14}C$ comparison of CO_2 against OC fractions at the 5 carbonate-free sites where CO_2 and at least two OC fractions were measured concurrently (Table 5.3, 1996 samples from sites 6, 24, 28, 32 & 40) yields mixed results. CO_2 is considerably younger than DOC (the primary OC fraction) in 2 out of 3 observations, but is undistinguishable from FPOC ($\Delta^{14}C$-CO_2 = 122±15‰ vs. $\Delta^{14}C$-FPOC = 129±11‰, n=5); in these rivers, FPOC on average makes up only ¼ of total OC and is characterized by low fine

suspended sediment (FSS) concentrations and high %weight (Table 5.2). CPOC is also older than CO_2 but makes up a very small fraction of total OC.

While the above CO_2-OC $\Delta^{14}C$ comparison is limited, it can be extended first with samples from the Rio Negro mouth and several small Negro streams where DIC and DOC samples were collected 7 years apart (Table 5.3, 2002 vs. 1995, sites 32, 33, 34, 37, 38, 39). OC in these clear and blackwater rivers is strongly dominated by DOC (Table 5.2). Comparing $\Delta^{14}C$ offsets against sampling year atmospheric $\Delta^{14}C$-CO_2, the DOC offset (62±66‰, n=8) is 3 times the CO_2 offset (19±12‰, n=8). While the difference in the means is not statistically significant ($p = 0.0894$), high DOC variance is largely the result of one outlier with an even larger atmospheric offset of 216‰. Excluding this value to reduce the variance yields a DOC offset of 40±25‰ and a marginally significant difference with respect to the CO_2 offset ($p = 0.0500$). Second, $\Delta^{14}C$-OC in lowland samples potentially influenced by carbonates (Table 5.3, 1996 samples from sites 10, 41, 43 & 45) is characterized by a similar DOC atmospheric $\Delta^{14}C$ offset of 72±64‰ (n=4). The FPOC offset (-80±35‰, n=4) indicates substantial aging at these sites which, except for the Guapore (site 10), are characterized by high FSS and low %weight FPOC values comparable to the Amazon mainstem (Table 5.2, see Hedges *et al.* 1986a). Therefore, while scatter is substantial, DOC – the dominant lowland OC fraction – is generally just under a decade in age; in carbonate-free lowland systems, DOC is older than CO_2. FPOC represents a more heterogeneous but less important component of total OC.

Carbonate-free lowland $\delta^{13}C$-CO_2 is generally enriched with respect to all OC fractions (Tables 5.3 & 5.4, Fig. 5.2). The separation for coincident samples is over 8‰ (Table 5.3), with $\delta^{13}C$-CO_2 = -20.1±3.5‰ (n=5), $\delta^{13}C$-DOC = -28.7±1.5‰ (n=3), $\delta^{13}C$-FPOC = -29.2±2.3‰ (n=5), and $\delta^{13}C$-CPOC = -28.4±0.9‰ (n=3). For Rio

Negro basin DIC and DOC samples collected 7 years apart, $\delta^{13}C\text{-}CO_2$ = -25.2±0.9‰ (n=8) and $\delta^{13}C$-DOC = -29.2±0.1‰ (n=8). ^{13}C separation between CO_2 and OC is smallest in the Rio Negro basin, where C_4 grasses are rare, and largest in the Ji-Parana basin, where deforestation has led to widespread replacement of forest by C_4 pastures, even along stream corridors (Bernardes *et al.* 2004). Lowland $\delta^{13}C$-OC observations in this study are similar to those obtained previously (Hedges *et al.* 1986a; Quay *et al.* 1992; Bernardes *et al.* 2004).

I conclude that *in situ* respiration is fueled in large part by an organic subfraction that cycles on the order of <5 years and is typically a small component of the total riverine OC load. This subfraction is younger and enriched in ^{13}C compared to bulk OC. Riparian and floodplain C_4 grasses, when present, may play a disproportionate role in fueling river respiration relative to C_3 contributions (Quay *et al.* 1992; Waichman 1996; Melack & Forsberg 2001). Direct CO_2 input from respiration of submerged tree and grass roots may be important at high waters (Devol *et al.* 1995), but is likely insignificant in my samples because they were predominantly collected during low water. Submerged grasses were present only in certain small Ji-Parana streams (sites 22 & 23).

Mountain and mixed river sites contain older dissolved CO_2 ($\Delta^{14}C$ = 96 to -749‰, Fig. 5.2) resulting in large part from carbonate mineral dissolution. Although the dissolution of carbonates increases DIC, it also increases pH, which in turn decreases dissolved free CO_2 concentrations and reduces evasion fluxes. Thus, while carbonate dissolution has a large impact on the isotopic signature of evaded CO_2, it can not be the main driver of outgassing. Observed CO_2 supersaturation must be maintained by a continuous flux of CO_2 from OC respiration or other CO_2 sources. These fluxes and the resulting CO_2 outgassing will gradually flush out DIC originally

exported from carbonates in terrestrial settings, replacing its isotopic signature with that of the new CO_2 source. Indeed, a CO_2 trend of increasing $\Delta^{14}C$ and decreasing $\delta^{13}C$ is observed from the Andes down to the mainstem Amazon (Fig. 5.2). However, this flushing is not rapid. In the mainstem of the forested middle and lower Ucayali basin, major ion geochemistry indicates that carbonate dissolution remains a dominant source of DIC from the Andean foothills to the sedimentary lowlands nearly 2000 km downstream (Stallard & Edmond 1983) (from site 56 to site 48, Figs. 5.1 & 5.4); consequently, $\Delta^{14}C$-CO_2 remains substantially depleted (-138‰ at downstream site 48) despite likely high respiratory inputs that steadily increase CO_2 concentrations from 560 to 3150 ppm (Table 5.2). Over the next 2000 km downstream (from site 48 to site 1) carbonate sediments become less prevalent and respired CO_2 gradually flushes out aged DIC, as observed in $\Delta^{14}C$-CO_2 increases from approximately -168‰ to 49‰, still below contemporary atmospheric $\Delta^{14}C$ levels. Therefore, all along the middle-lower Ucayali and western-central mainstem, inputs of young CO_2 from *in situ* respiration and tributary inflow drive large gas evasion fluxes of aged CO_2 originating from carbonate dissolution; partitioning of DIC from HCO_3^- to CO_2(aq) due to lower pH may be a significant CO_2 source only near the central mainstem (Table 4.2). In contrast, in the more arid Vilcanota river in the Ucayali headwaters above 3000 meters (sites 57, 58 & 59, Figs. 5.1 & 5.2), highly depleted $\Delta^{14}C$-CO_2 (< -500‰), enriched $\delta^{13}C$-CO_2 (~ -11‰), and substantial CO_2 supersaturation suggest that solid earth degassing is a large source of CO_2 at baseflow (dry season). While widely documented in other young, tectonically active mountain ranges (Kerrick 2001), this is the first time this process is reported at a large scale in the Andes outside active volcanic areas (Aravena & Suzuki 1990); its importance to other Andean rivers and during other seasons is unknown.

Control of respiration by a small fraction of OC does not imply that the bulk OC is unreactive. On the contrary, I find that measured OC fractions are mineralized all throughout the river system. The strongest line of evidence is that FPOC becomes generally younger and more depleted in ^{13}C as it moves downstream from mountain sites (Fig. 5.2, Table 4.4), where all OC fractions mirror the high altitude ^{13}C enrichment in plants of approximately 1‰ per 1000 m of elevation gain (Körner *et al.* 1991; Hedges *et al.* 2000). Within 1000 km from the mountain headwaters in the Ucayali above the Amazon mainstem (Fig. 1), $\delta^{13}C$-FPOC looks like lowland carbon. Given that FPOC is tightly associated with mineral surfaces (Hedges *et al.* 2000; Aufdenkampe *et al.* 2001) and that over 85% of the mineral load in the Amazon mainstem ultimately originates in the Andes (Gibbs 1967), this observation implies nearly complete mineralization of old Andean FPOC on transit in the river or during long-term flooplain storage; riverborne Andean FPOC is replaced with OC fixed in lowland ecosystems, possibly remobilized through erosion of floodplain sediments (Quay *et al.* 1992) (Tables 5.3 & 5.4). CPOC and DOC descending from the Andes follow identical trends of gradual ^{13}C depletion to lowland values (Fig. 5.2), although simple dilution by lowland OC can not be ruled out. DOC is generally modern (<50 years old) everywhere (Table 5.4, Fig. 5.2), demonstrating that old DOC does not escape from the basin. Exceptions do occur at two $\Delta^{14}C$-depleted mountain sites (sites 52 & 59) where algal fixation of old, $\delta^{13}C$-enriched DIC originating in carbonate dissolution is the likely DOC source (Aufdenkampe *et al.* submitted).

Organic and inorganic carbon fractions interact closely in river systems. However, in the Amazon basin, despite evidence for the mineralization of the OC load, bulk OC appears to operate on slower time scales compared to respiratory processes affecting DIC. ^{14}C and ^{13}C evidence for dominance of respiration fluxes by

a rapidly cycling, typically small fraction of total OC confirms the hypothesis posited in the Amazonian mainstem from previous respiration (Devol & Hedges 2001; Melack & Forsberg 2001), stable isotope (Quay *et al.* 1992; Waichman 1996), and mass balance studies (Quay *et al.* 1992; Richey *et al.* 2002). These findings may reconcile the apparently contradictory conclusions from radiocarbon studies from temperate systems (Cole & Caraco 2001; Raymond & Bauer 2001a; Raymond & Hopkinson 2003) through use of a framework where consumption or replacement of old fractions in bulk OC occurs in parallel with high rates of respiration of a highly labile OC subfraction. This paradigm has also been proposed for soils (Trumbore *et al.* 1995; Gaudinski *et al.* 2000; Trumbore 2000), providing strong conceptual linkage between aquatic and terrestrial carbon dynamics (Grimm *et al.* 2003). It suggests that deforestation in Amazonia may lead to immediate changes to the organic sources of river respiration, particularly when riparian forests are replaced by pasture, and argues that such impact is not inconsistent with the apparent lag times observed on bulk OC composition after deforestation (Bernardes *et al.* 2004). CO_2 evading from mid to large lowland rivers is largely contemporary, while in small streams the age of CO_2 ranges from contemporary to a few decades. When carbonate outcrops are present in the watershed, pumping of CO_2 from *in situ* respiration will drive outgassing of ^{14}C-depleted CO_2 for considerable distances downstream of the outcrops, as occurs in the Amazon mainstem. As riverine CO_2 evasion flux appears to be a significant component of continental carbon balances in the humid tropics (Richey *et al.* 2002), explicit accounting of ^{14}C and ^{13}C signatures of CO_2 outgassing from these river types may be required to accurately interpret isotope-based tropospheric CO_2 inversions at regional and local scales.

CONCLUSIONS

Rivers in humid tropics were recently shown to outgas CO_2 at much higher rates than previously appreciated, with evasion fluxes in Amazonian rivers (0.5 Pg C yr^{-1}) more than 10 times the exports to the ocean as total organic carbon (OC) or dissolved inorganic carbon (DIC) (Richey *et al.* 2002). However, little agreement exists about sources of CO_2, and the few direct estimates of respiratory source age range from contemporary to thousands of years (Cole & Caraco 2001; Raymond & Bauer 2001a; Raymond & Hopkinson 2003). Here I present results of an extensive survey of ^{13}C and ^{14}C composition of DIC and three OC size fractions in Amazonian rivers from small streams to the Amazon mainstem, and from Andean highlands to central lowlands. With few exceptions, respiration of completely contemporary organic matter (<5 years old) originating on land is the dominant source of excess CO_2 that drives outgassing in all mid to large rivers, despite observations that bulk OC fractions transported by these rivers range from tens to thousands of years in age. A small, rapidly cycling pool of OC is responsible for the large carbon fluxes from land to water to atmosphere in the humid tropics.

Table 5.1. Site and drainage area characterization. Latitude (Lat) and Longitude (Lon) are in decimal degrees. A few sites represent aggregated data from distinct sites in relative proximity. Site numbers 17 – 31 are in the Ji-Parana basin (see Fig. 5.1), and their site names correspond to codes used in previous studies (Bernardes *et al.* 2004). Continued on next page.

Site #	River	Site Name	Lat °S	Lon °W	Area km^2	Elevation		
						Site m	Basin Mean m	% > 1000 m
				Lowland				
6	Candeias	Candeias	8.766	63.708	13,200	77	179	0.2
7	Azul	Azul	9.627	64.942	4,030	103	184	0.0
9	Novo	Novo	14.172	59.742	150	295	314	0.0
10	Guaporé	Vila Bela	14.993	59.958	21,660	193	335	0.0
17	Ji-Paraná	JIP-5	8.147	62.787	73,410	69	246	0.0
18	Ji-Paraná	JIP-4	8.947	62.057	67,640	91	257	0.0
19	Machadinho	MAC	9.507	62.047	2,970	198	198	0.0
20	Ji-Paraná	JIP-3	10.092	61.977	43,580	181	284	0.0
21	Jarú	JARU	10.102	61.996	7,410	180	254	0.0
22	Boa Vista	NS1	10.757	62.368	< 10	296	297	0.0
23	Boa Vista	NS2	10.753	62.372	< 10	296	298	0.0
24	Ji-Paraná	JIP-2	10.937	61.957	29,770	192	293	0.0
25	Urupá	URUPA	10.902	61.962	4,820	191	264	0.0
26	Rolim de Moura	ROLIM	11.445	61.731	2,060	200	236	0.0
27	Ji-Paraná	JIP-1	11.452	61.463	19,170	200	325	0.0
28	Comemoração	COM-2	11.667	61.188	6,740	199	372	0.0
29	Comemoração	COM-1	12.718	60.173	160	594	598	0.0
30	Pimenta Bueno	PB-2	11.703	61.192	8,650	197	321	0.0
31	Pimenta Bueno	PB-1	12.847	60.343	130	495	491	0.0
32	Negro	Mouth	3.063	60.302	716,770	29	185	1.1
33	Barro Branco	Reserva Ducke 1	2.932	59.978	< 10	59	58	0.0
34	Cabeça Branca	Reser. Campinas 1	2.582	60.022	< 10	99	98	0.0
35	Cueiras	Cueiras	2.781	60.442	3,280	40	85	0.0
36	Asu	Reserva ZF2 1	2.608	60.216	< 10	67	67	0.0
37	Miratucu	Miratucu 4	1.963	61.848	520	34	32	0.0
38	Miratucu	Miratucu 3ag	2.031	61.853	450	34	32	0.0
39	Cobra	Miratucu 2c	2.027	61.813	< 10	34	34	0.0
40	Purus	Mouth	3.747	61.433	362,900	32	138	0.0
41	Purus	Boca do Acre	8.732	67.378	111,630	100	235	0.0
42	Acre	Brasileia	11.002	68.764	7,820	250	296	0.0
43	Juruá	Mouth	2.722	65.803	217,370	56	176	0.0
44	Japurá	Mouth	1.817	65.683	260,010	55	255	3.4
45	Juruá	Cruzeiro do Sul	7.622	72.637	43,960	188	259	0.0

Table 5.1 continued. Site and drainage area characterization.

Site #	River	Site Name	Lat °S	Lon °W	Area km^2	Elevation		
						Site m	Basin Mean m	% > 1000 m
				Mixed				
1	Amazon	Manacapuru	3.322	60.612	2,238,490	28	560	13.4
2	Amazon	Itapeua	4.053	63.017	1,818,270	38	661	16.5
3	Amazon	Vargem Grande	3.279	67.853	1,016,030	70	1040	28.3
4	Madeira	Mouth	3.450	58.798	1,381,590	20	501	11.7
5	Mamoré	Guayaramerin	10.848	65.347	601,470	120	541	12.5
8	Madeira	Madeira at Abunã	9.677	65.417	906,120	127	681	17.8
11	Beni	Riberalta Arriba	11.022	66.128	118,330	135	1372	46.2
46	Napo	Napo	3.295	72.632	110,300	103	651	16.5
47	Marañón	Marañón	4.528	73.568	358,170	113	1106	35.6
48	Ucayali	Ucayali	4.522	73.487	341,200	112	1658	41.7
50	Pachitea	Mouth	8.733	74.572	27,500	165	830	21.1
				Mountain				
12	Beni	Rurrenabaque	14.542	67.548	68,130	504	2191	79.0
13	Alto Beni	Sapecho	15.617	67.330	29,590	608	2735	91.6
14	Achumani	Achumani	16.472	68.063	230	3834	4565	100.0
15	Yara	Yara Caranavi	15.777	67.588	340	1012	1550	84.4
16	Zongo	Zongo	16.253	68.118	260	4555	4519	100.0
49	Ucayali	Ucayali at Pachitea	8.783	74.553	205,520	165	2500	65.7
51	Tambo	Mouth	10.787	73.773	121,290	286	3199	84.6
52	Apurimac	Cunyac	13.567	72.589	22,760	2425	4105	100.0
53	Urubamba	Mouth	10.757	73.712	61,070	288	1890	51.3
54	Yanatili	Quellouno	12.602	72.533	3,020	1083	3089	98.3
55	Urubamba	Sahuayaoti	12.646	72.538	13,920	824	3791	97.1
56	Urubamba	Quillabamba	12.867	72.682	12,640	1142	4001	99.3
57	Urubamba	Pachar	13.273	72.250	9,290	3106	4284	100.0
58	Salcca	Salcca	14.102	71.422	3,190	3792	4743	100.0
59	Vilcanota	Tinta	14.166	71.402	1,610	3571	4239	100.0
60	Lago Langui-Layo	Langui	14.437	71.292	470	3877	4276	100.0

Table 5.2. Average geochemical properties for isotopic sampling sites, based on samples analyzed for carbon isotopes. Data used for averages are based only on samples where a ^{14}C measurement was made. Continued on next page.

Site #	Temperature °C	pH	Alkalinity μeq L^{-1}	FSS mg L^{-1}	FPOC %wt	CO_2 ppm	DIC μmol L^{-1}	DOC mg L^{-1}	FPOC mg L^{-1}	CPOC mg L^{-1}
					Lowland					
6	25.4	5.92	98	19.1	7.13	7640	362	1.65	1.36	0.13
7	25.1	5.94	77	14.7	9.91	5723	275	0.69	1.46	
9	24.7	6.41	98	15.6	9.42	2476	184	0.68	1.47	0.93
10	20.9	6.53	410	14.4	7.83	7837	681	3.41	1.13	0.19
17	31.5	7.07	344	11.6		2099	404	2.04		
18	30.1	7.13	205	7.6		1063	236	2.57		
19	29.3	6.72	125	13.7		1653	175	2.02		
20	30.1	7.39	243	17.0		692	263	4.38		
21	29.6	7.45	532	14.4		1312	570	4.75		
22	25.9	6.31		9.2		10300				
23	25.7	6.60		6.7		7100				
24	26.5	6.97	248	21.9	5.71	1525	300	2.78	0.88	0.10
25	28.3	6.97	703	47.7		3193	797	8.43		
26	29.6	7.44		26.0				2.68		
27	29.3	7.15	131	14.8		643	150	2.43		
28	25.2	6.25	39	20.7	9.60	1346	85	2.49	1.12	0.18
29	23.6	5.32	3	15.0	1.96	1872	70	1.60	0.53	
30	28.9	7.12	197	14.0		1031	229	4.02		
31	25.5	5.83	4	6.3		565	25	1.36		
32	29.0	4.87	4	6.1	13.65	5197	184	10.24	0.61	0.01
33	24.9	4.15						3.54		
34	25.5	3.94						34.94		
35	30.3	3.84						6.74		
36	24.8	4.02						9.11		
37								7.02	0.77	
38								6.21	0.69	
39								6.09	0.39	
40	26.9	5.94	135	16.3	5.91	10048	482	4.02	0.96	0.01
41	26.4	7.68	2047	121.4	1.22	2757	2137	2.18	1.48	0.08
42	23.7	7.99	1467	70.2	2.92	964	1494	2.15	2.05	0.07
43	24.6	6.61	497	106.4	1.60	7824	767	3.50	1.70	0.05
44	25.7	5.30	15	19.9	3.64	4920	185	3.48	0.73	0.07
45	26.7	6.51	858	257.1	1.20	17173	1452	5.77	3.07	

Table 5.2 continued. Average geochemical properties for isotopic sampling sites, based on samples analyzed for carbon isotopes.

Site #	Temperature °C	pH	Alkalinity μeq L^{-1}	FSS mg L^{-1}	FPOC %wt	CO_2 ppm	DIC μmol L^{-1}	DOC mg L^{-1}	FPOC mg L^{-1}	CPOC mg L^{-1}
					Mixed					
1	27.7	6.37	338	161.7	1.14	8302	625	4.45	1.45	0.47
2		6.93	525	114.0	1.60	4010	663	3.98	1.79	
3		7.49	1269	203.0	1.00	2633	1358	2.68	1.95	
4	27.3	6.68	265	671.7	0.56	3551	388	2.57	3.76	0.20
5	27.3	6.67	570	421.9	0.56	8216	833	5.06	2.35	0.04
8	26.6	6.85	600	276.3	1.14	5482	789	3.59	3.15	
11	27.8	7.02	684	630.6	0.31	4431	823	1.98	1.93	0.47
46	29.7	6.94	270	178.9	1.51	2689	455	2.44	2.71	1.11
47	26.0	6.97	790	333.1	1.67	5356	957	4.66	5.58	1.49
48	28.0	7.43	1280	337.9	1.11	3149	1419	2.65	3.73	0.25
50	24.8	7.75	1290	269.2	1.84	1388	1257	2.21	4.95	7.24
					Mountain					
12	27.7	6.95	481	851.0	1.30	3658	597	1.89	8.40	0.61
13	23.9	7.76	762	1340.0	0.91	870	790	1.28	6.87	0.42
14	10.2	8.62	814	553.0	0.40	103	808	0.94	1.81	0.03
15	24.6	7.71	283			357	295	1.80	1.99	
16	6.7	7.01	203		0.73	1036	266	0.04	0.69	0.04
49	26.1	7.70	1170	288.5	1.24	1623	1315	1.80	3.58	0.73
51	25.7	7.91	1170	250.8	1.47	921	1192	2.35	3.69	0.11
52	22.1	8.75	1960	6.6	8.84	205	1833	1.57	0.59	0.00
53	27.0	8.06	960	268.5	1.67	587	1066	1.81	4.50	0.97
54	23.3	7.67	470	59.8	1.16	704	534	1.08	0.69	0.20
55	23.5	8.28	1230	46.7	2.44	446	1340	1.40	1.14	0.09
56	19.7	8.21	1390	55.0	2.73	562	1438	2.41	1.50	0.03
57	17.6	7.89	2960	183.6	3.84	2572	3183	3.40	7.04	0.01
58	15.1	7.55	2060	289.5	1.15	3872	2259	1.32	3.33	6.63
59	18.7	7.69	3320	4.5	16.16	4103	3252	2.63	0.72	0.01
60	11.9	8.46	1900	1.5	30.27	400	1821	1.90	0.45	

Table 5.3. Isotopic composition of each carbon fraction in each sample. Isotope values are reported in per mil (‰). Continued on next page.

Site #	Date	DIC	CO_2		DOC		FPOC		CPOC	
		$\delta^{13}C$	$\Delta^{14}C$	$\delta^{13}C$	$\Delta^{14}C$	$\delta^{13}C$	$\Delta^{14}C$	$\delta^{13}C$	$\Delta^{14}C$	$\delta^{13}C$
					Lowland					
6	7/2/1996	-19.32	99.5	-20.60			135.3	-30.77	206.6	-29.34
7	6/27/1996	-19.40	84.5	-20.77						
9	7/5/1996	-13.18	108.1	-16.82						
10	7/6/1996	-21.03	-145.9	-25.27	269.9	-26.59	-19.0	-31.64		
17	9/20/2000	-11.77	91.1	-17.72						
18	9/13/2000	-10.44	106.1	-16.65						
19	9/13/2000	-14.47	100.1	-19.45						
20	9/16/2000	-10.46	92.6	-17.14						
21	9/16/2000	-11.92	103.5	-18.73						
22	8/26/2002	-13.07	58.5	-16.81						
22	12/2/2002	-12.92	105.3	-14.29						
22	1/15/2003	-9.49	97.8	-13.92						
23	8/28/2002	-10.93	110.6	-16.39						
23	12/5/2002	-9.45	103.3	-13.16						
24	7/3/1996	-9.98	117.5	-15.60	244.4	-27.03	124.4	-25.61	11.4	-27.63
24	9/17/2000	-10.46	106.1	-17.32						
24	1/26/2003	-16.25	85.8	-20.31						
25	9/12/2000	-11.52	110.5	-17.84						
25	1/24/2003	-11.24	97.6	-16.50						
26	9/11/2000	-11.63	101.3	-18.43						
27	9/11/2000	-11.98	95.2	-18.30						
28	7/3/1996	-14.88	127.2	-17.70			138.1	-28.56	142.3	-28.14
28	9/11/2000	-15.96	100.2	-19.48						
28	1/18/2003	-20.40	87.5	-22.59						
29	7/4/1996	-20.49	61.0	-19.83						
29	9/10/2000	-21.83	74.2	-21.77						
30	9/11/2000	-12.94	94.0	-19.23						
31	9/10/2000	-19.02	27.5	-19.95						
32	1/31/1995				179.9	-29.10				
32	6/20/1995				334.6	-29.10	120.5	-29.10		
32	7/6/1996	-25.43	140.4	-24.44	129.0	-29.28	136.8	-29.75		
32	7/15/2002	-27.19	117.3	-26.15						
32	11/12/2002	-24.15	99.2	-24.11						
33	7/13/1995				150.4	-29.25				
33	7/13/2002	-25.02	114.2	-23.89						
34	12/12/1995				106.2	-29.08				
34	7/13/2002	-27.49	83.9	-26.34						
34	11/3/2002	-26.51	102.0	-25.36						
35	7/15/2002	-26.29	89.9	-25.16						
36	7/19/2002	-25.91	88.4	-24.74						
36	11/6/2002	-26.82	94.8	-25.71						
37	3/30/1995				168.4	-29.08				
38	3/29/1995				174.3	-29.17				
38	4/2/1995				170.2	-29.35				
39	4/2/1995				165.8	-29.39				
40	7/5/1996	-21.02	122.9	-22.38	94.9	-29.90	112.4	-31.55		

Table 5.3 continued. Isotopic composition of each carbon fraction in each sample.

Site #	Date	DIC	CO_2		DOC		FPOC		CPOC	
		$\delta^{13}C$	$\Delta^{14}C$	$\delta^{13}C$	$\Delta^{14}C$	$\delta^{13}C$	$\Delta^{14}C$	$\delta^{13}C$	$\Delta^{14}C$	$\delta^{13}C$
					Lowland					
41	6/23/1996	-13.79	70.9	-21.10	174.4	-29.34	28.6	-30.81		
42	6/22/1996	-14.62	1.8	-22.12						
43	7/1/1996	-17.90	112.7	-22.53	114.7	-29.88	58.1	-30.03		
44	7/2/1996	-17.57	109.5	-17.14						
45	6/25/1996	-15.35	67.1	-19.49	171.6	-29.72	54.1	-29.81	84.4	-28.71
					Mixed					
1	1/10/1995				199.6	-29.40	-86.0	-28.30	-184.0	-28.73
1	6/16/1995				137.5	-29.60	-157.1	-28.70	-127.5	-27.80
1	7/6/1996	-17.72	75.7	-21.41						
1	7/12/2002	-18.27	29.8	-20.53						
1	7/12/2002	-18.67	41.5	-20.37						
2	8/26/1991	-12.73	34.2	-18.62						
3	8/12/1991	-11.39	-30.4	-18.51						
4	1/19/1995				329.9	-28.70	-73.8	-27.40	-148.3	-27.40
4	7/8/1996	-15.75	95.7	-20.70	153.9	-28.79	-50.0	-29.82		
5	5/3/1995						-329.5	-27.27	-93.6	-26.14
8	6/27/1996	-13.77	48.6	-19.39	196.2	-27.97	-131.5	-28.30	-233.8	-26.53
11	5/6/1995				198.3	-28.64	-440.6	-26.77	-146.6	-27.64
46	11/7/1996	-13.65	21.7	-19.38	229.7	-29.60	-24.9	-28.87	-18.9	-28.44
47	11/8/1996	-11.61	-196.8	-17.71	156.4	-29.21	-7.0	-28.47	-43.4	-28.11
48	11/8/1996	-11.49	-138.5	-18.43	157.2	-29.46	-59.3	-28.59	-125.0	-28.24
50	11/5/1996	-11.07	-142.4	-18.67						
					Mountain					
12	11/14/1994	-9.90	-154.4	-15.81						
13	11/15/1994	-6.87	-116.9	-14.19						
13	5/11/1995								-30.7	-27.47
14	11/20/1994	-5.38	-61.3	-14.88						
15	11/16/1994	-6.91	14.3	-14.50						
16	5/15/1995						-221.4	-25.62	49.9	-27.60
49	11/5/1996				269.9	-28.70	-81.1	-28.07	34.2	-28.60
51	11/1/1996	-6.07	-155.6	-13.67	152.5	-27.92	-73.9	-27.63	78.8	-28.33
52	10/21/1996	-2.60	-148.9	-10.77	26.6	-21.84	18.2	-23.66	-19.9	-23.77
53	11/1/1996	-9.96	-151.2	-17.49	110.3	-28.95	-301.2	-27.11	74.6	-28.47
54	10/27/1996	-3.46	-45.3	-11.14						
55	10/27/1996	-3.34	-248.7	-11.31						
56	10/27/1996	-3.34	-273.6	-11.71	219.7	-25.23	-89.4	-24.33	16.5	-26.19
57	10/26/1996	-3.04	-645.2	-11.49						
58	10/23/1996	-2.35	-748.8	-10.69			-613.0	-24.65	-208.5	-25.89
59	10/23/1996	-2.77	-523.1	-10.94	-221.9	-23.28	-257.8	-24.59	-353.6	-26.35
60	10/24/1996	-2.04	-110.0	-11.33						

Table 5.4. Summary of ^{14}C and ^{13}C isotopic composition for each carbon fraction, by topographical site category. All carbonate-free sites are in the lowlands. Data are reported as mean ± standard deviation (number of samples), in per mil (‰). The number of samples for ^{13}C is the same as that shown for ^{14}C. $\delta^{13}C$-DIC summary values are -4.9 ± 2.7‰ (mountain), -14.2 ± 2.9‰ (mixed), -17.0 ± 5.9‰ (lowland), and -17.1 ± 6.2‰ (carbonate-free).

Site	CO_2		DOC		FPOC		CPOC	
Category	$\Delta^{14}C$	$\delta^{13}C$	$\Delta^{14}C$	$\delta^{13}C$	$\Delta^{14}C$	$\delta^{13}C$	$\Delta^{14}C$	$\delta^{13}C$
Mountain	-241 ± 232 (14)	-12.9 ± 2.2	93 ± 176 (6)	-26.0 ± 3.0	-202 ± 198 (8)	-25.7 ± 1.7	-40 ± 146 (9)	-27.0 ± 1.6
Mixed	-15 ± 99 (11)	-19.4 ± 1.2	195 ± 58 (9)	-29.0 ± 0.6	-136 ± 141 (10)	-28.2 ± 0.9	-125 ± 66 (9)	-27.7 ± 0.9
Lowland	89 ± 44 (43)	-20.1 ± 3.6	177 ± 64 (15)	-29.0 ± 0.9	89 ± 55 (10)	-29.8 ± 1.8	111 ± 83 (4)	-28.5 ± 0.7
Carbonate-free	98 ± 20 (38)	-19.8 ± 3.7	174 ± 67 (11)	-29.1 ± 0.7	128 ± 10 (6)	-29.2 ± 2.1	120 ± 99 (3)	-28.4 ± 0.9

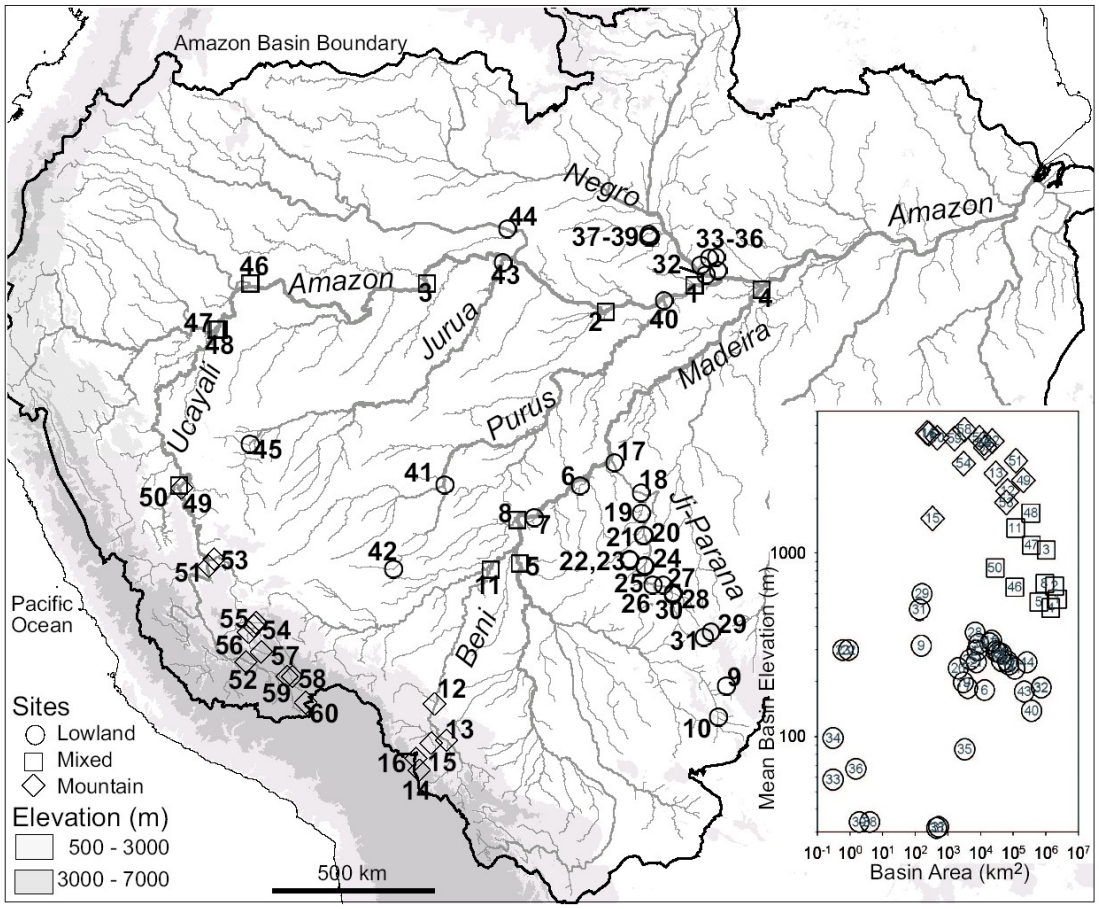

Figure 5.1. Amazon basin and river sites sampled for carbon isotopes. I used GTOPO30 elevation (Gesch *et al.* 1999) and a regional river network dataset (Mayorga *et al.* submitted) to categorize each site by topography according to the percent of the drainage area above 1000 meter elevation: mountain (diamond), ≥ 50% (16 sites); mixed (square), ≥ 10% (11 sites); and lowland (circle), < 10% (33 sites). Mountain sites are found only in the Andean Cordillera, while mixed sites are large rivers draining both mountain and lowland areas. Site numbers are displayed. The distribution of sites by drainage area (river size) and mean basin elevation is shown in the inset. See Table 5.1 for additional site information.

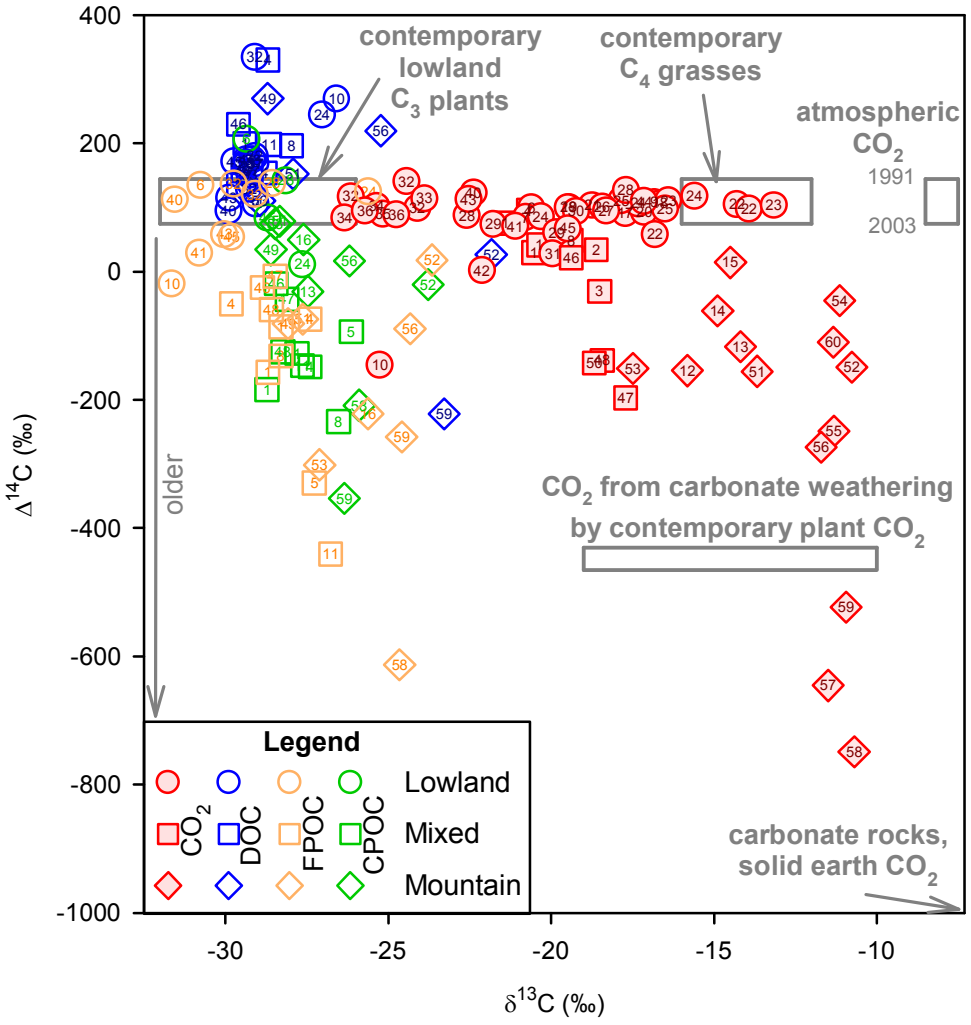

Figure 5.2. Distribution of ^{14}C and ^{13}C isotopes across all carbon fractions. More negative $\Delta^{14}C$ values indicate older carbon. Symbol shapes and numbers are the same as in Fig. 5.1, while symbol color indicates carbon fraction. Representative isotopic ranges of potential carbon sources are shown by gray boxes. Plant $\delta^{13}C$ ranges from -32‰ to -26‰ for lowland plant material fixed via the C_3 photosynthetic pathway typical of the majority of plants, to -16‰ to -12‰ for tropical grasses relying on the C_4 pathway (Hedges *et al.* 1986a; Bernardes *et al.* 2004). Phytoplankton take up dissolved CO_2 and impose ^{13}C fractionations of about 20‰, leading to observed and potential biomass $\delta^{13}C$ values of -32 to -40‰ in mixed and lowland rivers (Hedges *et al.* 1986a; Mook & Tan 1991; Clark & Fritz 1997; Devol & Hedges 2001), beyond the range found in lowland OC and CO_2 observations. Carbonate rocks and CO_2 from solid earth degassing are ^{14}C-free ($\Delta^{14}C$ = -1000‰) (Clark & Fritz 1997). $\delta^{13}C$ of carbonate rocks is approximately 0‰, whereas $\delta^{13}C$ of degassed CO_2 can range from -6‰ for volcanic to +10‰ for metamorphic sources (Clark & Fritz 1997). The carbonate weathering region represents CO_2 in equilibrium with HCO_3^- resulting from weathering by CO_2 derived from respired, contemporary C_3 or C_4 plant material (Clark & Fritz 1997).

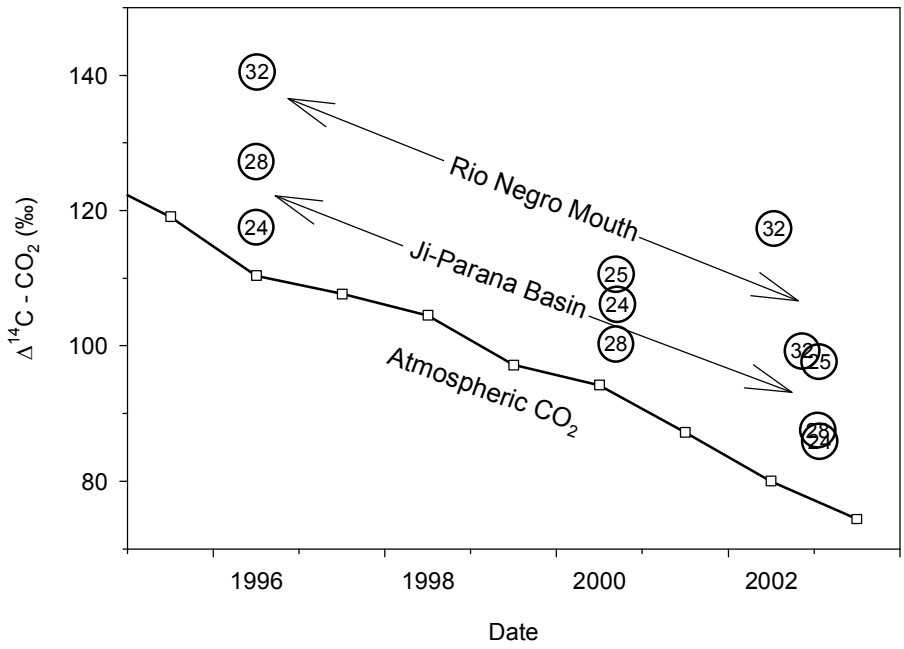

Figure 5.3. Temporal evolution of ^{14}C-CO_2 at four lowland sites from mid to large rivers in the Ji-Parana basin and Rio Negro, which drain continental Shields. Symbol shapes and numbers are the same as in Fig. 5.1. These sites were analyzed for ^{14}C-DIC 2–3 times between 1996 and 2003. Atmospheric $^{14}CO_2$ represents time-weighted annual means at Schauinsland, Germany (Levin & Kromer in press), plus a constant offset of +8‰ to account for the estimated gradient between Schauinsland and tropical South America. Natural regional and seasonal variability within the Amazon basin may be as high as 10‰.

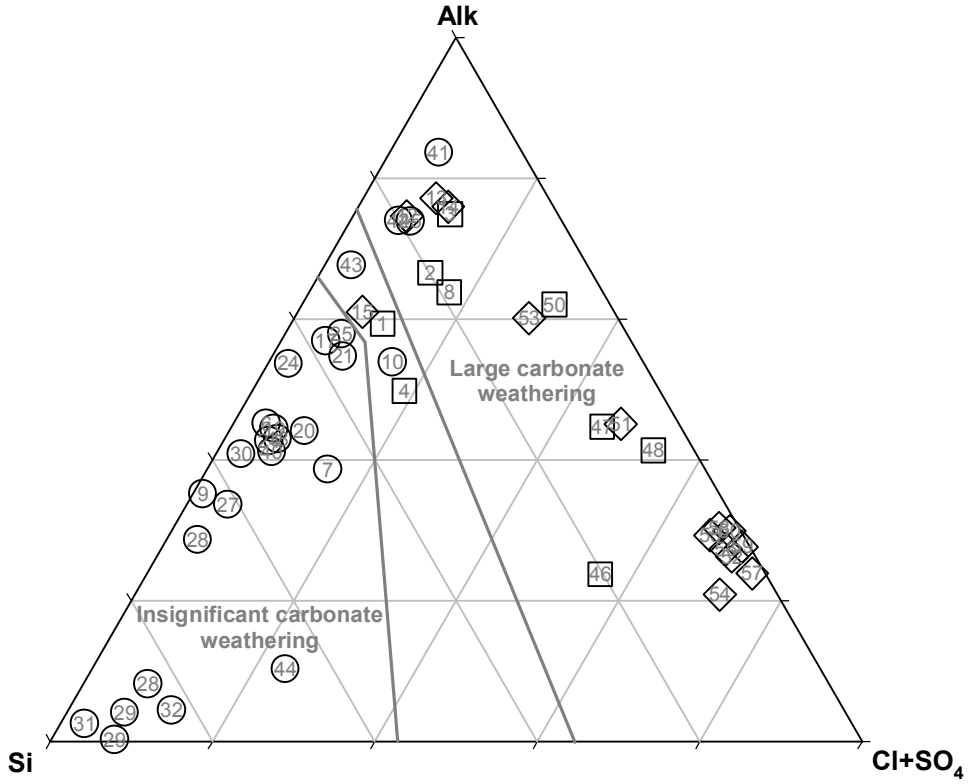

Figure 5.4. Relative proportions of silica (μmol L^{-1}), alkalinity (μeq L^{-1}), and $Cl^- + SO_4^{2-}$ (μeq L^{-1}), indicative of dominant weathering regimes controlling the dissolved load (Stallard & Edmond 1983). Symbol shapes and numbers are the same as in Fig. 5.1. Only samples with ^{14}C-DIC analyses are shown; data were not corrected for seasalt aerosols. Rivers falling near the alkalinity and $Cl^- + SO_4^{2-}$ vertices have high-solute waters draining primarily areas of carbonate sediments and evaporites, respectively. Evaporite dominance is typically associated with substantial carbonate outcrops, whereas relatively high alkalinity may also result from weathering of cation-rich aluminosilicates. Rivers draining cation-poor aluminosilicates cluster near the silica vertex. I delineated regions very likely to have high or insignificant weathering contributions from carbonates (Stallard & Edmond 1983). A heterogeneous set of 5 intermediate sites is more difficult to classify, but I assigned them to the carbonate influence group. 7 additional lowland sites where silica, alkalinity, and major anions were not measured were assumed to be carbonate-free based on dominant lithology, observations from neighboring rivers, or previous studies.

CHAPTER 6: ISOTOPIC TRENDS AND DISSOLVED INORGANIC CARBON CYCLING THROUGHOUT THE AMAZON RIVER SYSTEM

INTRODUCTION

Spanning a wide range of lithologies, topographic settings, vegetation communities, and climates (see Chapter 2), a continental-scale river system such as the Amazon presents unique opportunities for examining a variety of terrestrial DIC and CO_2 sources to streams; the impact of dynamic riverine processes with increasing river size in a variety of heterogeneous regions; and the mixing and integration of waters draining highly diverse landscapes. However, as discussed in Chapter 4, little work has been done in this regard outside the Amazon mainstem corridor, and ^{14}C-DIC has not been used at all.

To examine biogeochemical patterns and processes in tributaries across the basin, the CAMREX program conducted over the last decade a series of sampling expeditions to a variety of rivers of vastly different sizes from Andean and lowland headwater regions, including revisits to several Amazon mainstem sites (for results focused on organic matter, see Hedges *et al.* 2000; Bernardes *et al.* 2004; Aufdenkampe *et al.* submitted). In a collaborative project with A. Aufdenkampe (Stroud Water Research Center), I analyzed the ^{13}C and ^{14}C composition of DIC and three organic carbon fractions from a large collection of samples from these expeditions (see Chapter 5), representative of a wide range of rivers and watersheds. This isotopic dataset and supporting biogeochemical measurements carried out jointly may constitute the most comprehensive, integrated survey of riverine carbon cycling within a single large basin that exploits the dual isotopes. In Chapter 5, I used these isotopic observations to analyze the interactions between organic and inorganic fractions, concluding that while bulk OC fractions are eventually degraded during

their transit and long-term storage in the river system, in-channel respiration is largely fueled by a contemporary, uncharacterized organic fraction that typically makes up a small fraction of total OC and is generally a mixture of C_3 and C_4 plant material. This fraction is often isotopically distinct from bulk DOC, FPOC, or CPOC fractions. High rates of respiration in turn drive CO_2 evasion and ultimately lead to complete downstream replacement of terrestrially originated DIC with contemporary carbon.

In this chapter I concentrate on the use of ^{14}C and ^{13}C of DIC to address the following questions:

- What is the range in variability of isotopic composition across the basin, and the main sources of this variability?
- What are the primary terrestrial sources of DIC and CO_2 and their regional distribution?
- How do DIC and CO_2 evolve downstream from their sources across the basin in response to fluvial processes and a changing landscape composition draining into a growing river?
- Is there seasonal variability in the isotopic signatures? If so, what do they tell us about changing sources and processes?

As many of the sites were sampled only once, do not have associated discharge data, or form discontinuous longitudinal transects sampled on different years, construction of DIC mass balances by reach generally was not possible. Instead, I will examine trends in major ions, DIC, pCO_2, and carbon isotopes in several regions and longitudinal transects, using these observations as a baseline survey to characterize regional patterns of riverine DIC cycling and controlling processes across the basin. I conclude by summarizing the main trends and findings across the basin. This initial framework will be invaluable in future studies for

developing quantitative carbon models and constraining carbon budgets across specific transects.

Study Area

River samples analyzed in this study for carbon isotopes and related geochemistry were collected by several CAMREX teams on over a dozen expeditions all across the Amazon basin, between 1991 and 2003 (Fig. 6.1). These sampling programs are briefly described in Table 6.1. Sampled rivers range from first-order springs to the mainstem Amazon in the central part of the basin near Manaus (Table 5.1); their drainage areas span vegetation types from humid lowland forests to arid highlands and newly deforested lowlands converted to pastures. Lithology is also highly variable, ranging from freshly exposed and highly weatherable carbonate and evaporite sediments in the Andes to bleached white sands in the Precambrian Guyana Shield in the Rio Negro basin (Stallard & Edmond 1983; Putzer 1984; Sombroek 1984; Stallard 1985). The physical characteristics of the basin and general geochemical variability of its rivers are described in more detail in Chapters 2 and 4.

Sample collection and river environments along the Amazon mainstem and the mouths of its major tributaries have been described previously from a series of earlier cruises (Richey *et al.* 1986; Richey *et al.* 1990). These cruises traced a 1,800-km transect from Vargem Grande upstream near the border with Perú and Colombia, to Obidos, about 650 km upstream of the Amazon mouth (Fig. 5.1; see also Figs. 2.1, 2.2). The Mainstem 1991 cruise (MS91) followed that same transect, while the Mainstem 1996 cruise (MS96) had a reduced coverage and extended only from Tupé downstream to the mouth of Rio Madeira (Figs. 6.1, 5.1, 2.2).

Bolivian expeditions in 1994-95 (BO94 and BO95) focused on the Beni river draining the high Andes near the city of La Paz and extending for approximately 1,200 km to the confluence with the Rios Madre de Dios and Mamoré in the depositional lowlands, before the Beni meets the Mamoré to form the Rio Madeira near the border with Brazil (Figs. 6.1, 5.1, 2.2). Hedges *et al.* (2000) described organic matter cycling on this transect for the 1994 low-water expedition; the 1995 high-water expedition revisited largely the same transect. The geomorphology and geochemistry of the region has been described in detail elsewhere (Guyot *et al.* 1992; Guyot 1993; Guyot & Wasson 1994; Aalto *et al.* 2003).

The Peruvian 1996 expedition (PE96) focused on the Vilcanota-Urubamba-Ucayali transect, from the Altiplano headwaters of the Vilcanota South of Cusco, at an elevation of nearly 4,000 m; to the confluence of the Rios Ucayali and Marañón forming the Rio Amazonas in the lowlands 2,100 km downstream, and the mouth of the Rio Napo 200 km farther downstream (Figs. 6.1, 5.1, 2.2). Aufdenkampe *et al.* (submitted) described this transect in their study concentrating on organic matter cycling; with few exceptions (Stallard & Edmond 1983), rivers in the upper and central Ucayali region have never been characterized geochemically. The fluvial geomorphology and biogeography of the central and lower Ucayali has been described in detail elsewhere (Puhakka *et al.* 1992; Räsänen *et al.* 1992; Kalliola *et al.* 1993; Kvist & Nebel 2001), and the inorganic geochemistry of the lower Ucayali and upper Amazonas has been examined by Stallard & Edmond (1983).

The Southern Tributary Transect 1996 expedition (ST96) covered a large swath of southern lowland headwaters, from the Juruá near Cruzeiro do Sul in the West, going East through the Purus in Acre, and crossing the Madeira to Rondônia, and the Guaporé headwaters in the southern part of the Amazon basin near the

Bolivian border (Fig. 6.1, 5.1, 2.2). This region spans a climatological and lithological gradient from humid climates, cation-rich soils, and relatively pristine forests in the Western end, to more seasonal climates, more weathered soils, and savannas and highly deforested areas replaced with pastures in the Eastern end. The geochemistry of many of these rivers has never been examined before.

The Ji-Paraná river system in the Brazilian state of Rondônia (Fig. 5.1) has been the focus of intensive biogeochemical study as part of the LBA initiative, with 11 expeditions (JIP) conducted between 1998 and 2002 (Ballester *et al.* 2003; Bernardes *et al.* 2004; Krusche *et al.* in prep.). This basin represents a major deforestation front in the Brazilian Amazon (Roberts *et al.* 2002; Ballester *et al.* 2003). While it drains the weathered Precambrian Brazilian Shield, many of its Southern tributaries drain cation-rich lithologies (Ballester *et al.* 2003; Holmes *et al.* 2004). Nutrient, major ions, metabolism, and the impact of anthropogenic disturbance on rivers and streams have been studied previously in this region (Ferreira *et al.* 1988; Mortatti *et al.* 1989; Mortatti *et al.* 1992; Neill *et al.* 2001; Biggs *et al.* 2002; Biggs *et al.* 2004; Thomas *et al.* 2004).

Additional samples (AA) were obtained in 1995 and 2002-03 from small and mid-size streams north of Manaus, at the same Reserva Ducke and Reserva Campinas sites where McClain *et al.* (1997) conducted their hillslope and stream biogeochemistry studies, as well as from streams in the ZF-2 site at the Reserva Biologica do Cuieiras (Araújo *et al.* 2002; Luizão *et al.* 2004) and from the Cuieiras river draining the Reserva; the Solimões river near Marchantaria (Devol *et al.* 1995); and the mouths of the Negro and Madeira rivers. Also, samples from the Ji-Paraná basin in Rondônia were collected from many of the same sites included in the Ji-Paraná LBA transects.

METHODS

I will describe sampling and chemical methods only for CAMREX samples with unpublished major ion or DIC isotope data first presented here (see Table 6.1). Sample collection, field processing, and chemical analysis methods sometimes varied across expeditions. With few exceptions, they have been described in previous publications, as discussed above. Here I will summarize procedures commonly used and discuss in more detail sample processing and analysis for ^{13}C and ^{14}C of DIC.

Sampling

Samples were collected from boats and bridges, except in small streams where samples were grabbed directly near the surface. Samples for carbon isotopes of DIC were obtained from Niskin bottles near the middle of the channel or at the main flow section (thalweg) when it could be determined based on depth profiles. In most cases, a horizontal Niskin bottle oriented with the direction of flow was used, submerged to a depth of 6/10 the total water column (4/10 from the bottom). The procedure is described in Quay *et al.* (1992). Briefly, a 250 ml glass bottle was gradually overfilled (2x) from the bottom with water extracted from the Niskin bottle, without disturbing the water surface to avoid degassing or contamination by air. The unfiltered sample was then preserved with $HgCl_2$ to a concentration of 100 μM, and the bottle capped with a greased ground glass stopper and stored at ambient temperature. In the Ji-Parana program (JIP, Table 6.1), an additional sample for analysis of DIC concentration was extracted from the Niskin bottle and preserved with $HgCl_2$ to a concentration of 300 μM after filtering through pre-combusted 0.7 μm glass fiber filters (Whatman GFF) (Krusche *et al.* in prep.).

Samples for major ion, silica, and alkalinity were collected through different procedures. For Bolivia and the mainstem cruises, a collapsible-bag apparatus was used to collects depth-integrated, discharge-weighted samples (Richey *et al.* 1986; Hedges *et al.* 2000). PE96 and ST96 relied on a submersible pump at a depth of 6/10 from the surface to the bottom (Aufdenkampe *et al.* submitted). For JIP, samples were extracted from Niskin bottles (Ballester *et al.* 2003; Krusche *et al.* in prep.). Finally, AA used Niskin bottles for larger rivers and direct bottle submersion for small streams. Samples were preserved with $HgCl_2$ to a concentration of generally 50-100 μM; in such cases a separate, unpreserved and unfiltered sample was collected for Cl^- ion analysis. For all JIP expeditions except the first one (8/1998), major ion and silicate samples were preserved with thymol salt (Krusche *et al.* in prep.). All samples were passed through 47 μm Whatman GFF or 45 μm cellulose acetate filters soon after field collection, usually after sieving through a 63 μm Nitex screen.

Temperature, pH, dissolved oxygen, and electrical conductivity were measured in the field by submerging probes into the Niskin bottle or directly into the water column to a 6/10 depth from the surface. Different probes were sometimes used across expeditions; model types are listed in the corresponding publications (Table 6.1).

Chemical analyses

^{13}C-DIC and ^{14}C-DIC. ^{13}C of DIC was analyzed in the lab at the University of Washington (UW) according to the method presented in (Quay *et al.* 1992). Briefly, the top half of DIC samples was drawn into a vacuum line to avoid stirring particles settled at the bottom. Extracted DIC was stripped of all CO_2 after acidification. Cryogenically purified CO_2 was then analyzed for ^{13}C by dual-inlet isotope ratio mass spectrometry (IRMS). When sufficient mass remained after ^{13}C

analysis, CO_2 was reduced to graphite using hydrogen and a cobalt catalyst, and analyzed for radiocarbon by AMS (Vogel *et al.* 1987; Vogel 1992). More than 90% of the ^{14}C analyses were carried out at the Center for Accelerator Mass Spectrometry (CAMS), Lawrence Livermore National Laboratory; the rest were done at the University of Arizona AMS Laboratory.

^{13}C and ^{14}C are reported in the conventional $\delta^{13}C$ and $\Delta^{14}C$ per mil (‰) notation, respectively, as described in Chapter 4 (eqtns. 4.1 to 4.4). Absolute $\delta^{13}C$ and $\Delta^{14}C$ analysis errors (1σ) in this dataset are typically <0.2‰ and <6‰, respectively. For $\Delta^{14}C$, I did not apply a correction for the difference between sample collection year (z) and analysis year (y) as described in Chapter 4; however, given typical $^{14}R_{sample}$ values, typical y – z values of 5 years or less, and a maximum y – z value of 10 years (2001 – 1991), the correction is smaller than 1.5‰ and on average <1‰, less than the analysis error.

DIC, alkalinity, pCO_2, major ions, and silicate. DIC was measured manometrically during sample preparation for ^{13}C analysis. For JIP samples, DIC was measured at the Centro de Estudos Nucleares na Agricultura (CENA, Piracicaba, Brazil), using a Shimadzu 5000A TOC analyzer. When not measured directly, DIC was estimated from pH, alkalinity, and temperature (see below); the error incurred using values estimated with this approach has been shown to be <10% (Devol *et al.* 1987; Stallard & Edmond 1987; Devol *et al.* 1995). Alkalinity was measured using micro-Gran titration (Neal 2001) at the UW (MS91 and PE96), CENA (ST96 and JIP 1998 expedition), and at the Instituto Nacional de Pesquisas da Amazônia (INPA, Manaus, Brazil) (BO94 and BO95). When not measured, alkalinity was estimated from pH, DIC, and temperature measurements (see below). In nearly all cases free CO_2 partial pressure (pCO_2) was estimated from pH, DIC, temperature, and pressure

(see below); in the AA samples, pCO_2 was analyzed directly by headspace equilibration (A. Aufdenkampe, pers. comm.).

All major ion analyses were carried out at CENA. Major cations (Ca^{2+}, Mg^{2+}, Na^{+}, and K^{+}) were analyzed with Inductively Coupled Plasma – Atomic Emission Spectrometry (ICP-AES) for all expeditions before 1999. Major anions (Cl^{-} and SO_4^{2-}) from these samples were measured through colorimetry with flow injector analysis (FIA). Starting with 1999 JIP expeditions, major ions were analyzed with a Dionex DX500 liquid chromatograph. Major ions were not measured for MS91 and AA. Silicate was analyzed at CENA with ICP-AES (BO95, MS96, ST96, PE96, and JIP from 1999 and later), at INPA via colorimetry (MS91 and BO94), and at the UW with a colorimetric Technicon "AAII" Auto Analyzer (JIP 1998 expedition).

Previously published data

With the main exception of the Ji-Paraná sampling program (Ballester *et al.* 2003; Bernardes *et al.* 2004; Krusche *et al.* in prep.), most sites analyzed for carbon isotopes in this study were sampled only once or twice in this study. To place this new sample set within a more general context of seasonal and regional variability, I have gathered and included in my analysis relevant datasets from previously published studies. These additional sampling programs and the type of data available from them are listed in Table 6.1; site locations from these studies not sampled again during the 1990s CAMREX expeditions are shown with distinct symbols in Fig. 6.1. Sites from this new study also sampled previously are found mainly along the Amazon mainstem and in the Beni headwaters of the Madeira.

Most previous studies characterized major ions, pH, and titration alkalinity (Table 6.1), providing sufficient information to determine dominant weathering regimes in their drainage areas (for prominent examples, see Stallard & Edmond

1983; Guyot 1993). ^{14}C-DIC has never been measured before in Amazonian rivers. ^{13}C-DIC has been analyzed only along the Amazon mainstem, floodplain, and mouths of major tributaries, as part of the CAMREX program (Quay *et al.* 1989; Quay *et al.* 1992; Devol *et al.* 1995) and during the two Alpha-Helix cruises (Longinelli & Edmond 1983). A preliminary comparison of ^{13}C-DIC results from Longinelli & Edmond vs. CAMREX (including new analyses from this study) for river sites sampled under both programs suggests the occurrence of offsets of up to several per mil that may be the result of sampling or analytical differences. For this reason, I did not use ^{13}C-DIC results from Longinelli & Edmond (1983).

Site and basin characterizations

While the location of many sites was extracted from Global Position System (GPS) units, consistent analysis of basin characteristics and relative position along the river network requires georeferencing against a digital river network reach. All sites were manually georeferenced against the most likely sampling location in the river network dataset presented in Chapter 3; as the river network dataset has errors of up to a kilometer or more, georeferencing against the network may involve substantial distortions when accurate GPS location was available (see Chapter 2). Sites sampled by multiple programs were often aggregated into a single site when descriptive information warranted it (*e.g.*, Mamoré at Guayaramerin from BO94, BO95, BOLIRD, and BOLEP, Tables 6.1 and 5.1), or when sites were sufficiently near each other that geochemical differences can be expected to be negligible (*e.g.*, Manacapuru and Marchantaria on the central Amazon mainstem, MS91, MS96, AA, MS, MARCH, and AHSTA, Tables 6.1 and 5.1). Drainage area and distance along the river network was extracted using the methods discussed in Chapter 3. Site elevation was measured using field altimeters in some cases (BO94, BO95, and PE96) or by

extraction of elevation from the GTOPO30 gridded 1-km Digital Elevation Model (DEM) dataset (Gesch *et al.* 1999) for the river-georeferenced location. Mean basin elevation is the mean elevation from GTOPO30 over the extracted drainage boundaries. Mean monthly discharge was calculated by averaging multi-year daily data from the Brazilian agency ANA (Agencia Nacional das Aguas).

Regional and topographic site grouping

Fig. 6.1 shows the location of new and previously published sampling sites. Symbol shape represents site topographic classes, as presented in Chapter 5 (lowland, mixed, and mountain; see Fig. 5.1 and description therein). To facilitate the examination of DIC and CO_2 sources and trends, I have grouped all sites into 6 regions:

- The *Guyana* and *Brazilian Shield* sites (see Fig. 2.1 for maps of these two morphotectonic regions) drain largely lowland regions that are generally deeply weathered, including large white sand regions in the Guyana Shield (Putzer 1984; Bravard & Righi 1990); some regions are interspersed by abrupt sandstone and granite massifs (inselbergs or tepuis) or relatively elevated plateaus, especially in Roraima to the North and in eastern and southern sectors of the basin (Putzer 1984; Dubroeucq *et al.* 1991; Edmond *et al.* 1995). Isolated outcrops of silicate lithologies with high base cations can be found, particularly in the Brazilian Shield (e.g., Ballester *et al.* 2003; Holmes *et al.* 2004).
- The *Juruá and Purus basins* are southern tributaries in the central-western lowlands whose headwaters are relatively raised and dissected, and appear to drain significant carbonate outcrops that may represent uplifted former Andean depositional areas from an epoch when hydrographic drainage

patterns were dramatically different (R. Aalto, pers. comm.; also, anecdotal evidence of limestone caves and outcrops).

- *Subandean foreland and mainstem floodplain tributaries* represent a range of widely distributed, heterogeneous lowland sites not in the Shields or in the Juruá and Purus basins, but with either small Andean headwaters or draining through substantial Tertiary or Quaternary depositional sediments.
- *Peruvian Andes and Amazon mainstem* are all sites in central and southern Peru with substantial Andean drainages, and the large mainstem rivers issuing from them, including the Ucayali, Marañón, Solimoes, and Amazonas (see Figs. 2.2, 3.6).
- *Bolivian Andes and Madeira mainstem*, like the Peru-Amazonas class, includes Andean sites in Bolivia and the large mainstems issuing from them, including the Beni, Madre de Dios, Mamoré, and Madeira (see Figs. 2.2, 3.6).

Additional geomorphological, geological, pedological, and vegetation information may be found in RADAMBRASIL (1973-1984).

Geochemical equilibrium calculations

DIC, alkalinity, and pCO_2. Eqtn. 4.18 was used to estimate DIC when it was not analyzed directly but pH and alkalinity were, and to estimate alkalinity when only DIC and pH were analyzed. Equilibrium constants were corrected for temperature as described in Chapter 4. Water temperature in rivers throughout the Amazon basin spanned a large range, from approximately 6°C in the Andean mountains to 31°C in some open lowland rivers (see Table 5.2). When a temperature observation was not available for a sample (typically in the lowlands), I assumed a value of 27°C based on an average of 28±2°C in the Amazon mainstem (Devol *et al.* 1987; Devol *et al.* 1995) and the common occurrence of lower temperatures in the lowlands (Table 5.2).

Alkalinity was not corrected for the influence of dissolved organic acids as discussed by Devol *et al.* (1995) for the Amazon mainstem, as sites in this study represent a larger range of geochemical characteristics than the mainstem.

To estimate activity coefficients requires knowledge of ionic strength, which in turn commonly requires measurements of all major ions. In the datasets used in this study, some major ions were often not analyzed. However, except in salt springs in the Andes (Stallard & Edmond 1983), ionic strength is generally not very large; for unpublished, new datasets (Table 6.1), it reaches a maximum of 0.018 M in the Peru 1996 expedition and is much lower elsewhere (not shown, but see Table 5.2 for major ion concentrations). For these reasons, I did not correct for ionic strength in this study; equilibrium calculations are based on the assumption that $\gamma_z = 1$ and ${}^cK = K$ (see eqtns. 4.8 and 4.9).

As pCO_2 was rarely analyzed directly, I estimated it from DIC and pH via eqtn. 4.20. The degree of CO_2 saturation with respect to the atmosphere, pCO_2 / pCO_2^{atm}, was calculated by assuming a mean 1990s sea-level tropospheric pCO_2 of 360 ppm (Keeling *et al.* 1995; Rayner *et al.* 1999a; Keeling & Whorf 2004), and correcting this value for the effect of site elevation on atmospheric pressure (eqtn. 4.21).

^{13}C and ^{14}C of CO_2(g). Following the approach used in Chapter 5, I will discuss sources and cycling of DIC by examining the isotopic composition of CO_2(g) in equilibrium with bulk DIC. Relative to using the isotopic composition of DIC, this approach is more straightforward for comparing isotopic signatures against typical end-member sources like plant material and air, and for comparing observations from widely different geochemical environments by largely removing the possibly confounding effect of pH (Quay *et al.* 1992; Clark & Fritz 1997). pH- and

temperature-dependent calculations for $\delta^{13}C$ are discussed in Chapter 4 (eqtns. 4.22 to 4.26); $\Delta^{14}C$ does not require adjustments ($\Delta^{14}C\text{-}CO_2(g) = \Delta^{14}C\text{-DIC}$).

Results and Discussion

DIC isotopic data analyzed as part of this study are presented in Table 5.3. The number of DIC samples analyzed for ^{14}C in this study is more limited than those analyzed for ^{13}C (68 vs. 90), especially when previously published data are included (172 previous ^{13}C measurements). As ^{14}C and ^{13}C are closely linked, I expand on information gleaned from dual isotopes by placing such measurements in the context of overall ^{13}C-DIC variability from the same expeditions or previous data from the same sites. Likewise, I will discuss isotopic results in the context of concurrent and previously analyzed major ion, alkalinity, and DIC observations.

The DIC isotopic dataset collected for this study is extensive and spans large areas of the Amazon basin. However, its scattered nature and general absence of discharge data prevent the use of quantitative, mass-balance analyses. For this reason, the approach used will be more qualitative and descriptive. I first build on Stallard & Edmond's (1983) work using inorganic solutes to delineate dominant lithologies and weathering sources of DIC across the basin. Next, I examine broad isotopic, DIC, and pCO_2 trends by topographic class (lowland, mountain, and mixed) in each of the six regions (Fig. 6.1) to identify the primary terrestrial sources and channel processes controlling DIC cycling across the basin. After a examining regional variability in terrestrial DIC sources to smaller rivers and streams (< 9,000 km^2), I focus on downstream trends in DIC, alkalinity, pCO_2, pH, and CO_2 isotopes along several longitudinal transects in order to determine the changing, relative importance of processes such as gas exchange, respiration, and tributary inputs on the

downstream evolution of inorganic carbon. This approach is warranted by the unique combination of vegetation, climate, topography, and lithology found in each subbasin. Finally, I conclude by synthesizing individual subbasin trends into a basin-wide assessment of the importance and regional variability of terrestrial DIC sources and of processes controlling its fluvial cycling.

Weathering regimes and DIC sources

Stallard & Edmond (1983) introduced an approach to assess the relative importance of different lithologies and associated weathering regimes based on the concentrations of major inorganic solutes in rivers (see Chapter 5, and Stallard 1985; Stallard 1995; Edmond *et al.* 1996). This scheme relies on a ternary diagram where total cation concentration increases from the Si vertex, to the alkalinity vertex, to the $Cl^-+SO_4^{2-}$ vertex, as the dominant weathering source shifts from silicates, to carbonates, to evaporites, respectively. Fig. 6.2 presents data from all across the Amazon basin. As Cl^- and SO_4^{2+} were not analyzed at Vargem Grande and Itapeua in the 1991 expedition (MS91, Table 6.1), I used mean values from adjacent sites from the two Alpha-Helix cruises (AHSTA, Table 6.1). Major ions were not corrected for cyclic salts (marine aerosols). In the Andes, such correction is largely unnecessary as the presence of weatherable lithologies produces high major ion concentrations, and concentrations in rainfall are very diluted due to the large distance from the Atlantic Ocean source (Stallard & Edmond 1981; Guyot 1993; Edmond *et al.* 1996; Mortatti & Probst 2003). While the correction may be important in central and eastern parts of the basin, this geochemical data is used only qualitatively to characterize regional lithological patterns. Conclusions in this study are not affected by a lack of cyclic salt correction.

Shield sites cluster along the silicate weathering regime, with Guyana Shield sites tending closer towards the Si vertex; several Rio Negro samples would have plotted near the Si vertex, but were excluded because they had negative alkalinity. Highly weatherable silicate lithologies are apparent in many Brazilian Shield sites from the Ji-Paraná basin and nearby watersheds (Ferreira *et al.* 1988; Ballester *et al.* 2003; Holmes *et al.* 2004; Krusche *et al.* in prep.), as well as Rio Branco, a northern tributary to Rio Negro in the Guyana Shield (Stallard & Edmond 1983). Shield sites overlap partly with the Subandean Foreland sites, which extend into the alkalinity dominance region characteristic of carbonate dissolution and into the interior of the diagram that is influenced by sulfate originating from the oxidation of black shale (Stallard & Edmond 1983). Juruá and Purus sites, particularly in the headwaters, have reduced overlap with the silicate regime, and generally extend farther into the carbonate-dominated region compared to Shield and Foreland sites; this trend was first suggested in previous studies sampling the Juruá and Purus mouths (Stallard & Edmond 1983; Palmer & Edmond 1992).

Both Peru-Amazon and Bolivia-Madeira sites cluster in the carbonate dissolution region, but the former also extends into the $Cl^-+SO_4^{2-}$ vertex characteristic of evaporite dissolution, while the latter has extensive incursions into the lower interior of the diagram characteristic of black shales ("kerogen"). Carbonate dissolution in the Andes is therefore a source of DIC with high concentrations, depleted ^{14}C, and enriched ^{13}C (see discussion in Chapter 4). The presence of black shales in Bolivia-Madeira sites is supported by a general excess of SO_4^{2-} compared to Ca^{2+} in this region compared to Peru-Amazon (Fig. 6.3), indicative of oxidation of reduced sulfur from black shales in the former vs. gypsum ($CaSO_4$) dissolution in the latter (Stallard & Edmond 1983; Elbaz-Poulichet *et al.* 1999; Dalai *et al.* 2002; Millot

et al. 2003). An important consequence for the origin of DIC in Bolivia is that oxidation of black shales may provide both a direct source of aged CO_2 (Bacon & Keller 1998; Keller & Bacon 1998; Petsch *et al.* 2001; Berner *et al.* 2003) and a source of protons for dissolution of carbonates where the resulting HCO_3^- comes exclusively from carbonate minerals and is therefore ^{14}C-dead and highly enriched in ^{13}C (e.g., Galy & France-Lanord 1999; Yoshimura *et al.* 2001; Dalai *et al.* 2002; Millot *et al.* 2003).

Regional trends

Lowlands. Lowland river CO_2 is predominantly contemporary, has a $\delta^{13}C$ between the range of lowland C_3 (-32 to -26‰) and C_4 (-16 to -12‰) plant material, and is always relatively enriched in $\delta^{13}C$ compared to the lowland C_3 end member (Fig. 6.4; see Fig. 5.2 for end-member delineation and explanations). Lowland river DIC concentrations ranges from nearly zero in Shield and Subandean Foreland sites to >1,000 μM in the Juruá and Purus (Fig. 6.5), while pCO_2 ranges from atmospheric equilibrium (~ 360 ppm) to >13,000 ppm (Fig. 6.6). At ~ -8‰, atmospheric $\delta^{13}C$-CO_2 (see Chapters 4 and 5) is considerably more enriched than C_4 grasses and the most enriched lowland CO_2 sample; this isotopic separation together with high CO_2 supersaturation suggest that mixing with air may be a relatively minor influence on lowland CO_2.

The most $\delta^{13}C$-enriched lowland sites occur in Ji-Paraná basin in Rondônia in the Brazilian Shield, where C_4 pastures are abundant; the relative influence of air and respiration on river CO_2 in this region will be addressed in another section. The $\delta^{13}C$-CO_2 of Rio Negro (Guyana Shield) sites clusters closer to the C_3 end-member than all other lowland sites. Brazilian Shield sites span a wide range in $\delta^{13}C$ but also include the only lowland sites with $\delta^{13}C$-CO_2 fully overlapping the C_4 grass end-member;

these $\delta^{13}C$-enriched sites generally have higher DIC concentrations than the rest of that region (Fig. 6.5b). Shield DIC is low (<250 μM), except in the Ji-Paraná; while pCO_2 is as variable as lowland pCO_2 in general, it concentrates in the 2,000 to 6,000 ppm range (Fig. 6.6). The most $\delta^{13}C$-depleted Shield sites generally have the lowest DIC concentrations (Fig. 6.5b), suggesting C_3 sources in weathered lithologies.

Other lowland regions have $\delta^{13}C$-CO_2 intermediate between C_3 and C_4 end members. Subandean Foreland lowland sites (Rios Jutaí, Içá, and Japurá, see Fig. 3,6) show considerable variability in $\delta^{13}C$ (-24.84 to -17.14‰), low to intermediate DIC concentrations (Fig. 6.5b), and widely variable but generally highly supersaturated pCO_2 (Fig. 6.6) likely reflecting varying mixtures of CO_2 from C_3 and C_4 respiration, and relatively weatherable silicate lithologies in the Andean headwaters and lower depositional areas. The only $\Delta^{14}C$-CO_2 measurement available (Japurá mouth) reflects contemporary atmospheric CO_2, like most lowland CO_2. In contrast, Juruá and Purus sites have intermediate to high DIC, widely ranging but generally highly supersaturated pCO_2, fairly depleted $\delta^{13}C$ similar to the mainstem (Quay *et al.* 1992), and $\Delta^{14}C$ ranging from contemporary to depleted (1.8‰); this signature supports a diluted contribution from carbonate dissolution by soil CO_2 in forested (C_3) watersheds under largely open conditions (see Chapter 4 for discussion on carbonate dissolution).

Lowland $\Delta^{14}C$-CO_2 outliers are limited to an aged ($\Delta^{14}C$ = -145.9‰), $\delta^{13}C$-depleted (-25.27‰) Brazilian Shield observation in the Guaporé river South of Rondônia, which drains large wetland areas and has low oxygen content (Table 5.2); and an aged ($\Delta^{14}C$ = 1.8‰) site in the Purus headwaters, which together with two other relatively aged sites (below contemporary atmospheric $\Delta^{14}C$-CO_2) in the Purus and Juruá headwater, have substantially higher DIC concentrations compared to all

other lowland sites (Table 5.2, Figs. 6.5a, 6.5b), indicating a larger contribution from carbonate dissolution.

Mountains. All mountain sites are depleted in $\Delta^{14}C$, enriched in $\delta^{13}C$, have medium to very high DIC concentrations, and pCO_2 ranging from below saturation to ~ x10 atmospheric CO_2 (Figs. 6.4 to 6.6). Such composition is characteristic of areas highly influenced by carbonate weathering (see Chapter 4) and is consistent with the major ion trends discussed earlier. $\delta^{13}C$-CO_2 overall is more enriched than what would be expected from closed-system carbonate dissolution by biogenic soil CO_2 derived from C_3 plant material (~ -16‰) (Chapter 4, and Mook & Tan 1991; Clark & Fritz 1997; Aucour *et al.* 1999) dominant in mountain environments (Cabido *et al.* 1997; Ehleringer *et al.* 1997), even after accounting for the altitude enrichment effect on carbon fixed by plants (see Chapter 5, and Körner *et al.* 1991; Bird *et al.* 1994). Mixing with air in these generally turbulent and low-pCO_2 rivers may therefore play an important role (Stallard & Edmond 1987).

Peruvian Andes sites are generally more extreme in both isotopes and have much higher DIC concentrations compared to Bolivian sites (Figs. 6.4, 6.5), possibly the result of more abundant carbonate lithologies in Peru as indicated by major ion trends and lithological information (Stallard & Edmond 1983). However, three DIC-rich mountain sites in the upper Peruvian headwaters of the Vilcanota (Figs. 6.1, 5.1) have $\Delta^{14}C < -500‰$. Such a signature would require weathering under fully closed conditions with aged CO_2 or aging in aquifers. Groundwater residence times in mountainous regions are likely relatively short, leading to only limited aging along groundwater flowpaths. As discussed in Chapter 4, weathering commonly occurs under partially open conditions involving considerable exchange between DIC and biogenic soil CO_2, yielding waters with isotopic composition intermediate between

open and closed conditions, including $\Delta^{14}C > -500‰$ (see also Clark & Fritz 1997; Aucour *et al.* 1999). Instead, this baseflow, low-water signature may be influenced by carbonate weathering with ^{14}C-dead CO_2 degassed from the lithosphere (Fig. 5.2 and further discussion below) in this tectonically active cordillera.

Mixed sites. Mixed sites in the Subandean Foreland (Napo mouth), Peru-Amazonas, and Bolivia-Madeira regions clearly display transitions from mountain to lowland isotopic and DIC signatures, evolving towards younger, more $\delta^{13}C$-depleted CO_2, lower DIC concentrations, and higher pCO_2 (Figs. 6.4 to 6.6). This trend is probably the result of dilution of Andean influenced waters containing substantial carbonate dissolution contributions with lowland inputs from more weathered terrains, combined with high *in situ* respiratory fluxes of contemporary CO_2, as discussed in Chapter 5. However, while Rio Madeira CO_2 at the mouth appears isotopically undistinguishable from most large lowland rivers, the Solimoes-Amazonas at Manacapuru (Fig. 6.1) retains a relatively aged $\Delta^{14}C$ composition (29.8 to 75.7‰). If the OC fraction being respired is contemporary, as concluded in Chapter 5 from lowland sites, this aged signature suggests that a dynamic equilibrium between CO_2 evasion and respiration has not been reached with respect to $\Delta^{14}C$; this conclusion is in contrast with what has been postulated for CO_2 and $\delta^{13}C$ on the basis of mass balance, respiration experiments, and $\delta^{13}C$ analyses in the mainstem (see Chapter 5 discussion, and Quay *et al.* 1992).

Terrestrial sources of DIC

As rivers grow larger downstream, riverine processes such as gas exchange, photosynthesis, and respiration can swamp and erase the biogeochemical signature exported from *terra firme* components of the watershed (see Chapters 2 and 4 for

additional discussion). In order to identify terrestrial sources of DIC across the basin, I selected rivers draining relatively small areas, <9,000 km^2. While only a few of these are actually first- and second-order streams and many may be strongly influenced by fluvial processes, overall this set provides the best opportunity to examine the range of terrestrial inputs in this study. I have further separated smaller streams within this set, those draining areas <4,000 km^2.

Fig. 6.7a is analogous to Fig. 6.4 but focuses only on smaller rivers and a narrower, younger $\Delta^{14}C$ range. Only one river outside the shields is represented among lowland sites, implying a regionally biased view of lowland variability in terrestrial sources. Most small lowland rivers have contemporary CO_2 and $\delta^{13}C\text{-}CO_2$ reflecting an apparent mixture of C_3 and C_4 end members, indistinguishable from the isotopic signatures of larger lowland rivers. However, only the smallest streams have $\delta^{13}C\text{-}CO_2$ close to pure C_4 contributions; these occur in fully and partially deforested areas of the Ji-Paraná basin (NS1 and NS2, see Table 5.1). In addition, in carbonate-free regions only the large Guaporé river (see discussion above) and some of the smallest streams (NS1, PB-1, COM-1, and Azul, in Rondônia) show any significant aging, with atmospheric $\Delta^{14}C\text{-}CO_2$ offsets ranging from –66.7 to –20.0‰ for the small streams (refer to Chapter 5 and Table 5.3). $\delta^{13}C\text{-}CO_2$ of PB-1, COM-1, and Azul fall near the depleted end for Rondônia sites (–21.77 to –19.83‰), suggesting that soils and groundwater in that region can export aged CO_2 with substantial influence from C_3 respiration. The aged NS1 observation and the Guaporé have the lowest oxygen concentrations measured, 67.5 and 176 μM, respectively, where atmospheric saturation at 28°C is ~ 250 μM (Devol *et al.* 1995); they provide tentative evidence for decomposition of aged organic matter in low-oxygen environments such as wetlands.

In contrast, CO_2 in small Rio Negro streams (all <4,000 km^2) is contemporary and highly depleted in $\delta^{13}C$, though relatively enriched in $\delta^{13}C$ compared to C_3 plant material (see Fig. 5.2). All but one are first-order streams (Table 5.1), and their watersheds span a range of ecosystems from white-sand (spodosol), relatively open *campina* forest to closed forests above clayey Oxisols, and the larger Cuieiras stream draining a combination of both. They are unlikely to have any C_4 contributions, as most sites are canopy-covered streams where C_4 grasses are absent. However, their $\delta^{13}C$-CO_2 is within the range of clayey (Oxisol) forest soil CO_2 (-25 to -23‰) identified at the Paragominas site in eastern Amazonia (Trumbore *et al.* 1995; de Camargo *et al.* 1999); such CO_2 was also contemporary.

As discussed in Chapter 4, Telles *et al.* (2003) found that soil organic carbon in sandy Manaus Spodosols is more depleted in $\delta^{13}C$ and remains uniformly young with depth, while SOC in clayey Oxisols becomes enriched in $\delta^{13}C$ and much older with depth; in Rio Negro, clear-water streams with watersheds dominated by clay soils often have sandy valley soils (Bravard & Righi 1990; McClain *et al.* 1997; Telles *et al.* 2003; Luizão *et al.* 2004). Isotopic differences between small streams in Rondônia and in Rio Negro may result from such differences in SOC, which are in turn the product of different soil sorptive capacity. Nevertheless, both soil types produce acidic, low-conductivity streams, while certain soils in Rondônia yield more solute-rich and neutral streams (Fig. 6.7b).

Carbonate dissolution exerts considerable influence on the headwaters of the Juruá and Purus, and on mountain sites. This is especially noticeable in the small Acre river in the Purus (Fig. 6.7). Small mountain sites have a wide range of ion content (conductivity), but all tend to be $\delta^{13}C$-rich . As observed earlier, this is particularly true in Peru, where Vilcanota headwaters also appear to be influenced by

evaporite dissolution and $\Delta^{14}C$ that is unusually depleted compared to normal carbonate dissolution processes.

Downstream evolution

Ji-Paraná. As an extensive dataset was collected in the Ji-Paraná basin, I will examine regional and downstream trends closely in this region, highlighting regional variability within the basin (Fig. 6.8). As discussed earlier, small streams in the Comemoração (COM-1) and Pimenta Bueno (PB-1) headwaters are generally the most aged (Fig. 6.9a) – below contemporary atmospheric $\Delta^{14}C$-CO_2. These streams together with the larger, blackwater Rio Preto near the mouth of the Ji-Paraná, are generally the most acidic, solute poor, least supersaturated in pCO_2, and most $\delta^{13}C$-depleted waters in the Ji-Paraná basin (Figs. 6.9b, 6.10, 6.11). In contrast, small pasture streams (NS1 and NS2) in the southwestern tributaries are generally contemporary and are the most $\delta^{13}C$-rich waters, matching C_4 signatures closely. In these sites pastures often grow right into the streams (A. Aufdenkampe and A. Krusche, pers. comm.). These solute-rich sites (Fig. 6.11) are highly supersaturated in pCO_2 (Figs. 6.10a, 6.12) and are characteristic of the cation-rich lithologies of the southwestern tributaries to the Ji-Paraná (Biggs *et al.* 2002; Ballester *et al.* 2003; Biggs *et al.* 2004; Holmes *et al.* 2004; Krusche *et al.* in prep.).

Mid to large rivers in the Ji-Paraná basin have contemporary $\Delta^{14}C$ values (Fig. 6.9a), varying closely with atmospheric $\Delta^{14}C$-CO_2 (see Fig. 5.3). However, the southwestern tributaries are generally somewhat more $\delta^{13}C$-enriched than the Comemoração and Pimenta Bueno (Figs. 6.9b, 6.11a); this may be the result of more widespread deforestation and replacement by C_4 pastures in the southwestern tributaries (Ballester *et al.* 2003). In terms of $\delta^{13}C$ and conductivity, the Machadinho

is the most variable river in the basin; it appears to be influenced by both cation-rich and cation-poor lithologies, and by pastures, forests, and possibly by respiration of algal material. Finally, the mainstem is rather uniform isotopically and may be a mixture of C_4 and C_3 respiration, possibly with some additional $\delta^{13}C$ enrichment resulting from high evasion rates due to a relatively turbulent, wide, and shallow river bed with scattered rocky outcrops (pers. obs.).

Relatively low pCO_2 supersaturation in some samples in the region can result in substantial invasion of atmospheric CO_2 in these turbulent rivers. Contemporary mixtures of atmospheric CO_2 and respired CO_2 from C_3 and C_4 organic matter cannot be distinguished based on $\delta^{13}C$ alone. Increasing influence of atmospheric invasion at lower pCO_2 should be reflected in a negative correlation between $\delta^{13}C$-CO_2 and pCO_2; such correlation is not present (Fig. 6.12), indicating that the importance of atmospheric CO_2 invasion is not clearly established, though it cannot be discounted. See Chapter 5 for additional discussion.

Fig. 6.11 suggests largely two sources of water in the basin, one made up of the Comemoração, Pimenta Bueno, and Preto, which are solute-poor, acidic, and relatively depleted in $\delta^{13}C$ from lower deforestation extents and highly weathered lithologies; and another made up of solute-rich, neutral, and more enriched $\delta^{13}C$ from higher presence of pastures and more cation-rich lithologies (Ballester *et al.* 2003; Holmes *et al.* 2004; Krusche *et al.* in prep.). Fig. 6.11 also indicates a downstream evolution from small streams in each of these terrains. In solute-poor terrains, rivers become less acidic, more solute-rich, and more enriched in $\delta^{13}C$ downstream, possibly as a result of the inclusion of pasture areas and weatherable lithologies, and the effect of CO_2 evasion. In solute-rich terrains, rivers remain equally solute-rich, but become generally more basic and somewhat less depleted in $\delta^{13}C$. This change

appears to be the result of CO_2 evasion and the inclusion of respiration of organic matter from scattered forests in the larger tributaries, compared to the purer pasture composition of the small streams. Finally, near constancy in $\delta^{13}C$ and $\Delta^{14}C$ of CO_2 in the mainstem over ~ 600 km suggests the occurrence of a dynamic equilibrium between respiration, evasion, and possibly atmospheric invasion.

Rio Negro. Small streams and the mouth of the Rio Negro are very similar isotopically – all are contemporary and depleted in ^{13}C (Fig. 6.13; see also Fig. 6.4). However, smaller streams appear to be generally more acidic and somewhat $\delta^{13}C$-depleted overall, compared to the Rio Negro mouth. C_4 grasses are rare on the banks of the Rio Negro (see discussion in Chapter 4). This effect may then be the result of CO_2 evasion, which preferentially removes the lighter ^{12}C isotope and enriches the remaining CO_2, while leading to a small increase in pH.

Juruá and Purus. As discussed earlier, the headwaters of these basins appear to have substantial outcrops of carbonate sediments that are being weathered with forest soil CO_2. Alkalinity and major ion concentrations in these headwaters are as high as many Andean rivers draining carbonate sediments. No data are available from the middle of the basins, but at their mouths, these rivers are still rich in DIC and solutes compared to all other lowland rivers (Figs. 6.2, 6.5); the Juruá at low water has alkalinity values as high as Vargem Grande in the mainstem, and much higher than the Madeira near Bolivia. However, the isotopic signature of carbonate dissolution has been completely erased through the input of lower tributaries and respiratory inputs of contemporary organic matter fractions (see Chapter 5). Evidence of this transition can be gleaned from unpublished data from the HiBAM/IRD Amazon river geochemical program. They sampled the middle and lower Purus only a month before CAMREX sampled the headwaters. While only pH,

conductivity, and discharge data are available on their web site, these data clearly show a transition from higher conductivity and pH closer to the headwaters sampled by CAMREX, to lower conductivity and pH downstream. Replacement of DIC derived from carbonate dissolution by contemporary DIC derived from riverine respiration, and accompanying CO_2 evasion, are likely to take place along this transition zone in the middle of the basin

Bolivian Andes and Madeira mainstem. As discussed earlier and pointed out by Stallard & Edmond (1983), carbonate and evaporite sediments appear to be less common in the Bolivian Andes compared to the Peruvian Andes (Fig. 6.2), leading to overall lower concentrations of solutes and alkalinity (Fig. 6.5, where DIC may be used as a proxy for alkalinity). Alkalinity generally decreases from the mountains to the Madeira mouth in the Beni-Madeira system, a result from dilution with lowland rivers draining mostly weathered lithologies (Fig. 6.14b). Even in the mountains, Beni tributaries have low alkalinity relative to the Beni and the Peruvian Andes. In addition, the range of variability in alkalinity at the mixed "Riberalta Arriba" site (Fig. 5.1, Table 5.1) in the lowland depositional fan just before the confluence with the Madre de Dios, is similar to that in the Andean headwaters of the Beni. It appears that carbonate outcrops may be highly scattered across the Beni, intermixed with less weatherable silicate lithologies such as black shales.

Enriched $\delta^{13}C\text{-}CO_2$ in the mountains (first 500 km, Fig. 6.14a; see also Fig. 6.4) results partly from carbonate weathering inputs, as suggested by alkalinity (Fig. 6.14b), inorganic solute composition (Fig. 6.2), and depleted $\Delta^{14}C$ values (Fig. 6.4). Low pCO_2 levels (Fig. 6.14c) in these high-relief, turbulent rivers indicates that atmospheric CO_2 invasion is an important source of CO_2 in the mountains. Oxidation of black shales (Figs. 6.2, 6.3) may play a significant role as well, but its importance

can not be assessed quantitatively with current data. For the next 600-800 km downstream from the foothills, to the Madeira at Abuna near Rondônia, a $\delta^{13}C$ depletion and $\Delta^{14}C$ enrichment is accompanied by an increase in pCO_2 to supersaturation levels >10 x atmospheric pCO_2, while alkalinity remains nearly unchanged. These trends may be the result of lower atmospheric CO_2 invasion possibly combined with higher fluxes of respired CO_2 from C_3 organic matter. Farther downstream to the mouth of the Madeira there is an additional, small depletion in $\delta^{13}C$, while CO_2 becomes contemporary as a result of lowland tributary inputs and *in situ* respiration of contemporary organic matter. Ji-Paraná fluxes appear to have higher alkalinity and unusually enriched $\delta^{13}C$-CO_2 compared to other tributaries in the region.

Peru from Vilcanota Andean headwaters to Ucayali mouth. Compared to the Beni-Madeira transect, much more isotopic data are available for this transect. The transect may be divided into four reaches according to their geochemical and isotopic data (Figs. 6.15, 6.16). For the first 250 km in the Rio Vilcanota along the Altiplano to Pachar, site elevations decrease only from 3,900 to 3,100 meters and channel slope is generally gentle. In this relatively arid region, low-water samples show some of the highest alkalinity and major ions anywhere (Figs. 6.16a, 6.2); evaporite and carbonate dissolution are clearly widespread, with the latter leading to highly depleted $\Delta^{14}C$ and enriched $\delta^{13}C$ (Fig. 6.15). However, as pointed out earlier, the isotopic signatures are beyond the range of typical waters derived from carbonate dissolution (see Chapter 4, and Clark & Fritz 1997; Aucour *et al.* 1999). Several processes can lead to this anomaly, but highly elevated pCO_2 in the middle of this reach compared to most Andean sites (Fig. 6.16b, but also see Stallard & Edmond 1987) indicates an additional source of CO_2. High *in-situ* respiration from

agricultural runoff is unlikely because $\delta^{13}C$-CO_2 is too enriched and oxygen levels are near atmospheric saturation at the local temperature and elevation (not shown).

High pCO_2, highly depleted $\Delta^{14}C$ (<-500‰), enriched $\delta^{13}C$, high uplift rates, relative abundance of hot springs, and existence of Quaternary volcanism (R. Marocco, pers. comm.) all point to a substantial input of lithospheric CO_2 of volcanic or metamorphic (non-volcanic) origin (see Fig. 5.2). Volcanic CO_2 flux to rivers has been documented in the western Andes in Chile (Aravena & Suzuki 1990); metamorphic CO_2 flux is a phenomenon that has been widely documented elsewhere but not in the Andes, despite favorable geotectonic conditions (Rose & Davisson 1996; Kerrick & Caldeira 1998; Chiodini *et al.* 1999; Galy & France-Lanord 1999; James *et al.* 1999; Kerrick 2001; Yoshimura *et al.* 2001; Mörner & Etiope 2002; Yoshimura *et al.* 2004). Metamorphic, thermal decarbonation of carbonate sediments at depth produces CO_2 and dissolved Ca^{2+} which are then hydrothermally transported to the surface. This process may impact river DIC through direct input of ^{14}C-dead, $\delta^{13}C$-enriched lithospheric CO_2, and weathering of aquifer carbonates with lithospheric CO_2. Additional dry-season sampling of hot springs and groundwater is needed to isolate the occurrence of lithospheric degassing in this reach.

Over the next 150 km to Quillabamba on the Urubamba river, the river drops rapidly by about 2,000 meters. Alkalinity decreases and pCO_2 becomes close to equilibrium with the atmosphere (Fig. 6.16). $\Delta^{14}C$ is rapidly enriched to levels more typical of carbonate dissolution by contemporary CO_2 under partially open conditions. However, $\delta^{13}C$ remains highly enriched, possibly a result of atmospheric CO_2 invasion which would also enrich $\Delta^{14}C$. In the next 400 km to the mouth of the Urubamba at Atalaya, where the Ucayali begins at the confluence of the Tambo and Urubamba (Figs. 6.1, 5.1, 2.2), alkalinity and pCO_2 remain unchanged, but the major

shift is a large depletion in $\delta^{13}C$ accompanied by a smaller enrichment in $\Delta^{14}C$. In this forested and humid reach, carbonate dissolution appears to continue at high rates, but the CO_2 involved in weathering has shifted largely to soil CO_2 from forests (C_3). On the other hand, the Tambo and its upstream tributary (Cunyac, along the Apurimac river) are still enriched in $\delta^{13}C$, suggesting that they are not yet as impacted by lowland environments, as implied by the Tambo's higher mean basin elevation compared to that of the Urubamba (Table 5.1).

Over the next 1,400 km along the lowlands, alkalinity remains stable and high, and isotopes also remain nearly unchanged, suggesting that carbonate dissolution with CO_2 derived from lowland C_3 or possibly C_4 plants remain very important. However, pCO_2 increases from near atmospheric equilibrium to ~ 10 x atmospheric levels, more typical of lowland rivers and indicative of the growing influence of lowland inputs and *in-situ* respiration. This evolution and the persistent influence of carbonate dissolution indicate that the Ucayali is still a river in transition and not typical of lowland rivers or even the Amazon mainstem downstream. It is important to note that previous measurements (Stallard & Edmond 1983) of major ions and alkalinity at two reaches along the Urubamba and Ucayali (Fig. 6.16a) are in the same range as CAMREX measurements, suggesting that CAMREX observations are not anomalous. On the contrary, higher alkalinity measured by Stallard & Edmond (1983) in the middle Ucayali suggests that there may be periods of the hydrograph when carbonate dissolution is even more vigorous.

Amazon mainstem from Ucayali-Marañón confluence to Manacapuru. The Amazon mainstem (Solimões-Amazonas) from Vargem Grande to Manacapuru and Obidos has been studied before in detail (Longinelli & Edmond 1983; Stallard & Edmond 1983; Richey *et al.* 1990; Quay *et al.* 1992). Here I will discuss only some

salient points. First, $\delta^{13}C\text{-}CO_2$ appears to transition smoothly from the upstream end to Vargem Grande and Manacapuru (Fig. 6.17b), following the same gentle depletion trend already observed from Vargem Grande to Manacapuru (Martinelli *et al.* 1991; Quay *et al.* 1992) and possibly controlled by a $\delta^{13}C$ dynamic equilibrium between respiration and evasion postulated in previous studies (see Chapter 4, and Devol *et al.* 1987; Richey *et al.* 1990; Quay *et al.* 1992). $\Delta^{14}C\text{-}CO_2$, on the other hand, is still evolving and not in equilibrium, steadily increasing from the Ucayali and Marañón to Vargem Grande, Itapeua, and Manacapuru, over a distance of 2,100 km (Fig. 6.17a). Manacapuru $\Delta^{14}C$ has a bomb component but is still below contemporary atmospheric levels, implying that it is not in equilibrium with respiration of contemporary organic matter; see additional discussion on this issue above (*Regional trends*, mixed sites). Alkalinity decreases steadily from the Ucayali-Marañón confluence to Manacapuru, as a result of dilution by lowland tributaries (Fig. 6.18a). pCO_2 at the Ucayali and Marañón mouths appears to have already reached supersaturation levels typical of the mainstem (Fig. 6.18b), though additional observations are needed to assess the range of variability at those sites. Nevertheless, CAMREX Ucayali and Marañón alkalinity measurements are consistent with previous measurements from Stallard & Edmond (1983).

Seasonal variability

Seasonal cycles in river hydrographs can bring about large biogeochemical responses resulting both from differential contributions from different regions in large rivers as well as changing soil and in-channel processes (Richey *et al.* 1991; Devol *et al.* 1995; Richey *et al.* 2002). In this study, ^{14}C and ^{13}C DIC observations were sparse, rarely encompassing more than one sample per site (Table 5.3). To address

seasonal DIC and CO_2 cycles, I will focus on $\delta^{13}C\text{-}CO_2$, alkalinity, and pCO_2 at a range of representative sites with an adequate number of observations, including previously published data. As river discharge or stage data for sampling times were often not available, I will examine seasonal variability by matching each sample with the corresponding long-term monthly mean discharge for the sampling month. Plots for several sites are shown in Figs. 6.19 to 6.22.

In the lowlands (Ji-Paraná sites and Juruá and Purus mouths, Figs. 6.19, 6.20), there is a weak trend of depletion in $\delta^{13}C\text{-}CO_2$ with increasing discharge, and a well defined increase in pCO_2 supersaturation with discharge. These trends may be explained by higher depth-integrated respiration rates and higher CO_2 inputs from soils and inundated areas at high water, as suggested by Devol *et al.* (1995) for the Amazon mainstem. More depleted $\delta^{13}C\text{-}CO_2$ at high water may result from larger contribution by respiration of C_3 organic carbon, or conversely, increased atmospheric CO_2 invasion at low waters when shallower depths and lower river pCO_2 may facilitate exchange with the atmosphere. In the Purus and especially the Juruá, alkalinity increases substantially at low waters (Fig. 6.20), indicating a dilution of carbonate weathering DIC at high waters; therefore, in these systems depleted $\delta^{13}C\text{-}CO_2$ at high water may be partly the result of dilution of carbonate weathering DIC with waters originating in weathered regions of these basins. In contrast, the two Ji-Paraná sites and the Japurá mouth do not display any clear seasonal variability in alkalinity. Krusche *et al.* (in prep.) pointed out that alkalinity is indeed positively correlated with concurrently measured discharge at these Ji-Paraná sites, and suggested that these relatively dilute sites follow the soil-dominated pattern of Markewitz *et al.* (2001) for weathered soils, where cations and HCO_3^- are preferentially released during the wet season. In contrast, Ji-Paraná rivers draining

more weatherable silicate lithologies follow the more common pattern of dilution at high waters (Krusche *et al.* in prep.).

Seasonal variability at the mouth of Rio Madeira resembles that of the Purus mouth, although $\delta^{13}C\text{-}CO_2$ does not display clear seasonal changes (Fig. 6.21). At three sites in the Amazon mainstem (Fig. 6.22), pCO_2 and $\delta^{13}C\text{-}CO_2$ generally show the same trends described earlier, with increasing pCO_2 and decreasing $\delta^{13}C$ with discharge. However, the seasonal variability of alkalinity changes downstream, as pointed out by Probst *et al.* (1994). While at the most upstream site (Vargem Grande) alkalinity may increase slightly with discharge, farther downstream the relationship displays a hysteresis effect, with higher alkalinity at mid-range discharge levels (Fig. 6.22b); in contrast, at Obidos, the relationship becomes the more common dilution with discharge (not shown). The reasons for this downstream change are not clear, but likely involve differential seasonal contributions of large tributaries draining regions with strong contrasts in climate and lithology (Devol *et al.* 1995).

CONCLUSIONS

The geochemical survey presented in this study revealed large contrasts in DIC characteristics and controls across the basin. The dominant sources of basin-wide riverine isotopic variability are the presence of carbonate lithologies, the relative contribution of C_3 and C_4 organic carbon to respiration, and atmospheric CO_2 invasion in turbulent, low-pCO_2 rivers. Clear regional trends exist. Lowland rivers are predominantly supersaturated in pCO_2 and carry a DIC load that is at most only a few years old. ^{14}C-depleted DIC in the lowlands occurs only when carbonate lithologies are present (Juruá-Purus headwaters), in certain small streams receiving

aged groundwater CO_2 , and possibly in low-oxygen, wetland environments conducive to the decomposition of aged organic matter.

The isotopic signature of terrestrial DIC and CO_2 inputs into small streams varies across carbonate-free watersheds in the shields. Sandy soils north of Manaus and deforested regions in Rondônia export contemporary inorganic carbon, though the $\delta^{13}C$ of CO_2 reflects the dominant vegetation type. In contrast, weathered clayey soils in open and closed forests in the Ji-Paraná headwaters export aged inorganic carbon. C_4 vegetation, whether as riverine macrophytes or pastures in deforested areas, appears to exert a disproportionate influence on fluvial respiration and CO_2 in the lowlands. Riverine CO_2 is typically more supersaturated and more depleted in $\delta^{13}C$ at high water periods.

Carbonate lithologies are common throughout the Peruvian and Bolivian Andes, but are more abundant in Peru. Rapid, extensive erosion carries fresh, unweathered sediments into large depositional floodplains. As a result, carbonate dissolution occurs in depositional lowland environments as well as in mountainous areas, providing high DIC fluxes and distinctive isotopic signatures. The extensive presence of carbonate sediments above the Solimões results in slow replacement of ^{14}C-depleted DIC in the Amazon mainstem, in contrast with $\delta^{13}C$-DIC, which appears to reflect an equilibrium between evasion and respiration across the mainstem in addition to a very gradual downstream increase in contributions from C_3 respiration.

High rates of riverine respiration of contemporary organic carbon maintains CO_2 supersaturation with respect to the atmosphere, and will gradually "flush out" DIC of terrestrial origin via exchange with DIC and evasion of CO_2. Consequently, regardless of original sources, DIC in all rivers gradually becomes contemporary, approaching atmospheric ^{14}C-CO_2. High river turbulence can accelerate exchange

with the atmosphere; such conditions occur not only in steep Andean terrains, but also in rivers in the Brazilian and Guyana shields where rocky beds may be common.

In the Andes, tectonic activity and heterogeneity of lithologies can lead to local influence by marginal processes such as oxidation of black shales containing reduced sulfur, and volcanic and metamorphic lithospheric CO_2 degassing. At this point, further studies and surveys are needed to determine the regional extent of such processes. More generally, this study has only revealed the main patterns of DIC and CO_2 sources and cycling across the basin. Much more work is necessary to develop a solid, quantitative assessment of the regional extent of each end-member source and process identified in this study.

Table 6.1. Sampling programs with data used in this study. Columns DIC-^{14}C, DIC-^{13}C, and Major Ions indicate the type of geochemical data used from each program or expedition.

Program Code	Description and Regional Extent	Time Period	References	DIC ^{14}C	DIC ^{13}C	Major Ions
	CAMREX Datasets with Unpublished DIC Isotopes					
MS91	Amazon mainstem and mouths of major tributaries, from Vargem Grande to Obidos	8-9/1991		X	X	X
MS96	Central Amazon mainstem and mouths of major tributaries	7/1996		X	X	X
BO94	Bolivian low-water transect. Beni Andean headwaters; Beni, Madre de Dios, and Mamore confluences	11/1994	(Hedges *et al.* 2000)	X	X	X
BO95	High-water follow-up to 1994 Bolivian transect	5/1995				X
PE96	Peru low-water transect. Ucayali-Vilcanota Andean headwaters; Ucayali, Marañón, and Napo mouths	10-11/1996		X	X	X
ST96	Southern lowland tributary headwaters; Rio Jurua to Rondonia and Rio Guapore	6-7/1996		X	X	X
JIP	Rondonia Ji-Parana LBA expeditions (11 total)	8/1998 – 4/2002	(Ballester *et al.* 2003; Bernardes *et al.* 2004; Krusche *et al.* in prep.)	X	X	X
AA	Small and mid sized streams near Manaus and in Rondonia; Rio Solimoes near Marchantaria, and Madeira and Negro mouths. Collected by A. Aufdenkampe	1-12/1995, 7/2002 – 1/2003		X	X	
	Fully Published Datasets					
	CAMREX					
MS	12 cruises on the Amazon mainstem and mouths of major tributaries, from Vargem Grande to Obidos	5/1982 – 5/1990	(Richey *et al.* 1986; Richey *et al.* 1990; Quay *et al.* 1992)		X	X
MARCH	Monthly sample collection at Marchantaria, in the Rio Solimoes near Manaus	1983 – 1993	(Devol *et al.* 1995)		X	X
MAD	2 cruises along the Rio Madeira from Porto Velho to the mouth	4/1984, 1/1986	(Ferreira *et al.* 1988)			X
	OTHERS					
AHSTA	Alpha-Helix Amazon mainstem cruises, and additional collections from Peru, Bolivia, and central-lower Rio Negro by R. Stallard. ^{13}C data available but not used (see text)	5/1974 – 12/1978	(Stallard & Edmond 1983)			X
BOLIRD	PHICAB/IRD Bolivian Andes and lowland surveys. Only site average data are available	1983-1991	(Guyot *et al.* 1992; Guyot 1993; Guyot *et al.* 1996)			X
BOLEP	Bolivian Andes and lowland surveys	4,11/1994	(Elbaz-Poulichet *et al.* 1999)			X
PACH	5 Pachitea expeditions (Ucayali tributary) in Peruvian Andes, part of AARAM program	7/1998 – 8/2000	(Gómez *et al.* in press)			X

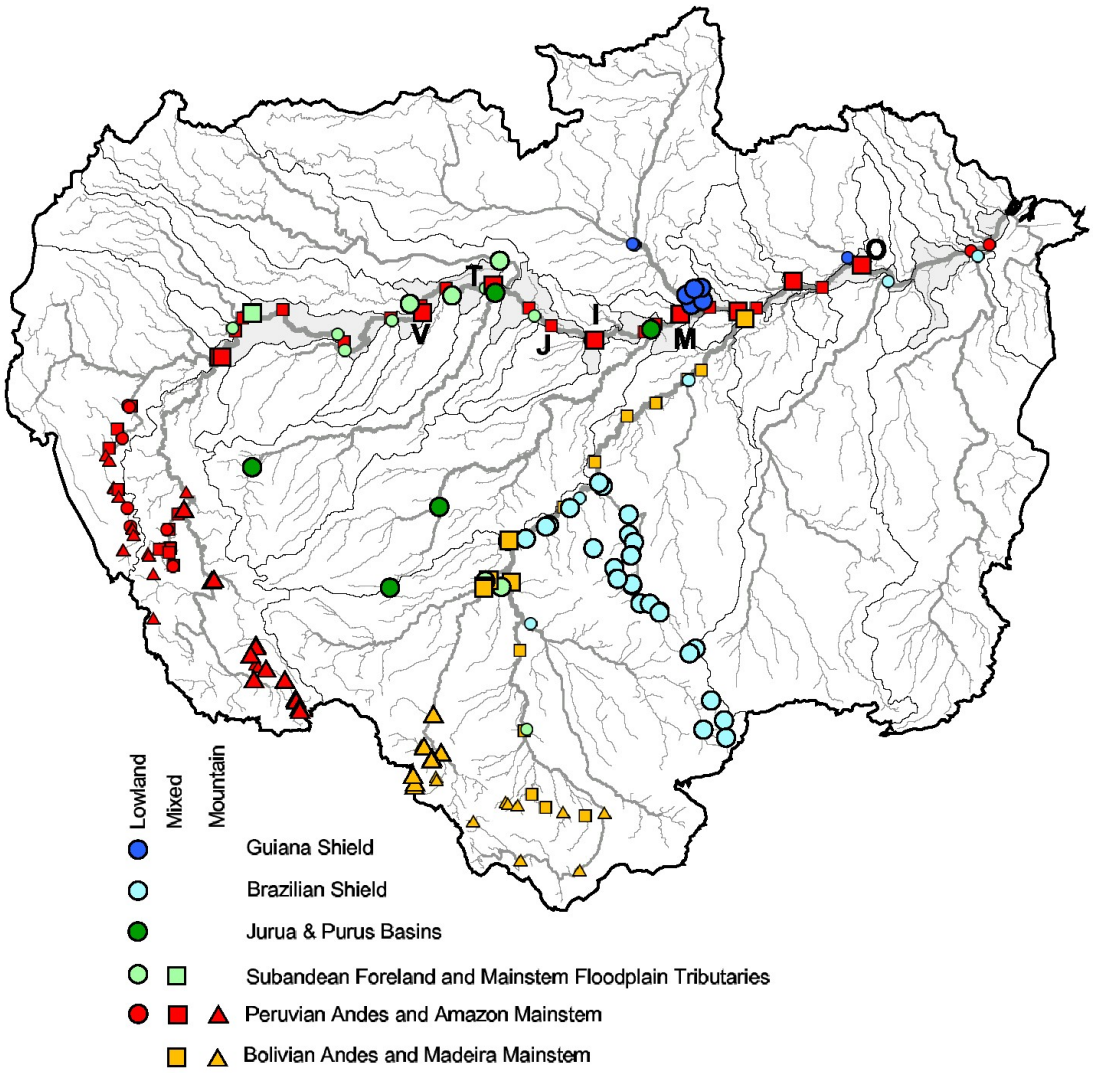

Figure 6.1. Amazon basin and sampling sites. Smaller site symbols represent sites with published ^{13}C-DIC or inorganic geochemistry data, not sampled in this study. Fig. 5.1 describes the topographic categories (lowland, mixed, and mountain). On the Amazon mainstem, V= Vargem Grande, T = Tupe, J = Jutica, M = Manacapuru-Marchantaria, and O = Obidos. Boundaries of major tributaries are shown; see Fig. 3.6 for tributary names.

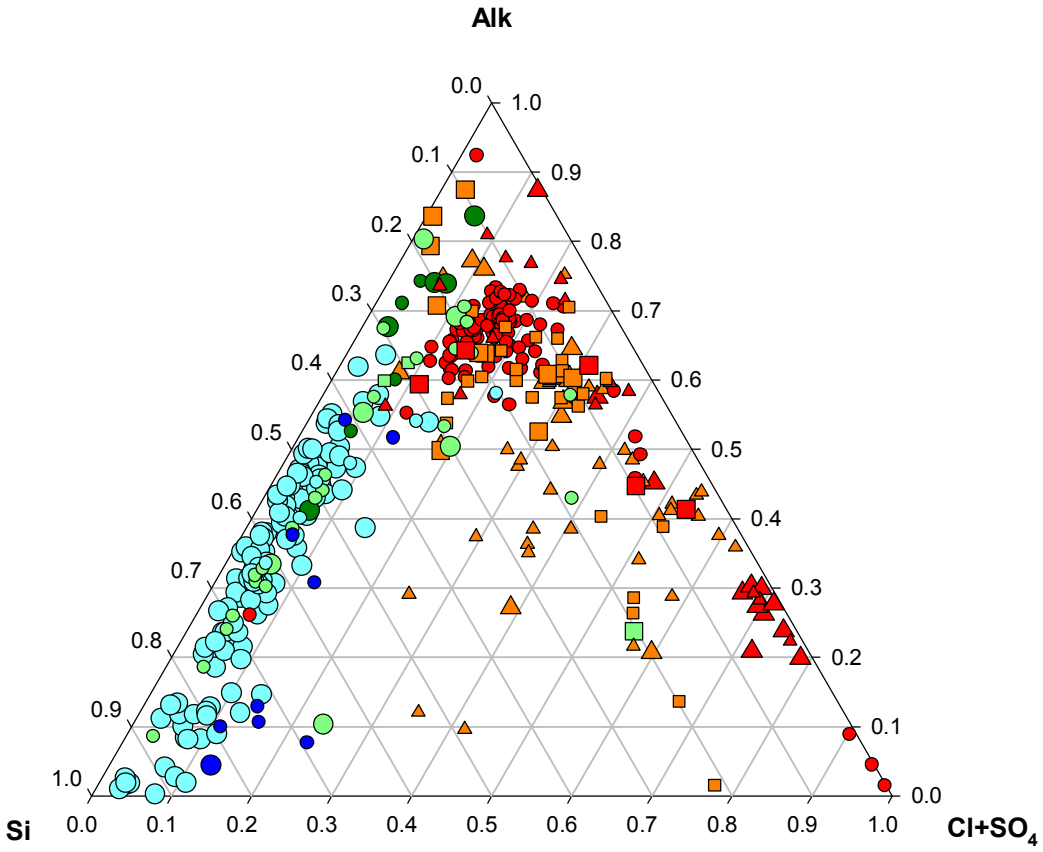

Figure 6.2. Major weathering regimes across the Amazon basin. Relative proportions of silica (µmol L^{-1}), alkalinity (µeq L^{-1}), and $Cl^- + SO_4^{2-}$ (µeq L^{-1}), indicative of dominant weathering regimes controlling the dissolved load. Symbology is the same as in Fig. 6.1.

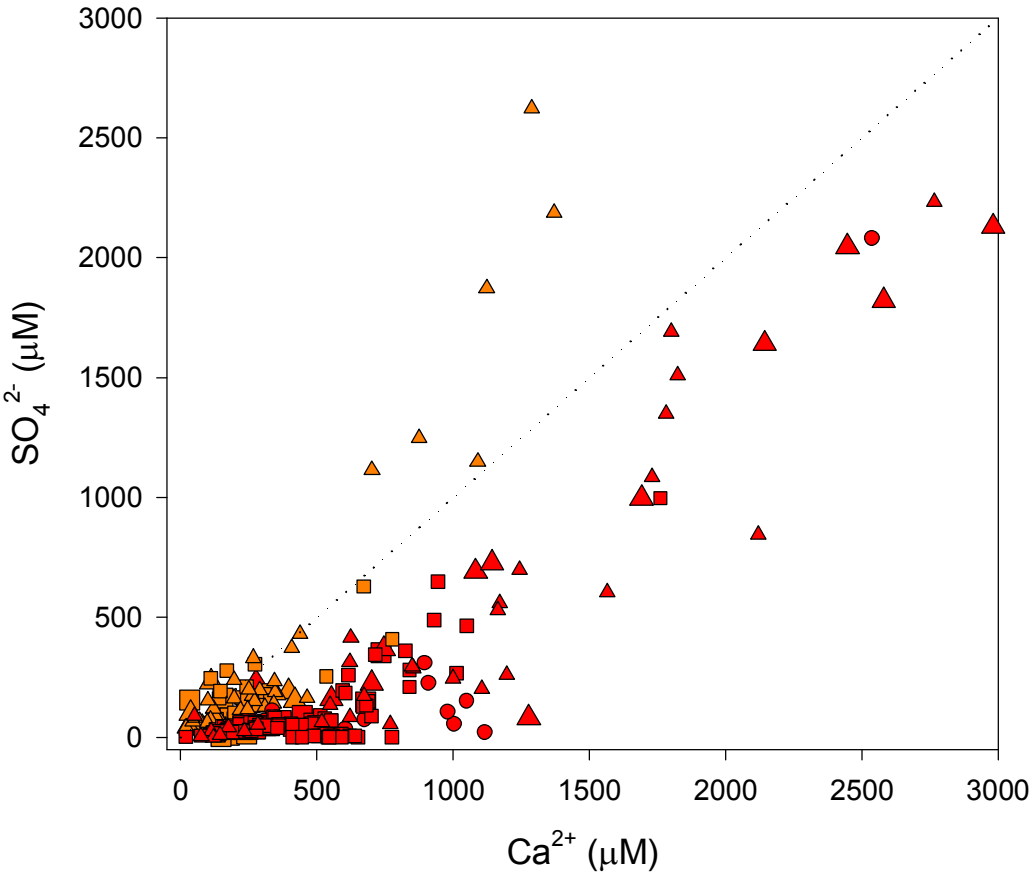

Figure 6.3. Sources of sulfate in rivers draining the Peruvian (red) and Bolivian (orange) Andes. Symbology is the same as in Fig. 6.1.

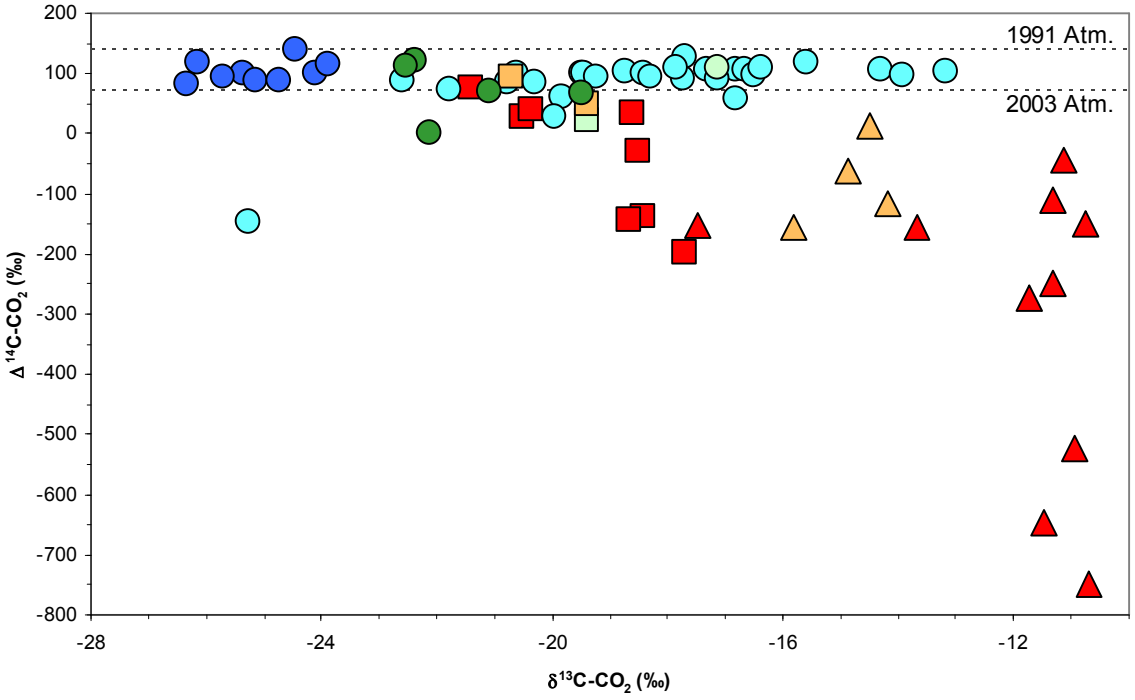

Figure 6.4. Basin wide CO_2 isotopic variability, $\Delta^{14}C$ vs. $\delta^{13}C$. Symbology is the same as in Fig. 6.1. Horizontal lines show the mean atmospheric $\Delta^{14}C$-CO_2 in tropical South America for the first and last sampling years (1991 and 2003, respectively). See Chapter 5.

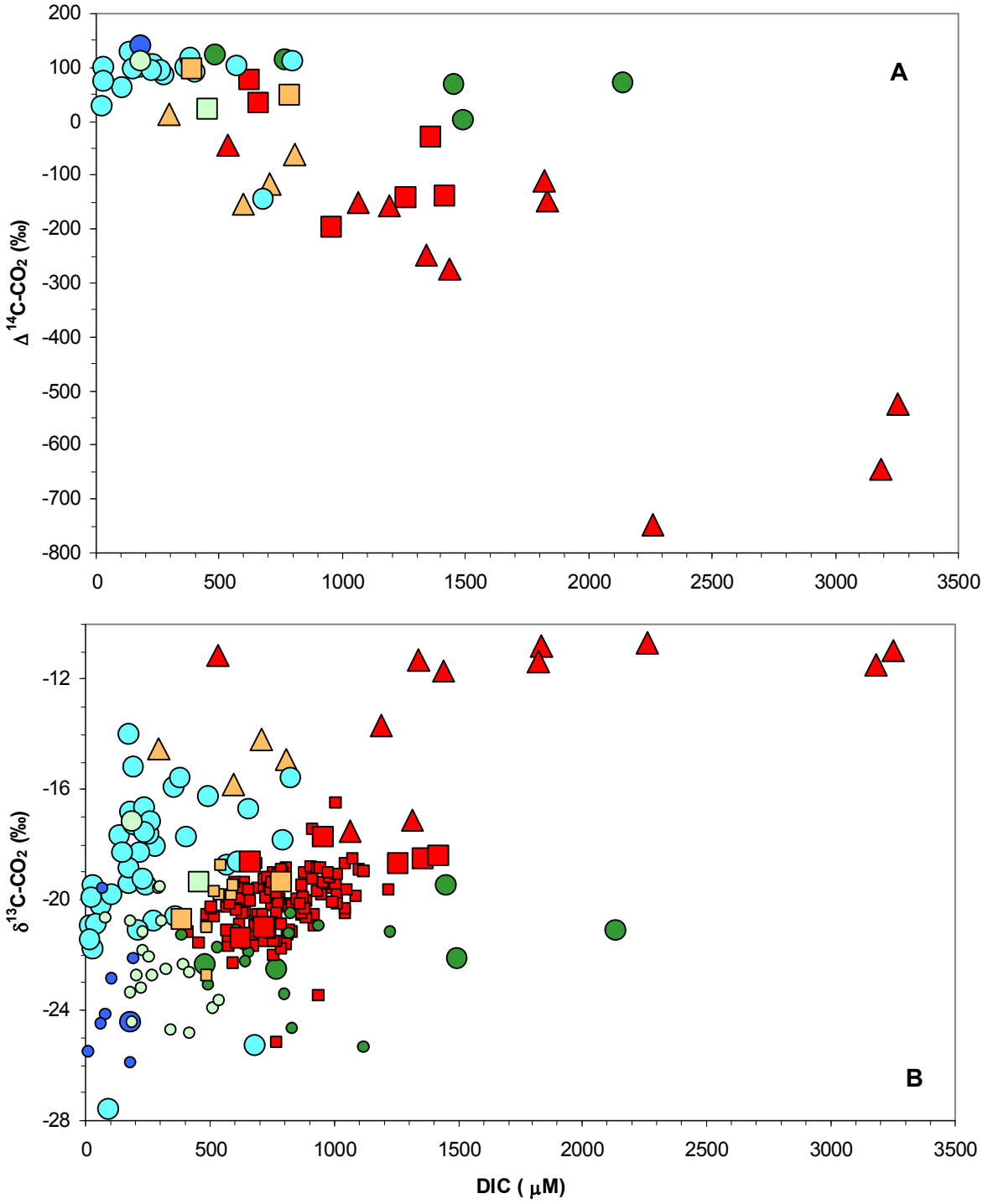

Figure 6.5. CO_2 isotopic variability with respect to DIC concentration. **A)** $\Delta^{14}C$. **B)** $\delta^{13}C$. Symbology is the same as in Fig. 6.1.

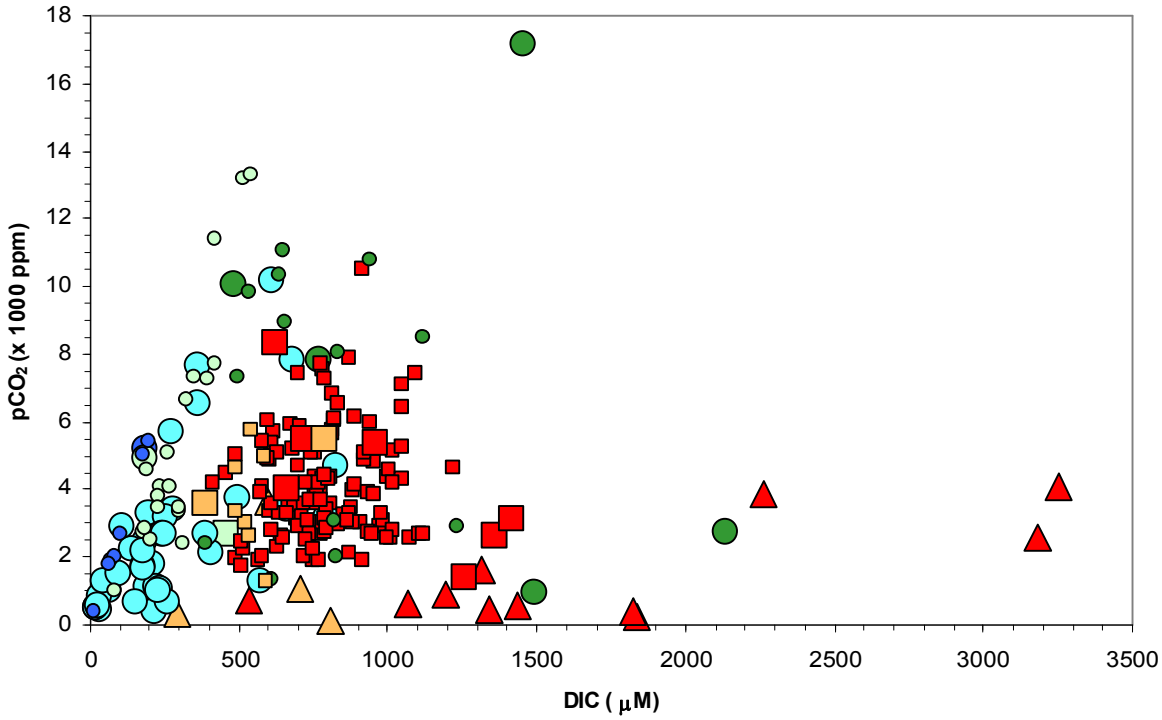

Figure 6.6. pCO_2 variability relative to DIC concentration. Symbology is the same as in Fig. 6.1.

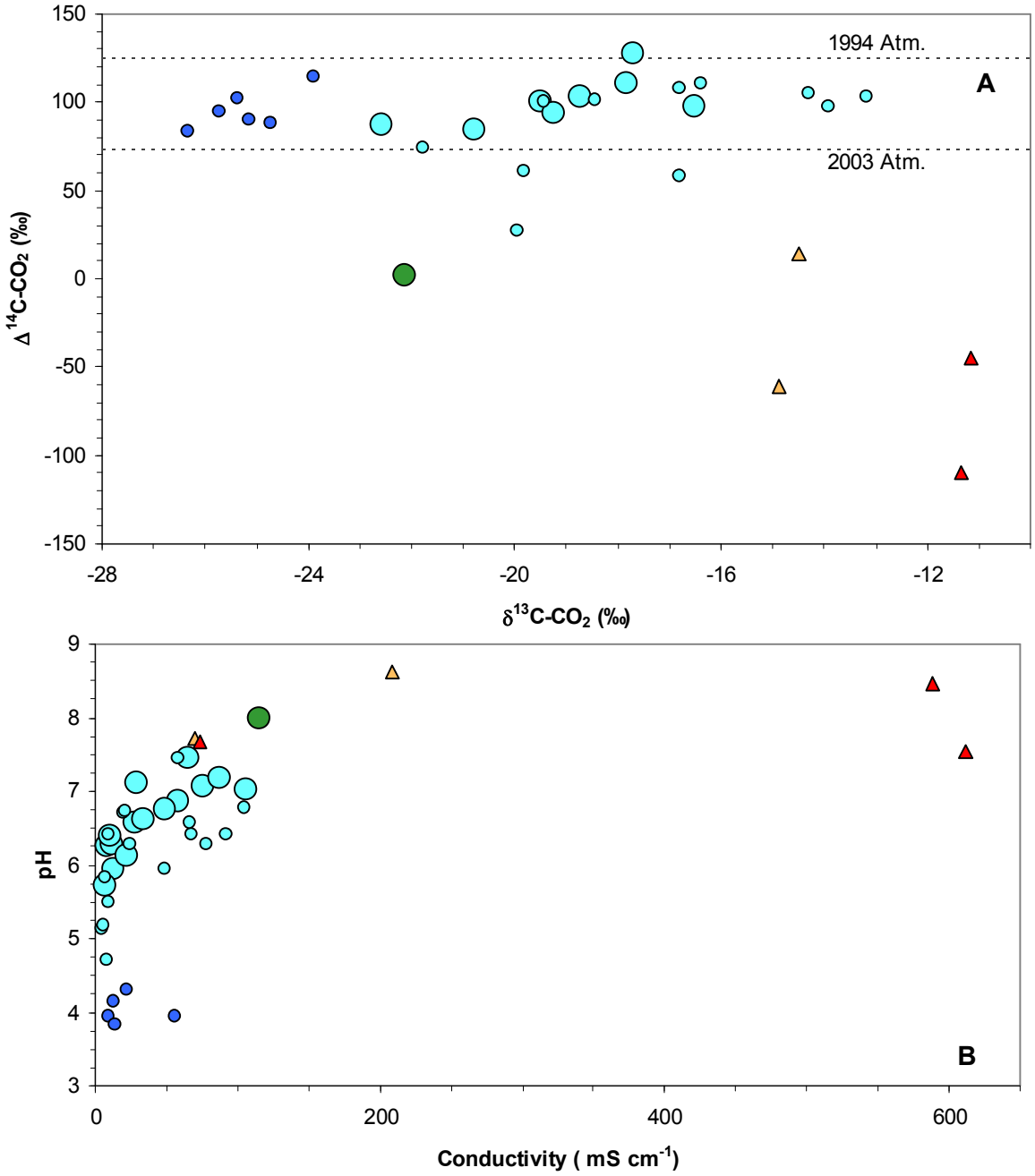

Figure 6.7. Sites with drainage area <9,000 km^2. Symbology is the same as in Fig. 6.1, but size does not distinguish previously published data. Small symbols represent sites with drainage area <4,000 km^2. **A)** $\Delta^{14}C\text{-}CO_2$ vs. $\delta^{13}C\text{-}CO_2$. Two sites in the Andean headwaters of the Ucayali are not shown, as their $\Delta^{14}C$ content is very low. Horizontal lines show the mean atmospheric $\Delta^{14}C\text{-}CO_2$ in tropical South America for the first and last sampling years in this sample set (1994 and 2003, respectively). **B)** pH vs conductivity. A site in the Andean headwaters of the Ucayali is not shown, as its conductivity is very high.

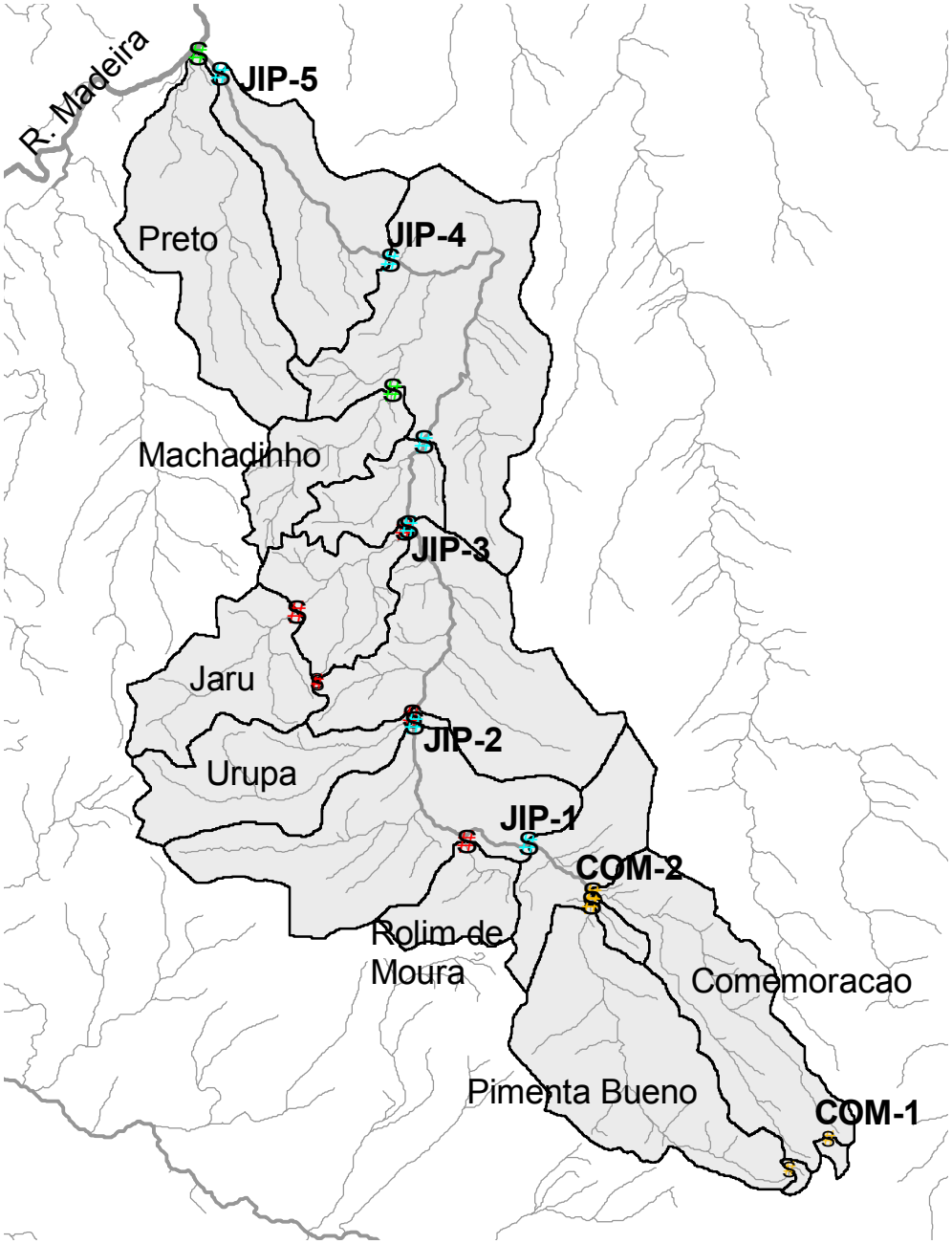

Figure 6.8. Ji-Paraná basin, sampling sites, and their drainage areas. Different colors are used for sites in the Ji-Paraná mainstem (light blue), upper headwaters (orange, Comemoração and Pimenta Bueno), cation-rich southern tributaries (red, Rolim de Moura, Urupá, Jarú, and Nossa Senhora stream), and northern tributaries in the lower reaches (green, Machadinho D'Oeste and Preto). Sites in small streams are shown with smaller symbols. No previously published data will be presented.

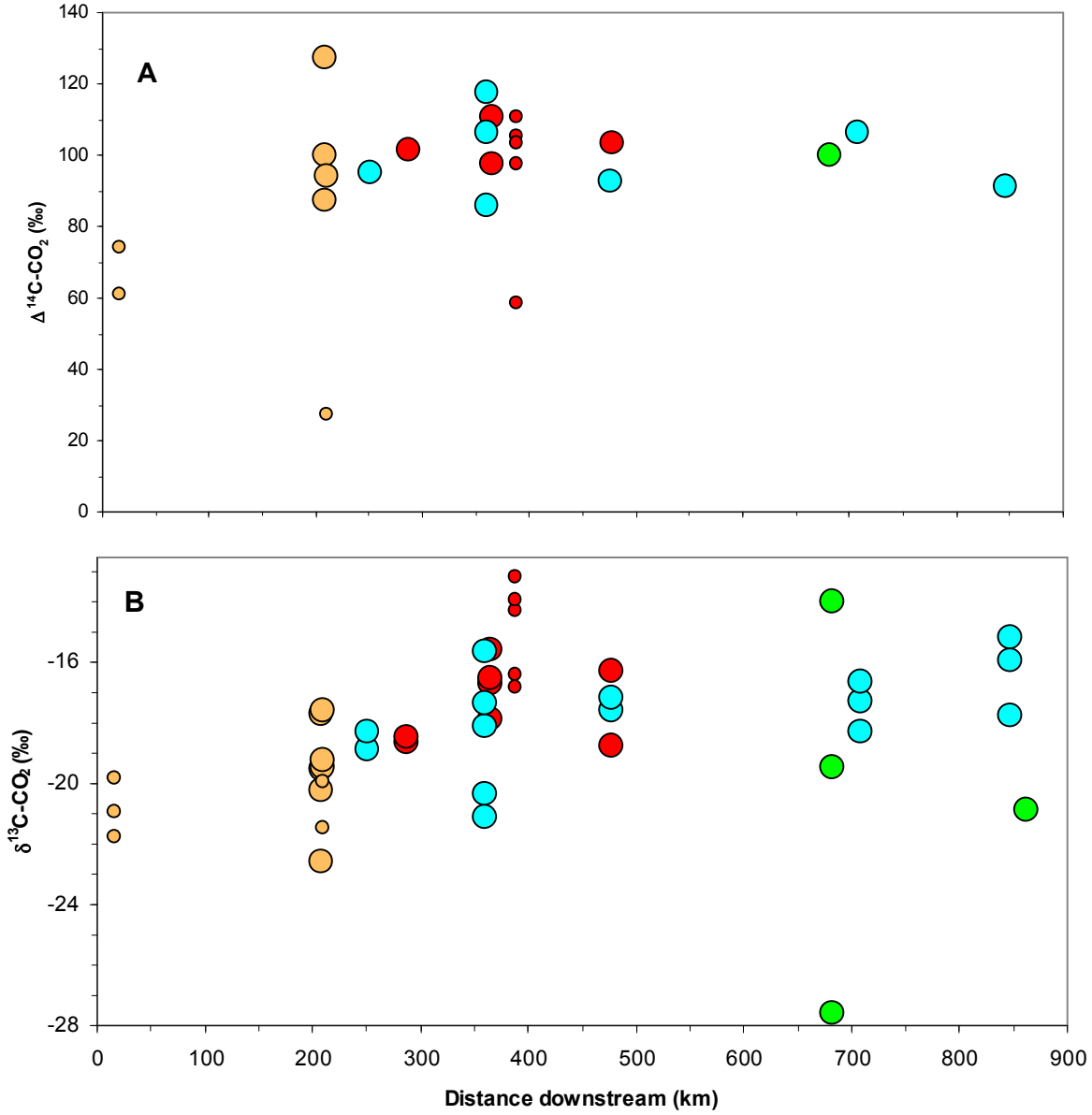

Figure 6.9. Downstream CO_2 isotopic evolution in the Ji-Paraná basin. The x-axis shows the distance from the source area upstream of COM-1. Tributary sites not draining directly into the mainstem are placed at the downstream location where they drain into the mainstem. Symbology is the same as in Fig. 6.8. **A)** $\Delta^{14}C$. **B)** $\delta^{13}C$.

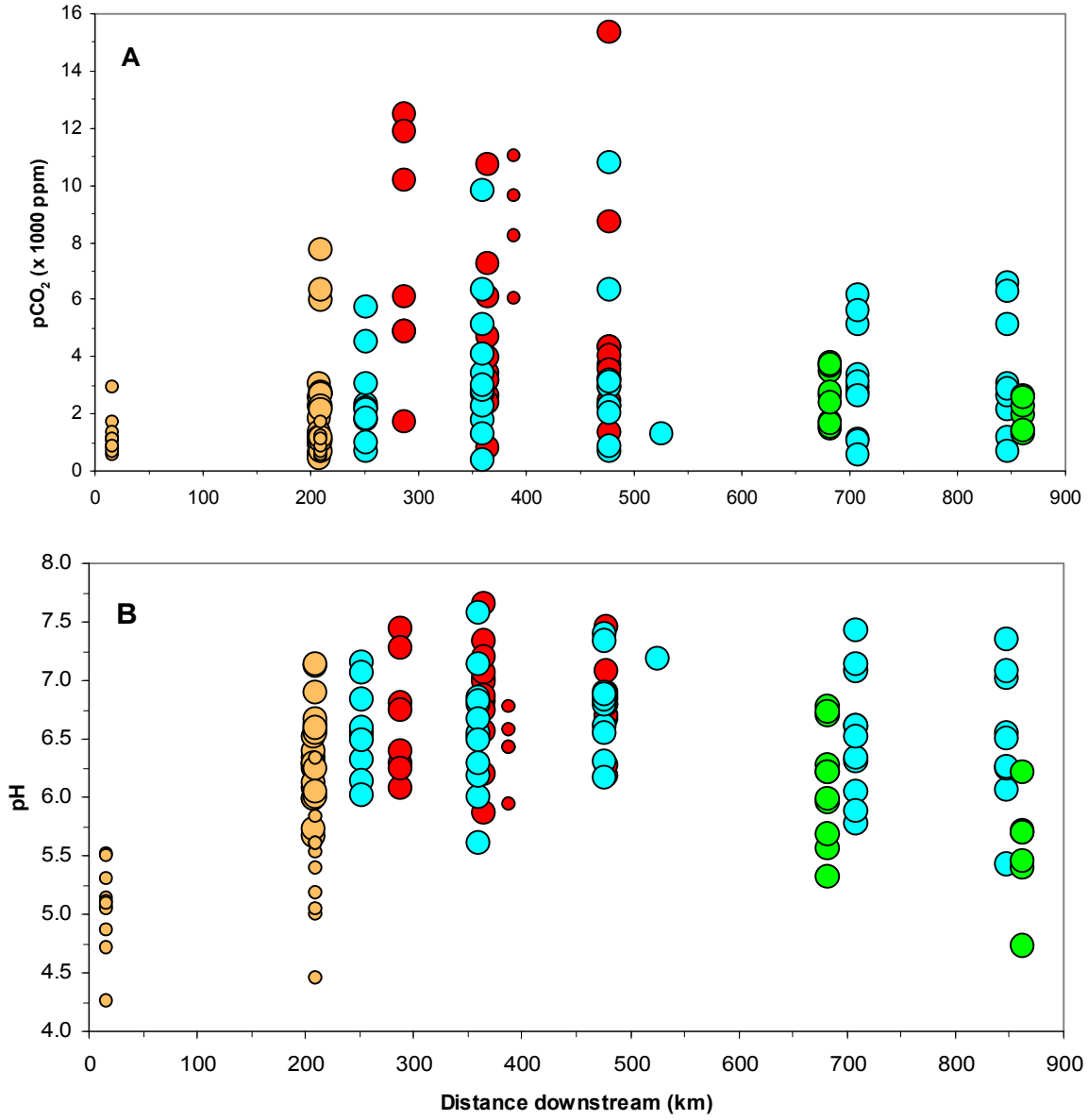

Figure 6.10. Downstream pCO_2 and pH evolution in the Ji-Paraná basin. Symbology is the same as in Fig. 6.8. **A)** pCO_2. **B)** pH.

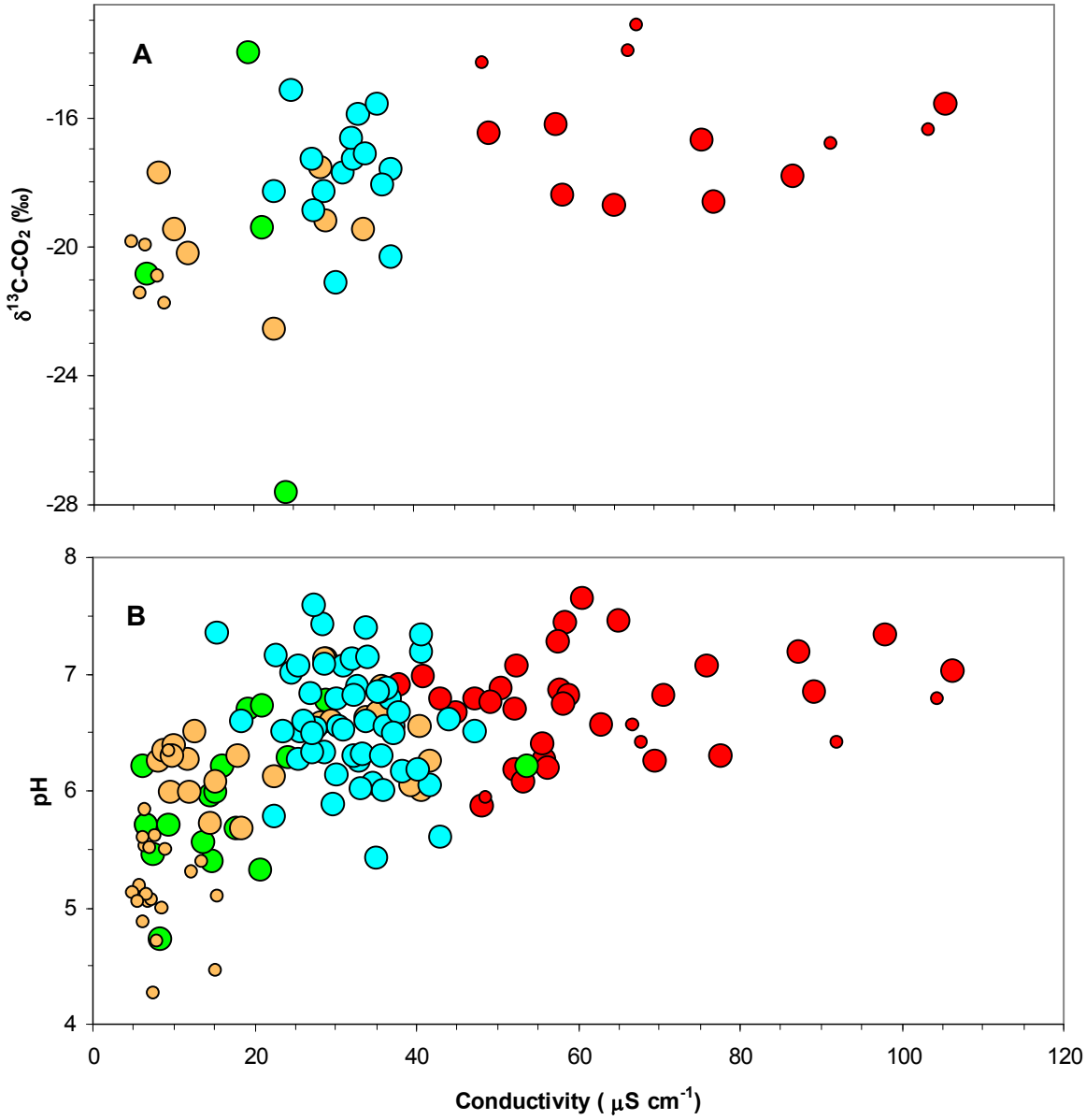

Figure 6.11. $\delta^{13}C\text{-}CO_2$ and pH variability with respect to conductivity in the Ji-Paraná basin. Symbology is the same as in Fig. 6.8. **A)** $\delta^{13}C\text{-}CO_2$. **B)** pH.

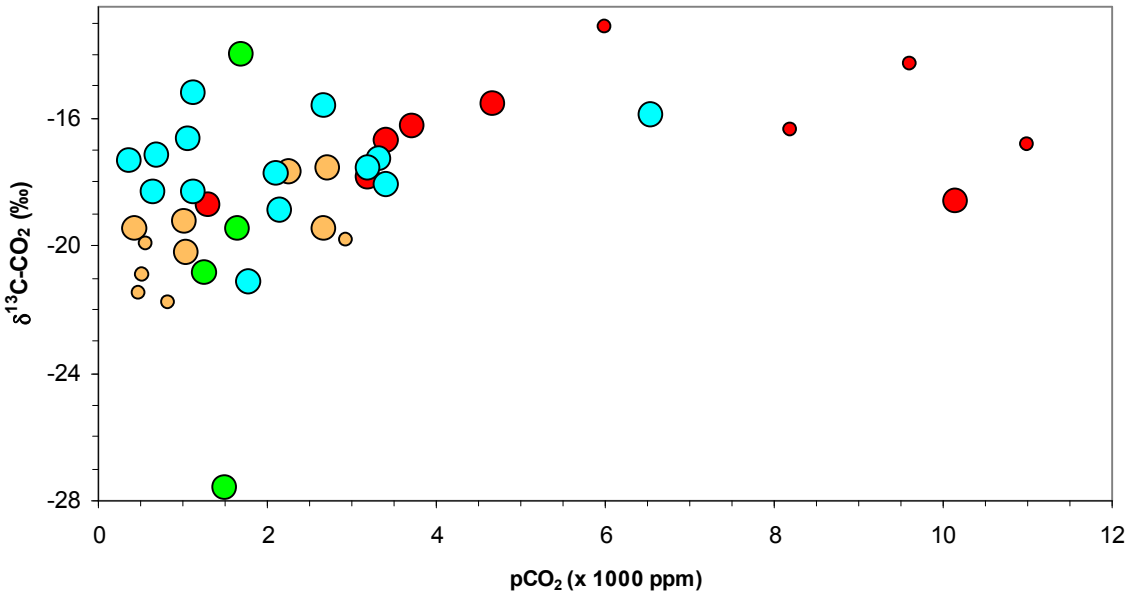

Figure 6.12. $\delta^{13}C\text{-}CO_2$ vs. pCO_2 in the Ji-Paraná basin. Symbology is the same as in Fig. 6.8.

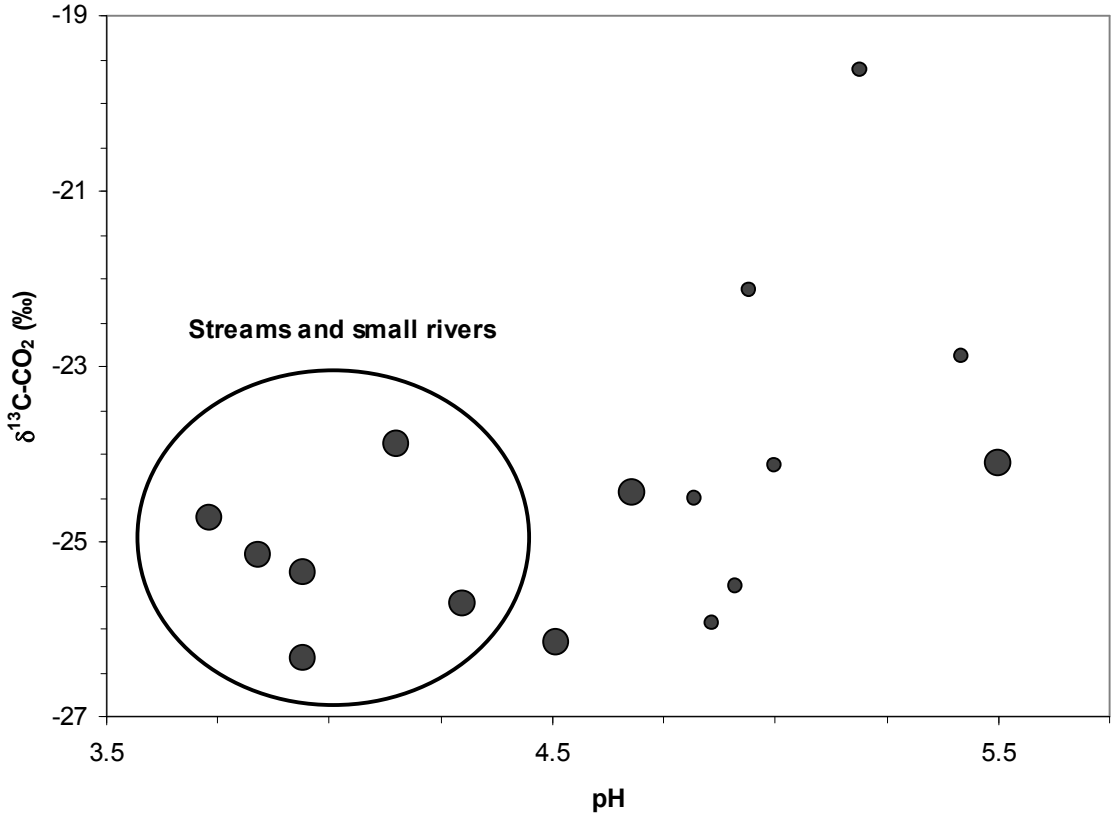

Figure 6.13. $^{13}C\text{-}CO_2$ vs. pH in small Rio Negro rivers and streams compared to the mouth, in the Guyana Shield. Symbol shape and size are the same as in Fig. 6.1.

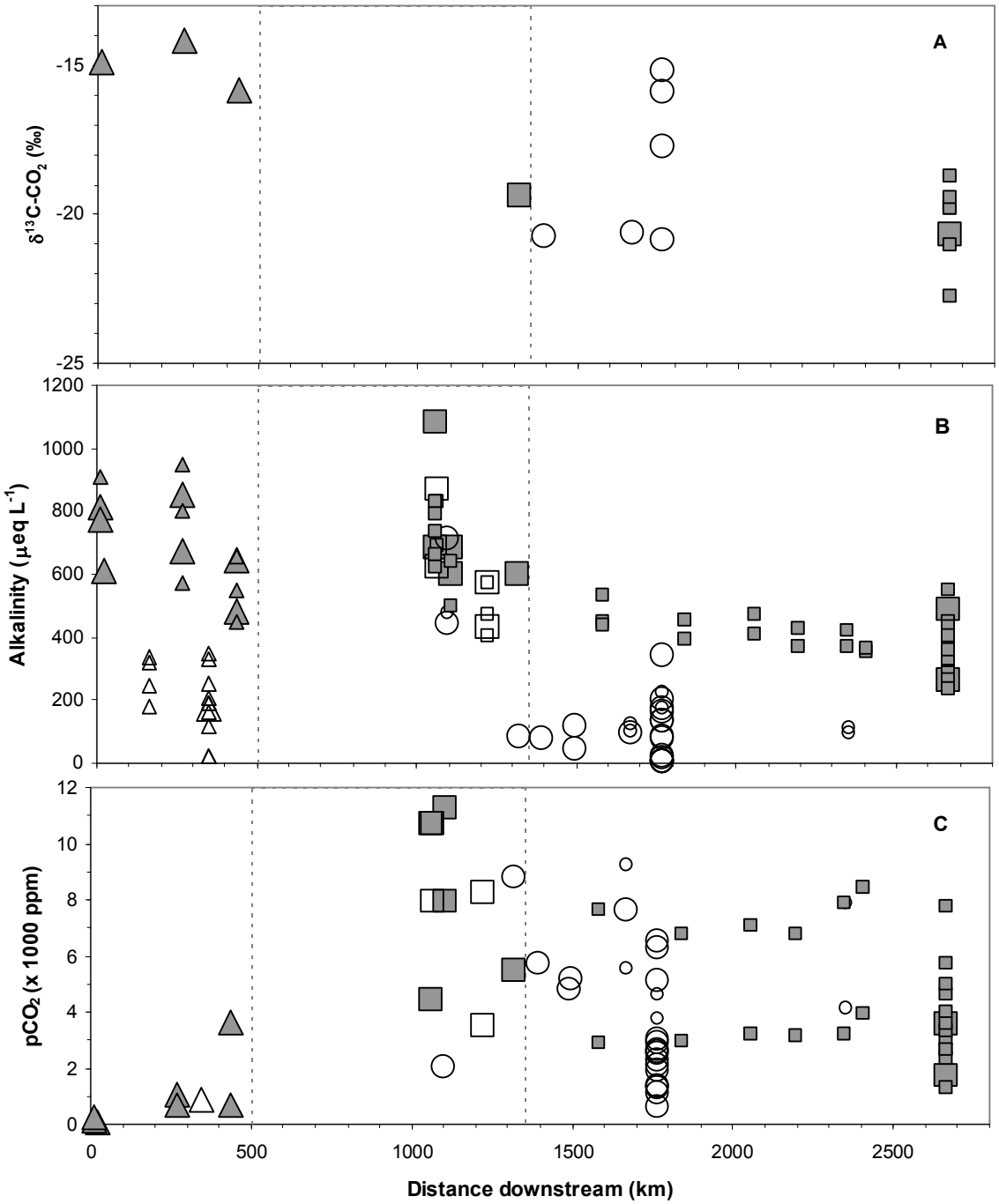

Figure 6.14. Downstream evolution from the Beni headwaters in the Bolivian Andes to the mouth of the Madeira. Symbology is the same as in Fig. 6.1, but dark gray represents the Beni-Madeira mainstem and white the immediate tributaries to that system. Dashed lines delineate the mountains to Rurrenabaque, depositional area to Rondônia, and lowland drainage to the mouth. **A)** $\delta^{13}C\text{-}CO_2$. **B)** Alkalinity. **C)** pCO_2.

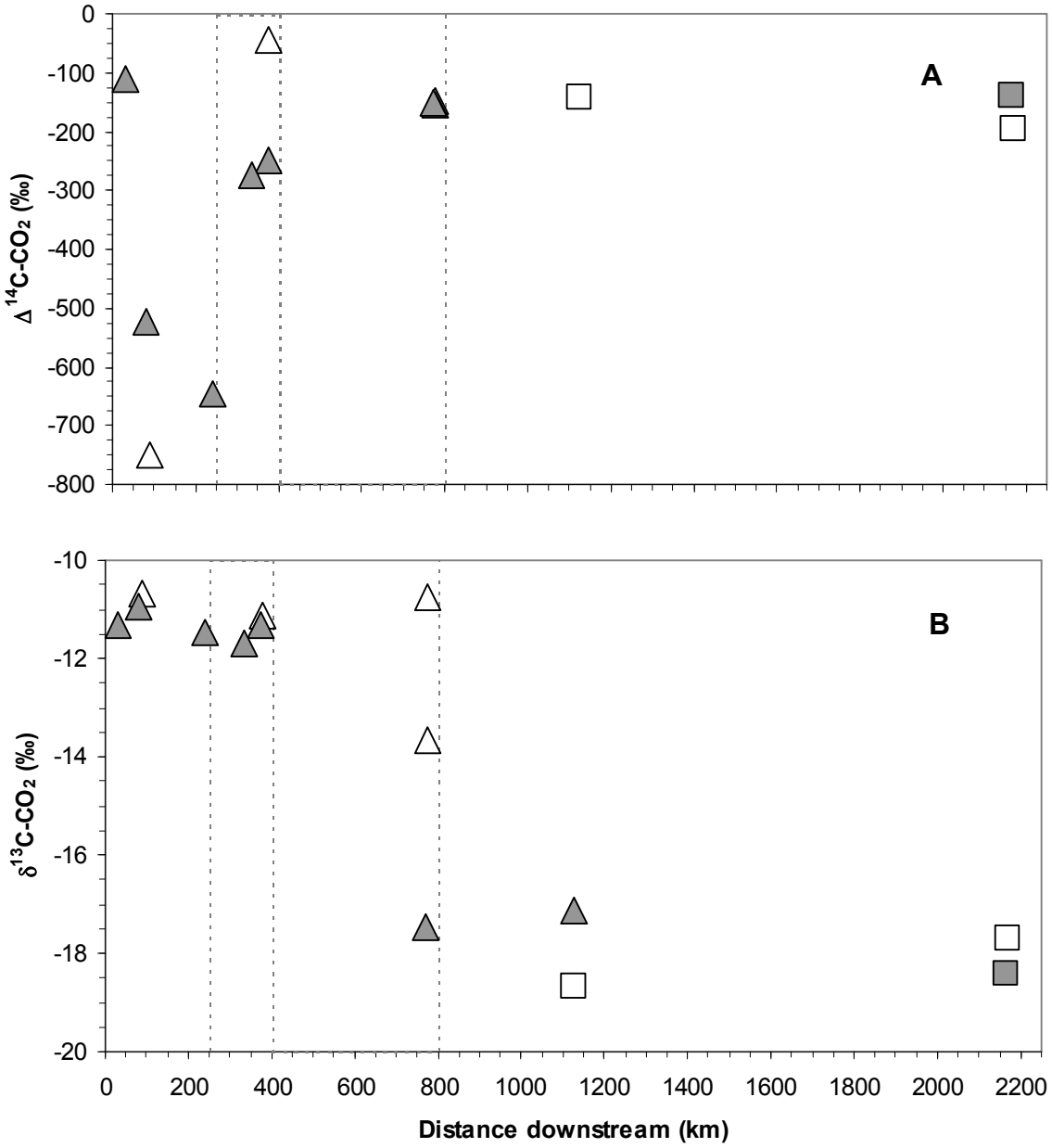

Figure 6.15. Downstream CO_2 isotopic evolution from the Vilcanota headwaters in the Peruvian Andes to the mouth of the Ucayali. Symbology is the same as in Fig. 6.1, but dark gray represents the Vilcanota-Urubamba-Ucayali mainstem and white the immediate tributaries to that system. Dashed lines delineate the upper mountainous Vilcanota, elevation drop off to Quillabamba, depositional area to the Urubamba-Tambo confluence, and lowland depositional drainage to the mouth. **A)** $\Delta^{14}C$. **B)** $\delta^{13}C$.

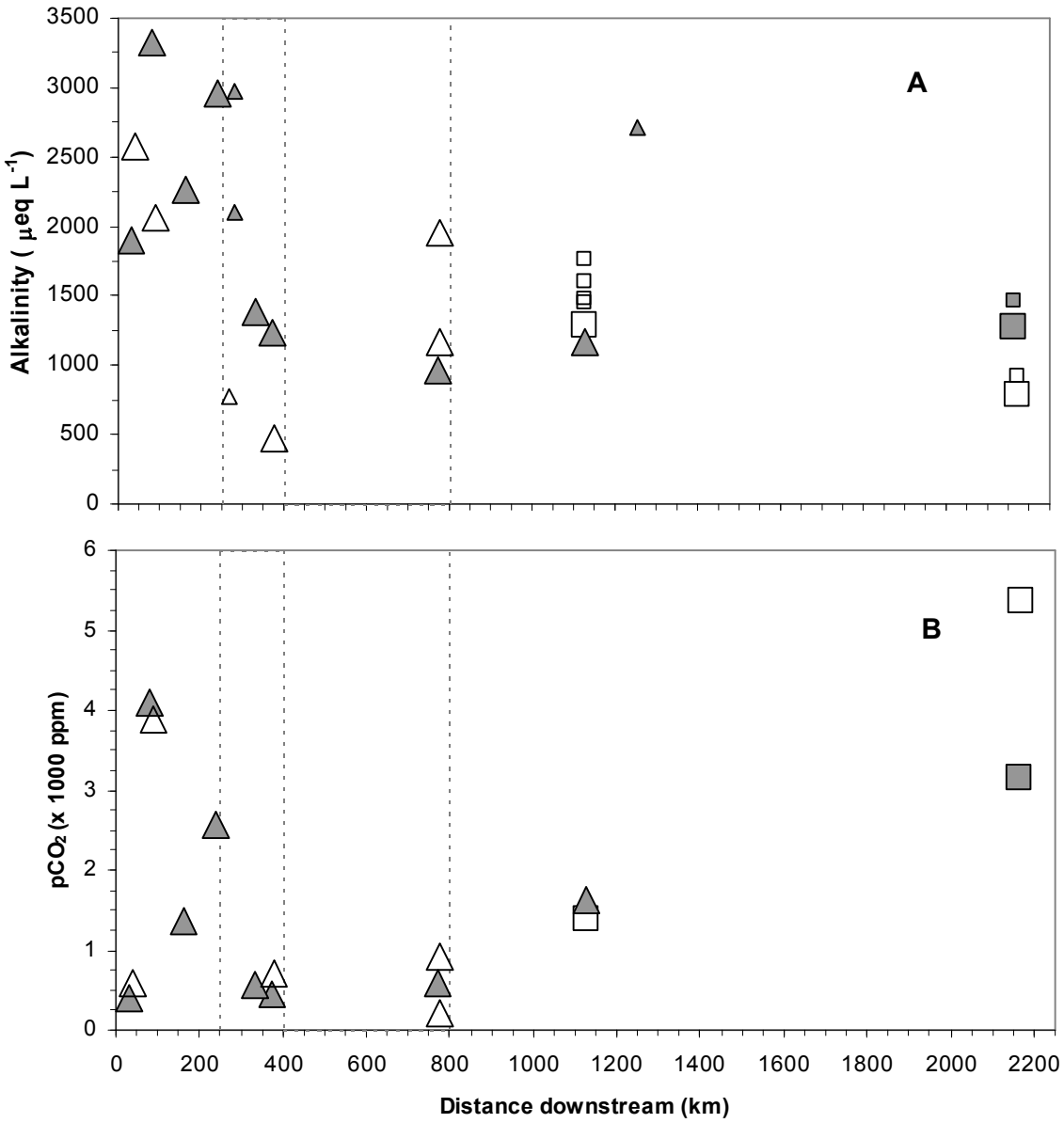

Figure 6.16. Downstream geochemical evolution from the Vilcanota headwaters in the Peruvian Andes to the mouth of the Ucayali. Symbology is the same as in Fig. 6.15. **A)** Alkalinity. **B)** pCO_2.

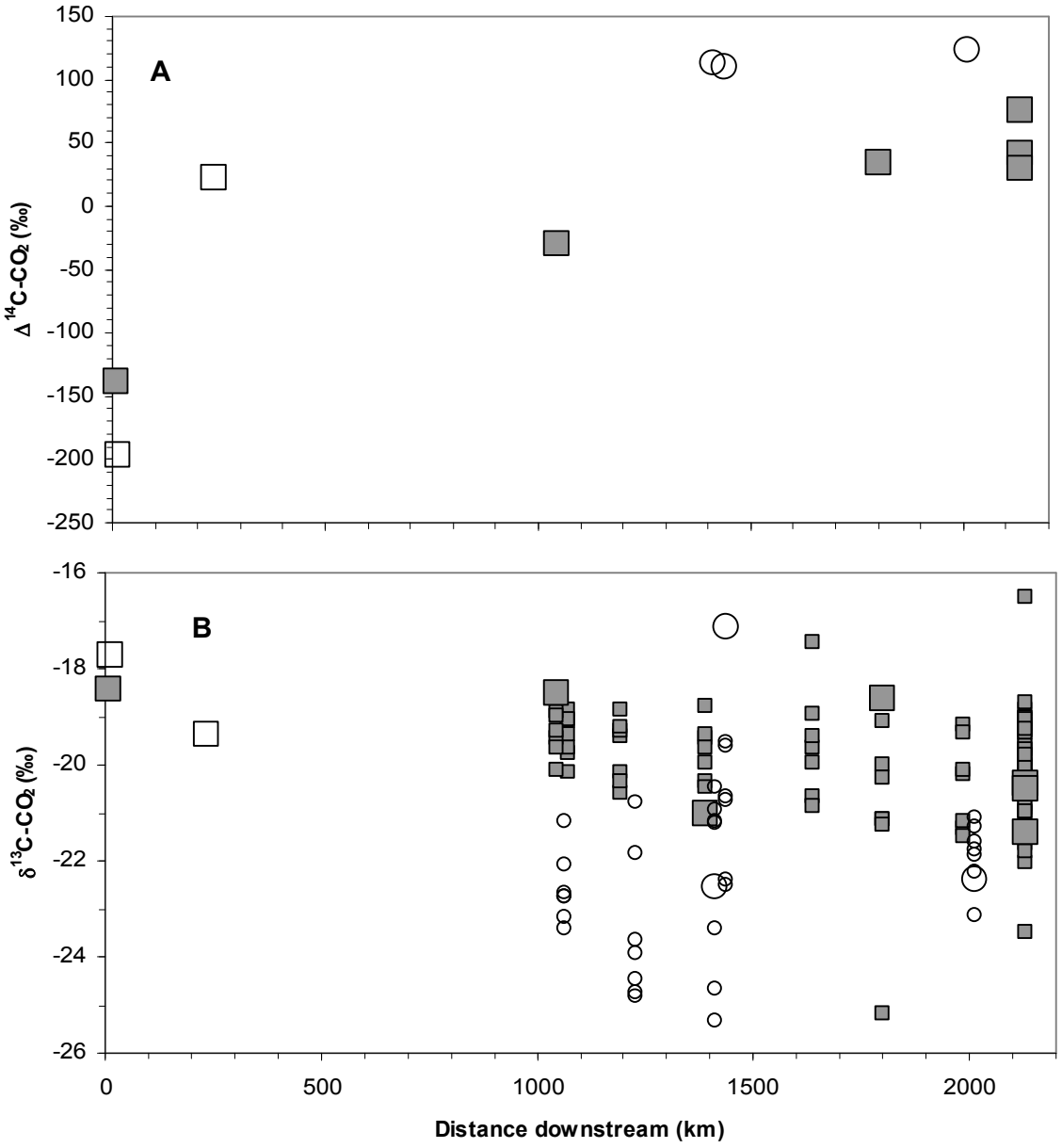

Figure 6.17. Downstream CO_2 isotopic evolution along the Amazon mainstem from the Ucayali-Marañón confluence to Manacapuru. Symbology is the same as in Fig. 6.1, but dark gray represents the Solimões-Amazonas mainstem and white the immediate tributaries to that system. **A)** $\Delta^{14}C$. **B)** $\delta^{13}C$.

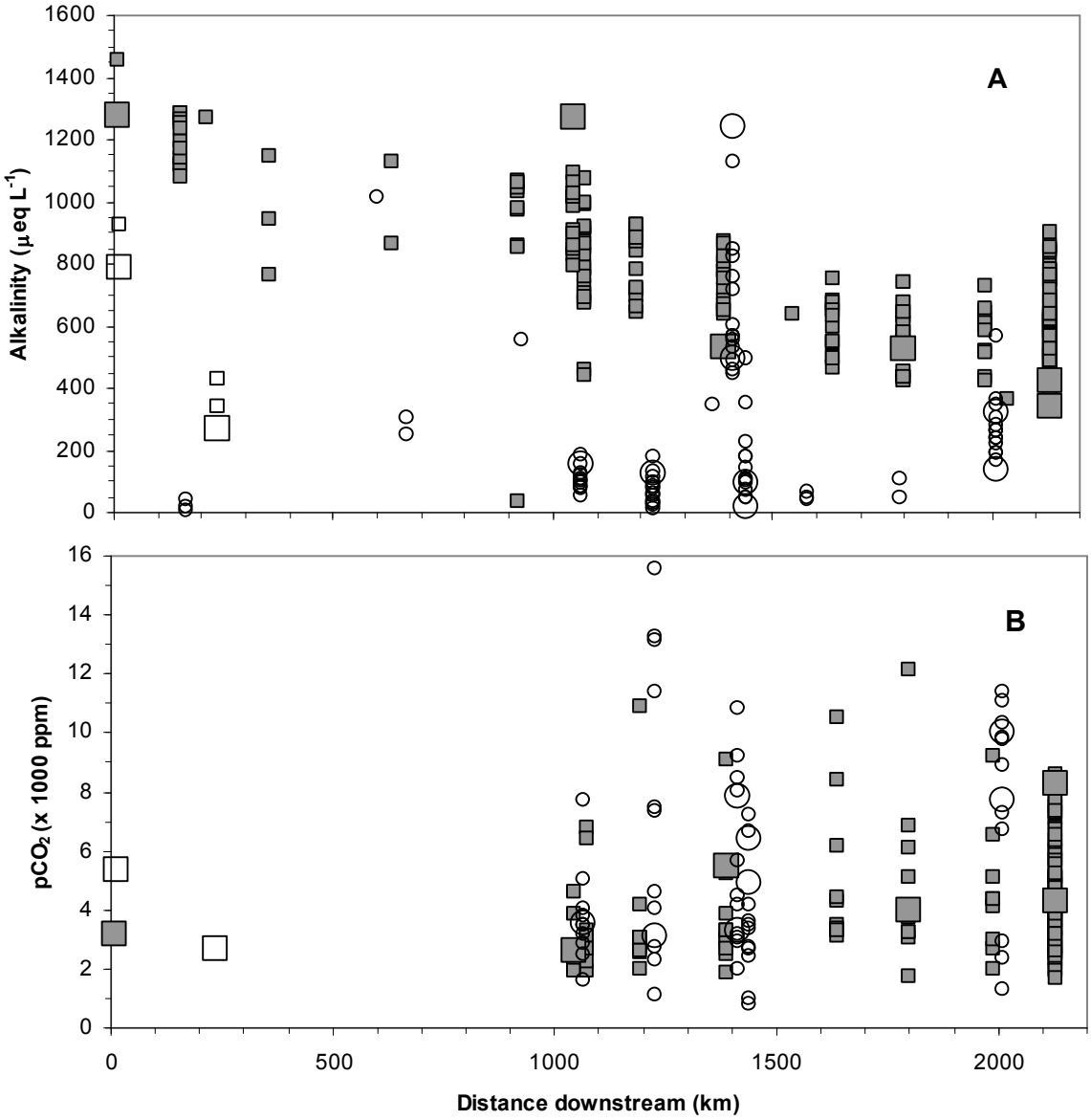

Figure 6.18. Downstream geochemical evolution along the Amazon mainstem from the Ucayali-Marañón confluence to Manacapuru. Symbology is the same as in Fig. 6.17. **A)** Alkalinity. **B)** pCO_2.

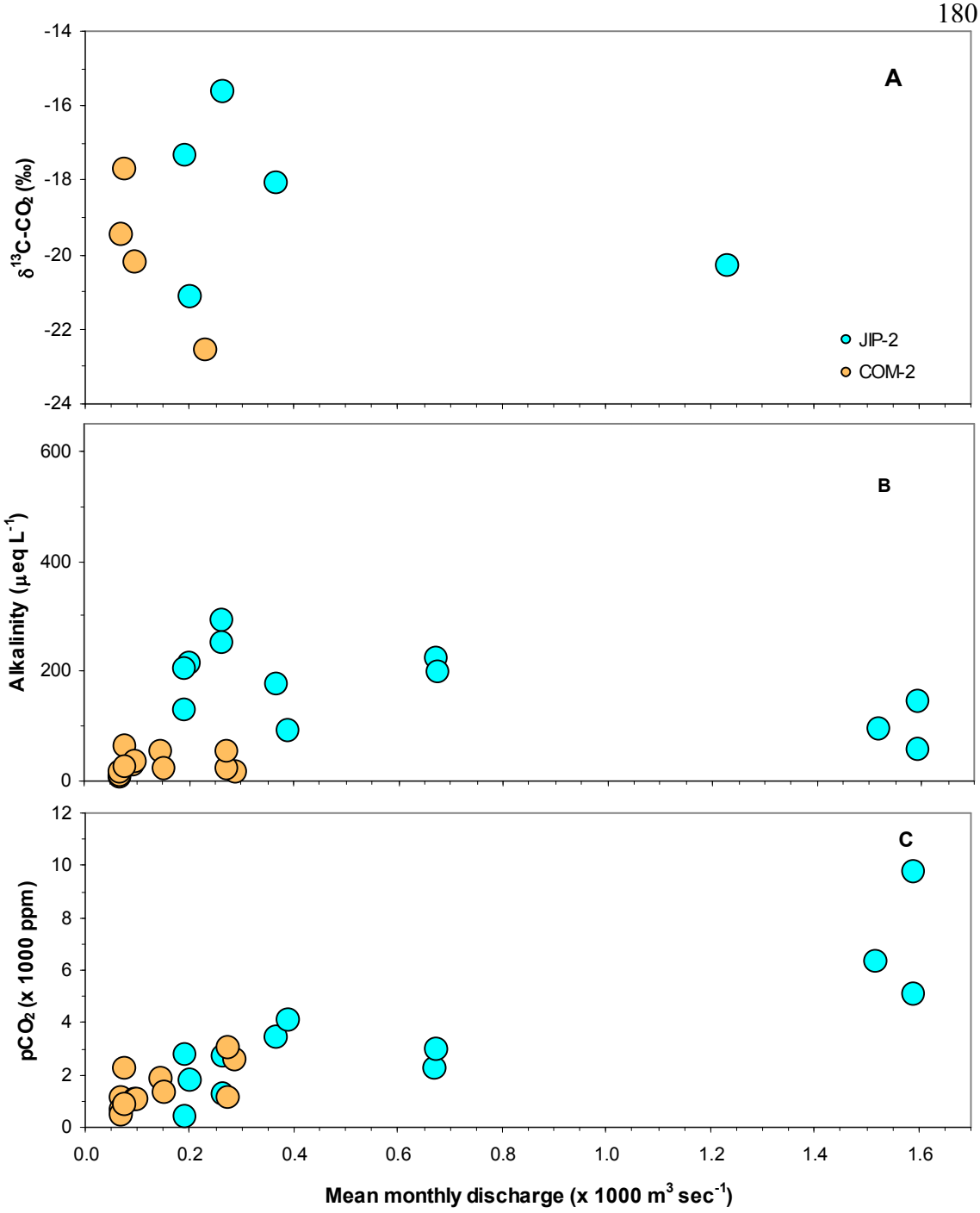

Figure 6.19. Seasonal variability at two sites in the Ji-Parana basin, JIP-2 (mainstem) and COM-2 (headwaters). This variability is depicted by plotting geochemical parameters against long-term mean monthly discharge for the sampling month, based on time series from a hydrographic gage located near each sampling site. Symbology is the same as in Fig. 6.8. **A)** $\delta^{13}C\text{-}CO_2$. **B)** Alkalinity. **C)** pCO_2.

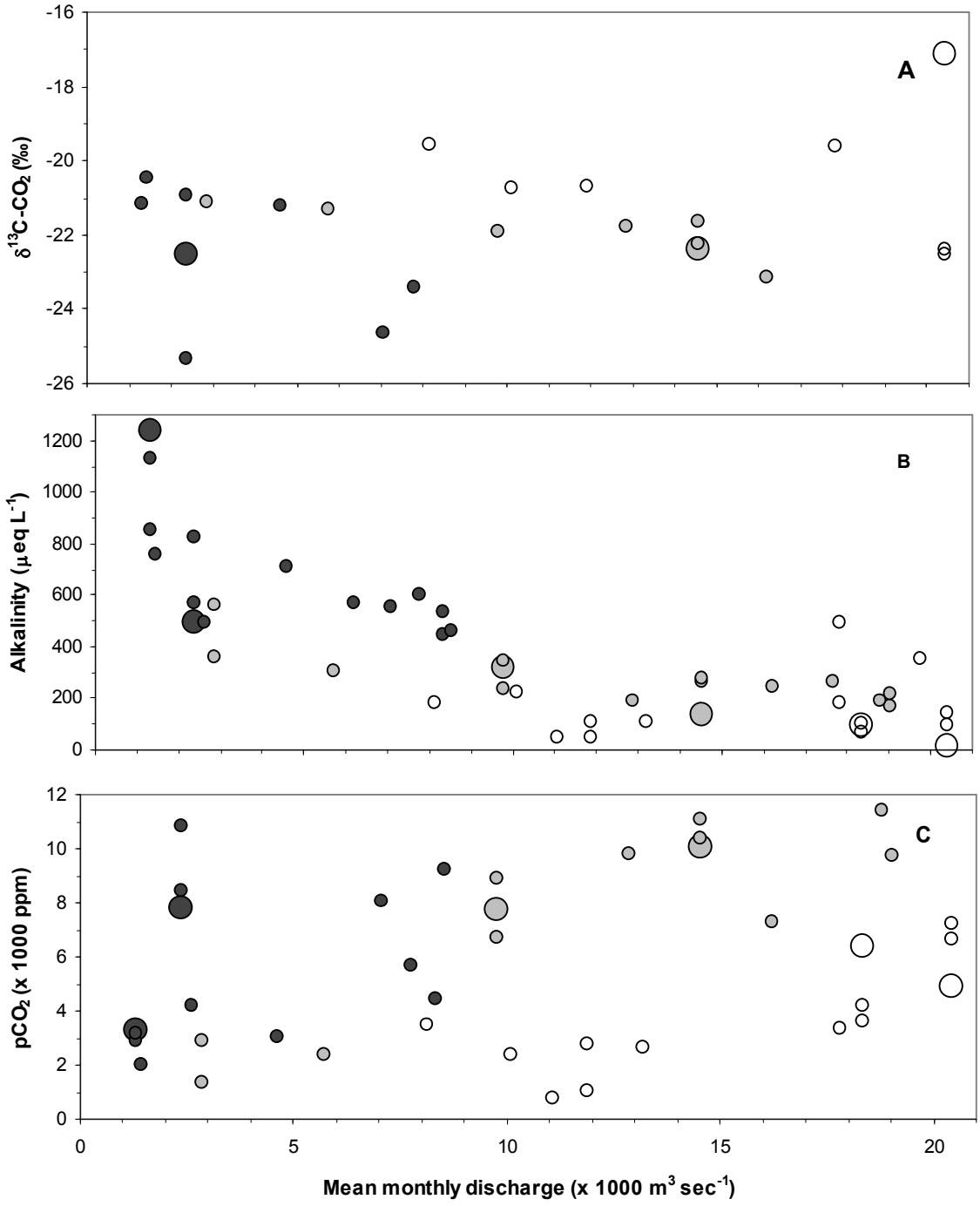

Figure 6.20. Same as Fig. 6.19, but for the mouths of Rios Juruá (black), Purus (gray), and Japurá (white). Symbol size and shape are the same as in Fig. 5.1.

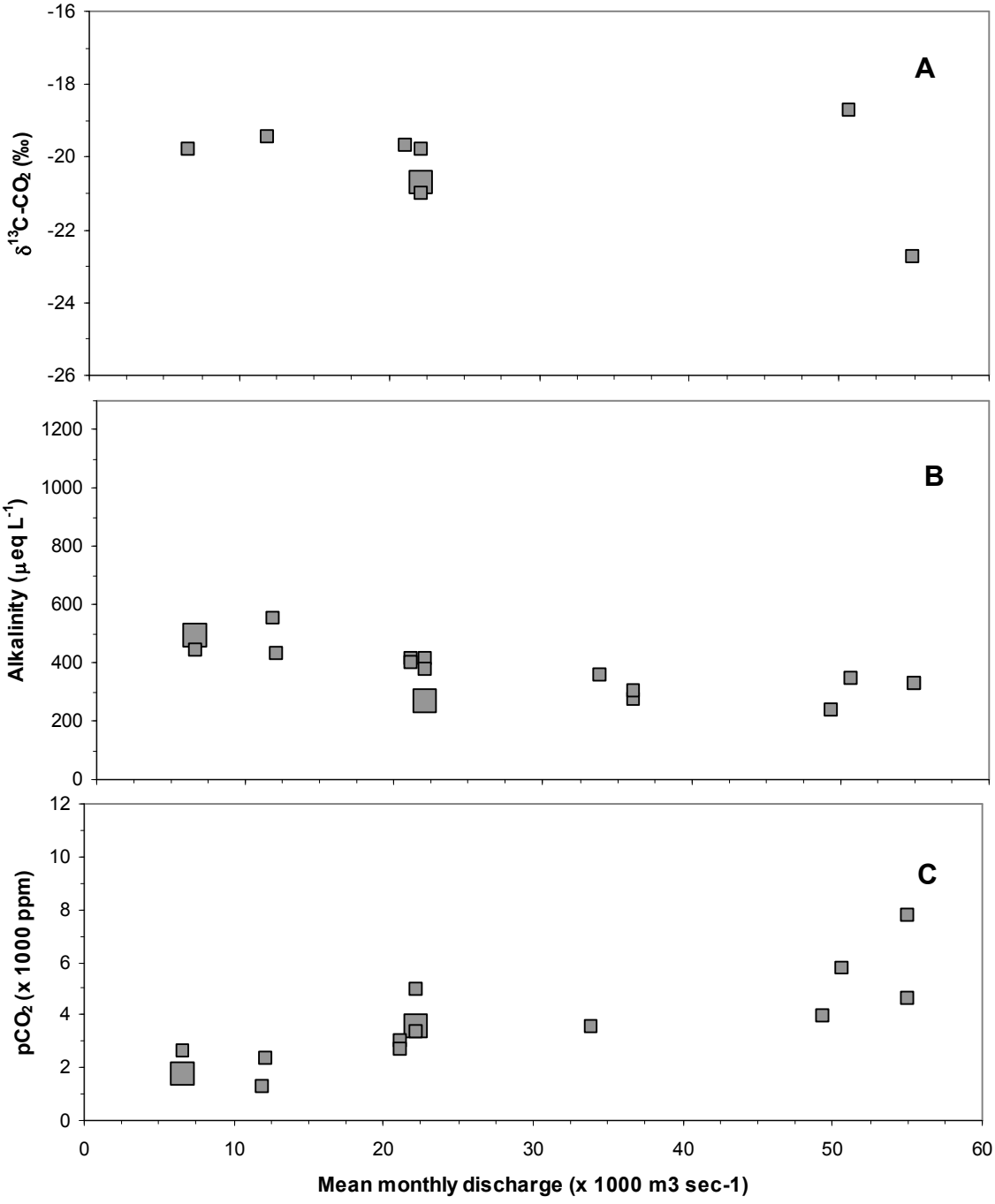

Figure 6.21. Same as Fig. 6.20, but for the mouth of Rio Madeira.

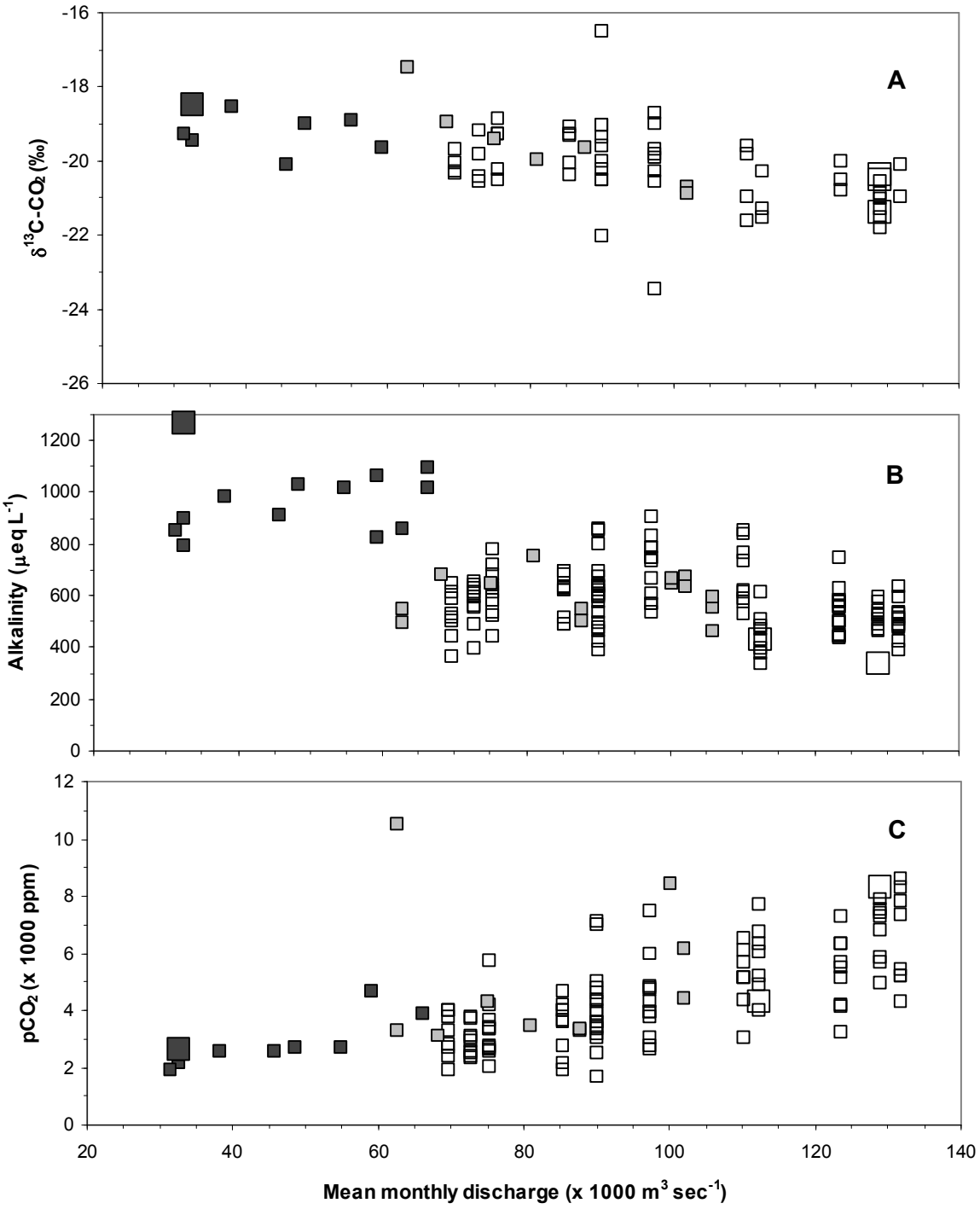

Figure 6.22. Same as Fig. 6.20, but for the Solimões-Amazonas mainstem at Vargem Grande (black), Jutica (gray), and Manacapuru/Marchantaria (white).

REFERENCES CITED

Aalto, R., Maurice-Bourgoin, L., Dunne, T., Montgomery, D. R., Nittrouer, C. A. & Guyot, J. L. (2003). Episodic sediment accumulation on Amazonian flood plains influenced by El Niño/Southern Oscillation. *Nature* **425**: 493-497.

Alves, D. S., Pereira, J. L. G., de Sousa, C. L., Soares, J. V. & Yamaguchi, F. (1999). Characterizing landscape changes in central Rondônia using Landsat TM imagery. *International Journal of Remote Sensing* **20**: 2877-2882.

Amiotte-Suchet, P. & Probst, J.-L. (1993). Modelling of atmospheric CO_2 consumption by chemical weathering of rocks: Application to the Garonne, Congo, and Amazon basins. *Chemical Geology* **107**: 205-210.

Amiotte-Suchet, P. & Probst, J.-L. (1995). A global model for present-day atmospheric/soil CO_2 consumption by chemical erosion of continental rocks (GEM-CO_2). *Tellus* **47B**: 273-280.

Amiotte-Suchet, P., Aubert, D., Probst, J.-L., Gauthier-Lafaye, F., Probst, A., Andreux, F. & Viville, D. (1999). $\delta^{13}C$ pattern of dissolved inorganic carbon in a small granitic catchment: The Strengbach case study (Vosges mountains, France). *Chemical Geology* **159**: 129-145.

Amiotte-Suchet, P., Probst, J.-L. & Ludwig, W. (2003). Worldwide distribution of continental rock lithology: Implications for the atmospheric/soil CO_2 uptake by continental weathering and alkalinity river transport to the oceans. *Global Biogeochemical Cycles* **17**: 1038, doi:10.1029/2002GB001891.

Amon, R. M. W. & Benner, R. (1996a). Bacterial utilization of different size classes of dissolved organic matter. *Limnology and Oceanography* **41**: 41-51.

Amon, R. M. W. & Benner, R. (1996b). Photochemical and microbial consumption of dissolved organic carbon and dissolved oxygen in the Amazon River system. *Geochimica et Cosmochimica Acta* **60**: 1783-1792.

Amundson, R., Stern, L., Baisden, T. & Wang, Y. (1998). The isotopic composition of soil and soil-respired CO_2. *Geoderma* **82**: 83-114.

Amundson, R. (2001). The carbon budget in soils. *Annual Review of Earth and Planetary Sciences* **29**: 535-562.

Anderson, S. P., Blum, J. D., Brantley, S. L., Chadwick, O. A., Chorover, J., Derry, L. A., Drever, J. I., Hering, J. G., Kirchner, J. W., Kump, L. R., Richter, D. D. & White, A. F. (2004). Proposed initiative would study Earth's weathering engine. *EOS Trans. AGU* **85**: 265-269.

Andreae, M. O., Artaxo, P., Brandão, C., Carswell, F. E., Ciccioli, P., da Costa, A. L., Culf, A. D., Esteves, J. L., Gash, J. H. C., Grace, J., Kabat, P., Lelieveld, J., Malhi, Y., Manzi, A. O., Meixner, F. X., Nobre, A. D., Nobre, C., Ruivo, M. d. L. P., Silva Dias, M. A. F., Stefani, P., Valentini, R., von Jouanne, J. & Waterloo, M. J. (2002). Biogeochemical cycling of carbon, water, energy, trace gases, and aerosols in Amazonia: The LBA-EUSTACH experiments. *Journal of Geophysical Research* **107**: 8066, doi:10.1029/2001JD000524.

Andrews, J. A. & Schlesinger, W. H. (2001). Soil CO_2 dynamics, acidification, and chemical weathering in a temperate forest with experimental CO_2 enrichment. *Global Biogeochemical Cycles* **15**: 149-162.

ANEEL. (1987). *Inventário das estações fluviométricas*. Agência Nacional de Energia Elétrica. Brasília, Brazil.

Araújo, A. C., Nobre, A. D., Kruijt, B., Elbers, J. A., Dallarosa, R., Stefani, P., von Randow, C., Manzi, A. O., Culf, A. D., Gash, J. H. C., Valentini, R. & Kabat, P. (2002). Comparative measurements of carbon dioxide fluxes from two nearby towers in a central Amazonian rainforest: The Manaus LBA site. *Journal of Geophysical Research* **107**: 8090, doi:10.1029/2001JD000676.

Araujo-Lima, C. A. R. M., Forsberg, B. R., Victoria, R. & Martinelli, L. (1986). Energy sources for detrivorous fishes in the Amazon. *Science* **234**: 1,256-1,258.

Aravena, R. & Suzuki, O. (1990). Isotopic evolution of river water in the northern Chile region. *Water Resources Research* **26**: 2887-2895.

Aravena, R., Schiff, S. L., Trumbore, S. E., Dillon, P. J. & Elgood, R. (1992). Evaluating dissolved inorganic carbon cycling in a forested lake watershed using carbon isotopes. *Radiocarbon* **34**: 636-645.

Asner, G. P., Townsend, A. R. & Braswell, B. H. (2000). Satellite observation of El Niño effects on Amazon forest phenology and productivity. *Geophysical Research Letters* **27**: 981-984.

Atekwana, E. A. & Krishnamurthy, R. V. (1998). Seasonal variations of dissolved inorganic carbon and $\delta^{13}C$ of surface waters: Application of a modified gas evolution technique. *Journal of Hydrology* **205**: 265-278.

Aucour, A.-M., Sheppard, S. M. F., Guyomar, O. & Wattelet, J. (1999). Use of ^{13}C to trace origin and cycling of inorganic carbon in the Rhône river system. *Chemical Geology* **159**: 87-105.

Aufdenkampe, A. K., Hedges, J. I., Richey, J. E., Krusche, A. V. & Llerena, C. A. (2001). Sorptive fractionation of dissolved organic nitrogen and amino acids onto fine sediments within the Amazon Basin. *Limnology and Oceanography* **46**: 1921-1935.

Aufdenkampe, A. K., Mayorga, E., Hedges, J. I., Llerena, C. A., Quay, P. D., Gudeman, J., Krusche, A. V. & Richey, J. E. (submitted). Organic matter in the Peruvian headwaters of the Amazon: A comparison to Bolivian tributaries and the lowland Amazon mainstem. *Organic Geochemistry.*

Aumont, O., Orr, J. C., Monfray, P., Ludwig, W., Amiotte-Suchet, P. & Probst, J.-L. (2001). Riverine-driven interhemispheric transport of carbon. *Global Biogeochemical Cycles* **15**: 393-405.

Avissar, R., Silva Dias, P. L., Silva Dias, M. A. F. & Nobre, C. (2002). The Large-Scale Biosphere-Atmosphere Experiment in Amazonia (LBA): Insights and future research needs. *Journal of Geophysical Research* **107**: 8086, doi:10.1029/2002JD002704.

Bacon, D. H. & Keller, C. K. (1998). Carbon dioxide respiration in the deep vadose zone: Implications for groundwater age dating. *Water Resources Research* **34**: 3069-3077.

Bade, D. L., Carpenter, S. R., Cole, J. J., Hanson, P. C. & Hesslein, R. H. (2004). Controls on δ^{13}C-DIC in lakes: Geochemistry, lake metabolism, and morphometry. *Limnology and Oceanography* **49**: 1160-1172.

Baldock, J. A. & Skjemstad, J. O. (2000). Role of the soil matrix and minerals in protecting natural organic materials against biological attack. *Organic Geochemistry* **31**: 697-710.

Ballester, M. V. R., Victoria, D. d. C., Krusche, A. V., Coburn, R., Victoria, R. L., Richey, J. E., Logsdon, M. G., Mayorga, E. & Matricardi, E. (2003). A Remote Sensing / GIS-based physical template to understand the biogeochemistry of the Ji-Paraná river basin (Western Amazônia). *Remote Sensing of Environment* **87**: 429-445.

Barnola, J.-M. (1999). Status of the atmospheric CO_2 reconstruction from ice core analyses. *Tellus* **51B**: 151-155.

Barth, J. A. C. & Veizer, J. (1999). Carbon cycle in St. Lawrence aquatic ecosystems at Cornwall (Ontario), Canada: Seasonal and spatial variations. *Chemical Geology* **159**: 107-128.

Barth, J. A. C., Cronin, A. A., Dunlop, J. & Kalin, R. M. (2003). Influence of carbonates on the riverine carbon cycle in an anthropogenically dominated catchment basin: Evidence from major elements and stable carbon isotopes in the Lagan River (N. Ireland). *Chemical Geology* **200**: 203-126.

Benedetti, M. F., Van Riemsdijk, W. H., Koopal, L. K., Kinniburgh, D. G., Gooddy, D. C. & Milne, C. J. (1996). Metal ion binding by natural organic matter: From the model to the field. *Geochimica et Cosmochimica Acta* **60**: 2503-2513.

Benner, R., Opsahl, S., Chin-Leo, G., Richey, J. E. & Forsberg, B. R. (1995). Bacterial carbon metabolism in the Amazon River system. *Limnology and Oceanography* **40**: 1262-1270.

Bernardes, M. C., Martinelli, L. A., Krusche, A. V., Gudeman, J., Moreira, M. Z., Victoria, R. L., Ometto, J. P. H. B., Ballester, M. V. R., Aufdenkampe, A. K., Richey, J. E. & Hedges, J. I. (2004). Riverine organic matter composition as a function of land use changes, Southwest Amazon. *Ecological Applications* **14**: S263-S279.

Berner, R. A., Lasaga, A. C. & Garrels, R. M. (1983). The carbonate-silicate geochemical cycle and its effect on atmospheric carbon dioxide over the past 100 million years. *American Journal of Science* **283**: 641-683.

Berner, R. A. & Lasaga, A. C. (1989). Modeling the geochemical carbon cycle. *Scientific American*, March 1989, p. 74-81.

Berner, R. A. (1991). A model for atmospheric CO_2 over Phanerozoic time. *American Journal of Science* **291**: 339-376.

Berner, R. A. (1994). GEOCARB II: A revised model of atmospheric CO_2 over Phanerozoic time. *American Journal of Science* **294**: 56-91.

Berner, R. A. & Berner, E. K. (1997). Silicate weathering and climate, p. 353-365. In: Ruddiman, W. F. (ed.), *Tectonic uplift and climate change*. Plenum Press. New York.

Berner, R. A. (1999). A new look at the long-term carbon cycle. *GSA Today* **9**: 1-6.

Berner, R. A. & Kothavala, Z. (2001). GEOCARB III: A revised model of atmospheric CO_2 over Phanerozoic time. *American Journal of Science* **301**: 182-204.

Berner, R. A. (2003). The long-term carbon cycle, fossil fuels and atmospheric composition. *Nature* **426**: 323-326.

Berner, R. A., Beerling, D. J., Dudley, R., Robinson, J. M. & Wildman Jr., R. A. (2003). Phanerozoic atmospheric oxygen. *Annual Review of Earth and Planetary Sciences* **31**: 105-134.

Bernoux, M., Cerri, C. C., Neill, C. & de Moraes, J. F. L. (1998). The use of stable carbon isotopes for estimating soil organic matter turnover rates. *Geoderma* **82**: 43-58.

Bidigare, R. R., Fluegge, A., Freeman, K. H., Hanson, K. L., Hayes, J. M., Hollander, D., Jasper, J. P., King, L. L., Laws, E. A., Milder, J., Millero, F. J., Pancost, R., Popp, B. N., Steinberg, P. A. & Wakeham, S. G. (1997). Consistent fractionation of ^{13}C in nature and in the laboratory: Growth-rate effects in some haptophyte algae. *Global Biogeochemical Cycles* **11**: 279-292.

Biggs, T. W., Dunne, T., Domingues, T. F. & Martinelli, L. A. (2002). Relative influence of natural watershed properties and human disturbance on stream solute concentrations

in the southwestern Brazilian Amazon basin. *Water Resources Research* **38**: doi: 10.1029/2001WR000271.

Biggs, T. W., Dunne, T. & Martinelli, L. A. (2004). Natural controls and human impacts on stream nutrient concentrations in a deforested region of the Brazilian Amazon basin. *Biogeochemistry* **68**: 227-257.

Bird, M. I., Haberle, S. G. & Chivas, A. R. (1994). Effect of altitude on the carbon-isotope composition of forest and grassland soils from Papua New Guinea. *Global Biogeochemical Cycles* **8**: 13-22.

Blair, N., Leu, A., Muñoz, E., Olse, J., Kwong, E. & Des Marais, D. (1985). Carbon isotopic fractionation in heterotrophic microbial metabolism. *Applied and Environmental Microbiology* **50**: 996-1001.

Blair, N. E., Leithold, E. L., Ford, S. T., Peeler, K. A., Holmes, J. C. & Perkey, D. W. (2003). The persistence of memory: The fate of ancient sedimentary organic carbon in a modern sedimentary system. *Geochimica et Cosmochimica Acta* **67**: 63-73.

Bluth, G. J. S. & Kump, L. R. (1994). Lithologic and climatologic controls of river chemistry. *Geochimica et Cosmochimica Acta* **58**: 2341-2359.

Boulton, A. J., Findlay, S., Marmonier, P., Stanley, E. H. & Valett, H. M. (1998). The functional significance of the hyporheic zone in streams and rivers. *Annual Review of Ecology and Systematics* **29**: 59-81.

Bousquet, P., Peylin, P., Ciais, P., Le Quéré, C., Friedlingstein, P. & Tans, P. P. (2000). Regional changes in carbon dioxide fluxes of land and oceans since 1980. *Science* **290**: 1342-1346.

Bowling, D. R., Pataki, D. E. & Ehleringer, J. R. (2003). Critical evaluation of micrometeorological methods for measuring ecosystem-atmosphere isotopic exchange of CO_2. *Agricultural and Forest Meteorology* **116**: 159-179.

Brandes, J. A., McClain, M. E. & Pimentel, T. P. (1996). ^{15}N evidence for the origin and cycling of inorganic nitrogen in a small Amazonian catchment. *Biogeochemistry* **34**: 45-56.

Bravard, S. & Righi, D. (1990). Podzols in Amazonia. *Catena* **17**: 461-475.

Braziunas, T. F., Fung, I. Y. & Stuiver, M. (1995). The preindustrial atmospheric $^{14}CO_2$ latitudinal gradient as related to exchanges among atmospheric, oceanic, and terrestrial reservoirs. *Global Biogeochemical Cycles* **9**: 565-584.

Brinkmann, W. L. F. (1985). Studies on hydrobiogeochemistry of a tropical lowland forest system. *GeoJournal* **11**: 89-101.

Broecker, W. S. & Sanyal, A. (1998). Does atmospheric CO_2 police the rate of chemical weathering? *Global Biogeochemical Cycles* **12**: 403-408.

Buchmann, N., Guehl, J.-M., Barigah, T. S. & Ehleringer, J. R. (1997). Interseasonal comparison of CO_2 concentrations, isotopic composition, and carbon dynamics in an Amazonian rainforest (French Guiana). *Oecologia* **110**: 120-131.

Bullen, T. D. & Kendall, C. (1998). Tracing of weathering reactions and water flowpaths: A multi-isotope approach, p. 611-646. In: Kendall, C. & McDonnell, J. J. (ed.), *Isotope tracers in catchment hydrology*. Elsevier. New York.

Cabido, M., Ateca, N., Astegiano, M. E. & Anton, A. M. (1997). Distribution of C_3 and C_4 grasses along an altitudinal gradient in Central Argentina. *Journal of Biogeography* **24**: 197-204.

Cai, D. L., Tan, F. C. & Edmond, J. M. (1988). Sources and transport of particulate organic carbon in the Amazon river and estuary. *Estuarine, Coastal and Shelf Science* **26**: 1-14.

Cameron, E. M., Hall, G. E. M., Veizer, J. & Krouse, H. R. (1995). Isotopic and elemental hydrogeochemistry of a major river system: Fraser river, British Columbia, Canada. *Chemical Geology* **122**: 149-169.

Canadell, J. G., Mooney, H. A., Baldocchi, D. D., Berry, J. A., Ehleringer, J. R., Field, C. B., Gower, S. T., Hollinger, D. Y., Hunt Jr., E. R., Jackson, R. B., Running, S. W., Shaver, G. R., Steffen, W., Trumbore, S. E., Valentini, R. & Bond, B. Y. (2000). Carbon metabolism of the terrestrial biosphere: A multitechnique approach for improved understanding. *Ecosystems* **3**: 115-130.

Carrasco N., L. M. & Bourges, J. 1992. Estudio del régimen del escurrimiento superficial en la cuenca Amazónica del rio Beni, p. 41-49. *In* Roche, M. A., Bourges, J., Salas R, E.

& Diaz E, C. (ed.), Seminario sobre el Programa Hidrológico y Climatológico de la Cuenca Amazónica de Bolivia (PHICAB). La Paz, Bolivia.

Cerling, T. E., Solomon, D. K., Quade, J. & Bowman, J. R. (1991). On the isotopic composition of carbon in soil carbon dioxide. *Geochimica et Cosmochimica Acta* **55**: 3403-3405.

Chambers, J. Q., Tribuzy, E. S., Toledo, L. C., Crispim, B. F., Higuchi, N., dos Santos, J., Araújo, A. C., Kruijt, B., Nobre, A. D. & Trumbore, S. E. (2004). Respiration from a tropical forest ecosystem: Partitioning of sources and low carbon use efficiency. *Ecological Applications* **14**: S72-S88.

Chen, J., Wang, F., Xia, X. & Zhang, L. (2002). Major element chemistry of the Changjiang (Yangtze River). *Chemical Geology* **187**: 231-255.

Cheng, S. (1992). Reaction-path formulation of a simple dissolution model for radiocarbon dating groundwater. *Radiocarbon* **34**: 646-653.

Chin, W.-C., Verdugo, P. & Orellana, M. (1998). Spontaneous assembly of marine dissolved organic matter into polymer gels. *Nature* **391**: 568-572.

Chiodini, G., Frondini, F., Kerrick, D. M., Rogie, J., Parello, F., Peruzzi, L. & Zanzari, A. R. (1999). Quantification of deep CO_2 fluxes from Central Italy. Examples of carbon balance for regional aquifers and of soil diffuse degassing. *Chemical Geology* **159**: 205-222.

Choi, J., Hulseapple, S. M., Conklin, M. H. & Harvey, J. W. (1998). Modeling CO_2 degassing and pH in a stream-aquifer system. *Journal of Hydrology* **209**: 297-310.

Cirpka, O., Reichert, P., Wanner, O., Müller, S. R. & Schwarzenbach, R. P. (1993). Gas exchange at river cascades: Field experiments and model calculations. *Environmental Science & Technology* **27**: 2086-2097.

Clark, D. A. (2002). Are tropical forests an important carbon sink? Reanalysis of the long-term plot data. *Ecological Applications* **12**: 3-7.

Clark, I. & Fritz, P. (1997). *Environmental isotopes in hydrogeology*. Lewis Publishers. Boca Raton.

Cleveland, C. C., Neff, J. C., Townsend, A. R. & Hood, E. (2004). Composition, dynamics, and fate of leached dissolved organic matter in terrestrial ecosystems: Results from a decomposition experiment. *Ecosystems* **7**: 275-285.

Cohen, A. S., Coe, A. L., Harding, S. M. & Schwark, L. (2004). Osmium isotope evidence for the regulation of atmospheric CO_2 by continental weathering. *Geology* **32**: 157-160.

Cole, J. J., Caraco, N. F., Kling, G. W. & Kratz, T. K. (1994). Carbon dioxide supersaturation in the surface waters of lakes. *Science* **256**: 1568-70.

Cole, J. J. & Caraco, N. F. (2001). Carbon in catchments: Connecting terrestrial carbon losses with aquatic metabolism. *Marine and Freshwater Research* **52**: 101-110.

Congalton, R. G. (1997). Exploring and evaluating the consequences of vector-to-raster and raster-to-vector conversion. *Photogrammetric Engineering & Remote Sensing* **63**: 425-434.

Conway, T. J., Tans, P. P., Waterman, L. S., Thoning, K. W., Kitzis, K. R., Masarie, K. A. & Zhang, N. (1994). Evidence for interannual variability of the carbon cycle from the National Oceanic and Atmospheric Administration/Climate Monitoring and Diagnostics Laboratory Global Air Sampling Network. *Journal of Geophysical Research* **99**: 22,831-22,855.

Cook, P. G., Favreau, G., Dighton, J. C. & Tickell, S. (2003). Determining natural groundwater influx to a tropical river using radon, chlorofluorocarbons and ionic environmental tracers. *Journal of Hydrology* **277**: 74-88.

Costa, M. H., Oliveira, C. H. C., Andrade, R. G., Bustamante, T. R., Silva, F. A. & Coe, M. T. (2002). A macroscale hydrological data set of river flow routing parameters for the Amazon Basin. *Journal of Geophysical Research* **107**: doi:10.1029/2001JD000309.

Costa-Cabral, M. C. & Burges, S. J. (1994). Digital elevation model networks (DEMON): A model of flow over hillslopes for computation of contributing and dispersal areas. *Water Resources Research* **30**: 1681-1692.

Cowie, G. L. & Hedges, J. I. (1984). Determination of Neutral Sugars in Plankton, Sediments, and Wood by Capillary Gas Chromatography of Equilibrated Isomeric Mixtures. *Analytical Chemistry* **56**: 497-504.

Cowie, G. L. & Hedges, J. I. (1992). Sources and reactivities of amino acids in a coastal marine environment. *Limnology and Oceanography* **37**: 703-724.

Crowley, T. J. & Berner, R. A. (2001). CO_2 and climate change. *Science* **292**: 870-872.

Curtis, W. F., Meade, R. H., Nordin Jr., C. F., Price, N. B. & Sholkovitz, E. R. (1979). Non-uniform vertical distribution of fine sediment in the Amazon River. *Nature* **280**: 381-383.

Dalai, T. K., Krishnaswami, S. & Sarin, M. M. (2002). Major ion chemistry in the headwaters of the Yamuna river system: Chemical weathering, its temperature dependence and CO_2 consumption in the Himalaya. *Geochimica et Cosmochimica Acta* **66**: 3397-3416.

Danko, D. M. (1992). The digital chart of the world. *GeoInfo Systems* **2**: 29-36.

Davidson, E. A. & Trumbore, S. E. (1995). Gas diffusivity and production of CO_2 in deep soils of the eastern Amazon. *Tellus* **47B**: 550-565.

Davidson, E. A., Belk, E. & Boone, R. D. (1998). Soil water content and temperature as independent or confounded factors controlling soil respiration in a temperate mixed hardwood forest. *Global Change Biology* **4**: 217-227.

Davidson, E. A., Verchot, L. V., Cattânio, J. H., Ackerman, I. L. & Carvalho, J. E. M. (2000). Effects of soil water content on soil respiration in forests and cattle pastures of eastern Amazonia. *Biogeochemistry* **48**: 53-69.

Davidson, E. A. & Artaxo, P. (2004). Globally significant changes in biological processes of the Amazon Basin: Results of the Large-scale Biosphere-Atmosphere Experiment. *Global Change Biology* **10**: 519-529.

Dawson, J. J. C., Hope, D., Cresser, M. S. & Billett, M. F. (1995). Downstream changes in free carbon dioxide in an upland catchment from Northeastern Scotland. *Journal of Environmental Quality* **24**: 699-706.

Dawson, J. J. C., Billett, M. F., Neal, C. & Hill, S. (2002). A comparison of particulate, dissolved and gaseous carbon in two contrasting upland streams in the UK. *Journal of Hydrology* **257**: 226-246.

de Camargo, P. B., Trumbore, S. E., Martinelli, L. A., Davidson, E. A., Nepstad, D. C. & Victoria, R. L. (1999). Soil carbon dynamics in regrowing forest of eastern Amazonia. *Global Change Biology* **5**: 693-702.

Deines, P., Langmuir, D. & Harmon, R. S. (1974). Stable carbon isotope ratios and the existence of a gas phase in the evolution of carbonate ground waters. *Geochimica et Cosmochimica Acta* **38**: 1147-1164.

Desjardins, T., Andreux, F., Volkoff, B. & Cerri, C. C. (1994). Organic carbon and ^{13}C contents in soils and soil size-fractions, and their changes due to deforestation and pasture installation in eastern Amazonia. *Geoderma* **61**: 103-118.

Dettinger, M. D. & Ghil, M. (1998). Seasonal and interannual variations of atmospheric CO_2 and climate. *Tellus* **50B**: 1-24.

Devol, A. H., Quay, P. D., Richey, J. E. & Martinelli, L. A. (1987). The role of gas exchange in the inorganic carbon, oxygen, and ^{222}Rn budgets of the Amazon River. *Limnology and Oceanography* **32**: 235-248.

Devol, A. H., Richey, J. E., Forsberg, B. R. & Martinelli, L. A. (1994). Environmental methane in the Amazon river floodplain, p. 151-165. In: Mitsch, W. J. (ed.), *Global wetlands: Old world and new*. Elsevier. Amsterdam.

Devol, A. H., Forsberg, B. R., Richey, J. E. & Pimentel, T. P. (1995). Seasonal variation in chemical distributions in the Amazon (Solimões) River: A multiyear time series. *Global Biogeochemical Cycles* **9**: 307-328.

Devol, A. H. & Hedges, J. I. (2001). Organic matter and nutrients in the mainstem Amazon River, p. 275-306. In: McClain, M. E., Victoria, R. L. & Richey, J. E. (ed.), *The biogeochemistry of the Amazon basin*. Oxford University Press. New York.

Döll, P. & Lehner, B. (2002). Validation of a new global 30-min drainage direction map. *Journal of Hydrology* **258**: 214-231.

Dörr, H. & Münnich, K. O. (1980). Carbon-14 and carbon-13 in soil CO_2. *Radiocarbon* **22**: 909-918.

Drever, J. I. (1988). *The geochemistry of natural waters*. Prentice Hall. Englewood Cliffs.

Drever, J. I. (1994). The effect of land plants on weathering rates of silicate minerals. *Geochimica et Cosmochimica Acta* **58**: 2325-2332.

Dubroeucq, D., Volkoff, B. & Pedro, G. (1991). La couverture pedologique du Bouclier du nord de l'Amazonie (bassin du Haut Rio Negro). Sequence evolutive des sols et son role dans l'aplanissement generalise des zones tropicales perhumides. *C.R.Acad.Sci.Paris, Serie II* **312**: 663-671.

Duivenvoorden, J. F. & Lips, J. M. 1995. *A Land-Ecological Study of Soils, Vegetation, and Plant Diversity in Colombian Amazonia.* TROPENBOS Series 12, Backhuys Publishers. Leiden.

Dunne, T., Mertes, L. A. K., Meade, R. H., Richey, J. E. & Forsberg, B. R. (1998). Exchanges of sediment between the flood plain and channel of the Amazon river in Brazil. *Geological Society of America Bulletin* **110**: 450-467.

Edmond, J. M., Palmer, M. R., Measures, C. I., Grant, B. & Stallard, R. F. (1995). The fluvial geochemistry and denudation rate of the Guayana Shield in Venezuela, Colombia, and Brazil. *Geochimica et Cosmochimica Acta* **59**: 3301-3325.

Edmond, J. M., Palmer, M. R., Measures, C. I., Brown, E. T. & Huh, Y. (1996). Fluvial geochemistry of the eastern slope of the northeastern Andes and its foredeep in the drainage of the Orinoco in Colombia and Venezuela. *Geochimica et Cosmochimica Acta* **60**: 2949-2976.

Edmond, J. M. & Hu, Y. (1997). Chemical weathering yields from basement and orogenic terrains in hot and cold climates, p. 329-351. In: Ruddiman, W. F. (ed.), *Tectonic uplift and climate change*. Plenum Press. New York.

Ehleringer, J. R. & Monson, R. K. (1993). Evolutionary and ecological aspects of photosynthetic pathway variation. *Annual Review of Ecology and Systematics* **24**: 411-439.

Ehleringer, J. R., Cerling, T. E. & Helliker, B. R. (1997). C_4 photosynthesis, atmospheric CO_2, and climate. *Oecologia* **112**: 285-299.

Ehleringer, J. R., Buchmann, N. & Flanagan, L. B. (2000). Carbon isotope ratios in belowground carbon cycle processes. *Ecological Applications* **10**: 412-422.

Ekblad, A. & Högberg, P. (2001). Natural abundance of ^{13}C in CO_2 respired from forest soils reveals speed of link between tree photosynthesis and root respiration. *Oecologia* **127**: 305-308.

Ekblad, A., Nyberg, G. & Högberg, P. (2002). ^{13}C-discrimination during microbial respiration of added C_3-, C_4- and ^{13}C-labelled sugars to a C_3-forest soil. *Oecologia* **131**: 245-249.

Elbaz-Poulichet, F., Seyler, P., Maurice-Bourgoin, L., Guyot, J. L. & Dupuy, C. (1999). Trace element geochemistry in the upper Amazon drainage basin (Bolivia). *Chemical Geology* **157**: 319-334.

Elsenbeer, H., Lack, A. & Cassel, K. (1995). Chemical fingerprints of hydrological compartments and flow paths at La Cuenca, western Amazonia. *Water Resources Research* **31**: 3051-3058.

Elsenbeer, H., Lack, A. & Cassel, K. (1996). The stormflow chemistry at La Cuenca, Western Amazonia. *Interciencia* **21**: 133-139.

Emblanch, C., Zuppi, G. M., Mudry, J., Blavoux, B. & Batiot, C. (2003). Carbon 13 of TDIC to quantify the role of the unsaturated zone: The example of the Vaucluse karst systems (Southeastern France). *Journal of Hydrology* **279**: 262-274.

Ertel, J. R., Hedges, J. I., Devol, A. H. & Richey, J. E. (1986). Dissolved humic substances of the Amazon River system. *Limnology and Oceanography* **31**: 739-754.

ESRI. (1997). *ARC/INFO version 7.1.1*. ESRI Press. Redlands, California.

Falkowski, P., Scholes, R. J., Boyle, E., Canadell, J., Canfield, D. E., Elser, J., Gruber, N., Hibbard, K., Högberg, P., Linder, S., Mackenzie, F. T., III, B. M., Pedersen, T., Rosenthal, Y., Seitzinger, S., Smetacek, V. & Steffen, W. (2000). The global carbon cycle: A test of our knowledge of Earth as a system. *Science* **290**: 291-296.

Farr, T. & Kobrick, M. (2000). Shuttle Radar Topography Mission produces a wealth of data. *EOS Trans. AGU* **81**: 583-585.

Feigl, B. J., Steudler, P. A. & Cerri, C. C. (1995). Effects of pasture introduction on soil CO_2 emissions during the dry season in the state of Rondônia, Brazil. *Biogeochemistry* **31**: 1-14.

Ferreira, J. R., Devol, A. H., Martinelli, L. A., Forsberg, B. R., Victoria, R. L., Richey, J. E. & Mortatti, J. (1988). Chemical composition of the Madeira river: Seasonal trends and total transport. *Mitt. Geol. Paläont. Inst.* **66**: 63-75.

Fessenden, J. E. & Ehleringer, J. R. (2003). Temporal variation in $\delta^{13}C$ of ecosystem respiration in the Pacific Northwest: Links to moisture stress. *Oecologia* **136**: 129-136.

Filius, J. D., Lumsdon, D. G., Meeussen, J. C. L. & others, a. (2000). Adsorption of fulvic acid on goethite. *Geochimica et Cosmochimica Acta* **64**: 51-60.

Finlay, J. C. (2003). Controls of streamwater dissolved inorganic carbon dynamics in a forested watershed. *Biogeochemistry* **62**: 231-252.

Fisher, T. R. (1979). Plankton and primary production in aquatic systems of the Central Amazon Basin. *Comparative Biochemistry and Physiology* **62(A)**: 31-38.

Fisher, T. R., Jr. & Parsley, P. E. (1979). Amazon lakes: Water storage and nutrient stripping by algae. *Limnology and Oceanography* **24**: 547-553.

Flintrop, C., Hohlmann, B., Jasper, T., Korte, C., Podlaha, O. G., Scheele, S. & Veizer, J. (1996). Anatomy of pollution: Rivers of North Rhine-Westphalia, Germany. *American Journal of Science* **296**: 58-98.

Forsberg, B. R., Devol, A. H., Richey, J. E., Martinelli, L. A. & dos Santos, H. (1988). Factors controlling nutrient concentrations in Amazon floodplain lakes. *Limnology and Oceanography* **33**: 41-56.

Forsberg, B. R., Araujo-Lima, C. A. R. M., Martinelli, L. A., Victoria, R. L. & Bonassi, J. A. (1993). Autotrophic carbon sources for fish of the Central Amazon. *Ecology* **74**: 643-652.

Forti, N. C. & Neal, C. (1992). Hydrochemical cycles in tropical rainforest: An overview with emphasis on Central Amazonia. *Journal of Hydrology* **134**: 103-115.

France-Lanord, C. & Derry, L. A. (1997). Organic carbon burial forcing of the carbon cycle from Himalayan erosion. *Nature* **390**: 65-67.

Francey, R. J., Allison, C. E., Etheridge, D. M., Trudinger, C. M., Enting, I. G., Leuenberger, M., Langenfelds, R. L., Michel, E. & Steele, L. P. (1999). A 1000-year high precision record of $\delta^{13}C$ in atmospheric CO_2. *Tellus* **51B**: 170-193.

Franken, W. & Leopoldo, P. R. (1984). Hydrology of catchment areas of Central-Amazonian forest streams, p. 501-519. In: Sioli, H. (ed.), *The Amazon: Limnology and Landscape Ecology of a Mighty Tropical River and its Basin*. W. Junk Publishers. Dordrecht.

Fread, D. L. (1992). Flow routing, p. 10.1-10.36. In: Maidment, D. R. (ed.), *Handbook of hydrology*. McGraw-Hill. New York.

Freitas, H. A., Pessenda, L. C. R., Aravena, R., Gouveia, S. E. M., Ribeiro, A. S. & Boulet, R. (2001). Late Quaternary vegetation dynamics in the Southern Amazon basin inferred from carbon isotopes in soil organic matter. *Quaternary Research* **55**: 39-46.

Furch, K. (1984). Water chemistry of the Amazon basin: The distribution of chemical elements among freshwaters, p. 167-199. In: Sioli, H. (ed.), *The Amazon: Limnology and Landscape Ecology of a Mighty Tropical River and its Basin*. W. Junk Publishers. Dordrecht.

Gaillardet, J., Dupré, B., Allègre, C. J. & Négrel, P. (1997). Chemical and physical denudation in the Amazon River Basin. *Chemical Geology* **142**: 141-173.

Gaillardet, J., Dupré, B., Louvat, P. & Allègre, C. J. (1999). Global silicate weathering and CO_2 consumption rates deduced from the chemistry of large rivers. *Chemical Geology* **159**: 3-30.

Galy, A. & France-Lanord, C. (1999). Weathering processes in the Ganges-Brahmaputra basin and the riverine alkalinity budget. *Chemical Geology* **159**: 31-60.

Gaudinski, J. B., Trumbore, S. E., Davidson, E. A. & Zheng, S. (2000). Soil carbon cycling in a temperate forest: Radiocarbon-based estimates of residence times, sequestration rates and partitioning of fluxes. *Biogeochemistry* **51**: 33-69.

Genereux, D. P. & Hemond, H. F. (1992). Determination of gas exchange rate constants for a small stream on Walker Branch watershed, Tennessee. *Water Resources Research* **28**: 2365-2374.

Gérard, J. C., Nemry, B., François, L. M. & Warnant, P. (1999). The interannual change of atmospheric CO_2: Contribution of subtropical ecosystems? *Geophysical Research Letters* **26**: 243-246.

Gesch, D. B., Verdin, K. L. & Greenlee, S. K. (1999). New land surface digital elevation model covers the Earth. *EOS* **80**: 70-71.

Gibbs, M. T., Bluth, G. J. S., Fawcett, P. J. & Kump, L. R. (1999). Global chemical erosion over the last 250 My: Variations due to changes in paleogeography, paleoclimate, and paleogeology. *American Journal of Science* **299**: 611-651.

Gibbs, R. J. (1967). The geochemistry of the Amazon River System: Part I. The factors that control the salinity and the composition and concentration of the suspended solids. *Geological Society of America Bulletin* **78**: 1203-1232.

Gómez, Z., Llerena, C. A. & McClain, M. E. (in press). Variabilidad espacio-temporal del nitrógeno e iones mayores en la cuenca del río Pachitea, Perú. *Revista Forestal del Perú*

Gonfiantini, R. & Zuppi, G. M. (2003). Carbon isotope exchange rate of DIC in karst groundwater. *Chemical Geology* **197**: 319-336.

Goni, M. A. & Hedges, J. I. (1992). Lignin dimers: Structures, distribution, and potential geochemical applications. *Geochimica et Cosmochimica Acta* **56**: 4025-4043.

Goulden, M. L., Miller, S. D., da Rocha, H. R., Menton, M. C., de Freitas, H. C., Figueira, A. M. S. & de Sousa, C. A. D. (2004). Diel and seasonal patterns of tropical forest CO_2 exchange. *Ecological Applications* **14**: S42-S54.

Gove, H. E. (2000). Some comments on accelerator mass spectrometry. *Radiocarbon* **42**: 127-135.

Graham, S. T., Famiglietti, J. S. & Maidment, D. R. (1999). Five-minute, 1/2°, and 1° data sets of continental watersheds and river networks for use in regional and global hydrologic and climate system modeling studies. *Water Resources Research* **35**: 583-587.

Gregory, S. V., Swanson, F. J., McKee, W. A. & Cummins, K. W. (1991). An ecosystem perspective of riparian zones. *BioScience* **41**: 540-551.

Grimm, N. B., Gergel, S. E., McDowell, W. H., Boyer, E. W., Dent, C. L., Groffman, P. M., Hart, S. C., Harvey, J. W., Johnston, C. A., Mayorga, E., McClain, M. E. & Pinay, G. (2003). Merging aquatic and terrestrial perspectives of nutrient biogeochemistry. *Oecologia* **442**: 485–501.

Guggenberger, G. & Kaiser, K. (2003). Dissolved organic matter in soil: Challenging the paradigm of sorptive preservation. *Geoderma* **113**: 293-310.

Gurney, K. R., Law, R. M., Denning, A. S., Rayner, P. J., Baker, D., Bousquet, P., Bruhwiler, L., Chen, Y.-H., Ciais, P., Fan, S.-M., Fung, I. Y., Gloor, M., Heimann, M., Higuchi, K., John, J., Maki, T., Maksyutov, S., Masarie, K., Peylin, P., Prather, M., Pak, B. C., Randerson, J. T., Sarmiento, J. L., Taguchi, S., Takahashi, T. & Yuen, C.-W. (2002). Towards robust regional estimates of CO_2 sources and sinks using atmospheric transport models. *Nature* **415**: 626-630.

Gu, B., Schmitt, J., Chen, Z., Liang, L. & McCarthy, J. F. (1995). Adsorption and desorption of different organic matter fractions on iron oxide. *Geochimica et Cosmochimica Acta* **59**: 219-229.

Guyot, J. L. 1993. *Hydrogeochimie des fleuves de l'Amazonie bolivienne, Ph.D. Thesis.* Editions de l'ORSTOM. Paris.

Guyot, J. L., Bourges, J., Hoorelbecke, R., Roche, M. A., Calle, H., Cortes, J. & Barragan Guzman, M. C. (1988). Exportation de matieres en suspension des Andes vers l'Amazonie par le Rio Beni, Bolivie. *IAHS Publ.* **174**: 443-451.

Guyot, J. L., Bourges, J., Calle, H., Cortes, J., Hoorelbecke, R. & Roche, M. A. 1989. Transport of suspended sediments to the Amazon by the Andean river: The River

Mamore, Bolivia, p. 106-113. *In* Fourth International Symposium on River Sedimentation. Beijing, China: ISRS.

Guyot, J. L., Quintanilla, J., Callidonde, M. & Calle, H. 1992. Distribución regional de la hidroquímica en la cuenca Amazónica de Bolivia, p. 135-144. *In* Roche, M. A., Bourges, J., Salas R, E. & Diaz E, C. (ed.), Seminario sobre el Programa Hidrológico y Climatológico de la Cuenca Amazónica de Bolivia (PHICAB). La Paz, Bolivia:

Guyot, J. L. & Wasson, J. G. (1994). Regional pattern of riverine dissolved organic carbon in the Amazon drainage basin of Bolivia. *Limnology and Oceanography* **39**: 452-458.

Guyot, J. L., Filizola, N., Quintanilla, J. & Cortez, J. (1996). Dissolved solids and suspended sediment yields in the Rio Madeira basin, from the Bolivian Andes to the Amazon. *IAHS Publ. no.* **236**: 55-63.

Guyot, J. L., Filizola, N. & Guimaraes, V. (1998). Amazon suspended sediment yield measurements using an Acoustic Doppler Current Profiler (ADCP): First results. *IAHS Publ. no.* **253**:

Guyot, J. L., Jouanneau, J. M. & Wasson, J. G. (1999). Characterization of river bed and suspended sediments in the Rio Madeira drainage basin (Bolivian Amazonia). *Journal of South American Earth Sciences* **12**: 401-410.

Hanson, P. J., Edwards, N. T., Garten, C. T. & Andrews, J. A. (2000). Separating root and soil microbial contributions to soil respiration: A review of methods and observations. *Biogeochemistry* **48**: 115-146.

Hedges, J. I., Clark, W. A., Quay, P. D., Richey, J. E., Devol, A. H. & Santos, U. d. M. (1986a). Compositions and fluxes for particulate organic material in the Amazon River. *Limnology and Oceanography* **31**: 717-738.

Hedges, J. I., Ertel, J. R., Quay, P. D., Grootes, P. M., Richey, J. E., Devol, A. H., Farwell, G. W., Schmidt, F. W. & Salati, E. (1986b). Organic carbon-14 in the Amazon River system. *Science* **231**: 1129-1131.

Hedges, J. I., Cowie, G. L., Richey, J. E., Quay, P. D., Benner, R., Strom, M. & Forsberg, B. R. (1994). Origins and processing of organic matter in the Amazon River indicated by carbohydrates and amino acids. *Limnology and Oceanography* **39**: 743-761.

Hedges, J. I. & Keil, R. G. (1995). Sedimentary organic matter preservation: An assessment and speculative synthesis. *Marine Chemistry* **49**: 81-115.

Hedges, J. I., Mayorga, E., Tsamakis, E., McClain, M. E., Aufdenkampe, A., Quay, P., Richey, J. E., Benner, R., Opsahl, S., Black, B., Pimentel, T., Quintanilla, J. & Maurice, L. (2000). Organic matter in Bolivian tributaries of the Amazon River: A comparison to the lower mainstem. *Limnology and Oceanography* **45**: 1449-1466.

Hélie, J.-F., Hillaire-Marcel, C. & Rondeau, B. (2002). Seasonal changes in the sources and fluxes of dissolved inorganic carbon through the St. Lawrence River -- isotopic and chemical constraint. *Chemical Geology* **186**: 117-138.

Henn, M. R. & Chapela, I. H. (2000). Differential C isotope discrimination by fungi during decomposition of C_3- and C_4-derived sucrose. *Applied and Environmental Microbiology* **66**: 4180-4186.

Högberg, P., Nordgren, A., Buchmann, N., Taylor, A. F. S., Ekblad, A., Högberg, M. N., Nyberg, G., Ottoson-Löfvenius, M. & Read, D. J. (2001). Large-scale forest girdling shows that current photosynthesis drives soil respiration. *Nature* **411**: 789-792.

Hogg, J., McCormack, J. E., Roberts, S. A., Gahegan, M. N. & Hoyle, B. S. (1997). Automated derivation of stream-channel networks and selected catchment characteristics from digital elevation models, p. 211-235. In: Mather, P. M. (ed.), *Geographical information handling: Research and applications*. John Wiley & Sons. Chichester.

Holmes, K. W., Roberts, D. A., Sweeney, S., Numata, I., Matricardi, E., Biggs, T. W., Batista, G. & Chadwick, O. A. (2004). Soil databases and the problem of establishing regional biogeochemical trends. *Global Change Biology* **10**: 796-814.

Hope, D., Billett, M. F. & Cresser, M. S. (1994). A review of the export of carbon in river water: Fluxes and processes. *Environmental Pollution* **84**: 301-324.

Hope, D., Palmer, S. M., Billett, M. F. & Dawson, J. J. C. (2001). Carbon dioxide and methane evasion from a temperate peatland stream. *Limnology and Oceanography* **46**: 847-857.

James, E. R., Manga, M. & Rose, T. P. (1999). CO_2 degassing in the Oregon Cascades. *Geology* **27**: 823-826.

Johnsson, M. J. & Meade, R. H. (1990). Chemical weathering of fluvial sediments during alluvial storage: The Macuapanim Island point bar, Solimões River, Brazil. *Journal of Sedimentary Petrology* **60**: 827-842.

Jones, J. B. & Mulholland, P. J. (1998a). Carbon dioxide variation in a hardwood forest stream: An integrative measure of whole catchment soil respiration. *Ecosystems* **1**: 183-196.

Jones, J. B. & Mulholland, P. J. (1998b). Influence of drainage basin topography and elevation on carbon dioxide and methane supersaturation of stream water. *Biogeochemistry* **40**: 57-72.

Junk, W. J. (1989). The use of amazonian floodplains under an ecological perspective. *Interciencia* **14**: 317-322.

Kaiser, K. & Zech, W. (1997). Competitive sorption of dissolved organic matter fractions to soils and related mineral phases. *Soil Science Society of America Journal* **61**: 64-69.

Kaiser, K. (1998). Fractionation of dissolved organic matter affected by polyvalent metal cations. *Organic Geochemistry* **28**: 849-854.

Kaiser, K. & Guggenberger, G. (2000). The role of DOM sorption to mineral surfaces in the preservation of organic matter in soils. *Organic Geochemistry* **31**: 711-725.

Kaiser, K., Guggenberger, G. & Zech, W. (2001). Isotopic fractionation of dissolved organic carbon in shallow forest soils as affected by sorption. *European Journal of Soil Science* **52**: 585-597.

Kalbitz, K., Solinger, S., Park, J.-H., Michalzik, B. & Matzner, E. (2000). Controls on the dynamics of dissolved organic matter in soils: A review. *Soil Science* **165**: 277-304.

Kalliola, R., Linna, A., Puhakka, M., Salo, J. & Räsänen, M. (1993). Mineral nutrients in fluvial sediments from the Peruvian Amazon. *Catena* **20**: 333-349.

Karim, A. & Veizer, J. (2000). Weathering processes in the Indus River Basin: Implications from riverine carbon, sulfur, oxygen, and strontium isotopes. *Chemical Geology* **170**: 153-177.

Keeling, C. D., Whorf, T. P., Wahlen, M. & van der Plicht, J. (1995). Interannual extremes in the rate of rise of atmospheric carbon dioxide since 1980. *Nature* **375**: 666-670.

Keeling, C. D. & Whorf, T. P. (2004). Atmospheric CO_2 records from sites in the SIO air sampling network. In: (ed.), *Trends: A Compendium of Data on Global Change*. Carbon Dioxide Information Analysis Center, Oak Ridge National Laboratory, U.S. Department of Energy. Oak Ridge, Tenn., U.S.A.

Keil, R. G., Montluçon, D. B., Prahl, F. G. & Hedges, J. I. (1994). Sorptive preservation of labile organic matter in marine sediments. *Nature* **370**: 549-552.

Keil, R. G., Mayer, L. M., Quay, P. D., Richey, J. E. & Hedges, J. I. (1997). Losses of organic matter from riverine particles in deltas. *Geochimica et Cosmochimica Acta* **61**: 1507-1511.

Keller, C. K. & Bacon, D. H. (1998). Soil respiration and georespiration distinguished by transport analyses of vadose CO_2, $^{13}CO_2$, and $^{14}CO_2$. *Global Biogeochemical Cycles* **12**: 361-372.

Keller, M., Alencar, A., Asner, G. P., Braswell, B. H., Bustamante, M. M. C., Davidson, E. A., Feldpausch, T., Fernandes, E., Goulden, M. L., Kabat, P., Kruijt, B., Luizão, F. J., Miller, S., Markewitz, D., Nobre, A. D., Nobre, C. A., Filho, N. P., da Rocha, H. R., Silva Dias, P., von Randow, C. & Vourlitis, G. L. (2004). Ecological research in the Large-Scale Biosphere-Atmosphere Experiment in Amazonia: Early results. *Ecological Applications* **14**: S3-S16.

Kendall, C., Sklash, M. G. & Bullen, T. D. (1995). Isotope tracers of water and solute sources in catchments, p. 261-303. In: Trudgill, S. T. (ed.), *Solute modelling in catchment systems*. John Wiley & Sons. Chichester.

Kerrick, D. M. & Caldeira, K. (1998). Metamorphic CO_2 degassing from orogenic belts. *Chemical Geology* **145**: 213-232.

Kerrick, D. M. (2001). Present and past nonanthropogenic CO_2 degassing from the solid earth. *Reviews of Geophysics* **39**: 565-585.

Klinge, H. & Ohle, W. (1964). Chemical properties of rivers in the Amazonian area in relation to soil conditions. *Verhandlungen - Internationale Vereinigung fur Theoretische und Angewandte Limnologie* **15**: 1067-1076.

Konhauser, K. O., Fyfe, W. S. & Kronberg, B. I. (1994). Multi-element chemistry of some Amazonian waters and soils. *Chemical Geology* **111**: 155-175.

Körner, C., Farquhar, G. D. & Roksandic, Z. (1988). A global survey of carbon isotope discrimination in plants from high altitude. *Oecologia* **74**: 623-632.

Körner, C., Farquhar, G. D. & Wong, S. C. (1991). Carbon isotope discrimination by plants follows latitudinal and altitudinal trends. *Oecologia* **88**: 30-40.

Koutika, L.-S., Bartoli, F., Andreux, F., Cerri, C. C., Burtin, G., Chone, T. & Philippy, R. (1997). Organic matter dynamics and aggregation in soils under rain forest and pastures of increasing age in the eastern Amazon Basin. *Geoderma* **76**: 87-112.

Krusche, A. V., Bernardes, M. C., Ballester, M. V. R., Victoria, R. L., Martinelli, L. A., Aufdenkampe, A. K., Richey, J. E., Gomes, B. M., Leite, N. K. & Molson, M. (in prep.). Natural and anthropogenic influences on the biogeochemistry of a meso-scale (75,000 km^2) river undergoing deforestation in Southwest Amazon (Ji-Paraná river, Rondônia).

Krysanova, V., Müller-Wohlfeil, D.-I. & Becker, A. (1998). Development and test of a spatially distributed hydrological/water quality model for mesoscale watersheds. *Ecological Modelling* **106**: 261-289.

Küchler, I. L., Miekeley, N. & Forsberg, B. R. (1994). Molecular mass distributions of dissolved organic carbon and associated metals in waters from Rio Negro and Rio Solimões. *Science of the Total Environment* **156**: 207-216.

Kump, L. R., Brantley, S. L. & Arthur, M. A. (2000). Chemical weathering, atmospheric CO_2, and climate. *Annual Review of Earth and Planetary Sciences* **28**: 611-617.

Kvist, L. P. & Nebel, G. (2001). A review of Peruvian flood plain forests: Ecosystems, inhabitants and resource use. *Forest Ecology and Management* **150**: 3-26.

Laws, E. A., Popp, B. N., Bidigare, R. R., Kennicutt, M. C. & Macko, S. A. (1995). Dependence of phytoplankton carbon isotopic composition on growth rate and $[CO_2]_{aq}$: Theoretical considerations and experimental results. *Geochimica et Cosmochimica Acta* **59**: 1131-1138.

Leenheer, J. A. (1980). Origin and nature of humic substances in the waters of the Amazon River Basin. *Acta Amazonica* **10**: 513-526.

Lenz, P. H., Melack, J. M., Robertson, B. & Hardy, E. A. (1986). Ammonium and phosphate regeneration by the zooplankton of an Amazon floodplain lake. *Freshwater Biology* **16**: 821-830.

Leopold, L. B. (1994). *A View of the River*. Harvard University Press. Cambridge.

Lesack, L. F. W. & Melack, J. M. (1996). Mass balance of major solutes in a rainforest catchment in the Central Amazon: Implications for nutrient budgets in tropical rainforests. *Biogeochemistry* **32**: 115-142.

Levin, I. & Hesshaimer, V. (2000). Radiocarbon -- A unique tracer of global carbon cycle dynamics. *Radiocarbon* **42**: 69-80.

Levin, I. & Kromer, B. (in press). The tropospheric $^{14}CO_2$ level in mid latitudes of the Northern Hemisphere (1959-2003). *Radiocarbon*

Lewis, W. M., Hamilton, S. K. & Saunders, J. F. (1995). Rivers of northern South America, p. 219-256. In: Cushing, C. E., Cummins, K. W. & Minshall, G. W. (ed.), *River and stream ecosystems*. Elsevier. Amsterdam.

Liang, C. & Mackay, D. S. (2000). A general model of watershed extraction and representation using globally optimal flow paths and up-slope contributing area. *International Journal of Geographical Information Science* **14**: 337-358.

Lloyd, J. & Farquhar, G. D. (1994). ^{13}C discrimination during CO_2 assimilation by the terrestrial biosphere. *Oecologia* **99**: 201-215.

Lohmann, D., Lettenmaier, D. P., Liang, X., Wood, E. F., Boone, A., Chang, S., Chen, F., Dai, Y., Desborough, C., Dickinson, R. E., Duan, Q., Ek, M., Gusev, Y. M., Habets, F., Irannejad, P., Koster, R., Mitchell, K. E., Nasonova, O. N., Noilhan, J., Schaake, J., Schlosser, A., Shao, Y., Shmakin, A. B., Verseghy, D., Warrach, K., Wetzel, P.,

Xue, Y., Yang, Z.-L. & Zeng, Q.-C. (1998). The Project for Intercomparison of Land-surface Parameterization Schemes (PILPS) Phase 2(c) Red-Arkansas River basin experiment: 3. Spatial and temporal analysis of water fluxes. *Global and Planetary Change* **19**: 161-179.

Longinelli, A. & Edmond, J. M. (1983). Isotope geochemistry of the Amazon Basin: A reconnaissance. *Journal of Geophysical Research* **88**: 3703-3717.

Ludwig, W., Probst, J. L. & Kempe, S. (1996). Predicting the oceanic input of organic carbon by continental erosion. *Global Biogeochemical Cycles* **10**: 23-41.

Luizão, R. C. C., Luizão, F. J., Paiva, R. Q., Monteiro, T. F., Sousa, L. S. & Kruijt, B. (2004). Variation of carbon and nitrogen cycling processes along a topographic gradient in a central Amazonian forest. *Global Change Biology* **10**: 592-600.

Maidment, D. R. (1993). GIS and hydrologic modeling, p. 147-167. In: Goodchild, M. F., Parks, B. O. & Steyaert, L. T. (ed.), *Environmental modeling with GIS*. Oxford University Press. New York.

Malhi, Y. & Grace, J. (2000). Tropical forests and atmospheric carbon dioxide. *Trends in Ecology & Evolution* **15**: 332-337.

Marengo, J. A. & Nobre, C. A. (2001). General characteristics and variability of climate in the Amazon Basin and its links to the global climate system, p. 17-41. In: McClain, M. E., Victoria, R. L. & Richey, J. E. (ed.), *The biogeochemistry of the Amazon basin*. Oxford University Press. New York.

Markewitz, D., Davidson, E. A., Figueiredo, R. O., Victoria, R. L. & Krusche, A. V. (2001). Control of cation concentrations in stream waters by surface soil processes in an Amazonian watershed. *Nature* **410**: 802-805.

Martinelli, L. A., Devol, A. H., Victoria, R. L. & Richey, J. E. (1991). Stable carbon isotopic variation in C_3 and C_4 plants along the Amazon River. *Nature* **353**: 57-59.

Martinelli, L. A., Victoria, R. L., Trivelin, P. C. O., Devol, A. H. & Richey, J. E. (1992). ^{15}N natural abundance in plants of the Amazon River floodplain and potential atmospheric N_2 fixation. *Oecologia* **90**: 591-596.

Martinelli, L. A., Victoria, R. L., Dematte, J. L. I., Richey, J. E. & Devol, A. H. (1993). Chemical and mineralogical composition of Amazon River floodplain sediments, Brazil. *Applied Geochemistry* **8**: 391-402.

Martinelli, L. A., Victoria, R. L., Forsberg, B. R. & Richey, J. E. (1994). Isotopic composition of major carbon reservoirs in the Amazon floodplain. *International Journal of Ecology and Environmental Sciences* **20**: 31-46.

Martinelli, L. A., Victoria, R. L., Sternberg, L. S. L., Ribeiro, A. & Moreira, M. Z. (1996a). Using stable isotopes to determine sources of evaporated water to the atmosphere in the Amazon Basin. *Journal of Hydrology* **183**: 191-204.

Martinelli, L. A., Pessenda, L. C. R., Espinosa, E., Camargo, P. B., Telles, E. C., Cerri, C. C., Victoria, R. L., Aravena, R., Richey, J. & Trumbore, S. (1996b). Carbon-13 variation with depth in soils of Brazil and climate change during the Quaternary. *Oecologia* **106**: 376-381.

Martinelli, L. A., Almeida, S., Brown, I. F., Moreira, M. Z., Victoria, R. L., Sternberg, L. S. L., Ferreira, C. A. C. & Thomas, W. W. (1998). Stable carbon isotope ratio of tree leaves, boles and fine litter in a tropical forest in Rondônia, Brazil. *Oecologia* **114**: 170-179.

Martinelli, L. A., Victoria, R. L., de Camargo, P. B., Piccolo, M. C., Mertes, L. A. K., Richey, J. E., Devol, A. H. & Forsberg, B. R. (2003). Inland variability of carbon-nitrogen concentrations and $\delta^{13}C$ in Amazon floodplain (várzea) vegetation and sediment. *Hydrological Processes* **17**: 1419-1430.

Martz, L. W. & Garbrecht, J. (1992). Numerical definition of drainage network and subcatchment areas from digital elevation models. *Computers & Geosciences* **18**: 747-761.

Mayer, L. M. (1994). Relationships between mineral surfaces and organic carbon concentrations in soils and sediments. *Chemical Geology* **114**: 347-363.

Mayer, L. M., Keil, R. G., Macko, S. A., Joye, S. B., Ruttenberg, K. C. & Aller, R. C. (1998). Importance of suspended particulates in riverine delivery of bioavailable nitrogen to coastal zones. *Global Biogeochemical Cycles* **12**: 573-579.

Mayer, L. M. (1999). Extent of coverage of mineral surfaces by organic matter in marine sediments. *Geochimica et Cosmochimica Acta* **63**: 207-215.

Mayorga, E., Logsdon, M. G., Ballester, M. V. R. & Richey, J. E. (submitted). Estimating cell-to-cell land surface flow paths from digital channel networks, with an application to the Amazon basin. *Journal of Hydrology.*

McClain, M. E., Richey, J. E. & Pimentel, T. P. (1994). Groundwater nitrogen dynamics at the terrestrial-lotic interface of a small catchment in the Central Amazon Basin. *Biogeochemistry* **27**: 113-127.

McClain, M. E., Richey, J. E. & Victoria, R. L. (1995). Andean contributions to the biogeochemistry of the Amazon river system. *Bulletin de l'Institut Français des Etudes Andine* **24**: 425-437.

McClain, M. E., Richey, J. E., Brandes, J. A. & Pimentel, T. P. (1997). Dissolved organic matter and terrestrial-lotic linkages in the Central Amazon basin of Brazil. *Global Biogeochemical Cycles* **11**: 295-311.

McClain, M. E. & Elsenbeer, H. (2001). Terrestrial inputs to Amazon streams and internal biogeochemical processing, p. 185-208. In: McClain, M. E., Victoria, R. L. & Richey, J. E. (ed.), *The biogeochemistry of the Amazon basin*. Oxford University Press. New York.

Meade, R. H., Nordin Jr., C. F., Curtis, W. F., Rodrigues, F. M. C., Vale, C. M. D. & Edmond, J. M. (1979). Sediment loads in the Amazon River. *Nature* **278**: 161-163.

Meade, R. H., Dunne, T., Richey, J. E., Santos, U. d. M. & Salati, E. (1985). Storage and remobilization of suspended sediments in the Lower Amazon River of Brazil. *Science* **228**: 488-490.

Meade, R. H. (1994). Suspended sediments of the modern Amazon and Orinoco Rivers. *Quaternary International* **21**: 29-39.

Meir, P., Grace, J., Miranda, A. & Lloyd, J. (1996). Soil respiration in a rainforest in Amazonia and in cerrado in central Brazil, p. 319-351. In: Gash, J. H. C., Nobre, C. A., Roberts, J. M. & Victoria, R. L. (ed.), *Amazonian Deforestation and Climate*. John Wiley & Sons. Chichester.

Melack, J. M. & Forsberg, B. R. (2001). Biogeochemistry of Amazon floodplain lakes and associated wetlands, p. 235-274. In: McClain, M. E., Victoria, R. L. & Richey, J. E. (ed.), *The biogeochemistry of the Amazon basin*. Oxford University Press. New York.

Mertes, L. A. K., Smith, M. O. & Adams, J. B. (1993). Estimating suspended sediment concentrations in surface waters of the Amazon River wetlands from Landsat images. *Remote Sensing of Environment* **43**: 281-301.

Mertes, L. A. K., Dunne, T. & Martinelli, L. A. (1996). Channel-floodplain geomorphology of the Solimões-Amazon River, Brazil. *Geological Society of America Bulletin* **108**: 1089-1107.

Mertes, L. A. K. (1997). Documentation and significance of the perirheic zone on inundated floodplains. *Water Resources Research* **33**: 1749-1762.

Meybeck, M. (1982). Carbon, nitrogen, and phosphorus transport by world rivers. *American Journal of Science* **282**: 401-450.

Meyer, J. L., McDowell, W. H., Bott, T. L., Elwood, J. W., Ishizaki, C., Melack, J. M., Peckarsky, B. L., Peterson, B. J. & Rublee, P. A. (1988). Elemental dynamics in streams. *Journal of the North American Benthological Society* **7**: 410-432.

Michalzik, B., Tipping, E., Mulder, J., Gallardo Lancho, J. F., Matzner, E., Bryant, C. L., Clarke, N., Lofts, S. & Vicente Esteban, M. A. (2003). Modelling the production and transport of dissolved organic carbon in forest soils. *Biogeochemistry* **66**: 241-264.

Millot, R., Gaillardet, J., Dupré, B. & Allègre, C. J. (2003). Northern latitude chemical weathering rates: Clues from the Mackenzie River Basin, Canada. *Geochimica et Cosmochimica Acta* **67**: 1305-1329.

Mook, W. G. & Tan, F. C. (1991). Stable carbon isotopes in rivers and estuaries, p. 245-264. In: Degens, E. T., Kempe, S. & Richey, J. E. (ed.), *Biogeochemistry of major world rivers*. John Wiley & Sons.

Moore, I. D., Grayson, R. B. & Ladson, A. R. (1991). Digital terrain modelling: A review of hydrological, geomorphological, and biological applications. *Hydrological Processes* **5**: 3-30.

Moran, M. A. & Zepp, R. G. (1997). Role of photoreactions in the formation of biologically labile compounds from dissolved organic matter. *Limnology and Oceanography* **42**: 1307-1316.

Mörner, N.-A. & Etiope, G. (2002). Carbon degassing from the lithosphere. *Global and Planetary Change* **33**: 185-203.

Mortatti, J., Ferreira, J. R., Martinelli, L. A., Victoria, R. L. & Tancredi, A. C. F. (1989). Biogeochemistry of the Madeira river basin. *GeoJournal* **19**: 391-397.

Mortatti, J., Probst, J. L. & Ferreira, J. R. (1992). Hydrological and geochemical characteristics of the Jamari and Jiparana river basins (Rondonia, Brazil). *GeoJournal* **26**: 287-296.

Mortatti, J. & Probst, J.-L. (2003). Silicate rock weathering and atmospheric/soil CO_2 uptake in the Amazon basin estimated from river water geochemistry: Seasonal and spatial variations. *Chemical Geology* **197**: 177-196.

Mounier, S., Braucher, R. & Benaïm, J. Y. (1999). Differentiation of organic matter's properties of the Rio Negro basin by crossflow ultra-filtration and UV-spectrofluorescence. *Water Research* **33**: 2363-2373.

Mounier, S., Benedetti, M., Benaïm, J. Y. & Boulègue, J. (2002). Organic matter size dynamics in the Amazon River, p. 25-34. In: McClain, M. E. (ed.), *The Ecohydrology of South American Rivers and Wetlands*. IAHS Spec. Pub. no. 6, IAHS Press. Wallingford, UK.

Mulholland, P. J., Fellows, C. S., Tank, J. L., Grimm, N. B., Webster, J. R., Hamilton, S. K., Martí, E., Ashkenas, L. R., Bowden, W. B., Dodds, W. K., McDowell, W. H., Paul, M. J. & Peterson, B. J. (2001). Inter-biome comparison of factors controlling stream metabolism. *Freshwater Biology* **46**: 1503-1517.

Muller, F., Seyler, F. & Guyot, J. L. 1999. Utilisation d'imagerie radar (ROS) JERS-1 pour l'obtention de réseaux de drainage. Example du Rio Negro (Amazonie), p. 112. *In* Hydrological and Geochemical Processes in Large Scale River Basins. Manaus, Brazil: HiBAm.

Munhoven, G. (2002). Glacial-interglacial changes of continental weathering: Estimates of the related CO_2 and HCO_3^- flux variations and their uncertainties. *Global and Planetary Change* **33**: 155-176.

Neal, C., House, W. A. & Down, K. (1998a). An assessment of excess carbon dioxide partial pressures in natural waters based on pH and alkalinity measurements. *The Science of the Total Environment* **210/211**: 173-185.

Neal, C., House, W. A., Jarvie, H. P. & Eatherall, A. (1998b). The significance of dissolved carbon dioxide in major lowland rivers entering the North Sea. *The Science of the Total Environment* **210/211**: 187-203.

Neal, C. (2001). Alkalinity measurements within natural waters: Towards a standardised approach. *The Science of the Total Environment* **265**: 99-113.

Neff, J. C. & Asner, G. P. (2001). Dissolved organic carbon in terrestrial ecosystems: Synthesis and a model. *Ecosystems* **4**: 29-48.

Neill, C., Melillo, J. M., Steudler, P. A., Cerri, C. C., de Moraes, J. F. L., Piccolo, M. C. & Brito, M. (1997). Soil carbon and nitrogen stocks following forest clearing for pasture in the Southwestern Brazilian Amazon. *Ecological Applications* **7**: 1216-1225.

Neill, C. & Davidson, E. A. (2000). Soil carbon accumulation or loss following deforestation for pasture in the Brazilian Amazon, p. 197-211. In: Lal, R., Kimble, J. M. & Stewart, B. A. (ed.), *Global climate change and tropical ecosystems*. CRC Press. Boca Raton.

Neill, C., Deegan, L. A., Thomas, S. M. & Cerri, C. C. (2001). Deforestation for pasture alters nitrogen and phosphorus in small Amazonian streams. *Ecological Applications* **11**: 1817-1828.

Nelson, P. N., Baldock, J. A. & Oades, J. M. (1993). Concentration and composition of dissolved organic carbon in streams in relation to catchment soil properties. *Biogeochemistry* **19**: 27-50.

NGDC. (1988). *ETOPO5 Digital relief of the surface of the Earth, http://www.ngdc.noaa.gov*. NOAA, National Geophysical Data Center. Boulder, Colorado.

NGDC. (1997). *TerrainBase global terrain model, http://www.ngdc.noaa.gov*. NOAA, National Geophysical Data Center. Boulder, Colorado.

Nordin Jr., C. F., Meade, R. H., Curtis, W. F., Bósio, N. J. & Landim, P. M. B. (1980). Size distribution of Amazon River bed sediment. *Nature* **286**: 52-53.

Nortcliff, S. & Thornes, J. B. (1978). Water and cation movement in a tropical rainforest environment. 1. Objectives, experimental design and preliminary results. *Acta Amazonica* **8**: 245-258.

Nortcliff, S. & Thornes, J. B. (1988). The dynamics of a tropical floodplain environment with reference to forest ecology. *Journal of Biogeography* **15**: 49-59.

Nortcliff, S., Ross, S. M. & Thornes, J. B. (1990). Soil moisture, runoff and sediment yield from differentially cleared tropical rainforest plots, p. 419-436. In: Thornes, J. B. (ed.), *Vegetation and Erosion: Processes and Environments*. John Wiley & Sons. Chichester.

O'Leary, M. H. (1981). Carbon isotope fractionation in plants. *Phytochemistry* **20**: 553-567.

Ometto, J. P. H. B., Flanagan, L. B., Martinelli, L. A., Moreira, M. Z., Higuchi, N. & Ehleringer, J. R. (2002). Carbon isotope discrimination in forest and pasture ecosystems of the Amazon Basin. *Global Biogeochemical Cycles* **16**: 1109, doi:10.1029/2001GB001462.

Pacala, S. W., Hurtt, G. C., Baker, D., Peylin, P., Houghton, R. A., Birdsey, R. A., Heath, L., Sundquist, E. T., Stallard, R. F., Ciais, P., Moorcroft, P. R., Caspersen, J. P., Shevliakova, E., Moore III, B., Kohlmaier, G. H., Holland, E. A., Gloor, M., Harmon, M. E., Fan, S.-M., Sarmiento, J. L., Goodale, C. L., Schimel, D. S. & Field, C. B. (2001). Consistent land- and atmosphere-based U.S. carbon sink estimates. *Science* **292**: 2316-2320.

Palmer, M. R. & Edmond, J. M. (1992). Controls over the strontium isotope composition of river water. *Geochimica et Cosmochimica Acta* **56**: 2099-2111.

Palmer, S. M., Hope, D., Billett, M. F., Dawson, J. J. C. & Bryant, C. L. (2001). Sources of organic and inorganic carbon in a headwater stream: Evidence from carbon isotope studies. *Biogeochemistry* **52**: 321-338.

Pataki, D. E., Ehleringer, J. R., Flanagan, L. B., Yakir, D., Bowling, D. R., Still, C. J., Buchmann, N., Kaplan, J. O. & Berry, J. A. (2003). The application and interpretation of Keeling plots in terrestrial carbon cycle research. *Global Biogeochemical Cycles* **17**: 1022, doi:10.1029/2001GB001850.

Patel, N., Mounier, S., Guyot, J. L., Benamou, C. & Benaïm, J. Y. (1999). Fluxes of dissolved and colloidal organic carbon, along the Purus and Amazonas Rivers (Brazil). *Science of the Total Environment* **229**: 53-64.

Pessenda, L. C. R., Gomes, B. M., Aravena, R., Ribeiro, A. S., Boulet, R. & Gouveia, S. E. M. (1998a). The carbon isotope record in soils along a forest-cerrado ecosystem transect: Implications for vegetation changes in the Rondonia state, southwestern Brazilian Amazon region. *The Holocene* **8**: 599-603.

Pessenda, L. C. R., Gouveia, S. E. M., Aravena, R., Gomes, B. M., Boulet, R. & Ribeiro, A. S. (1998b). ^{14}C dating and stable carbon isotopes of soil organic matter in forest-savanna boundary areas in the southern Brazilian Amazon region. *Radiocarbon* **40**: 1013-1022.

Peterson, B. J., Wollheim, W. M., Mulholland, P. J., Webster, J. R., Meyer, J. L., Tank, J. L., Martí, E., Bowden, W. B., Valett, H. M., Hershey, A. E., McDowell, W. H., Dodds, W. K., Hamilton, S. K., Gregory, S. V. & Morrall, D. D. (2001). Controls of nitrogen export from watersheds by headwater streams. *Science* **292**: 86-90.

Petsch, S. T., Eglinton, T. I. & Edwards, K. J. (2001). ^{14}C-dead living biomass: Evidence for microbial assimilation of ancient organic carbon during shale weathering. *Science* **292**: 1127-1131.

Phillips, O. L., Malhi, Y., Higuchi, N., Laurence, W. F., Núñez Vargas, P., Vásquez Martínez, R., Laurence, S. G., Ferreira, L. V., Stern, M., Brown, S. & Grace, J. (1998). Changes in the carbon balance of tropical forests: Evidence from long-term plots. *Science* **282**: 439-442.

Poage, M. A. & Feng, X. (2004). A theoretical analysis of steady state $\delta^{13}C$ profiles of soil organic matter. *Global Biogeochemical Cycles* **18**: GB2016, doi:10.1029/2003GB002195.

Powers, J. S. & Schlesinger, W. H. (2002). Geographic and vertical patterns of stable carbon isotopes in tropical rain forest soils of Costa Rica. *Geoderma* **109**: 141-160.

Probst, J. L., Mortatti, J. & Tardy, Y. (1994). Carbon river fluxes and weathering CO_2 consumption in the Congo and Amazon river basins. *Applied Geochemistry* **9**: 1-13.

Puhakka, M., Kalliola, R., Rajasilta, M. & Salo, J. (1992). River types, site evolution and successional vegetation patterns in Peruvian Amazonia. *Journal of Biogeography* **19**: 651-665.

Putzer, H. (1984). The geological evolution of the Amazon basin and its mineral resources, p. 15-46. In: Sioli, H. (ed.), *The Amazon: Limnology and landscape ecology of a mighty tropical river and its basin*. W. Junk Publishers. Dordrecht.

Quay, P. D., Emerson, S. R., Quay, B. M. & Devol, A. H. (1986). The carbon cycle for Lake Washington -- A stable isotope study. *Limnology and Oceanography* **31**: 596-611.

Quay, P. D., King, S., Wilbur, D., Wofsy, S. & Richey, J. (1989). $^{13}C/^{12}C$ of atmospheric CO_2 in the Amazon Basin: forest and river sources. *Journal of Geophysical Research* **94**: 18,327-18,336.

Quay, P. D., Wilbur, D. O., Richey, J. E., Hedges, J. I., Devol, A. H. & Victoria, R. L. (1992). Carbon cycling in the Amazon River: Implications from the ^{13}C composition of particles and solutes. *Limnology and Oceanography* **37**: 857-871.

Quay, P. D., Wilbur, D. O., Richey, J. E., Devol, A. H., Benner, R. & Forsberg, B. R. (1995). The $^{18}O/^{16}O$ of dissolved oxygen in rivers and lakes in the Amazon Basin: a tracer of respiration and photosynthesis. *Limnology and Oceanography* **40**: 718-729.

RADAMBRASIL. (1973-1984). *Levantamento de recursos naturais. Vol. 3-20, 22, 25, 26*. Departamento Nacional da Producão Mineral. Rio de Janeiro.

Raich, J. W. & Potter, C. S. (1995). Global patterns of carbon dioxide emissions from soils. *Global Biogeochemical Cycles* **9**: 23-36.

Raich, J. W., Potter, C. S. & Bhagawati, D. (2002). Interannual variability in global soil respiration, 1980-94. *Global Change Biology* **8**: 800-812.

Randerson, J. T., Enting, I. G., Schuur, E. A. G., Caldeira, K. & Fung, I. Y. (2002). Seasonal and latitudinal variability of troposphere $\Delta^{14}CO_2$: Post bomb contributions from fossil fuels, oceans, the stratosphere, and the terrestrial biosphere. *Global Biogeochemical Cycles* **16**: 1112, doi:10.1029/2002GB001876.

Räsänen, M. E., Neller, R., Salo, J. & Junger, H. (1992). Recent and ancient fluvial deposition systems in the Amazonian foreland basin, Peru. *Geological Magazine* **129**: 293-306.

Raymond, P. A., Bauer, J. E. & Cole, J. J. (2000). Atmospheric CO_2 evasion, dissolved inorganic carbon production, and net heterotrophy in the York River estuary. *Limnology and Oceanography* **45**: 1707-1717.

Raymond, P. A. & Bauer, J. E. (2001a). Riverine export of aged terrestrial organic matter to the North Atlantic Ocean. *Nature* **409**: 497-500.

Raymond, P. A. & Bauer, J. E. (2001b). DOC cycling in a temperate estuary: A mass balance approach using natural ^{14}C and ^{13}C isotopes. *Limnology and Oceanography* **46**: 655-667.

Raymond, P. A. & Cole, J. J. (2001). Gas exchange in rivers and estuaries: Choosing a gas transfer velocity. *Estuaries* **24**: 312-317.

Raymond, P. A. & Hopkinson, C. S. (2003). Ecosystem modulation of dissolved carbon age in a temperate marsh-dominated estuary. *Ecosystems* **6**: 694-705.

Rayner, P. J., Enting, I. G., Francey, R. J. & Langenfelds, R. (1999a). Reconstructing the recent carbon cycle from atmospheric CO_2, $\delta^{13}C$ and O_2/N_2 observations. *Tellus* **51B**: 213-232.

Rayner, P. J. & Law, R. M. (1999). The interannual variability of the global carbon cycle. *Tellus* **51B**: 210-212.

Rayner, P. J., Law, R. M. & Dargaville, R. (1999b). The relationship between tropical CO_2 fluxes and the El Niño-Southern Oscillation. *Geophysical Research Letters* **26**: 493-496.

Reichstein, M., Rey, A., Freibauer, A., Tenhunen, J. D., Valentini, R., Banza, J., Casals, P., Cheng, Y., Grunzweig, J. M., Irvine, J., Joffre, R., Law, B. E., Loustau, D., Miglietta, F., Oechel, W., Ourcival, J.-M., Pereira, J. S., Peresotti, A., Ponti, F., Qi, Y., Rambal, S., Rayment, M., Romanya, J., Rossi, F., Tedeschi, V., Tironi, G., Xu, M. & Yakir, D. (2003). Modeling temporal and large-scale spatial variability of soil respiration from soil water availability, temperature and vegetation productivity indices. *Global Biogeochemical Cycles* **17**: 1104, doi:10.1029/2003GB002035.

Renssen, H. & Knoop, J. M. (2000). A global river routing network for use in hydrological modeling. *Journal of Hydrology* **230**: 230-243.

Richey, J. E., Brock, J. T., Naiman, R. J., Wissmar, R. C. & Stallard, R. F. (1980). Organic carbon: oxidation and transport in the Amazon River. *Science* **207**: 1348-1351.

Richey, J. E., Meade, R. H., Salati, E., Devol, A. H., Nordin, C. F. & dos Santos, U. (1986). Water discharge and suspended sediment concentrations in the Amazon River: 1982-1984. *Water Resources Research* **22**: 756-764.

Richey, J. E., Devol, A. H., Wofsy, S. C., Victoria, R. & Ribeiro, M. N. G. (1988). Biogenic gases and the oxidation and reduction of carbon in the Amazon River and floodplain waters. *Limnology and Oceanograpy* **33**: 551-561.

Richey, J. E., Nobre, C. & Deser, C. (1989a). Amazon River discharge and climate variability: 1903 to 1985. *Science* **246**: 101-103.

Richey, J. E., Mertes, L. A. K., Dunne, T., Victoria, R. L., Forsberg, B. R., Tancredi, A. C. N. S. & Oliveira, E. (1989b). Sources and routing of the Amazon River flood wave. *Global Biogeochemical Cycles* **3**: 191-204.

Richey, J. E., Hedges, J. I., Devol, A. H. & Quay, P. D. (1990). Biogeochemistry of carbon in the Amazon River. *Limnology and Oceanography* **35**: 352-371.

Richey, J. E., Victoria, R. L., Salati, E. & Forsberg, B. R. (1991). The biogeochemistry of a major river system: The Amazon case study, p. 57-74. In: Degens, E. T., Kempe, S.

& Richey, J. E. (ed.), *Biogeochemistry of major world rivers*. John Wiley & Sons. New York.

Richey, J. E., Wilhelm, S. R., McClain, M. E., Victoria, R. L., Melack, J. M. & Araujo-Lima, C. (1997). Organic matter and nutrient dynamics in river corridors of the Amazon basin and their response to anthropogenic change. *Ciência e Cultura* **49**: 98-110.

Richey, J. E., Melack, J. M., Aufdenkampe, A. K., Ballester, M. V. & Hess, L. L. (2002). Outgassing from Amazonian rivers and wetlands as a large tropical source of atmospheric CO_2. *Nature* **416**: 617-620.

Roberts, D. A., Numata, I., Holmes, K. W., Batista, G., Krug, T., Monteiro, A., Powell, B. & Chadwick, O. A. (2002). Large area mapping of land-cover change in Rondônia using multitemporal spectral mixture analysis and decision tree classifiers. *Journal of Geophysical Research* **107**: 8073, doi:10.1029/2001JD000374.

Rose, T. P. & Davisson, M. L. (1996). Radiocarbon in hydrologic systems containing dissolved magmatic carbon dioxide. *Science* **273**: 1367-1370.

Rosenqvist, A., Forsberg, B. R., Pimentel, T., Rauste, Y. A. & Richey, J. E. (2002). The use of spaceborne radar data to model inundation patterns and trace gas emissions in the central Amazon floodplain. *International Journal of Remote Sensing* **23**: 1303-1328.

Royer, D. L., Berner, R. A., Montañez, I. P., Tabor, N. J. & Beerling, D. J. (2004). CO_2 as a primary driver of Phanerozoic climate. *GSA Today* **14**: 4-10.

Ruddiman, W. F., ed. (1997). *Tectonic uplift and climate change*. Plenum Press. New York.

Ruddiman, W. F., Raymo, M. E., Prell, W. L. & Kutzbach, J. E. (1997). The uplift-climate connection: A synthesis, p. 471-515. In: Ruddiman, W. F. (ed.), *Tectonic uplift and climate change*. Plenum Press. New York.

Salimon, C. I., Davidson, E. A., Victoria, R. L. & Melo, A. W. F. (2004). CO_2 flux from soil in pastures and forests in southwestern Amazonia. *Global Change Biology* **10**: 833-843.

Salo, J., .Kalliola, R., Häkkinen, I., Mäkinen, Y., Niemelä, P., Puhakka, M. & Coley, P. D. (1986). River dynamics and the diversity of Amazon lowland forest. *Nature* **322**: 254-258.

Sanaiotti, T. M., Martinelli, L. A., Victoria, R. L., Trumbore, S. E. & Camargo, P. B. (2002). Past vegetation changes in Amazon savannas determined using carbon isotopes of soil organic matter. *Biotropica* **34**: 2-16.

Sarmiento, J. L. & Gruber, N. (2002). Sinks for anthropogenic carbon. *Physics Today* **55**: 30-36.

Savage, K. E. & Davidson, E. A. (2001). Interannual variation of soil respiration in two New England forests. *Global Biogeochemical Cycles* **15**: 337-350.

Schaefer, D. A., McDowell, W. H., Scatena, F. N. & Asbury, C. E. (2000). Effects of hurricane disturbance on stream water concentrations and fluxes in eight tropical watersheds of the Luquillo Experimental Forest, Puerto Rico. *Journal of Tropical Ecology* **16**: 189-207.

Schimel, D. S., House, J. I., Hibbard, K. A., Bousquet, P., Ciais, P., Peylin, P., Braswell, B. H., Apps, M. J., Baker, D., Bondeau, A., Canadell, J. G., Churkina, G., Cramer, W., Denning, A. S., Field, C. B., Friedlingstein, P., Goodale, C. L., Heimann, M., Houghton, R. A., Melillo, J. M., Moore III, B., Murdiyarso, D., Noble, I., Pacala, S. W., Prentice, I. C., Raupach, M. R., Rayner, P. J., Scholes, R. J., Steffen, W. L. & Wirth, C. (2001). Recent patterns and mechanisms of carbon exchange by terrestrial ecosystems. *Nature* **414**: 169-172.

Schindler, J. E. & Krabbenhoft, D. P. (1998). The hyporheic zone as a source of dissolved organic carbon and carbon gases to a temperate forested stream. *Biogeochemistry* **43**: 157-174.

Schlesinger, W. H. & Andrews, J. A. (2000). Soil respiration and the global carbon cycle. *Biogeochemistry* **48**: 7-20.

Sekulin, A. E., Bullock, A. & Gustard, A. (1992). Rapid calculation of catchment boundaries using an automated river network overlay technique. *Water Resources Research* **28**: 2101-2109.

Sholkovitz, E. R. & Price, N. B. (1980). The major-element chemistry of suspended matter in the Amazon Estuary. *Geochimica et Cosmochimica Acta* **44**: 163-171.

Siegenthaler, U. & Munnich, K. O. (1981). $^{13}C/^{12}C$ fractionation during CO_2 transfer from air to sea, p. 249-257. In: Bolin, B. (ed.), *Carbon Cycle Modelling*. John Wiley. New York.

Sioli, H. (1984a). The Amazon and its main affluents: Hydrography, morphology of the river courses, and river types, p. 127-165. In: Sioli, H. (ed.), *The Amazon: Limnology and Landscape Ecology of a Mighty Tropical River and its Basin*. W. Junk Publishers. Dordrecht.

Sioli, H., ed. (1984b). *The Amazon: Limnology and Landscape Ecology of a Mighty Tropical River and its Basin*. W. Junk Publishers. Dordrecht.

Sippel, S. J., Hamilton, S. K., Melack, J. M. & Novo, E. M. M. (1998). Passive microwave observations of inundation area and the area/stage relation in the Amazon River floodplain. *International Journal of Remote Sensing* **19**: 3055-3074.

Siqueira, P., Hensley, S., Shaffer, S., Hess, L., McGarragh, G., Chapman, B. & Freeman, A. (2000). A continental-scale mosaic of the Amazon basin using JERS-1 SAR. *IEEE Transactions on Geoscience and Remote Sensing* **38**: 2638-2644.

Smith, R. A., Schwarz, G. E. & Alexander, R. B. (1997). Regional interpretation of water-quality monitoring data. *Water Resources Research* **33**: 2781-2798.

Smith, S. V. & Kroopnick, P. (1981). Carbon-13 isotopic fractionation as a measure of aquatic metabolism. *Nature* **294**: 252-253.

Sombroek, W. G. (1984). Soils of the Amazon region, p. 521-535. In: Sioli, H. (ed.), *The Amazon: Limnology and landscape ecology of a mighty tropical river and its basin*. W. Junk Publishers. Dordrecht.

Sotta, E. D., Meir, P., Malhi, Y., Nobre, A. D., Hodnett, M. G. & Grace, J. (2004). Soil CO_2 efflux in a tropical forest in the central Amazon. *Global Change Biology* **10**: 601-607.

Spitzy, A. & Ittekkot, V. (1991). Dissolved and particulate organic matter in rivers, p. 5-17. In: Mantoura, R. F. C., Martin, J.-M. & Wollast, R. (ed.), *Ocean Margin Processes in Global Change*. John Wiley & Sons. Berlin.

St. John, T. V. & Anderson, A. B. (1982). A re-examination of plant phenolics as a source of tropical black water rivers. *Tropical Ecology* **23**: 151-154.

Stallard, R. F. & Edmond, J. M. (1981). Geochemistry of the Amazon. 1. Precipitation chemistry and the marine contribution to the dissolved load at the time of peak discharge. *Journal of Geophysical Research* **86**: 9844-9858.

Stallard, R. F. & Edmond, J. M. (1983). Geochemistry of the Amazon: 2. The influence of geology and weathering environment on the dissolved load. *Journal of Geophysical Research* **88**: 9671-9688.

Stallard, R. F. (1985). River chemistry, geology, geomorphology, and soils in the Amazon and Orinoco Basins, p. 293-316. In: Drever, J. I. (ed.), *The chemistry of weathering*. D. Reidel. Dordrecht.

Stallard, R. F. & Edmond, J. M. (1987). Geochemistry of the Amazon. 3. Weathering chemistry and limits to dissolved inputs. *Journal of Geophysical Research* **92**: 8293-8302.

Stallard, R. F. (1988). Weathering and erosion in the humid tropics, p. 225-246. In: Lerman, A. & Meybeck, M. (ed.), *Physical and Chemical Weathering in Geochemical Cycles*. Kluwer Academic Publishers. Dordrecht.

Stallard, R. F. (1995). Tectonic, environmental, and human aspects of weathering and erosion: A global review using a steady-state perspective. *Annual Review of Earth and Planetary Sciences* **23**: 11-39.

Stallard, R. F. (1998). Terrestrial sedimentation and the carbon cycle: Coupling weathering and erosion to carbon burial. *Global Biogeochemical Cycles* **12**: 231-257.

Stark, N. M. & Jordan, C. F. (1978). Nutrient retention by the root mat of an Amazonian rain forest. *Ecology* **59**: 434-437.

Still, C. J., Berry, J. A., Collatz, G. J. & DeFries, R. S. (2003). Global distribution of C_3 and C_4 vegetation: Carbon cycle implications. *Global Biogeochemical Cycles* **17**: 1006, doi:10.1029/2001GB001807.

Sternberg, H. O. (1975). *The Amazon River of Brazil*. Franz Steiner Verlag GMBH. Wiesbaden, Germany.

Stuiver, M. & Robinson, S. W. (1974). University of Washington GEOSECS North Atlantic carbon-14 results. *Earth and Planetary Science Letters* **23**: 87-90.

Stuiver, M. & Polach, H. A. (1977). Discussion: Reporting of ^{14}C data. *Radiocarbon* **19**: 355-363.

Stumm, W. & Morgan, J. J. (1981). *Aquatic Chemistry*, 2nd ed. John Wiley & Sons. New York.

Sundquist, E. T. (1993). The global carbon dioxide budget. *Science* **259**: 934-941.

Szaran, J. (1998). Carbon isotope fractionation between dissolved and gaseous carbon dioxide. *Chemical Geology* **150**: 331-337.

Tan, F. C. & Edmond, J. M. (1993). Carbon isotope geochemistry of the Orinoco Basin. *Estuarine, Coastal and Shelf Science* **36**: 541-547.

Taylor, C. B. (1997). On the isotopic composition of dissolved inorganic carbon in rivers and shallow groundwater: A diagrammatic approach to process identification and a more realistic model of the open system. *Radiocarbon* **39**: 251-268.

Taylor, C. B., Trompetter, V. J., Brown, L. J. & Bekesi, G. (2001). The Manawatu aquifers, North Island, New Zealand: Clarification of hydrogeology using a multidisciplinary environmental tracer approach. *Hydrological Processes* **15**: 3269-3286.

Telles, E. C. C., de Camargo, P. B., Martinelli, L. A., Trumbore, S. E., da Costa, E. S., Santos, J., Higuchi, N. & Oliveira Jr., R. C. (2003). Influence of soil texture on carbon dynamics and storage potential in tropical forest soils of Amazonia. *Global Biogeochemical Cycles* **17**: 1040, doi:10.1029/2002GB001953.

Telmer, K. & Veizer, J. (1999). Carbon fluxes, pCO_2 and substrate weathering in a large northern river basin, Canada: Carbon isotope perspectives. *Chemical Geology* **159**: 61-86.

Thomas, S. M., Neill, C., Deegan, L. A., Krusche, A. V., Ballester, M. V. & Victoria, R. L. (2004). Influences of land use and stream size on particulate and dissolved materials in a small Amazonian stream network. *Biogeochemistry* **68**: 135-151.

Tian, H., Melillo, J. M., Kicklighter, D. W., Mcguire, A. D., Helfrich III, J. V. K., Moore III, B. & Vörösmarty, C. J. (1998). Effect of interannual climate variability on carbon storage in Amazonian ecosystems. *Nature* **396**: 664-667.

Tiessen, H., Chacon, P. & Cuevas, E. (1994). Phosphorus and nitrogen status in soils and vegetation along a toposequence of dystrophic rainforests on the upper Rio Negro. *Oecologia* **99**: 145-150.

Townsend, A. R., Asner, G. P., White, J. W. C. & Tans, P. P. (2002). Land use effects on atmospheric ^{13}C imply a sizable terrestrial CO_2 sink in tropical latitudes. *Geophysical Research Letters* **29**: doi:10.1029/2001GL013454.

Trolier, M., White, J. W. C., Tans, P. P., Masarie, K. A. & Gemery, P. A. (1996). Monitoring the isotopic composition of atmospheric CO_2: Measurements from the NOAA Global Air Sampling Network. *Journal of Geophysical Research* **101**: 25,897-25,916.

Trumbore, S. E. (1993). Comparison of carbon dynamics in tropical and temperate soils using radiocarbon measurements. *Global Biogeochemical Cycles* **7**: 275-290.

Trumbore, S. E., Davidson, E. A., Camargo, P. B. d., Nepstad, D. C. & Martinelli, L. A. (1995). Belowground cycling of carbon in forests and pastures of Eastern Amazonia. *Global Biogeochemical Cycles* **9**: 515-528.

Trumbore, S. E. (2000). Age of soil organic matter and soil respiration: Radiocarbon constraints on belowground C dynamics. *Ecological Applications* **10**: 399-411.

USA-CERL. (1991). *GRASS 4.0 User's Manual*. United States Army Corps of Engineers Construction Engineering Research Laboratory. Champaign, Illinois.

USGS. (1998). *HYDRO1k, http://edcwww.cr.usgs.gov/landdaac/gtopo30/hydro/*. U.S. Geological Survey, Earth Resour. Obs. Syst. Data Center. Sioux Falls, SD.

Vannote, R. L., Minshall, G. W., Cummings, K. W., Sedell, J. R. & Cushing, C. E. (1980). The river continuum concept. *Canadian Journal of Fisheries and Aquatic Sciences* **37**: 130-137.

Vasconcelos, S. S., Zarin, D. J., Capanu, M., LIttell, R., Davidson, E. A., Ishida, F. Y., Santos, E. B., Araújo, M. M., Aragão, D. V., Rangel-Vasconcelos, L. G. T., Oliveira, F. A., McDowell, W. H. & de Carvalho, C. J. R. (2004). Moisture and substrate

availability constrain soil trace gas fluxes in an eastern Amazonian regrowth forest. *Global Biogeochemical Cycles* **18**: GB2009, doi:10.1029/2003GB002210.

Verdin, K. L. & Verdin, J. P. (1999). A topological system for delineation and codification of the Earth's river basins. *Journal of Hydrology* **218**: 1-12.

Victoria, R., Martinelli, L. A., Richey, J. E., Devol, A. H., Forsberg, B. R. & Ribeiro, M. N. G. (1989). Spatial and temporal variations in soil chemistry on the Amazon floodplain. *GeoJournal* **19**: 45-52.

Victoria, R. L., Martinelli, L. A., Trivelin, P. C. O., Matsui, E., Forsberg, B. R., Richey, J. E. & Devol, A. H. (1992). The use of stable isotopes in studies of nutrient cycling: Carbon isotope composition of Amazon varzea sediments. *Biotropica* **24**: 240-249.

Vogel, J. S., Nelson, D. E. & Southon, J. R. (1987). ^{14}C background levels in an accelerator mass spectrometry system. *Radiocarbon* **29**: 323-333.

Vogel, J. S. (1992). A rapid method for preparation of biomedical targets for AMS. *Radiocarbon* **34**: 344-350.

Vogel, J. S., Turteltaub, K. W., Finkel, R. & Nelson, D. E. (1995). Accelerator mass spectrometry. *Analytical Chemistry* **A**: 353-359.

Vörösmarty, C. J., Fekete, B. M., Meybeck, M. & Lammers, R. B. (2000a). Global system of rivers: Its role in organizing continental land mass and defining land-to-ocean linkages. *Global Biogeochemical Cycles* **14**: 599-621.

Vörösmarty, C. J., Fekete, B. M., Meybeck, M. & Lammers, R. B. (2000b). Geomorphometric attributes of the global system of rivers at 30-minute spatial resolution. *Journal of Hydrology* **237**: 17-39.

Waichman, A. V. (1996). Autotrophic carbon sources for heterotrophic bacterioplankton in a floodplain lake of central Amazon. *Hydrobiologia* **341**: 27-36.

Waliser, D. E. & Gautier, C. (1993). A satellite-derived climatology of the ITCZ. *Journal of Climate* **6**: 2162-2174.

Waliser, D. E. & Somerville, R. C. J. (1994). Preferred latitudes of the Intertropical Convergence Zone. *Journal of the Atmospheric Sciences* **51**: 1619-1639.

Wallace, A. R. (1853). *Narrative of travels on the Amazon and Rio Negro*. Reeve. London.

Wang, Y., Huntington, T. G., Osher, L. J., Wassenaar, L. I., Trumbore, S. E., Amundson, R. G., Harden, J. W., McKnight, D. M., Schiff, S. L., Aiken, G. R., Lyons, W. B., Aravena, R. O. & Baron, J. S. (1998). Carbon cycling in terrestrial environments, p. 577-610. In: Kendall, C. & McDonnell, J. J. (ed.), *Isotope tracers in catchment hydrology*. Elsevier. New York.

Wang, Y., Amundson, R. & Niu, X.-F. (2000). Seasonal and altitudinal variation in decomposition of soil organic matter inferred from radiocarbon measurements of soil CO_2 flux. *Global Biogeochemical Cycles* **14**: 199-211.

Wanninkhof, R. & Knox, M. (1996). Chemical enhancement of CO_2 exchange in natural waters. *Limnology and Oceanography* **41**: 689-697.

White, A. F. & Blum, A. E. (1995). Effects of climate on chemical weathering in watersheds. *Geochimica et Cosmochimica Acta* **59**: 1729-1747.

Williams, M. R. & Melack, J. M. (1997). Solute export from forested and partially deforested catchments in the central Amazon. *Biogeochemistry* **38**: 67-102.

Williams, P. M. (1968). Organic and inorganic constituents of the Amazon River. *Nature* **218**: 937-938.

Wissmar, R. C., Richey, J. E., Stallard, R. F. & Edmond, J. M. (1981). Plankton metabolism and carbon processes in the Amazon River, its tributaries, and floodplain waters, Peru-Brazil, May-June 1977. *Ecology* **62**: 1622-1633.

Yang, C., Telmer, K. & Veizer, J. (1996). Chemical dynamics of the "St. Lawrence" riverine system: δD_{H2O}, $\delta^{18}O_{H2O}$, $\delta^{13}C_{DIC}$, $\delta^{34}S_{sulfate}$, and dissolved $^{87}Sr/^{86}Sr$. *Geochimica et Cosmochimica Acta* **60**: 851-866.

Yoshimura, K., Nakao, S., Noto, M., Inokura, Y., Urata, K., Chen, M. & Lin, P.-W. (2001). Geochemical and stable isotope studies on natural water in the Taroko Gorge karst area, Taiwan -- chemical weathering of carbonate rocks by deep source CO_2 and sulfuric acid. *Chemical Geology* **177**: 415-430.

Yoshimura, K., Liu, Z., Cao, J., Yuan, D., Inokura, Y. & Noto, M. (2004). Deep source CO_2 in natural waters and its role in extensive tufa deposition in the Huanglong Ravines, Sichuan, China. *Chemical Geology* **205**: 141-153.

Zeebe, R. E. & Wolf-Gladrow, D. (2001). *CO_2 in seawater: Equilibrium, kinetics, isotopes*. Elsevier. Amsterdam.

Zhang, J., Quay, P. D. & Wilbur, D. O. (1995). Carbon isotope fractionation during gas-water exchange and dissolution of CO_2. *Geochimica et Cosmochimica Acta* **59**: 107-114.

Vita
EMILIO MAYORGA

EDUCATION

Ph.D. 2004. Chemical Oceanography, University of Washington. Advisor: Jeffrey E. Richey. Dissertation: *Isotopic constraints on sources and cycling of riverine dissolved inorganic carbon in the Amazon basin.*

M.Sc. 1997. Chemical Oceanography, University of Washington. Advisor: Jeffrey E. Richey. Dissertation: *Basin-scale controls on organic carbon exports from mesoscale to large Amazonian rivers.*

B.S. 1992. Civil Engineering, Massachusetts Institute of Technology. Interdisciplinary environmental studies focusing on biogeochemistry and hydrology.

PUBLICATIONS

Mayorga, E., A.K. Aufdenkampe, C.A. Masiello, A.V. Krusche, J.I. Hedges, P.D. Quay and J.E. Richey. Submitted. Respiration of contemporary organic matter drives outgassing of CO_2 from Amazonian rivers. *Nature*.

Mayorga, E., M.G. Logsdon, M.V.R. Ballester and J.E. Richey. Submitted. Extracting cell-to-cell land surface drainage paths from digital channel networks, with an application to the Amazon basin. *Journal of Hydrology*.

Ballester, M.V., D. de C. Victoria, A.V. Krusche, R. Coburn, R.L. Victoria, J.E. Richey, M.G. Logsdon, **E. Mayorga** and E. Matricardi. 2003. A Remote Sensing / GIS-based physical template to understand the biogeochemistry of the Ji-Paraná river basin (Western Amazonia). *Remote Sensing of Environment* **87**: 429-445.

Grimm, N.B., S.E. Gergel, W.H. McDowell, E.W. Boyer, C.L. Dent, P.M. Groffman, S.C. Hart, J.W. Harvey, C.A. Johnston, **E. Mayorga**, M.E. McClain and G. Pinay. 2003. Merging aquatic and terrestrial perspectives of nutrient biogeochemistry. *Oecologia* **442**: 485-501.

McClain, M.E., E.W. Boyer, C.L. Dent, S.E. Gergel, N.B. Grimm, P.M. Groffman, S.C. Hart, J.W. Harvey, C.A. Johnston, **E. Mayorga**, W.H. McDowell and G. Pinay. 2003. Biogeochemical hot spots and hot moments at the interface of terrestrial and aquatic ecosystems. *Ecosystems* **6**: 301-312.

Mayorga, E. and A.K. Aufdenkampe. 2002. Processing of bioactive elements in the Amazon River system, p. 1-24. In: McClain, M. E. (ed.), *The Ecohydrology of South American Rivers and Wetlands*. IAHS Spec. Pub. no. 6, IAHS Press. Wallingford, UK.

Hedges, J.I., **E. Mayorga**, E. Tsamakis and others. 2000. Organic matter in Bolivian tributaries of the Amazon River: A comparison to the lower mainstem. *Limnology and Oceanography* **45**: 1449-1466.